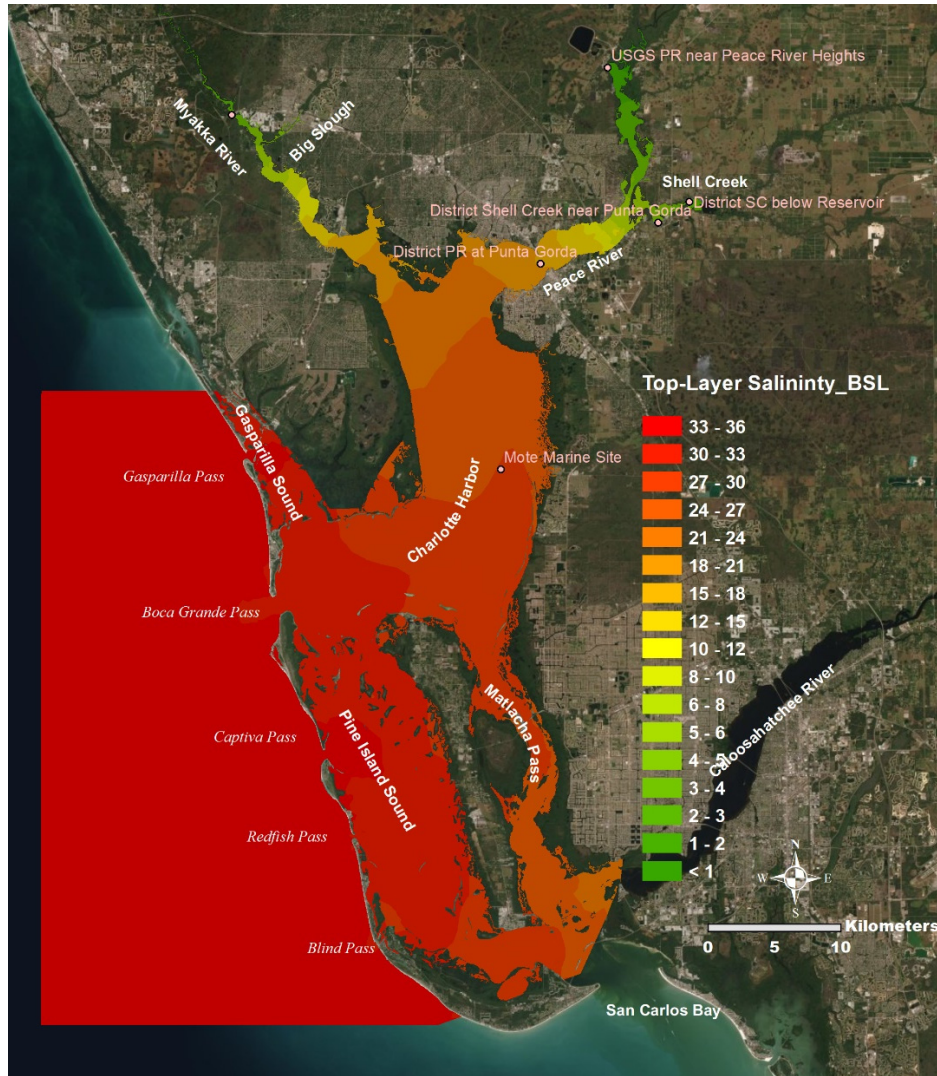


Simulating Hydrodynamics in Charlotte Harbor and its Major Tributaries

XinJian Chen, Ph.D., P.E.



Southwest Florida
Water Management District

September 2020

Contents

Summary	3
1. Introduction	5
2. Dynamic Coupling of LAMFE with UnLESS3D.....	9
3. Model Calibration and Verification.....	12
4. Simulations for the Determination of MFLs	42
5. Conclusions	68
6. References	70
7. Appendix A.....	72
8. Appendix B.....	96
9. Appendix C.....	106
10. Appendix D.....	111
11. Appendix E	126

Summary

To determine the regulatory minimum freshwater inflows to the lower Peace River (LPR) and the lower Myakka River (LMR), a sophisticated hydrodynamic model was developed in 2007 that simulated circulations and salt transport processes in a simulation domain that comprises the LPR, the LMR, the upper portion of the Charlotte Harbor (UCH), and lower Shell Creek (LSC). The 2007 model used for the complex LPR - LMR - UCH system is a coupled 3D – 2DV model named LESS, which dynamically links a laterally averaged two-dimensional hydrodynamic model (LAMFE) with a three-dimensional hydrodynamic model (LESS3D). Although the LESS model was successfully used in the minimum flow and level (MFL) evaluations of the LPR and LMR, there are a couple of shortcomings in the 2007 hydrodynamic modeling study of the estuarine system, including relative short calibration/verification periods, a relative wet summer for the calibration period, lack of any calibration station near the east side of Charlotte Harbor (CH), and that the simulation domain excluded areas south of the boundary of the Southwest Florida Water Management District (SWFWMD.)

As required by the existing rules, the MFL for the LPR is to be re-evaluated by 2018. The current modeling study is to support the re-evaluations of the MFLs of the LPR and LSC, with an intention of eliminating the abovementioned shortcomings in the LESS model developed in 2007 for the LPR-LMR-UCH system. The new model is also a coupled 3D-2DV model, which dynamically couples the LAMFE model with a 3D unstructured Cartesian grid model named UnLESS3D. The new model developed in this study is named UnLESS.

When applying the UnLESS model in the re-evaluations of MFLs for the LPR and LSC, the simulation domain was extended further downstream to cover the entire Charlotte Harbor, including the LPR, the LMR, LSC, Gasparilla Sound, Pine Island Sound, Matlacha Pass, and the most downstream portion of Caloosahatchee River. The simulation domain also included an offshore area that is about 20 - 30 kilometers into the Gulf of Mexico (GOM.)

Comparing to a 13-month calibration/verification period in the 2007 modeling study (SWFWMD, 2007), the new calibration and verification period is a 20-month period from January 1, 2013 to September 1, 2014. Similar to the 2007 hydrodynamic modeling, data used to drive the UnLESS model included measured freshwater inflows at upstream boundaries, meteorological data (rain, solar radiation, air temperature, air humidity, and wind) measured in the Charlotte Harbor system, estimated ungauged flows, and the downstream boundary conditions of tides, salinity, and temperature. Downstream boundary conditions came from another model simulation effort that simulated the West Florida Shelf, including Charlotte Harbor.

The UnLESS model was calibrated and verified against measured real-time data collected during the period January 2013 to August 2014 by different agencies at five stations inside the simulation domain, including a Mote Marine Laboratory (Mote) station, a US Geological Survey (USGS) station, and three stations by the Southwest Florida Water Management District (SWFWMD.) The model calibration period was from August 2013 to August 2014, while the model verification period was from January 2013 to July 2013. The calibrated model was used to determine minimum flows for both the LPR and LSC. For this purpose, various model runs were conducted for a 92-months period from January 2007 to August 2014 under various flow reduction scenarios of the LPR and LSC.

Based on simulated salinity results, salinity habitats, including volumes, bottom areas, and shoreline lengths for various salinity ranges, were calculated for all the flow reduction scenarios. An analysis of these simulated salinity habitats has shown that if flow reductions during the

extremely dry, dry, and wet seasons were not larger than 13%, 23%, and 40%, respectively, the most sensitive salinity habitat in the LPR and LSC would not decline 15% or more. In other words, the minimum flows for the LPR and LSC during extremely dry, dry, and wet seasons are respectively 87%, 77%, and 60% of their baseline flow rates.

1. Introduction

Charlotte Harbor, located on southwest coast of the Florida Peninsula, is one of the largest estuaries in Florida that was identified by the US Environmental Protection Agency as an estuary with national significance. The northern half of the estuary is managed by the SWFWDM, while its southern half is within the jurisdiction of the South Florida Water Management District (SFWMD). The estuary receives freshwater loadings mainly from three rivers: The Peace and Myakka Rivers in the north and the Caloosahatchee River in the south (Figure 1).



Figure 1 An aerial photo of the entire Charlotte. The yellow dashed line denotes the boundary between the SWFWDM and the SFWMD. Pink dots represent locations where real-time data were collected for model calibration and verification.

The Peace River has a length of approximately 120 KM and runs southwestward into the northeast portion of the Charlotte Harbor, while the Myakka River is about 106 KM long and flows first southwestward and then southeastward into the northwest portion of the Charlotte Harbor. The entire Peace River watershed is about 6213 KM². The most downstream segment of the Peace River, from Arcadia to the mouth, is the lower Peace River (LPR) that is about 58 KM long. About 84% of the Peace River watershed is gauged, and the remaining 16% of the Peace River watershed is ungauged with unknown freshwater contribution to the Charlotte Harbor. Gaged flow includes those measured by the United States Geological Survey (USGS) at Arcadia station in the Peace River and in two tributaries downstream of Arcadia: Joshua and Horse Creeks (SWFWMD, 2001). Another major tributary to the LPR is Shell Creek, which drains a sub-basin of about 1124 KM² and flows to the LPR at about 14.5 KM upstream of the mouth of the LPR. Shell Creek is impounded at about 8.3 KM upstream of the confluence with the LPR, forming a reservoir, which is primarily for the water supply for the City of Punta Gorda. The LPR and LSC are generally narrow and meandering, except for areas near the mouth of the LPR where the river becomes wider with islands. Majority of the 58 KM long LPR is tidal influenced, and the tidal limit extends to roughly 50 KM upstream from the mouth.

On the Myakka River side, the lower Myakka River (LMR) is about 40 KM long and starts at the downstream side of the lower Myakka Lake (Downs' Dam) in the Myakka River State Park. The Myakka River watershed is approximately 608 KM². Only about 50% of the Myakka River watershed is gauged at the USGS Myakka Head station and a few tributary stations downstream of the Downs' Dam, and thus the ungauged area is about half the watersheds for the Myakka River. Similar to the Peace River, the Myakka River is also narrow and meandering, except for its very downstream portion where the river is wider and has several islands. The entire lower Myakka River is tidally influenced, as tides can reach to the base of Downs' Dam.

The Caloosahatchee River and Estuary are about 102 kilometers long, with the estuarine portion being roughly 42 KM in length (SFWMD, 2005.) The system drains a watershed, which includes rural areas on the northern edge of Everglades, of about 3,370 KM² (SFWMD, et al., 2009.) The Caloosahatchee River and Estuary connect Lake Okeechobee to the GOM and occasionally receives a large amount of freshwater flow from the nutrient-rich lake. A series of locks and spillways exist along the Caloosahatchee River for the control of the river flow, which eventually enters the San Carlos Bay to reach the GOM at the southern tip of the Charlotte Harbor. The Caloosahatchee River system is outside of the boundary of the SWFWMD and is managed by the US Army Corps of Engineers and the South Florida Water Management District. Although a small portion of the Caloosahatchee Estuary was included in the model, the river has only very minor influence on the LPR and LSC.

Even though the LPR, LMR, and the Charlotte Harbor (CH) are often treated as three individual water bodies in many cases, they are interconnected with different degrees of interactions among themselves. On one hand, the LPR and LMR provide the CH freshwater inflows that are ecologically critical for the health of the harbor. On the other hand, hydrodynamics and salinity in the CH play a very important role in keeping the ecosystems of the LPR and LMR in balance as both rivers are tidally influenced. Tides and salinity transport processes in the downstream estuary directly affect habitat distributions in both rivers. To manage the water resources and protect the ecosystems of the LPR, LSC, and LMR, it is important to understand the hydraulic interactions among these water bodies and the Charlotte Harbor. As such, it is necessary to develop a numerical model that can provide detailed information of circulations and salinity and

temperature distributions in all the water bodies of the estuarine system with the same degree of accuracy.

As mentioned in previous publications (Chen, 2005, 2007a, 2007b), the flow pattern in the Charlotte Harbor is generally three-dimensional, a 3D hydrodynamic model is needed to accurately simulate hydrodynamics in the estuary. To include the LPR and the LMR in the simulation, one can extend the 3D model domain upstream to cover the entire reach of the LPR and LMR. However, this way of including the tributary in the simulation is apparently not efficient. In addition, it is difficult to correctly represent the cross section of the LPR and LMR in a 3D model because only limited number of grids (usually five or less grids, sometimes just one grid) are used to discretize the width of the river (e.g., Johnson et al, 1991; Sucsy et al, 1997; Mendelsohn et al, 1997). For example, it is impossible to accurately resolve the cross section shown in Figure 2 with just three grids in the latitudinal direction of the tributary (perpendicular to the tributary).

Although the flow pattern in Charlotte Harbor is three-dimensional, it is generally vertically two-dimensional in most segments of the LPR, LSC, and LMR because of their narrow widths. It is much efficient to use a laterally averaged 2D (2DV) model for the narrow and meandering portions of the LPR, LSC, and LMR than to use a 3D model. With enough number of layers in the vertical direction (generally ten or more), a 2DV model resolves the bathymetry of a tributary better than a 3D model that has only a limited number of grids in the latitudinal direction. Also, a 2DV model automatically handles the wetting/drying phenomenon in the tributary, while a 3D model often needs a lot of computational efforts to deal with the temporal shoreline change in the narrow and meandering tributary. The cross section shown in Figure 2 is typical in the narrow portions of the LPR, LSC, and LMR. As can be seen from the figure, the cross section is composed of a main channel and two flood plains at both sides of the river. While the main channel can be very narrow and in the order of 10 – 20 m, the flood plain can be as wide as a few kilometers. When flow is low, water only exists in the main channel. However, during a major storm event, the flood plains will be submerged and used as conveyance for the flood. For a better understanding of the ecological system in the rivers, it is critical to accurately simulate the emerging/submerging feature of the flood plain. In this circumstance, information is needed about the total flow rate and the water elevation, not the detailed velocity distribution in the narrow portions of the LPR and LMR. Evidently, it is much harder for a 3D model to handle these areas of the rivers even if it can do so. The emerging/submerging feature of the cross section can be automatically simulated in a laterally averaged 2D model without any special treatment often seen in a 3D model, simply because the river width is included in the governing equations for the 2DV model (see Section 3).

To effectively simulate the interactions among upper Charlotte Harbor, the LPR, and the LMR, a dynamically coupled 3D-2DV model similar to that used in the previous MFL evaluations of LPR and LMR was developed and used for the re-evaluations of MFLs for the LPR and LSC. In the following sections, the dynamically coupled 3D-2DV hydrodynamic model UnLESS is briefly presented, followed by a description of model calibration and verification, including a discussion of data used to drive the model and to calibrate/verify the model. The use of the calibrated UnLESS model for the LPR – LMR - CH system to conduct hydrodynamic simulations in order to evaluate effects of freshwater flow reductions in the LPR and LSC on salinity habitats in both water bodies is presented. Model results of flow reduction scenarios, including those with the consideration of the sea level rise predictions from 2010 to 2035 for both the baseline flows and MFLs, are presented and discussed, before conclusions of the study are drawn.

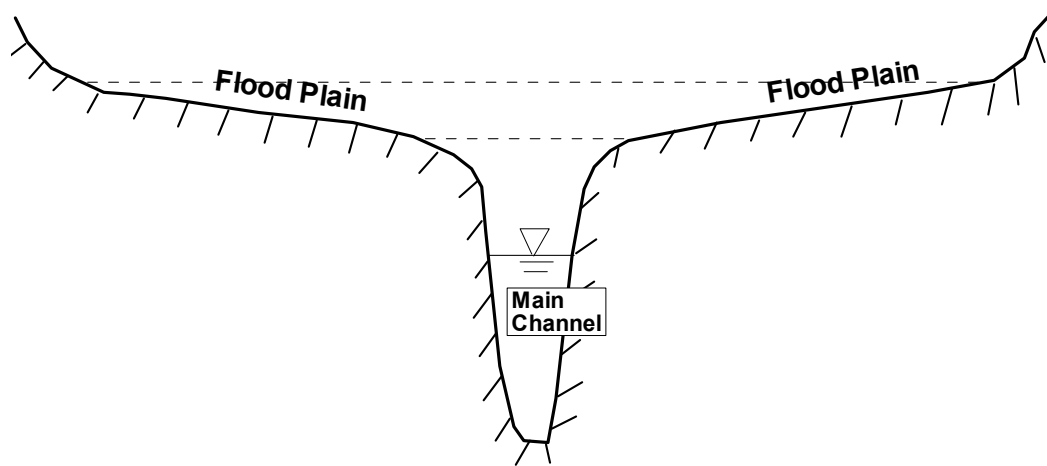


Figure 2 A typical cross section of the narrow part of the Peace (or Myakka) River. It is comprised of a main channel and two flood plains. Most of the time, flow only exists in the main channel. During a major storm event, the flood plains can be submerged to convey the flood.

2. Dynamic Coupling of LAMFE with UnLESS3D

The hydrodynamic model used for the modeling study of the Charlotte Harbor is the UnLESS model, which is a dynamic, two-way coupled model of a laterally averaged 2D hydrodynamic model named LAMFE (Chen and Flannery, 1997; Chen et al., 2000; Chen, 2003a and 2004a) and an unstructured Cartesian grid model named UnLESS3D (Chen, 2011, 2012).

This section is a brief description of the UnLESS model. Details about numerical methods employed in the UnLESS and how dynamic coupling of the LAMFE and UnLESS3D models is achieved are described in Chen (2020).

2.1 Governing Equations

In the LAMFE model, the following governing equations are solved:

$$\frac{\partial ub}{\partial x} + \frac{\partial wb}{\partial z} = v \quad (1)$$

$$\frac{\partial u}{\partial t} + \mathbf{u} \frac{\partial u}{\partial x} + \mathbf{w} \frac{\partial u}{\partial z} = -\frac{\tau_{wx}}{\rho_0 b} - g \frac{\partial \eta}{\partial x} - \frac{g}{\rho_0} \int_z^\eta \frac{\partial \rho}{\partial x} d\zeta + \frac{1}{b} \frac{\partial}{\partial x} \left(b A_h \frac{\partial u}{\partial x} \right) + \frac{1}{b} \frac{\partial}{\partial z} \left(b A_v \frac{\partial u}{\partial z} \right) \quad (2)$$

$$b \frac{\partial c}{\partial t} + \frac{\partial ubc}{\partial x} + \frac{\partial wbc}{\partial z} = \frac{\partial}{\partial x} \left(b B_h \frac{\partial c}{\partial x} \right) + \frac{\partial}{\partial z} \left(b B_v \frac{\partial c}{\partial z} \right) + v c_t + S_s \quad (3)$$

where t is time; x is the horizontal coordinate along the river/estuary, z is the vertical coordinate, u and w denote velocity components in x - and z -directions, respectively; v is the lateral velocity from lateral inputs (sheet flow of direct runoff, tributary, etc.); b , p , g , and η denote the width, pressure, gravity acceleration, and the free surface elevation, respectively; ρ_0 is the reference density; τ_{wx} represents the shear stress due to the friction acting on the side wall ($= \rho C_w u [u^2 + w^2]^{1/2}$, where C_w is a non-dimensional friction coefficient for side walls); A_h and A_v are kinetic eddy viscosities in the x - and z -directions, respectively; c is concentration (can be temperature, salinity, suspended sediment concentrations, nutrient concentrations, etc.); c_t is concentration in lateral inputs; B_h and B_v are eddy diffusivities in the x - and z -directions, respectively; S_s denotes source/sink terms; and ρ is density which is a function of salinity and temperature (UNESCO, 1983). In the above transport equation, if the material simulated involves settling, w in the advective term includes the settling velocity of the material.

In the UnLESS3D model, the governing equations are

$$\frac{\partial u}{\partial x} + \frac{\partial v}{\partial y} + \frac{\partial w}{\partial z} = 0 \quad (4)$$

$$\frac{\partial u}{\partial t} + \frac{\partial uu}{\partial x} + \frac{\partial vu}{\partial y} + \frac{\partial wu}{\partial z} = f v - \frac{1}{\rho_0} \frac{\partial p}{\partial x} + \frac{\partial}{\partial x} \left(A_h \frac{\partial u}{\partial x} \right) + \frac{\partial}{\partial y} \left(A_h \frac{\partial u}{\partial y} \right) + \frac{\partial}{\partial z} \left(A_v \frac{\partial u}{\partial z} \right) \quad (5)$$

$$\frac{\partial v}{\partial t} + \frac{\partial uv}{\partial x} + \frac{\partial vv}{\partial y} + \frac{\partial wv}{\partial z} = -f u - \frac{1}{\rho_0} \frac{\partial p}{\partial y} + \frac{\partial}{\partial x} \left(A_h \frac{\partial v}{\partial x} \right) + \frac{\partial}{\partial y} \left(A_h \frac{\partial v}{\partial y} \right) + \frac{\partial}{\partial z} \left(A_v \frac{\partial v}{\partial z} \right) \quad (6)$$

$$p = g \int_z^\eta \rho d\zeta \quad (7)$$

$$\frac{\partial c}{\partial t} + \frac{\partial uc}{\partial x} + \frac{\partial vc}{\partial y} + \frac{\partial wc}{\partial z} = \frac{\partial}{\partial x} \left(B_h \frac{\partial c}{\partial x} \right) + \frac{\partial}{\partial y} \left(B_h \frac{\partial c}{\partial y} \right) + \frac{\partial}{\partial z} \left(B_v \frac{\partial c}{\partial z} \right) + S_s \quad (8)$$

where x , y , and z are Cartesian coordinates (x is from west to east, y is from south to north, and z is vertical pointing upward); u , v , and w are velocities in the x -, y -, and z -directions, respectively; f denotes Coriolis parameter; and A_h and A_v represent horizontal and vertical eddy viscosities,

and \mathbf{q} is a square matrix of the order $M \times M$ and M is the total number of grids in the horizontal plane in the 3D subdomain. \mathbf{q} is a sparse matrix, with its diagonal elements being no less than 1 and its off-diagonal elements being no greater than 0. The non-zero elements are functions of the total side area of the grid cell and the grid sizes in x - and y -directions. Locations of the non-zero elements are determined by the connectivity of the unstructured Cartesian grids.

Equations (9) and (12) can be merged together as follows

$$\begin{bmatrix} \hat{\mathbf{q}} & \mathbf{p} \\ \mathbf{s} & \hat{\mathbf{r}} \end{bmatrix} \begin{bmatrix} \Delta\eta_{3D} \\ \Delta\eta_{2DV} \end{bmatrix} = \begin{bmatrix} \Delta\eta_{3D}^* \\ \Delta\eta_{2DV}^* \end{bmatrix} \quad (14)$$

where \mathbf{p} and \mathbf{s} are rectangular matrices of orders $M \times N$ and $N \times M$, respectively. They are needed to ensure a proper modeling of the two-way interaction between the 3D and 2DV subdomains. Both \mathbf{p} and \mathbf{s} only have a limited number of non-zero elements. In fact, the number of non-zero elements in \mathbf{p} and \mathbf{s} is the same as the number of grids that are involved in the patching of the 3D and 2DV subdomains. Accordingly, elements for the original matrixes for the 3D subdomain (\mathbf{q}) and the 2DV subdomain (\mathbf{r}), which are associated with the patching, are slightly modified for proper connections of the 3D and 2DV subdomains, resulting in $\hat{\mathbf{q}}$ and $\hat{\mathbf{r}}$ shown in the above equation.

The sparse matrix system shown in Equation (14) is similar to those in Equations (9) and (12), and can be efficiently solved using the bi-conjugate gradient method of Van der Vorst (1992). After Equation (14) is solved, the final free surface location is found for the entire simulation area, including both the 3D and 2DV subdomains.

Final velocities at the new time step can be calculated after the final free surface elevations in both the 3D and 2DV subdomains are found. The transport equations are then solved to update distributions of simulated constituents (salinity, temperature, suspended sediment concentration etc.). Details on the numerical schemes for calculating velocities and concentrations can be found in Chen (2003a, 2003b, 2007a, 2011).

3. Model Calibration and Verification

3.1 Model Setup

The UnLESS model that dynamically couples LAMFE and UnLESS3D was applied to Charlotte Harbor using 4790 grids in the horizontal plane and 17 layers in the vertical direction to discretize the 3D simulation subdomain and 311 grids and 17 layers to discretize the 2DV simulation subdomain. The 3D subdomain includes the entire Charlotte Harbor, the downstream 16.13 kilometers of the LPR, the downstream 12.64 kilometers of the LMR, and the most downstream 1.74 KM portion of the LSC, and an offshore area in the GOM.

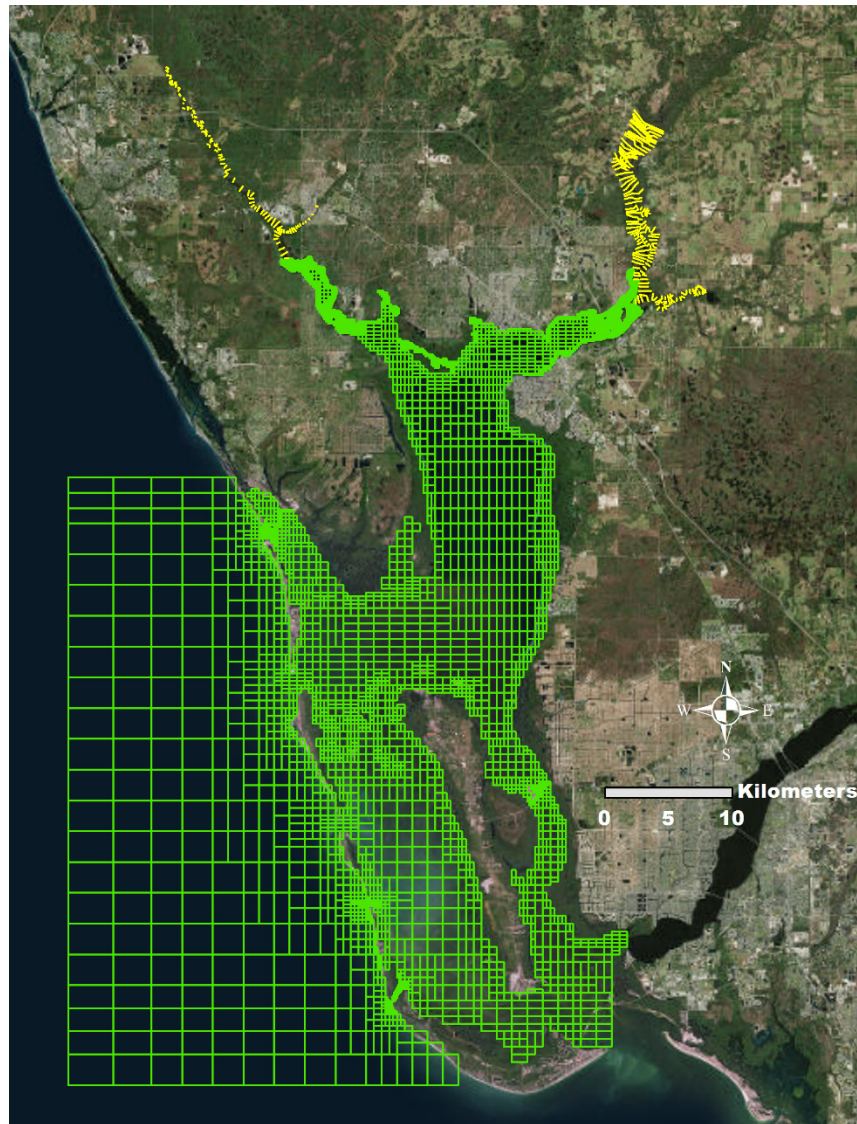


Figure 3. UnLESS mesh used for the Charlotte Harbor hydrodynamic modeling. Green rectangular tiles are model grids for the 3D simulation subdomain, while 2DV grids are bounded by cross sections drawn with yellow lines.

The dimension of the unstructured Cartesian grids varies between $37.5 \text{ m} \times 37.5 \text{ m}$ in the Peace River and Shell Creek to $3,500 \text{ m} \times 2,400 \text{ m}$ for the offshore area. Figure 3 shows the UnLESS mesh used for the simulation domain, with 3D grids consisting of different sizes of rectangular bricks (tiles) plotted in green and 2DV grids being bounded by cross-sections plotted in red in the figure.

Bathymetry data used in the grid generation consisted of cross-sectional surveys by the SWFWMD (WGI, 2015; Wang, 2003 & 2012) for Charlotte Harbor, LPR, LMR, LSC, and Myakkahatchee, LiDAR data for the LPR and LPR watersheds, and bathymetry data used in the University of South Florida (USF) West Florida Coastal Ocean Model (WFCOM) for the offshore area.

The grid size showing in Figure 3 varied from $37.5 \text{ m} \times 37.5 \text{ m}$ to $3,500 \text{ m} \times 2,400 \text{ m}$, in x- and y-directions, respectively, in the 3D subdomain. In the 2DV subdomain, the spacing along the river varied between 39 m to 4,147m. The vertical layer thickness for the 3D and 2DV subdomains are the same and varied between 0.4 m and 4 m.

The simulation period for model calibration and verification was from January 2013 to August 2014. The model calibration period was from August 2013 to August 2014, while the model verification period was from January 2013 to July 2013. Model calibration involves adjusting model parameters such as bottom roughness, eddy viscosities and diffusivities, etc. in 3D and 2DV subdomains to obtain best match between model results and field data at the five measurement stations shown in Figure 1.

3.2 Input Data

Boundary conditions of water level, salinity, and temperature at the downstream open boundaries in the GOM and Caloosahatchee River during the 20-month simulation period were provided by Zheng and Weisberg (2014) of College of Marine Science at the USF, from their WFCOM model. Figure 4 shows the USF WFCOM model mesh, which includes Charlotte Harbor. Gauged USGS flows were included in the USF WFCOM model.

Although the USF WFCOM model had 31 σ layers in the vertical directions, with higher resolution in the surface to better resolve the surface boundary layer (Zheng and Weisberg, 2004), water levels, salinities, and temperatures in eight equal-spacing σ layers were provided along the south, west, and north open boundaries in the Gulf as well as in the Caloosahatchee River (Figure 3). Because the UnLESS model is a z-level model, salinity and temperature results from the WFCOM model were interpolated from the eight σ layers to eight fixed elevations before they were read to the UnLESS model, which further interpolates these boundary conditions from the eight fixed elevations to the 17 z-level layers in UnLESS each time step.

Figure 5 shows water level boundary conditions at the centers of the south, west, and north open boundaries in the Gulf as well as in the middle of Caloosahatchee River. It can be seen that tides on the three sides of the open boundaries are similar, with comparable short-term and long-term variabilities; however, because of the attenuation of the tidal waves as they propagate into the Caloosahatchee River, the water level near the river mouth has a much smaller magnitude of short-term variation than those at the open boundaries in the Gulf. Salinity and temperature boundary conditions at the top and bottom layers of these locations are shown in Figures 6 and 7. As can be seen from Fig. 6, salinity along the open boundaries in the Gulf is well-mixed, except during the wet season, when salinity at the south and west side can have a difference up to about

1.5 psu between the top and bottom layer. In the Caloosahatchee River near the mouth, salinity varies from 0 psu during high flow days to about 32 psu during very dry days.

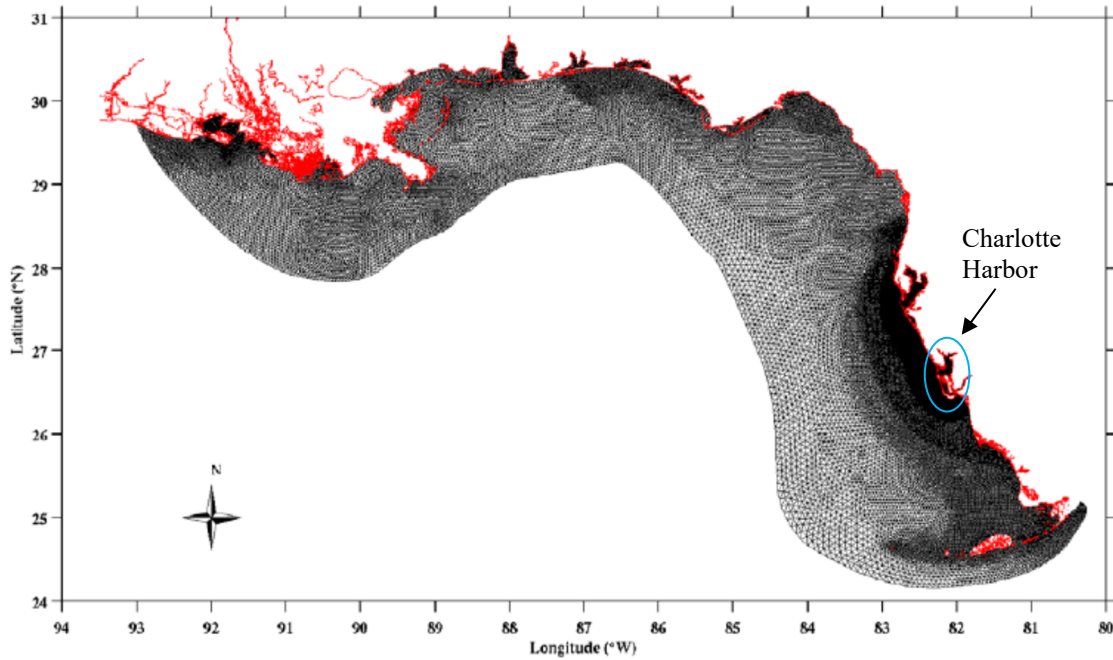


Figure 4. University of South Florida WFCOM model mesh.

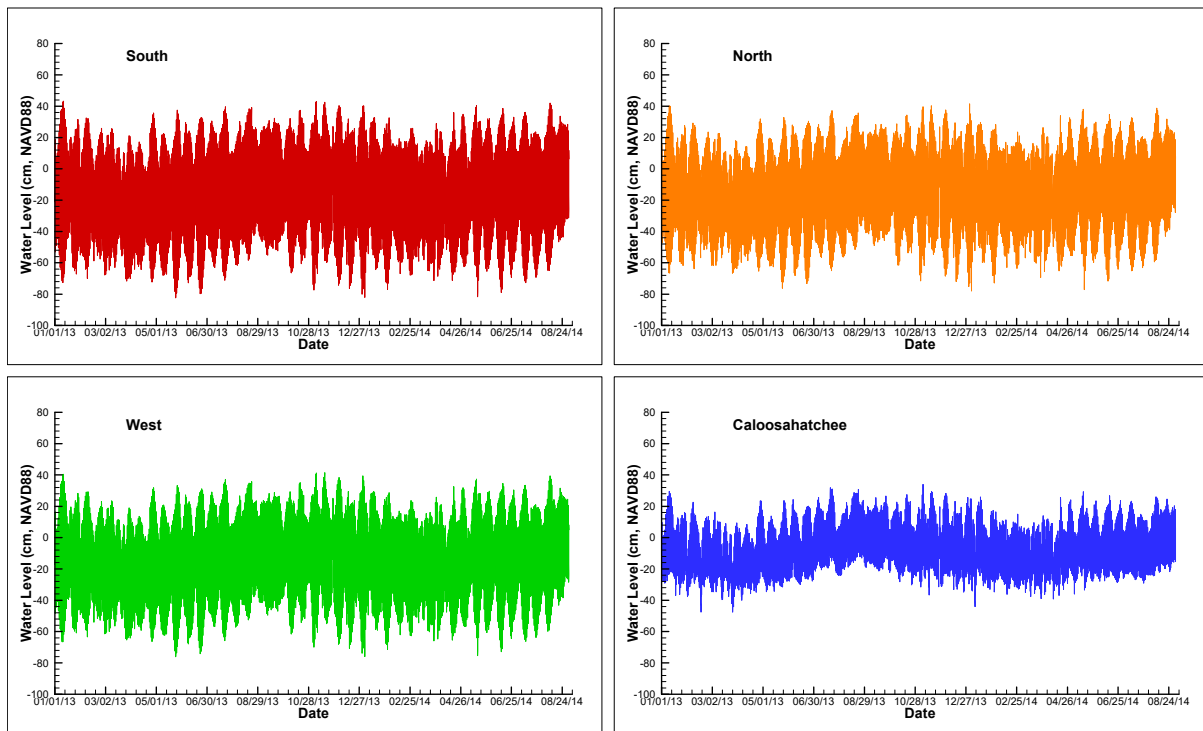


Figure 5. Water level results of the WFCOM model at the centers of the southern, western, northern open boundaries as well as in the middle of the Caloosahatchee River.

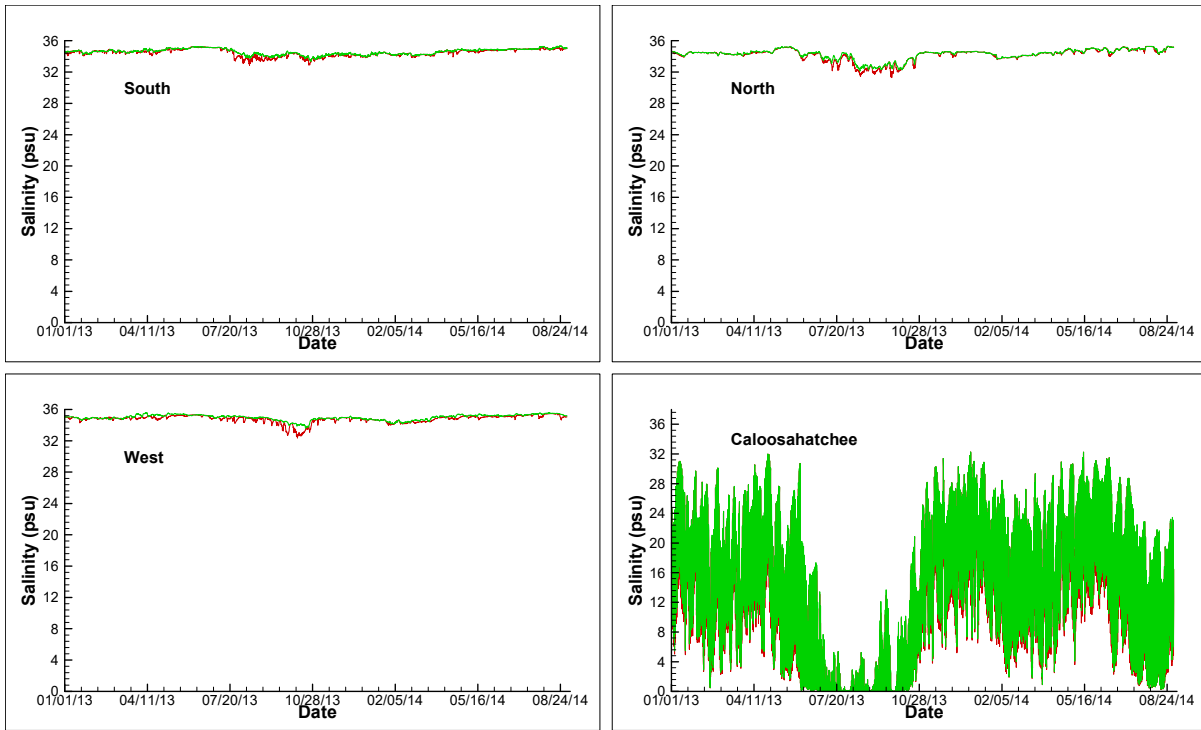


Figure 6. Top and bottom salinity boundary conditions at the centers of the southern, western, northern open boundaries as well as in the middle of the Caloosahatchee River.

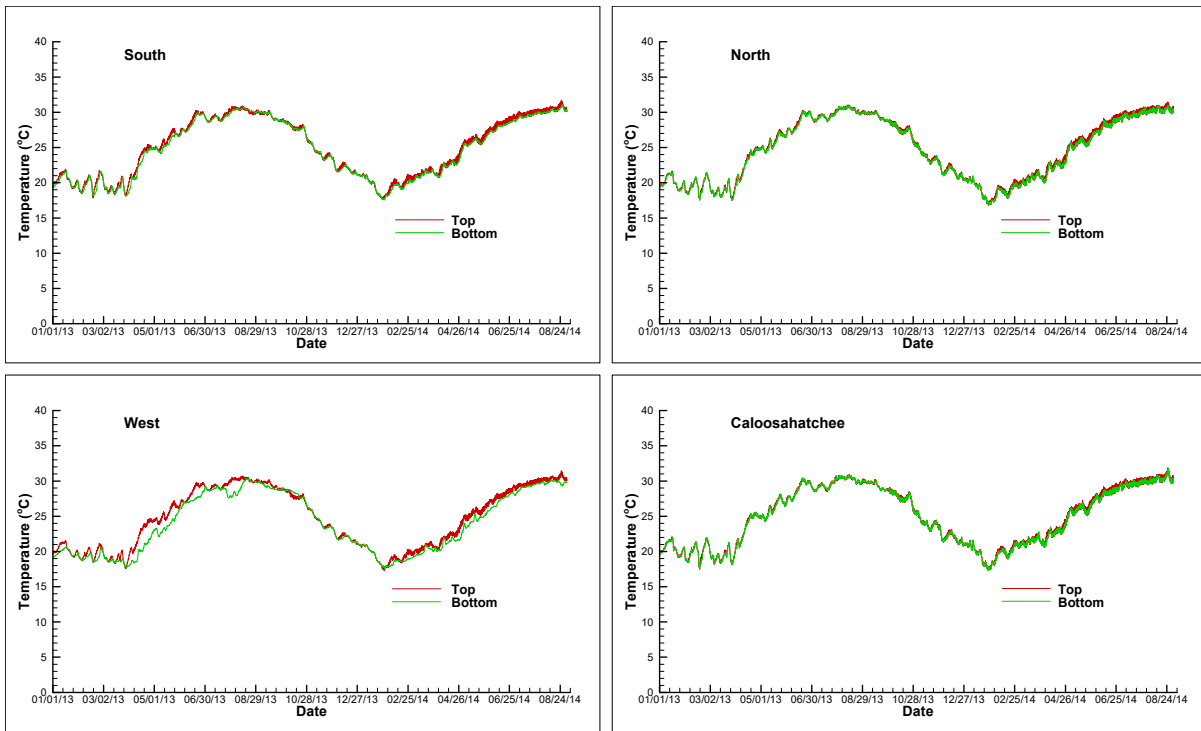


Figure 7. Top and bottom temperature boundary conditions at the centers of the southern, western, northern open boundaries as well as in the middle of the Caloosahatchee River.

At the upstream boundaries of LPR, LSC, and LMR, including Blackburn Canal and Myakkahatchee, (also called Big Slough Canal), freshwater flows were specified, which included both gauged and estimated flows. Gauged flow used at the upstream boundary of the LPR included data measured at USGS stations of Peace River at Arcadia, Joshua Creek at Nocatee, and Horse Creek near Arcadia. At the upstream boundary of LSC, gauged flow used was from the USGS Shell Creek near Punta Gorda station. For Myakka River, gauged flows were these measured at USGS stations of Myakka River near Sarasota, Big Slough Canal at Tropicaire, and Blackburn Canal near Venice.

In addition to gauged USGS flows, there are also ungauged flows that contribute a significant portion of the total freshwater budget to upper Charlotte Harbor. As mentioned before, the Peace River watershed has an ungauged area of about 16%, while for the Myakka River, about one half of the watershed is ungauged. These ungauged areas contribute a big fraction of the total freshwater budget to the Charlotte Harbor and have significant effects on salinity distributions in the simulation domain. Because freshwater inflows directly affect salinity distributions in the estuary, a good estimation of ungauged flows into the simulation domain is important. In the 2007 study, freshwater flows from the ungauged sub-basins of the watershed were estimated by Ross et al (2005) using the Hydrological Simulation Program - FORTTRAN (HSPF) (Bicknell, 1997).

As discussed in Chen (2007), it is very challenging to obtain reasonable estimates of ungauged flows from a very complex system such as the Peace - Myakka River watershed. Although the HSPF model is a popular model that has been used in many areas of the country, including Florida, it cannot guarantee good model results, especially when it is used as an extrapolation tool for an area that is quite different from the gauged areas in terms of land-use and hydro-geological properties. Moreover, due to the unavailability of freshwater flow data to the tidal reaches, it is impossible to determine the severity of the errors and the confidence interval of the simulated ungauged flows. The unknown errors in the estimated ungauged flow will inevitably cause errors in model results of the coupled 3D-2DV model. Unfortunately, without a better way to estimate ungauged flows, simulated results using the HSPF model by Ross et al. (2005) appeared to be the only choice available for a rough estimate of the freshwater contribution from the ungauged areas of the watershed. During the calibration process of the model, it was found that the model under-predicted salinity during the wet months of the simulation period (see below), suggesting that ungauged flows by Ross et al. (2005) could be over-estimated. As such, the 2007 study compared the HSPF results to those estimated by Janicki Environmental using a simple method developed by SDI Environmental Services (SWFWMD, 2007). It was found that the estimated ungauged flows using the SDI method are generally 50 – 60% lower than the HSPF results, except for the few peak flows in the first couple of months of the simulation period which are much higher than HSPF peak flows. Based on this comparison, the daily ungauged flow values generated by the HSPF model were adjusted before they were used in the model simulation.

In the current model simulations, adjusted ungauged flows in the 2007 study were analyzed and the relationship between ungauged flow and rainfall received for each sub-basin was studied with the consideration of different land use coverages and soil types within the sub-basin. Details about the method used to estimate ungauged flows for the Peace and Myakka Rivers can be found in Ghile and Leeper (2015.)

Figure 8 shows the total gauged flows in the Peace and Myakka River watersheds and the total ungauged flows to the LPR and LMR during 2007 - 2014. The sum of the total gaged and ungauged flows, which represents the total hydrologic loading to the system during the 8-year

period, is also shown in the figure (blue dashed line.) As can be seen from the figure, 2007 – 2011 were relatively dry, while 2012 – 2014 were relatively wet with higher flow peaks.

Because some of the freshwater inflows were taken away by withdrawal before reaching Charlotte Harbor, this freshwater loss was considered in the model simulations. The Peace River/Manasota Regional Water Supply Authority withdraws water from the LPR, with its withdrawal point being roughly 3.5 KM upstream of USGS Peace River Heights station (Figure 1). Withdrawal by the City of Punta Gorda is from the upstream of the Shell Creek dam, and thus was already included in the LSC flow data. Another freshwater loss is through Blackburn Canal, which drains Myakka River. The canal connects the Donna/Roberts Bay on the Florida Gulf Coast to the Myakka River. The USGS gauged flow in the Blackburn Canal during the period March 4, 2004 to May 4, 2013. The gauging station was unfortunately discontinued since May 5, 2013 and thus flow data during May 5, 2013 - September 1, 2014 needed to be estimated. Although it drains the Myakka River most of the time, the Blackburn Canal occasionally flows to the Myakka River, depending on the water levels in the Myakka River and in Donna/Roberts Bay. Because water level in Donna/Roberts Bay has tidal signals, flow gauged in Blackburn Canal also has significant tidal signals. This study used USGS tide-filtered (residual) daily mean flow before May 5, 2013 and estimated the daily Blackburn Canal flow using a correlation between gauged flow at USGS Myakka River near Sarasota and that in Blackburn Canal.

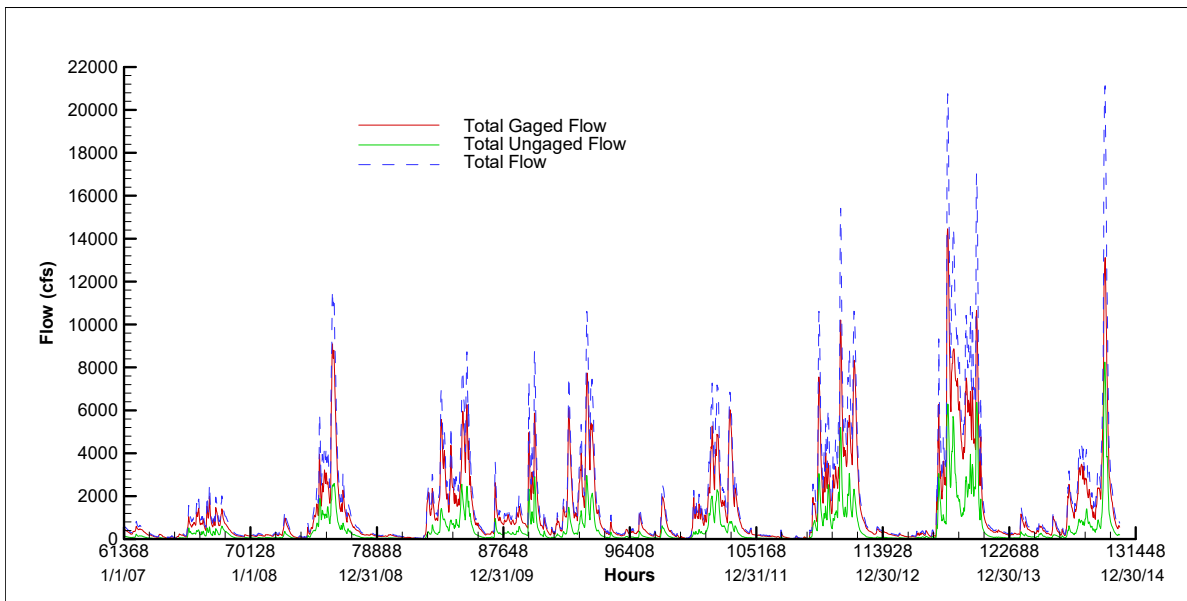


Figure 8. Total gaged flow (red line), total ungauged flows (green line), and total flow (blue dashed line) to the Charlotte Harbor during the 8-year period of 2007 - 2014.

In the previous MFL evaluation (Chen, 2007), a correlation between flows at USGS Myakka River near Sarasota and in Blackburn Canal was found to be as follows

$$Q_b = \begin{cases} 0.057Q_m, & Q_m \leq 457 \\ 0.169Q_m - 51.2, & Q_m > 457 \end{cases} \quad (15)$$

where Q_b is the flow rate that drains Myakka River through the Blackburn Canal, and Q_m is the Myakka River flow at the USGS station near Sarasota. The units in the above equation are cubic feet per second.

It should be noted that the above equation only estimates flow leaving the Myakka River, as Q_b calculated from the equation is always positive. From the available Blackburn Canal flow data, the negative flow rate is generally very small in magnitude (≤ 2.2 cfs) and occurs infrequently.

The above correlation was derived based on available Blackburn Canal flow data at the time the analysis was conducted, during a 209-day period of March 6, 2004 - September 30, 2004. With more data available during the current study, the above equation was updated. Figure 9 is a plot of measured flow at the USGS Blackburn Canal station versus measured flow at the USGS Myakka River near Sarasota station (blue dots) during the period March 6, 2004 to May 4, 2013.

As can be seen in Fig. 9, measured Blackburn Canal flow is well correlated with measured Myakka River near Sarasota. The best fit of the correlation between flow at USGS Myakka River near Sarasota and that in Blackburn Canal takes the following polynomial form:

$$Q_b = 9 \times 10^{-12} Q_m^4 - 8 \times 10^{-8} Q_m^3 + 0.0002 Q_m^2 + 0.023 Q_m + 2.4058 \quad (16)$$

Estimated flows in Blackburn Canal from May 5, 2013 to September 1, 2014 using the above equation are plotted in Figure 5 with orange dots. Similar to Equation (15), the above equation only estimates flow leaving the Myakka River, as Q_b calculated from in the equation is always positive.

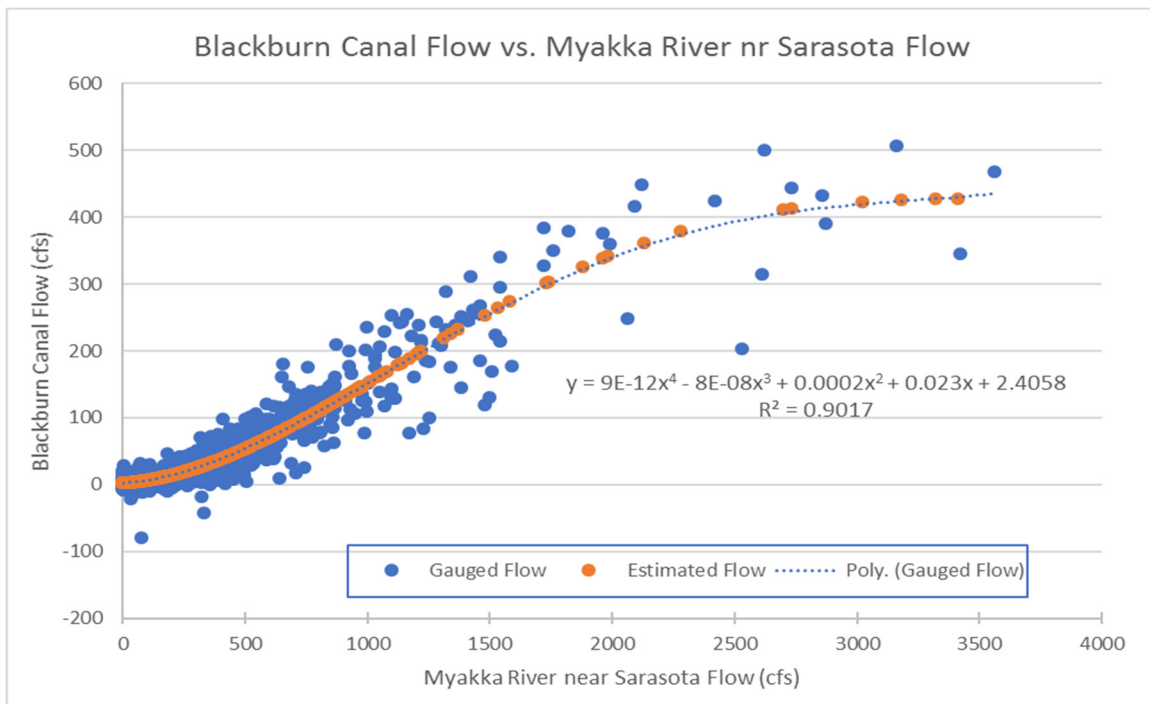


Figure 9 Blackburn Canal flow versus Myakka River near Sarasota flow during the period March 6, 2004 - May 4, 2013.

Weather data used for the Charlotte Harbor UnLESS model included rainfall, wind speed and direction, solar radiation, air humidity, and air temperature. These data were measured at the Mote Marine Laboratory station in Charlotte Harbor during February 7, 2013 – August 31, 2014. For time periods prior to February 7, 2013, average rainfall data at the following SWFWMD sites in the watershed, which are close to the simulation domain, were used: New Charlotte South (SID 24710), Punta Gorda 4 ESE NWS (SID 25105), Punta Gorda NWS (SID 24711), ROMP TR1-2

Tropical Gulf (SID 25220), and ROMP TR3-1 Point Lonesome (SID 25218). Measured solar radiation, air humidity, air temperature, and wind speed and direction at the SWFWMD site Peace River II ET (SID 24571) were used prior to February 7, 2013.

Figure 10 shows daily rainfall data used in the UnLESS model for the period between January 1, 2013 and August 31, 2014, while Figure 11 shows wind speed and direction data during the same time period. Measured data used in the model for solar radiation, air temperature, and air humidity during the period January 1, 2013 – August 31, 2014 are plotted in Figures 12, 13, and 14, respectively.

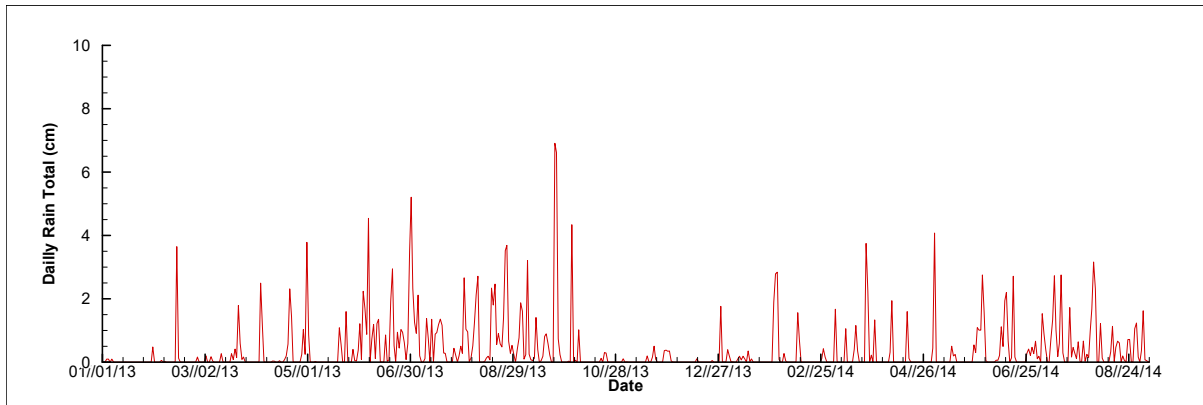


Figure 10. Daily rainfall data used in the model for the simulation period between January 1, 2013 and August 31, 2014.

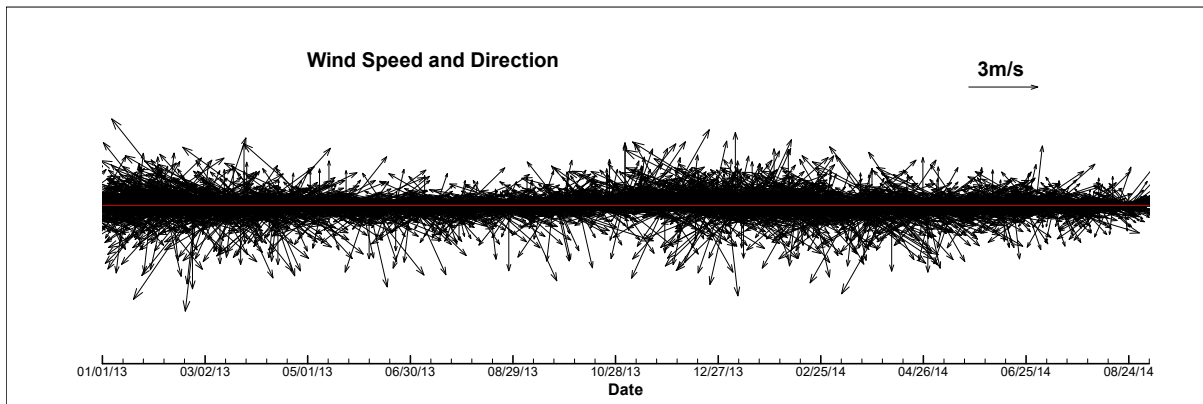


Figure 11. Wind speed and direction data used in the model for the simulation period between January 1, 2013 and August 31, 2014.

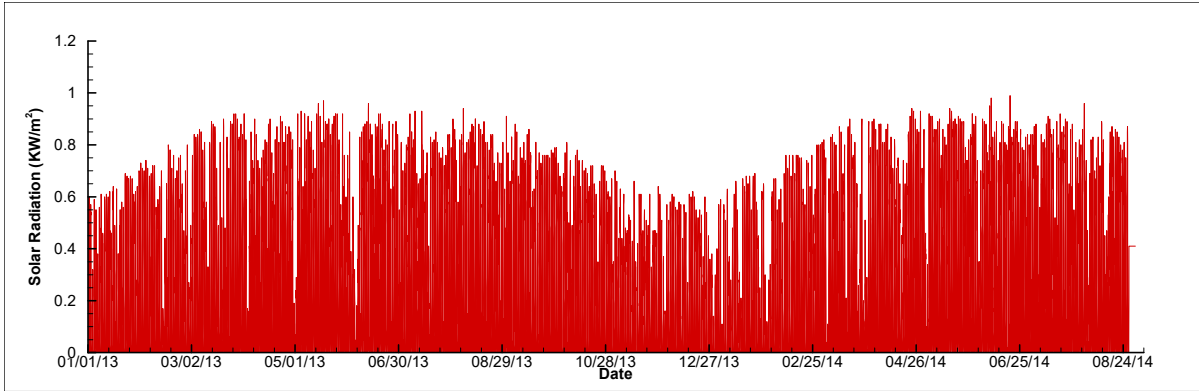


Figure 12. Solar radiation data used in the model for the simulation period between January 1, 2013 and August 31, 2014.

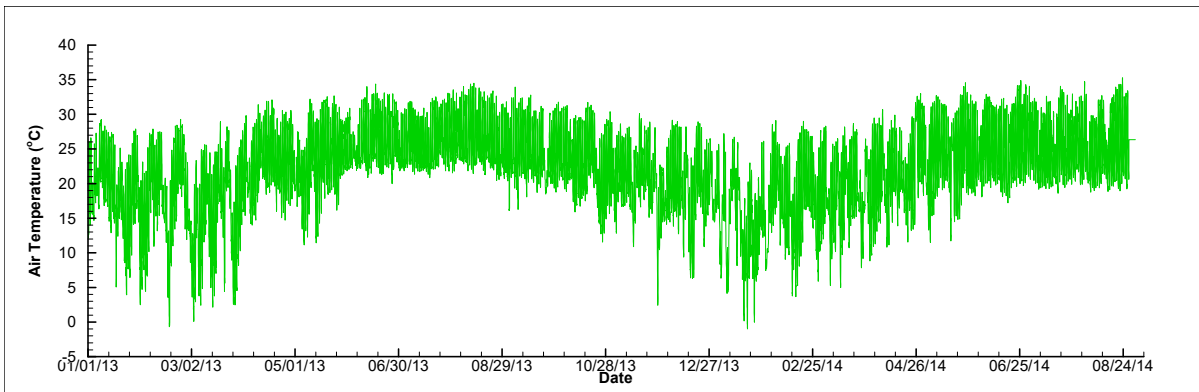


Figure 13. Air temperature data used in the model for the simulation period between January 1, 2013 and August 31, 2014.

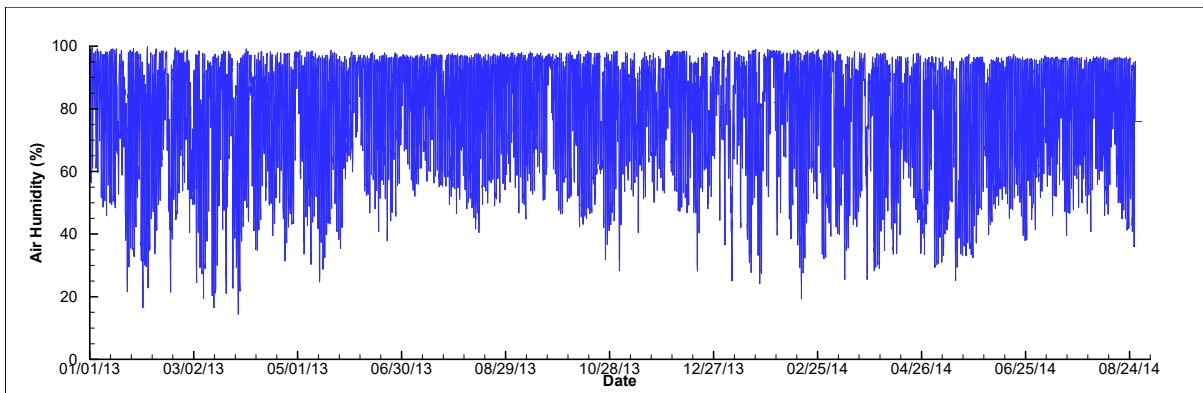


Figure 14. Air humidity data used in the model for the simulation period between 1/1/2013 and 8/31/2014.

3.3 Results of Model Calibration and Verification

As mentioned above, the UnLESS model was calibrated and verified against measured data at five stations inside the simulation domain. As can be seen in Figure 1, in Charlotte Harbor, there was a Mote station. In the LPR, there were two stations: one at Punta Gorda (PR_PG) operated by the SWFWMD and one near Peace River Heights (PR_HT) by the USGS. In LSC, the SWFWMD had two stations: one near Punta Gorda (SC_PG) and one below the reservoir (SC_BR).

Measured data at these stations included water levels, salinities, and temperatures. Except for the Mote station, where top, mid-depth, and bottom salinities and temperatures were measured, all other stations have top and bottom salinity and temperature measurements. At the Mote station, currents were also measured, in six layers, each with a thickness of 0.5 m. The middle of the bottom layer was roughly at the elevation of -3.0 m, NAVD88, while the middle of the top layer was about 0.5 m below the NAVD88 datum. Clearly, the top two layers could be exposed to air during low waters.

It would be ideal that the elevations at which salinity and temperature were measured are consistent during the entire simulation period. Unfortunately, this was not the case for this study. At the Mote station, elevations of salinity and temperature sensors had to be adjusted to avoid certain unfavorable conditions (salinity was measured through the measurement of specific conductance and salinity sensor means conductance sensor in this document). For example, the initial sensor elevations were -0.5 m, -1.94 m, and -3.41 m, for the top, mid-depth, and bottom layers, respectively at the Mote station. The top sensor was lowered 0.1 m at Hour 116081 (Note: our 0 is at 12:00 AM, January 1, 2000; therefore Hour 116081 was 5:00 PM, EST, on March 29, 2013) to avoid being exposed to air during very low waters and the bottom sensor was raised 0.1m at Hour 116320.25 to avoid being affect by high suspended sediment concentration near the bottom. At the three SWFWMD stations (PR_PG, SC_PG, and SC_BR) top-layer sensors were floats about 0.5 m below the free surface, while the bottom-layer sensors were changed multiple times at the hours shown in Table 1.

Table 1. Time points, expressed as hours since 12:00 AM, January 1, 2000, when elevations of the bottom-layer salinity and temperature sensors were changed at SWFWMD stations. Units for sensor elevations are meters relative to the NAVD 88 datum with positive being above the datum.

PR_PG		SC_PG		SC_BR	
Hour	Elevation	Hour	Elevation	Hour	Elevation
113868.00	-2.346	113847.75	-1.058	113844.50	-1.368
114542.50	-2.321	114180.75	-1.139	114539.00	-1.345
114998.25	-2.536	114540.00	-1.148	114995.75	-1.372
115355.25	-2.517	114996.50	-1.123	115358.50	-1.412
115688.75	-2.504	115357.50	-1.303	115666.75	-1.414
116026.25	-2.461	115666.75	-1.271	116029.00	-1.393
116314.25	-2.477	116028.25	-1.175	116317.25	-1.387
116698.00	-2.470	116316.50	-1.178	116701.00	-1.384
117057.75	-2.473	116699.75	-1.172	117178.75	-0.943
117346.25	-2.483	117348.75	-1.186	117348.00	-0.940
117706.00	-2.510	117708.00	-1.177	117709.00	-0.964
118017.75	-2.446	118021.25	-1.146	118020.50	-0.933
118162.25	-2.438	118165.25	-1.171	118164.50	-0.958

118523.25	-2.463	118524.00	-1.249	118524.50	-0.956
119001.50	-2.405	119002.75	-1.173	119003.50	-0.939
119410.25	-2.402	119413.00	-1.106	119412.50	-0.942
119674.25	-2.440	119675.25	-1.172	120395.50	-0.951
120057.50	-2.458	120058.75	-1.146	120852.25	-0.936
120394.75	-2.464	120395.00	-1.151	121380.50	-0.943
120850.50	-2.509	120851.50	-1.148	121692.50	-0.932
121378.25	-2.441	121380.00	-1.156	122197.50	-0.952
121690.50	-2.427	121692.00	-1.162	123541.75	-0.944
122195.50	-2.425	122196.75	-1.159	124068.50	-0.954
122703.25	-2.430	122705.00	-1.164	124214.25	-0.739
123082.75	-2.417	123083.75	-1.163	125270.00	-0.858
123539.50	-2.422	123541.00	-1.156	125606.25	-0.840
124067.50	-2.419	124068.50	-1.158	125941.25	-0.822
124211.00	-1.715	124212.00	-1.286	126254.00	-0.881
124715.50	-1.602	124716.50	-1.090	126565.25	-0.815
125267.50	-1.653	125268.75	-1.097	126902.50	-0.835
125604.50	-1.612	125606.00	-1.096	127286.00	-0.869
125938.75	-1.641	125942.25	-1.054	127596.25	-0.836
126251.00	-1.658	126253.00	-1.158	128126.25	-0.805
126562.50	-1.608	126564.25	-1.069	128413.50	-0.809
126899.50	-1.667	126901.25	-1.089	128798.00	-0.804
127283.50	-1.672	127285.25	-1.127	129110.50	-0.812
127594.50	-1.619	127595.50	-1.111		
128124.00	-1.675	128127.25	-1.071		
128410.50	-1.590	128412.25	-0.971		
128795.75	-1.640	128799.25	-1.064		
129107.75	-2.149	129109.00	-1.082		

At the USGS PR_HT station, the top-layer sensors floated at about 0.5 m below the free surface, while the bottom sensor elevation was at -3.60 m, NAVD88.

3.2 Comparisons of Model Results with Measured Real-Time Data

The UnLESS model was calibrated against measured real-time data of water level, salinity, and temperature by adjusting bottom roughness, parameters associated with horizontal and vertical eddy viscosity and diffusivity estimations, and model implicitness in both the 3D and 2DV subdomains. A friction coefficient representing the roughness of the side wall in the 2DV subdomain was also adjusted in the model calibration process.

The calibration period was from August 1, 2013 to August 31, 2014. A 30-day spin-up run was first conducted to obtain reasonable spatial distributions of water level, water velocity, salinity, and temperature in the 3D and 2DV simulation subdomains at the end of the spin-up. The UnLESS model during the 30-day spin-up run was driven by input data in July 2013. The

verification period was from January 1, 2013 to August 1, 2013. After the model is calibrated and verified, the model was run for the entire 20-month period from January 2013 to August 2014.

Modeled salinities and temperatures at the top and bottom were interpolated to the exact elevations of the salinity and temperature sensors for comparison. Figure 15 shows comparisons of simulated water levels with measured data during the entire 20-month period from January 2013 to August 2014 at the Mote, PR_PG, PR_HT, SC_PG, and SC_BR stations, respectively. In the figure, red solid lines are simulated water levels, while blue dashed lines are measured water levels.

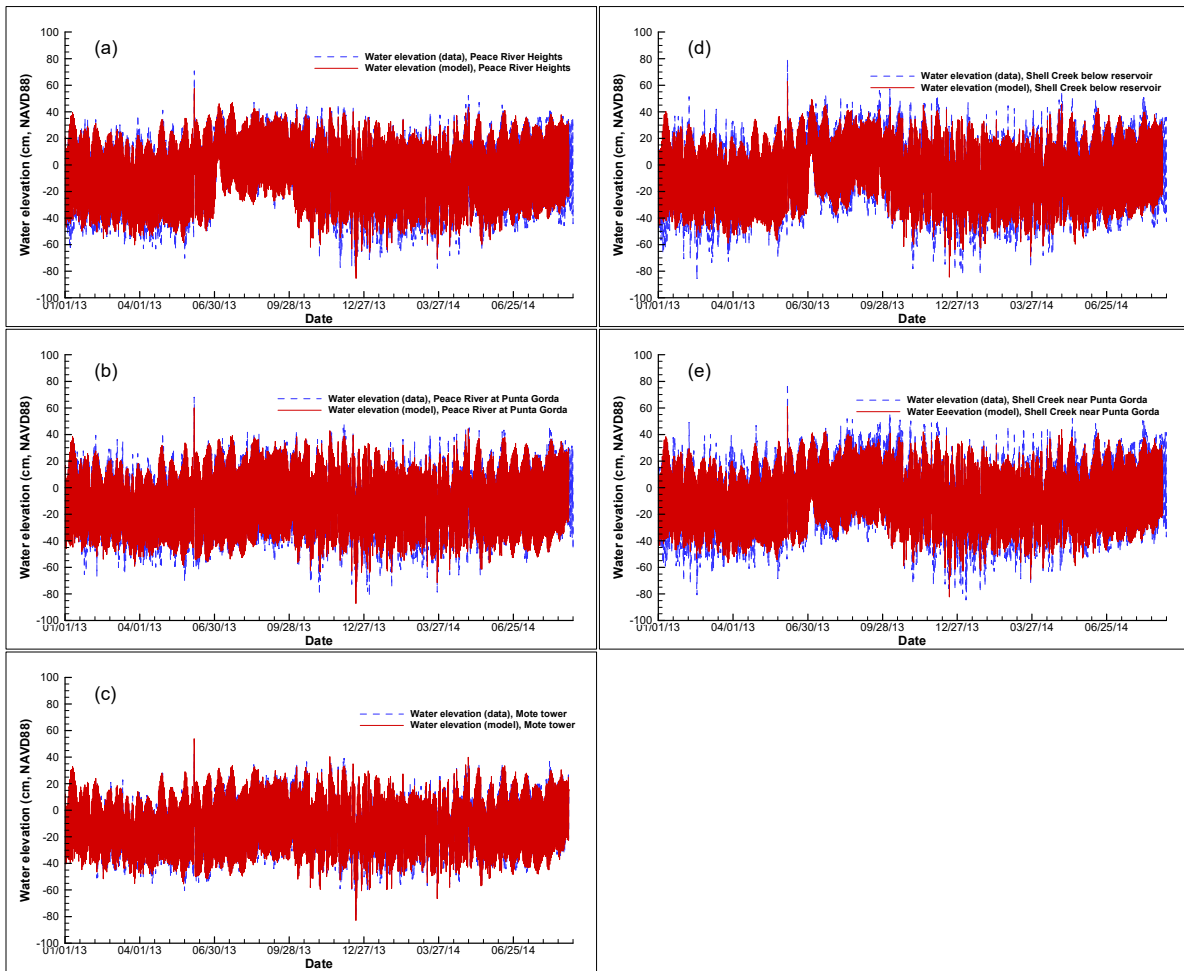


Figure 15. Comparisons of simulated water levels (red solid lines) and measured water levels (blue dashed lines) at the PR_HT (a), PR_PG (b), Mote (c), SC_BR (d), and SC (e) stations during the 20-month period from January 2013 to August 2014.

As demonstrated in Figure 15, the simulated water levels at all five stations match with measured data very well. Nevertheless, the model did miss a number of peaks, more so for the negative peaks than positive peaks. These missed negative peaks were more significant for the upstream stations than the downstream station in Charlotte Harbor.

Figure 16 shows comparisons of simulated and measured water levels for the month of January 2014, which had the most missed peaks in a month. Water level boundary conditions during the month at the middle of the west side of the open boundaries in the GOM are also shown

in the figure. One thing that can be seen is that simulated water levels at all five stations had similar tidal signals except for the phase and amplitude differences. Figure 16 shows that all missed peaks occurred at similar time points, when the lower low water occurred. An examination of the lower low waters at these data stations reveals that the lower low water level decreases from downstream to upstream in the estuarine system. This phenomenon is likely caused by the wind action during that time period, when the area experiences northern or northeastern winds most of the time in January. As the wind data are only available at the Mote station for the time period, it is not a surprise that simulated water elevation at the Mote station has the least misses of the negative peaks among the five data stations. The mismatches of the lower low waters in the two LPR stations and two LSC stations are likely caused by inaccurate wind used for these areas. As the relatively large negative peaks shown in measured water levels did not exist in the water level boundary conditions in the GOM, it is also possible wind speed and wind direction were not accurately represented in the WFCOM model.

Figures 17 and 18 show comparisons of simulated and measured water velocities at the Mote station in Charlotte Harbor. The v -velocities shown in Figure 17 are velocity components of simulated and measured water currents in the y -direction, with the positive value pointing to the north and negative value to the south. Similarly, v -velocities shown in Figure 18 are velocity components of simulated and measured water currents in the x -direction, with the positive value pointing to the east and negative value to the west. $v_1, v_2, v_3, v_4, v_5,$ and v_6 (or $u_1, u_2, u_3, u_4, u_5,$ and u_6) are v -velocities (or u -velocities) at Depths 1 through 6, respectively, with Depth 1 being near the bottom, at about -3 m, NAVD88, and Depth 6 being near the water surface.

Because the Mote station was located in the lower portion of upper Charlotte Harbor which runs roughly in the y -direction, currents in the y -direction are much larger than these in the x -direction. It can be seen from Figure 17 that simulated tidal currents in the y -direction match with measured data very well, except for some missed peaks, mainly during wet seasons. Like missed peaks in simulated water levels, missed v -velocity peaks might be due to less accurate representation of some local physical factors such as the bathymetry and wind speed and direction, in addition to errors in the WFCOM model for boundary conditions at the open boundaries in the GOM.

While v -velocities at the Mote station are dominated by tides, u -velocities shown in Figure 18 have relatively weak tidal signals, because currents in the x -direction are also affected by wind, Coriolis forces, and baroclinic forces at a comparable scale. As a result, the match of simulated u -velocities with measured data is not as accurate as that for v -velocities due to uncertainties contained in the input data such as those for freshwater inflows and wind.

Figure 19 shows comparisons simulated and measured v - and u -velocities at Depths 1, 3, and 5 at the Mote station during the month of January 2014. The mismatches mostly occurred for the surface layer velocities, suggesting that the wind could be a factor responsible for the mismatches. At the bottom and middle layers, both simulated and measured u -velocities are generally weak but have similar magnitudes. Furthermore, high frequency signals exist in both simulated and measured u -velocities. Although one may consider these high frequency variabilities as noise, they could be caused by some physical factors such as the nonlinear interactions among velocities as well as those between flow and the estuary bed.

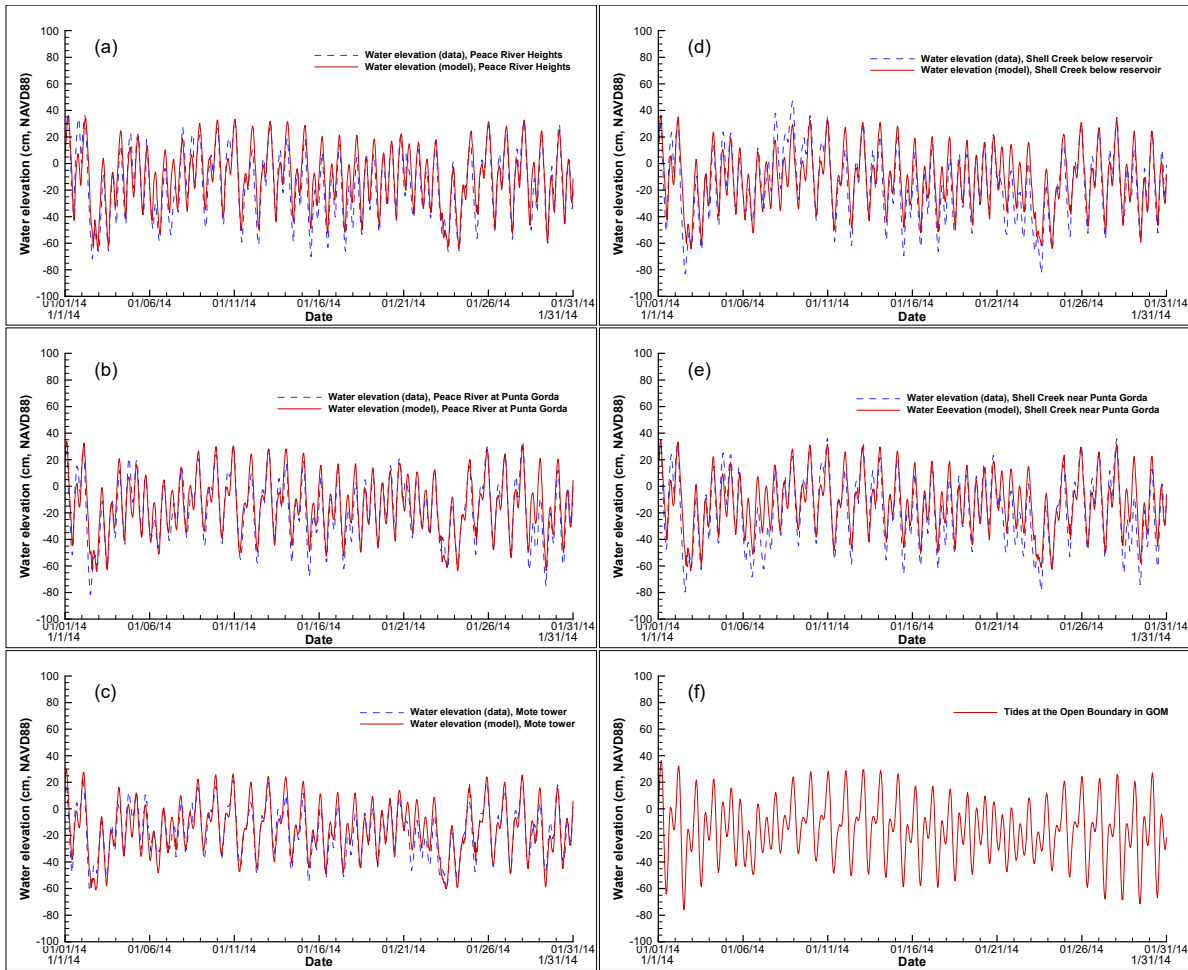


Figure 16 Comparisons of simulated water levels (red solid lines) and measured water levels (blue dashed lines) at the PR_HT (a), PR_PG (b), Mote (c), SC_BR (d), and SC (e) during the period January 1, 2014 - January 31, 2014. Water level boundary conditions at an open boundary in the GOM are also shown here in (f).

Figures 20 – 24 are comparisons of simulated salinities with measured data at the Mote, PR_PG, PR_HT, SC_PG, and SC_BR stations over the period January 2013 to August 2014. As shown in figures, except for the Mote station, there were large data gaps at the other four stations. These large data gaps occurred mainly during the summer season of 2013 when salinities at these four stations were very low.

Generally, simulated salinities at all five stations matched with measured data well in terms of short-term and longer-term variations; nonetheless, there are many mismatches where the model either over-estimates or under-estimates salinities. For example, at the Mote station, the model under-estimates salinities at all three depths, in terms of average and variability, during the summer of 2013; however, during the dry season of 2014, the model slightly over-estimates salinities at this station.

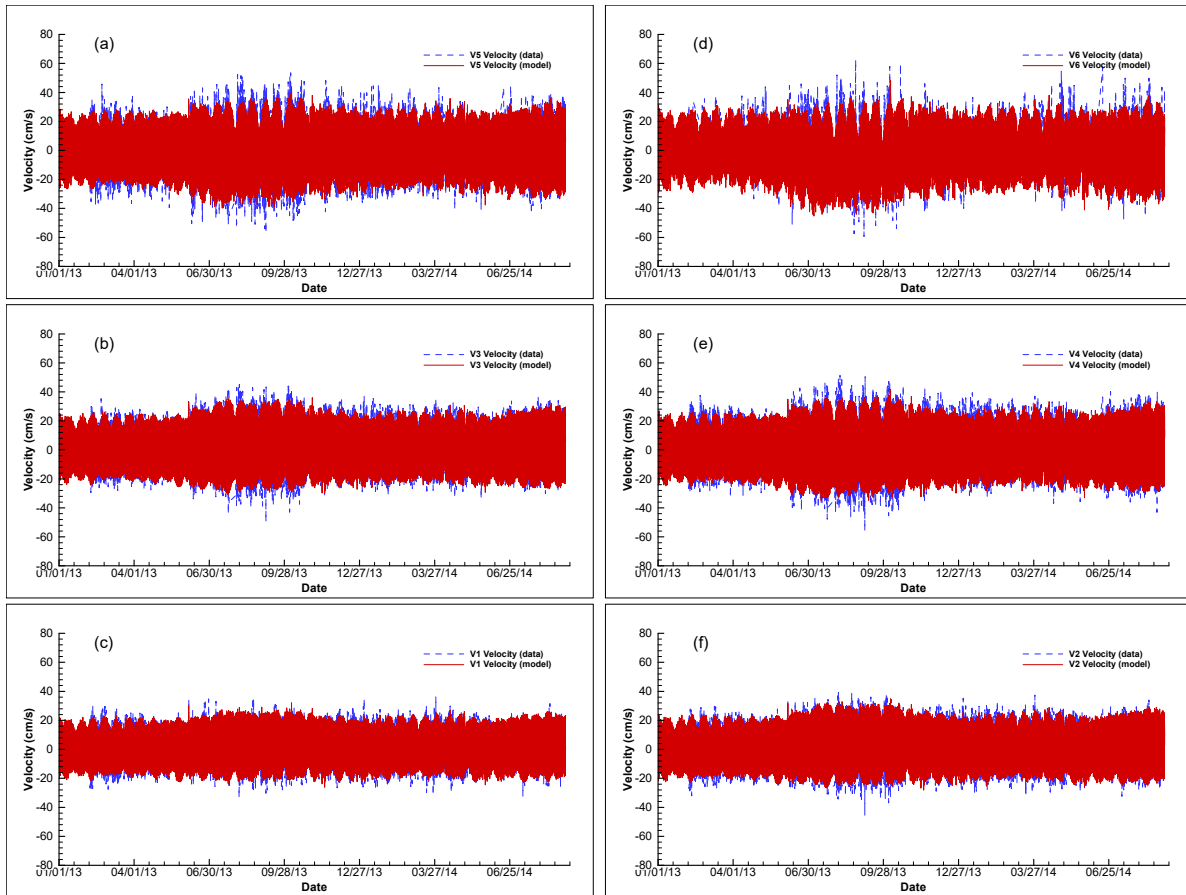


Figure 17. Comparisons of simulated v-velocities (red solid lines) with measured u-velocities (blue dashed lines) at six depths of the Mote station in Charlotte Harbor during the 20-month period from January 2013 to August 2014.

Because low salinity habitats are most sensitive to flow variation in dry months of the area when both rainfall and freshwater inflow are low, it is critical that simulated salinities match well with measured data during dry season. Figures 25 – 29 show comparisons of simulated and measured salinities for the month of April 2014, which was in the middle of the dry season for the area. It can be seen from Figures 25 – 29 that during April 2014, although salinities in all five stations were higher than during wet months, salinity variabilities in the dry month were relatively lower than those in wet months. This is because both rainfall and freshwater inflows during dry months were low with only small temporal variabilities.

Figures 30 – 34 show comparisons of simulated and measured temperatures at the five data collection stations during January 2013 through August 2014. As can be seen from these figures, simulated temperatures at the both the Mote station and the PR_PG station match very well for all the 20 months. At PR_HT, SC_PG, and SC_BR, simulated temperatures generally agree well with measured data, except during the coldest 60-day period, which occurred roughly between the middle of December 2013 and the middle of February of 2014, when the model under-predicted water temperature by a few degrees Celsius. Several sources of error could be responsible for these mismatches, including the wind data used in the model for areas near these three stations, where the Peace River or Shell Creek are much narrower than the PR_PG station or the Mote station in Charlotte Harbor

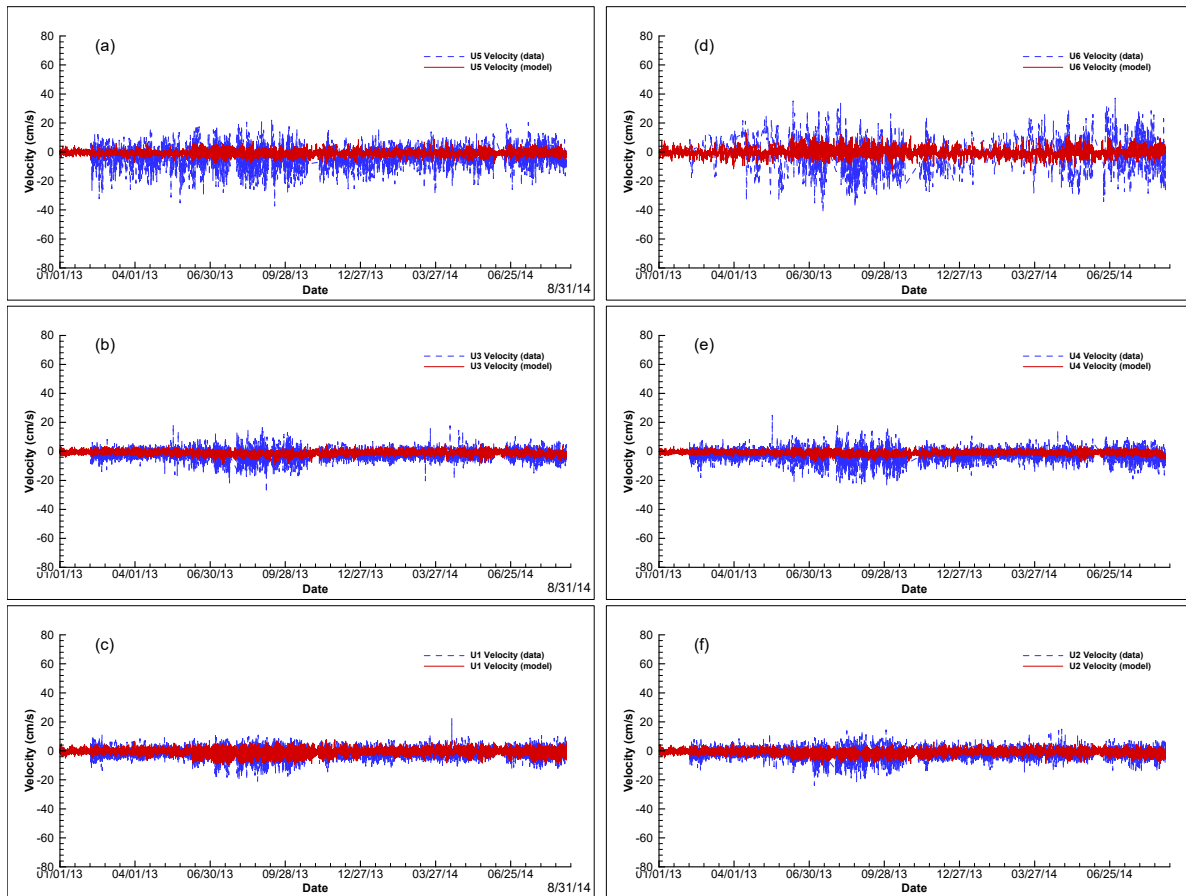


Figure 18. Comparisons of simulated u-velocities (red solid lines) with measured u-velocities (blue dashed lines) at six depths of the Mote station in Charlotte Harbor during the 20-month period from January 2013 to August 2014.

Because thermo-habitats were not a concern in the MFL re-evaluations for the LPR and LSC, a very good agreement between simulated and measured temperatures was not a major goal in this modeling study. As such, no extra effort was made to improve model calibration for the temperature simulation in the estuarine system

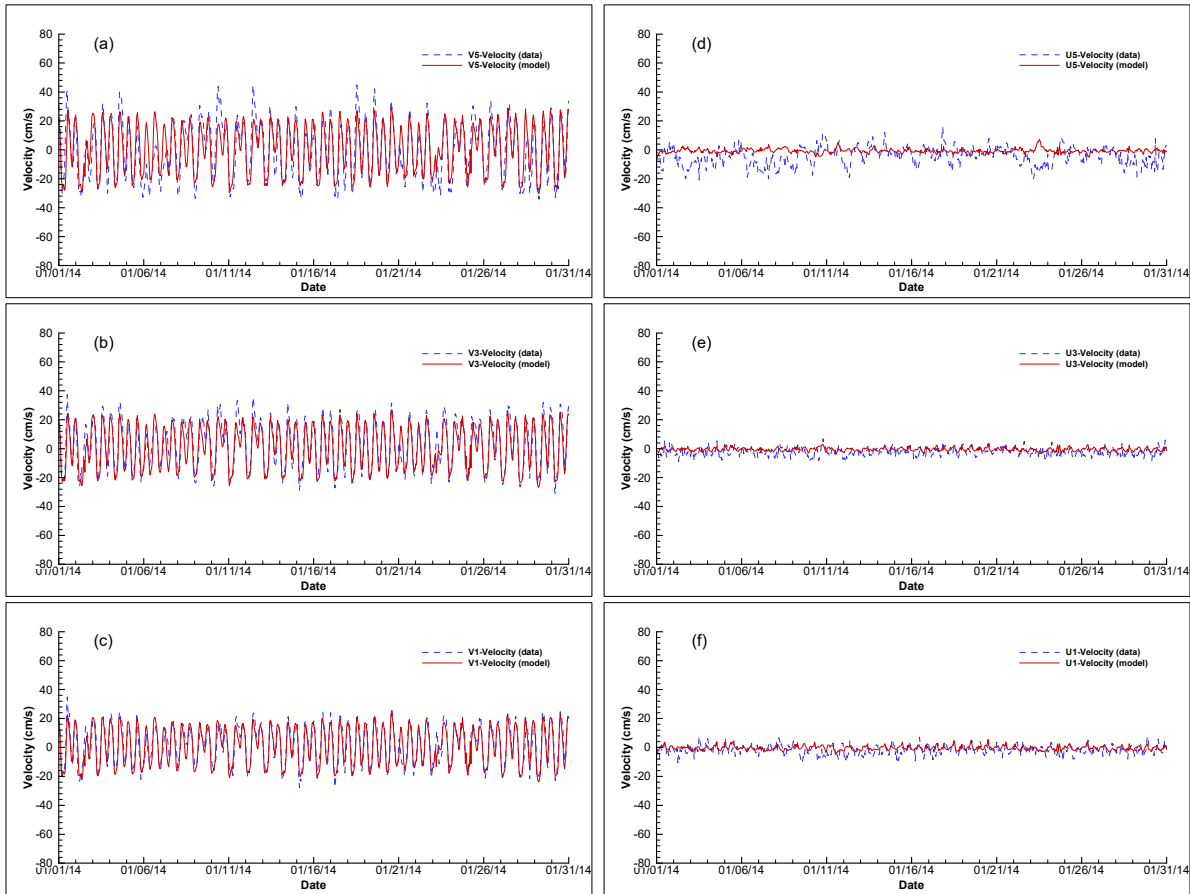


Figure 19. Comparisons of simulated (red solid lines) and measured (blue dashed lines) V- and U-velocities at Depths 1, 3, and 5 of the Mote station during January 2014.

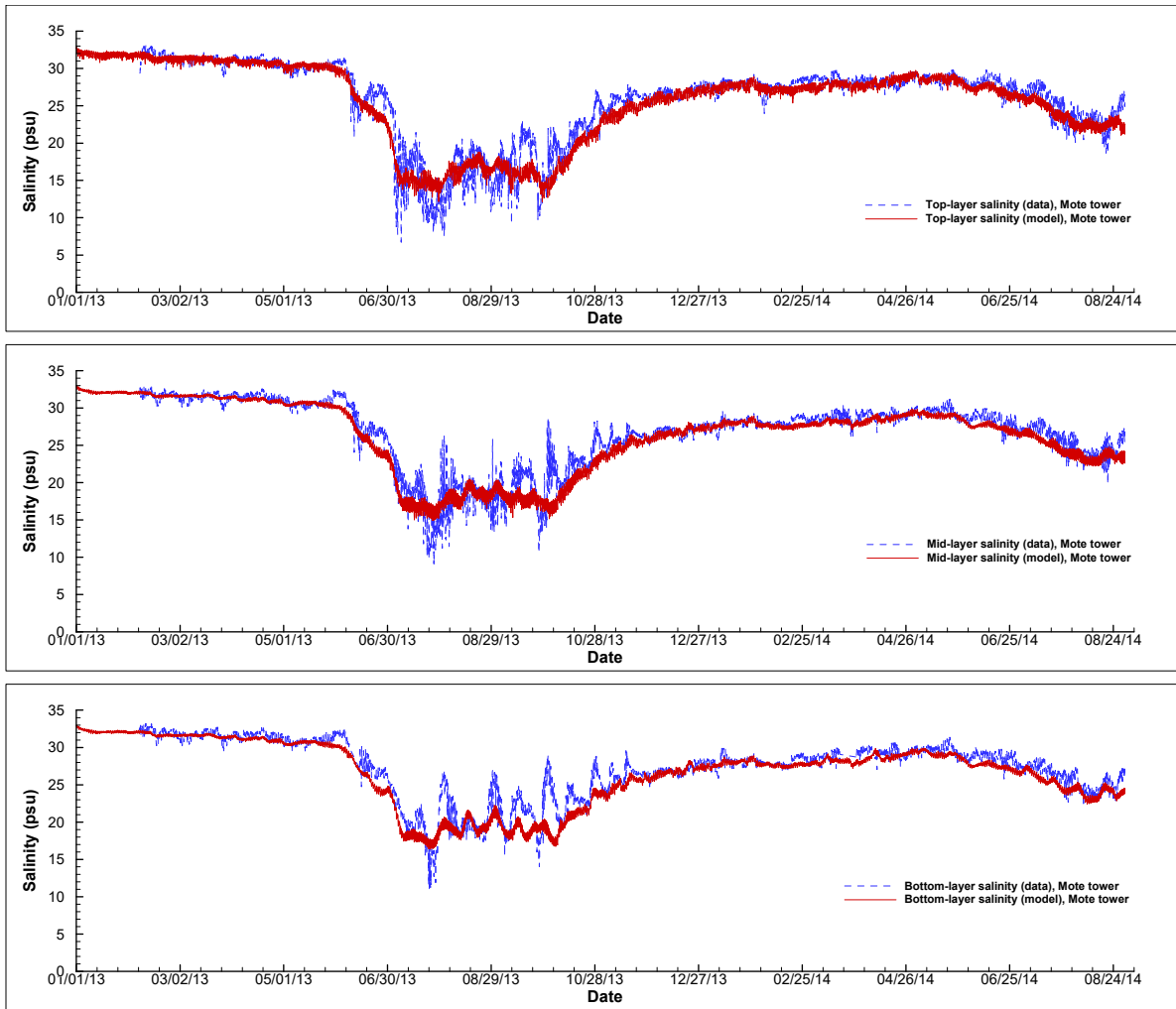


Figure 20. Comparisons of simulated (red solid lines) and measured (blue dashed lines) salinities at the top, middle, and bottom layers at the Mote station during the 20-month period between January 2013 and August 2014.

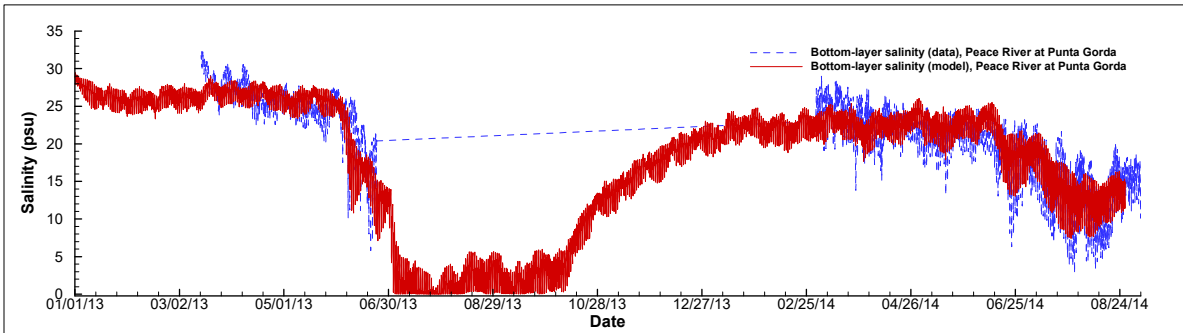
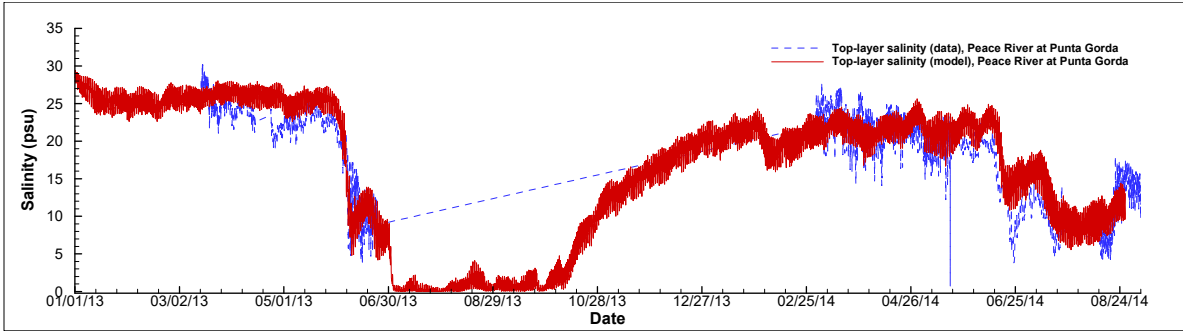


Figure 21. Comparisons of simulated (red solid lines) and measured (blue dashed lines) salinities at the top and bottom layers at the PR_PG station during the 20-month period between January 2013 and August 2014.

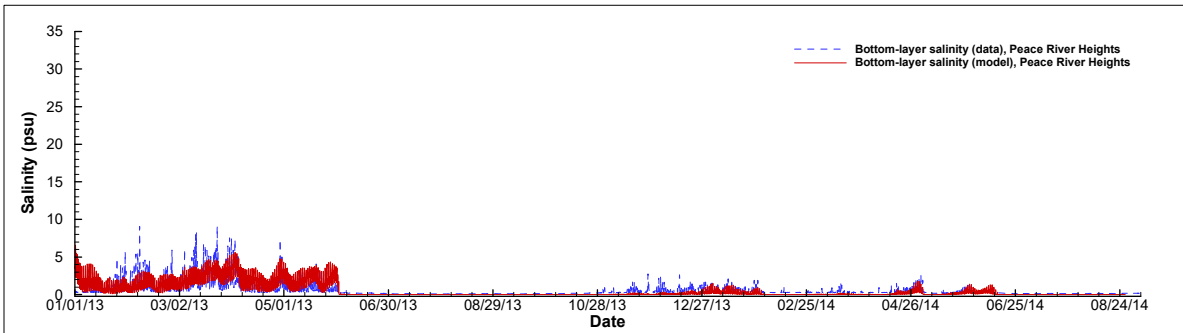
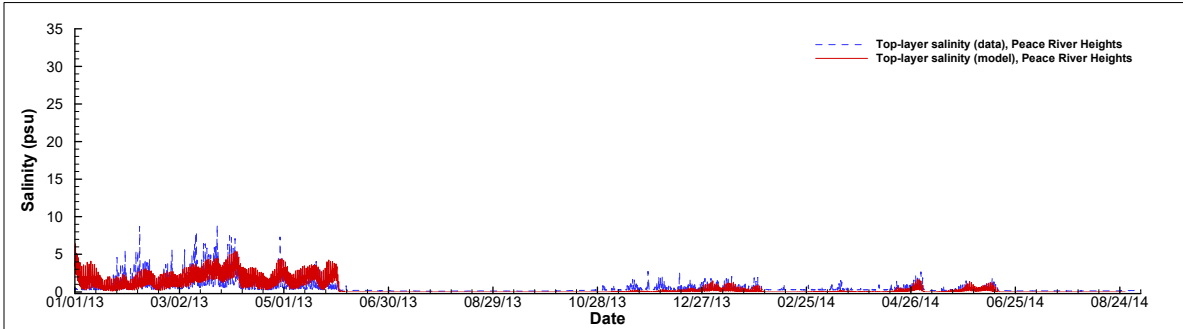


Figure 22. Comparisons of simulated (red solid lines) and measured (blue dashed lines) salinities at the top and bottom layers at the PR_HT station from January 2013 to August 2014.

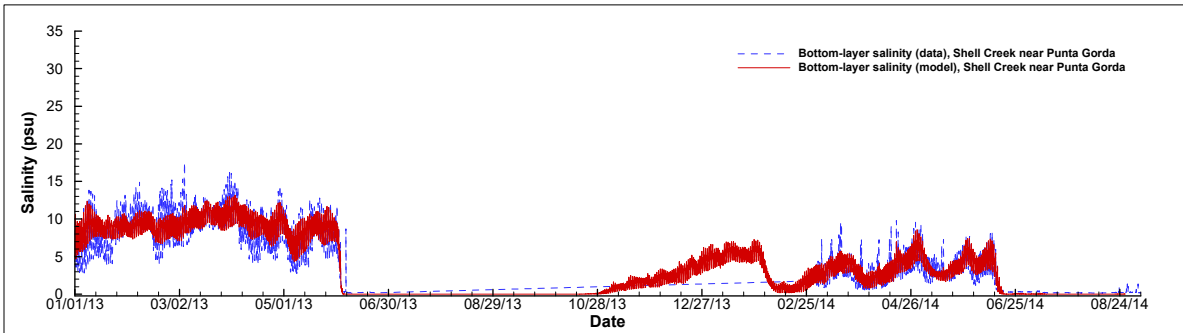
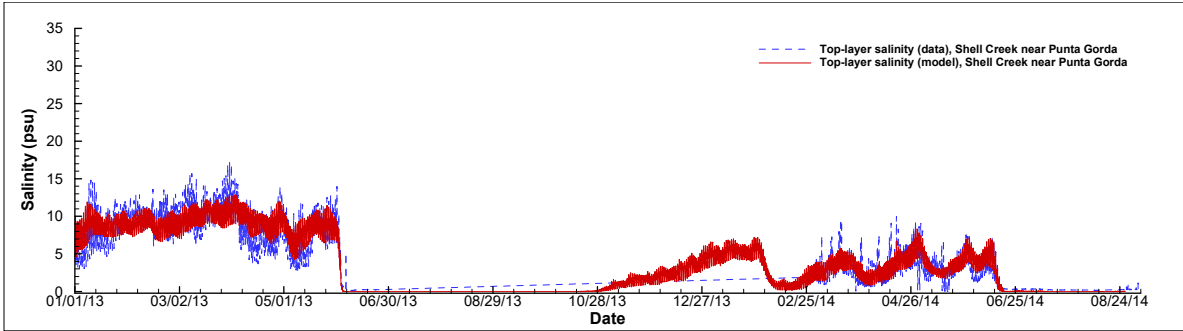


Figure 23. Comparisons of simulated (red solid lines) and measured (blue dashed lines) salinities at the top and bottom layers at the SC_PG station during the 20-month period between January 2013 and August 2014.

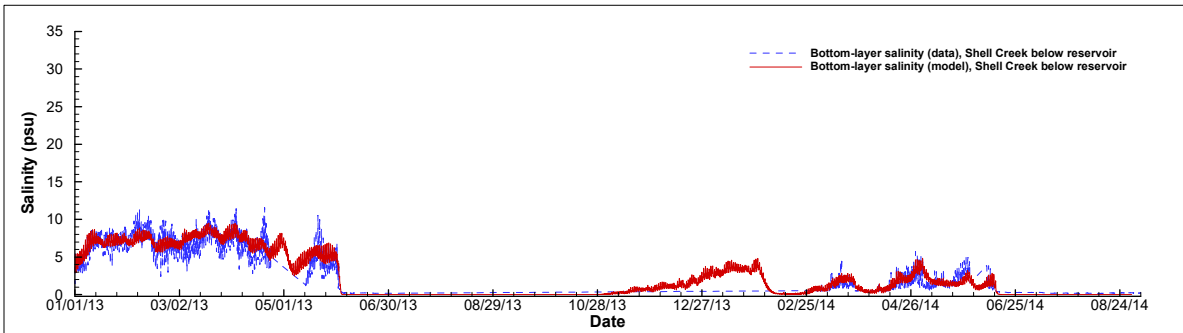
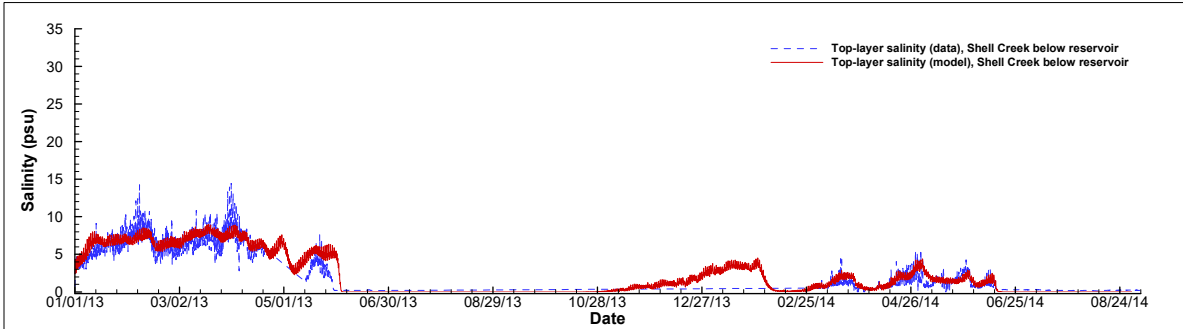


Figure 24. Comparisons of simulated (red solid lines) and measured (blue dashed lines) salinities at the top and bottom layers at the SC_BR station during the 20-month period between January 2013 and August 2014.

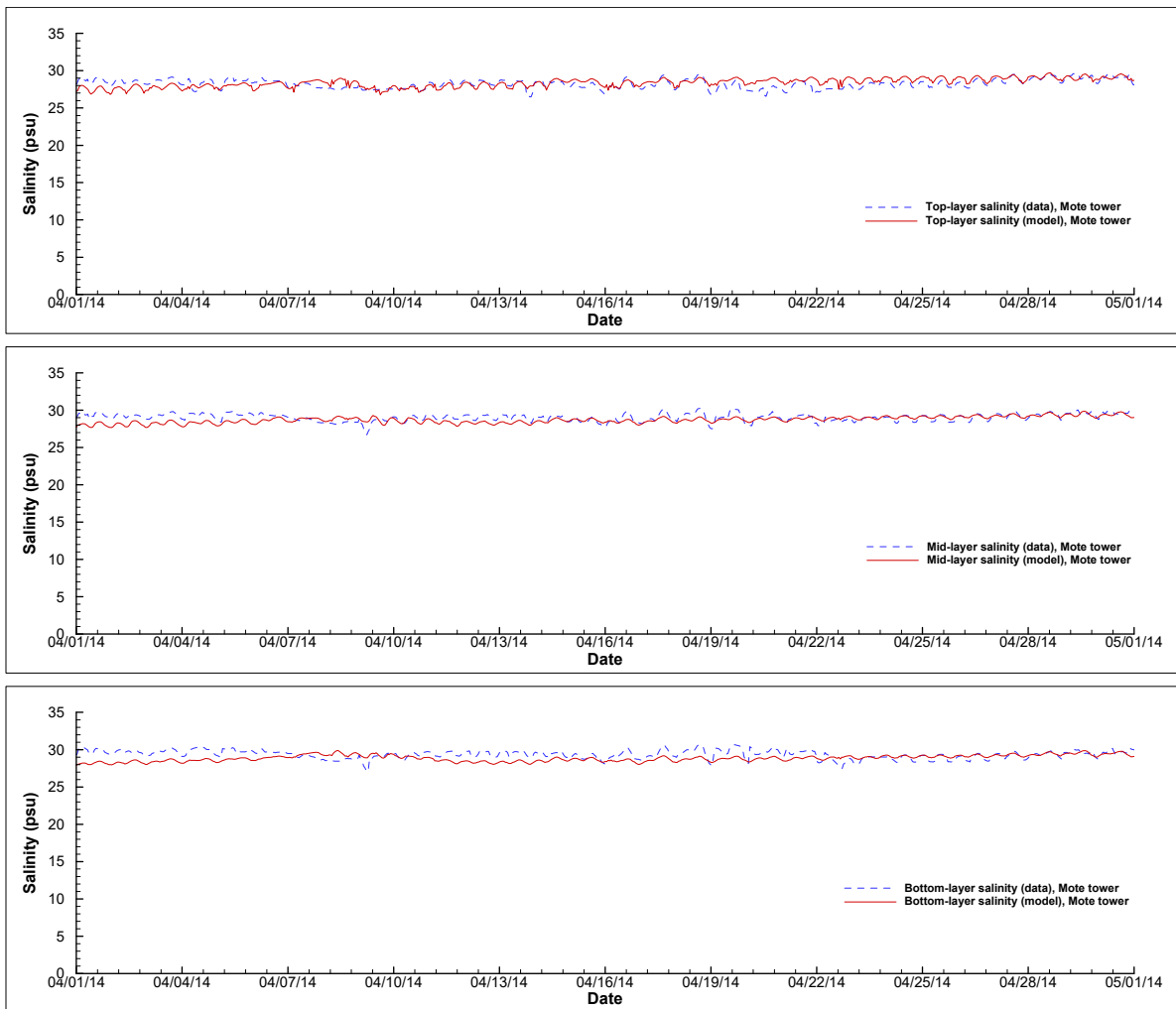


Figure 25. Comparisons of simulated (red solid lines) and measured (blue dashed lines) salinities at the top, middle, and bottom layers at the Mote station during April 2014.

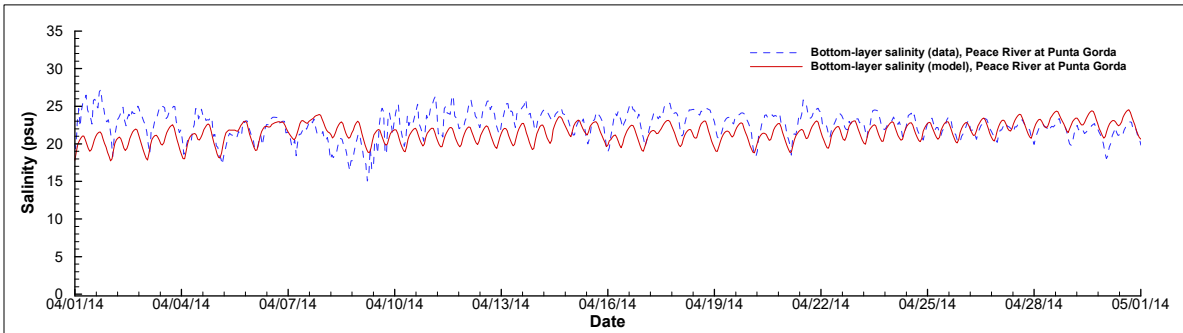
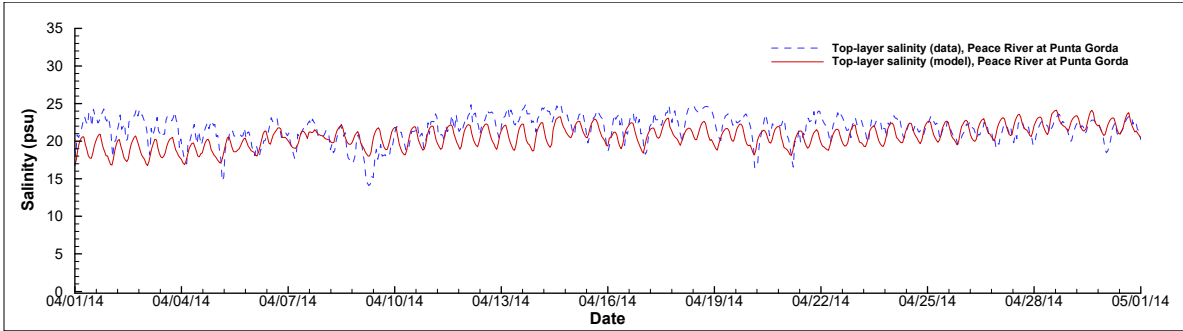


Figure 26. Comparisons of simulated (red solid lines) and measured (blue dashed lines) salinities at the top and bottom layers at the PR_PG station during April 2014.

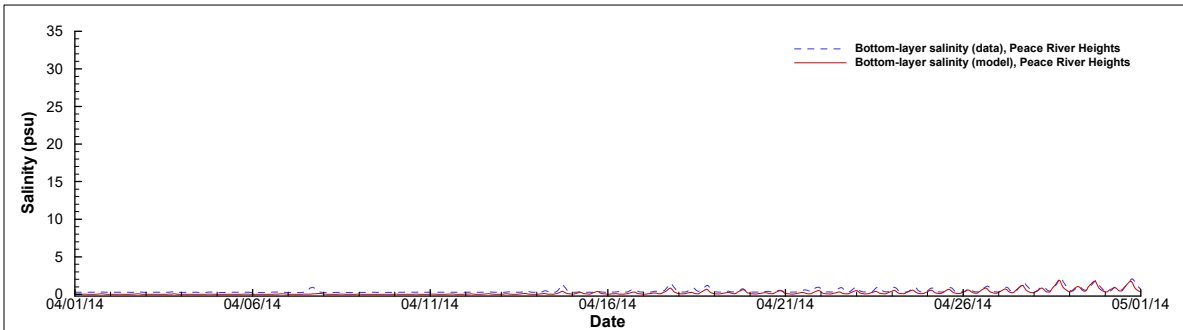
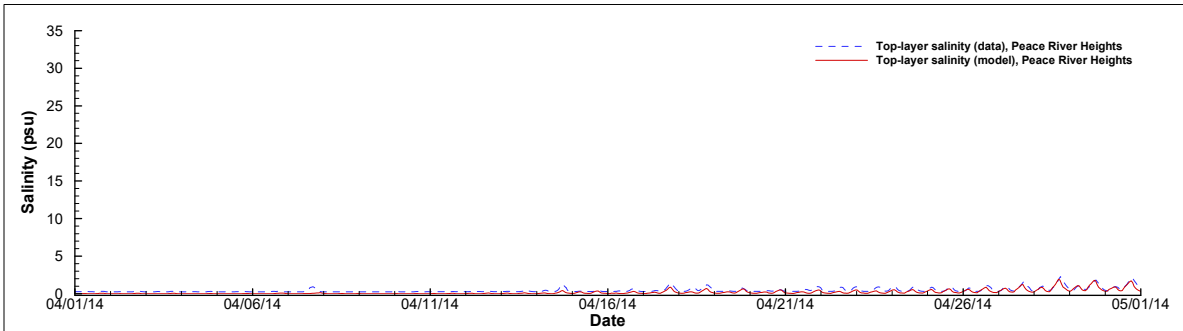


Figure 27. Comparisons of simulated (red solid lines) and measured (blue dashed lines) salinities at the top and bottom layers at the PR_HT station during April 2014.

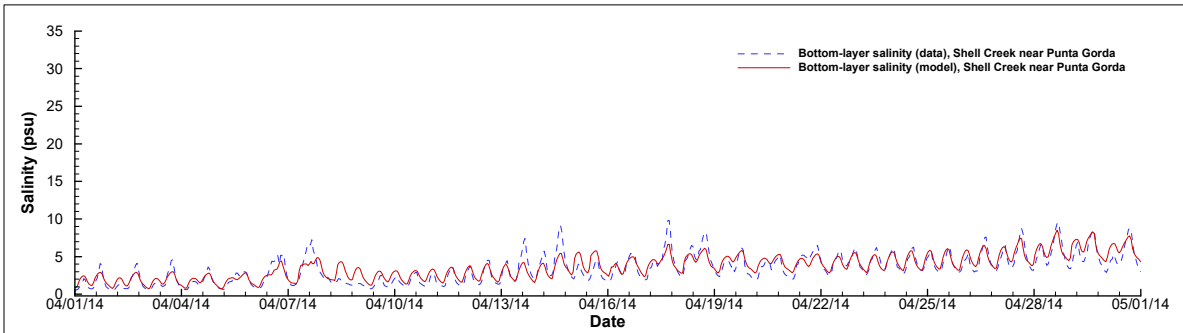
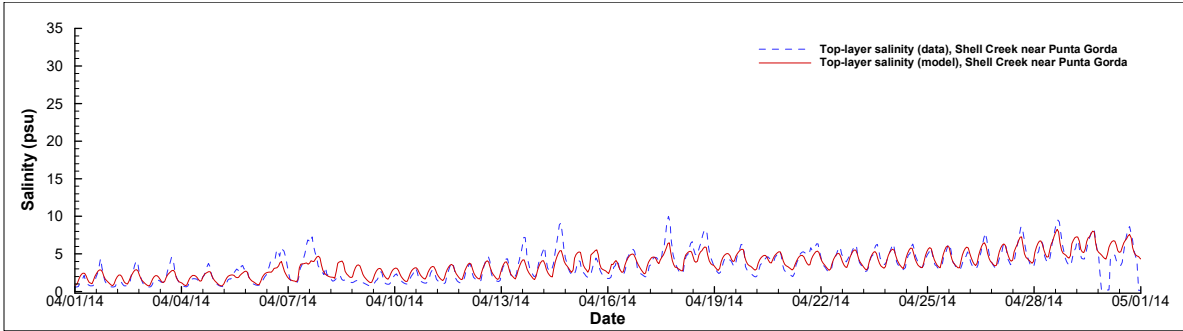


Figure 28. Comparisons of simulated (red solid lines) and measured (blue dashed lines) salinities at the top and bottom layers at the SC_PG station during April 2014.

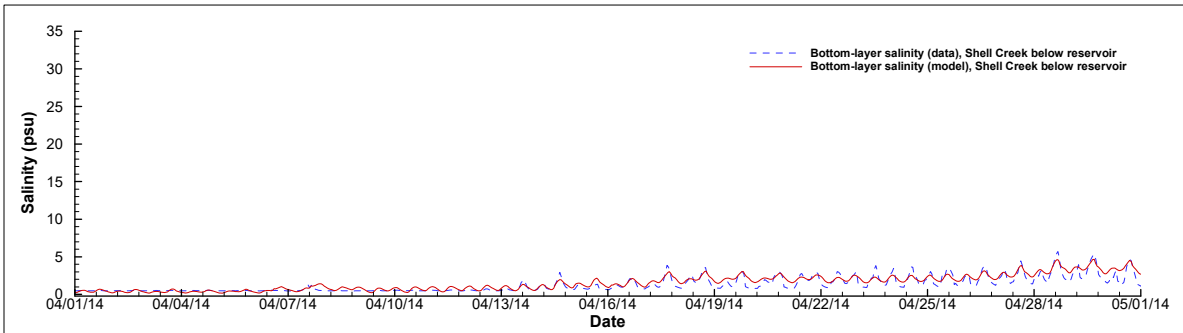
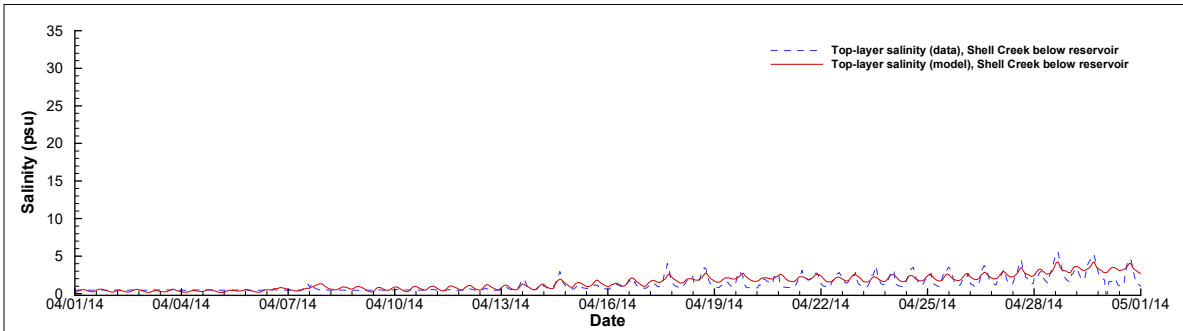


Figure 29. Comparisons of simulated (red solid lines) and measured (blue dashed lines) salinities at the top and bottom layers at the SC_BR station during April 2014.

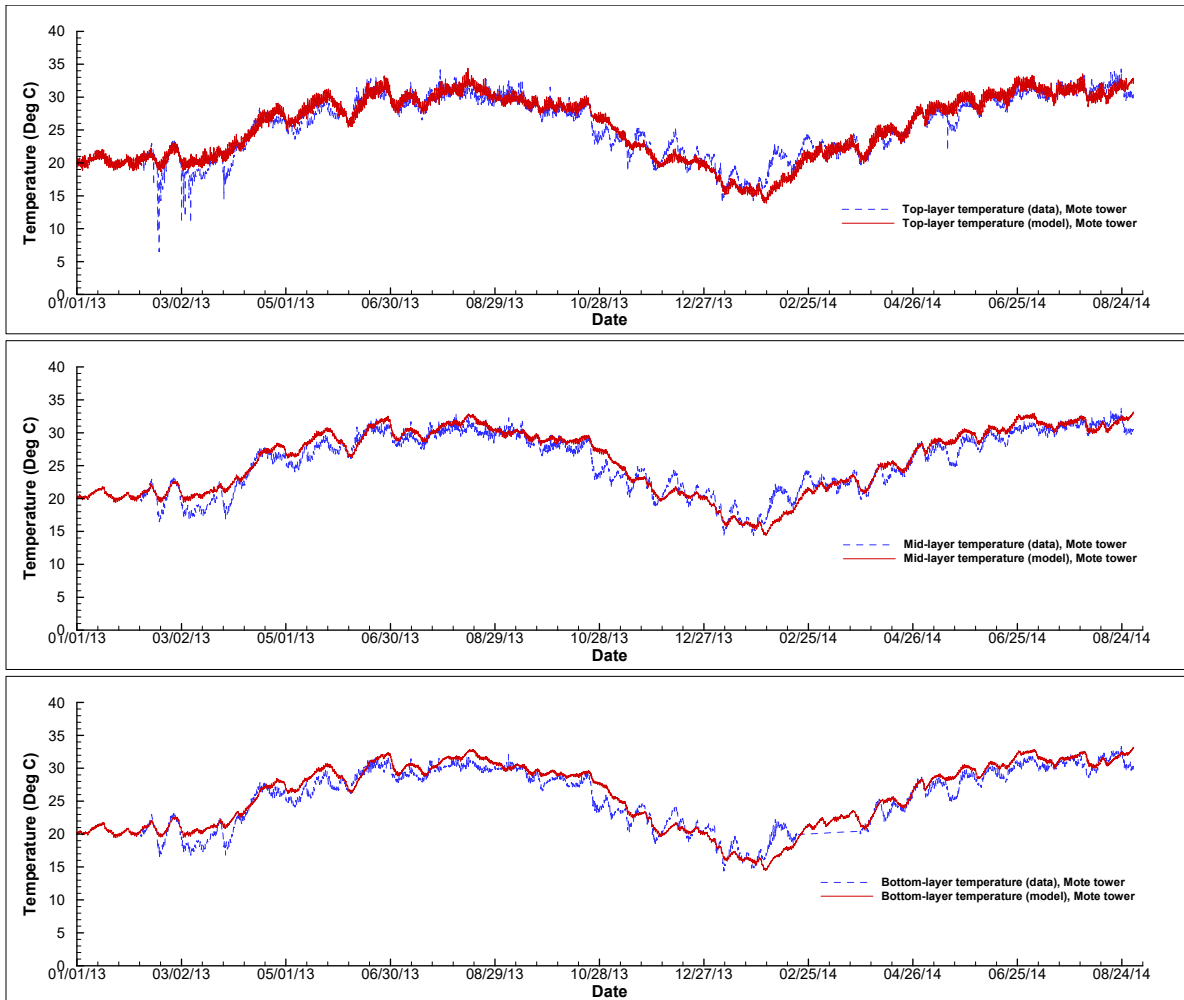


Figure 30. Comparisons of simulated (red solid lines) and measured (blue dashed lines) temperatures at the top, middle, and bottom layers at the Mote station during the 20-month period between January 2013 and August 2014.

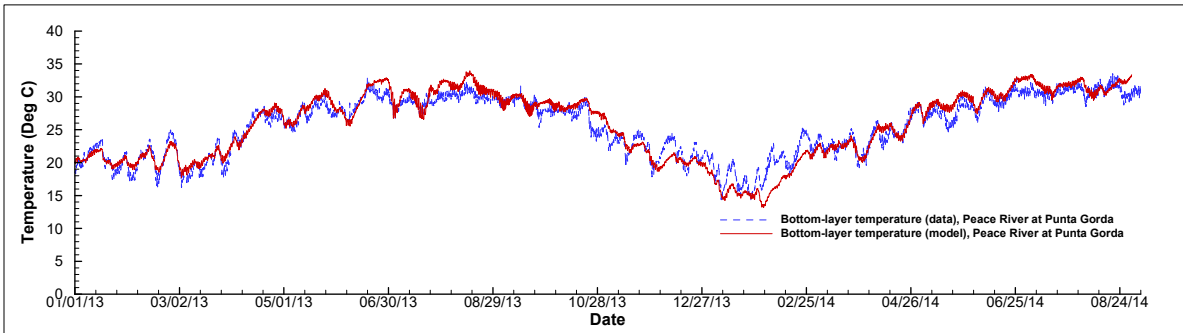
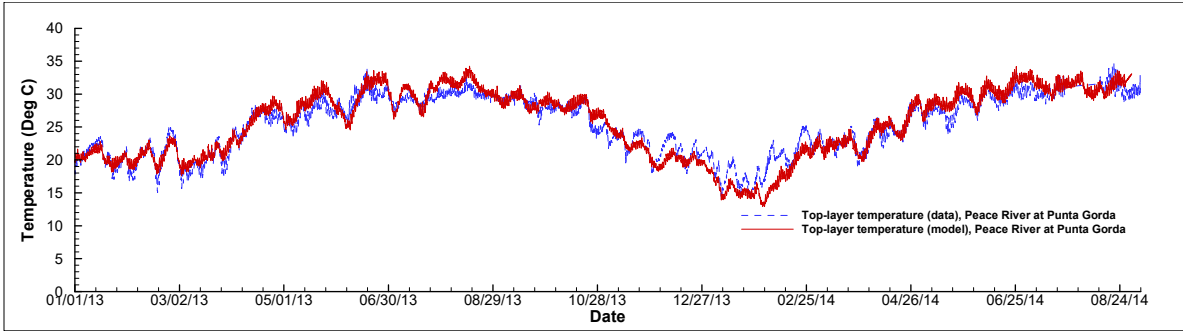


Figure 31. Comparisons of simulated (red solid lines) and measured (blue dashed lines) temperatures at the top and bottom layers at the PR_PG station during the 20-month period between January 2013 and August 2014.

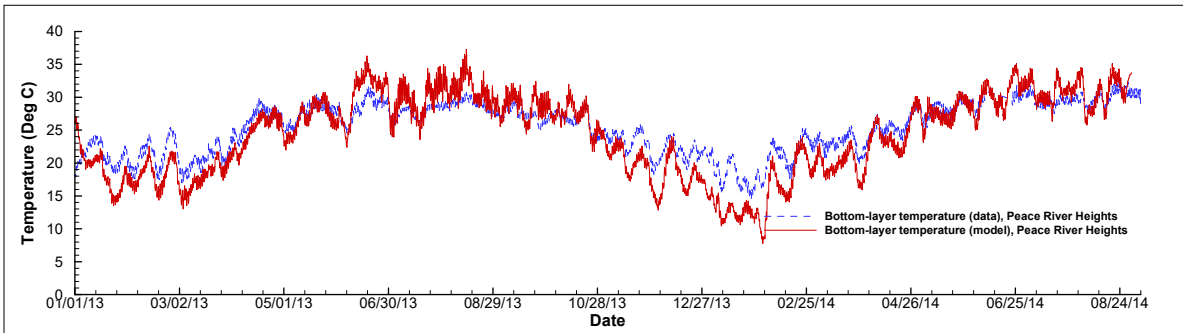
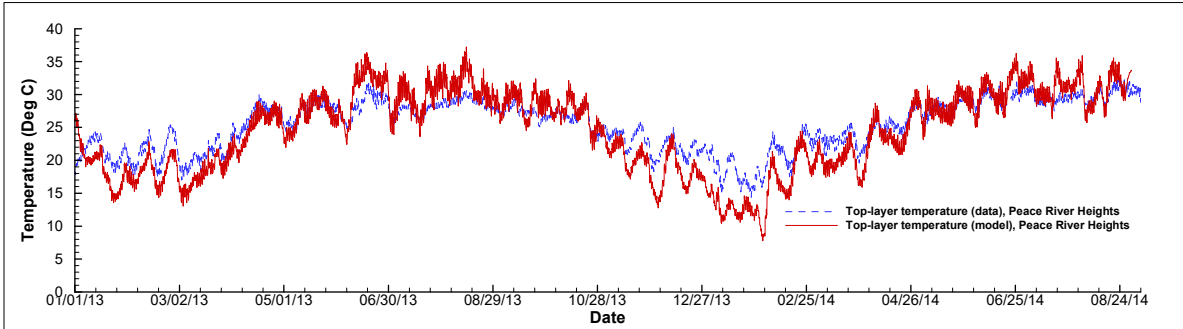


Figure 32. Comparisons of simulated (red solid lines) and measured (blue dashed lines) temperatures at the top and bottom layers at the PR_HT station during the 20-month period between January 2013 and August 2014.

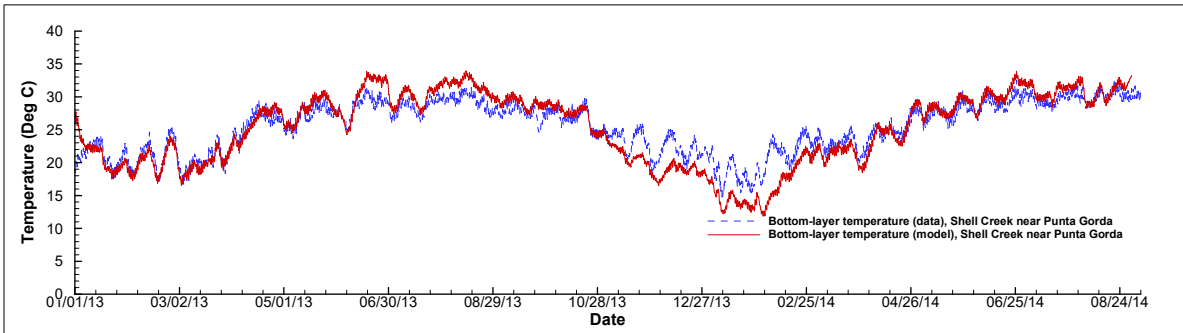
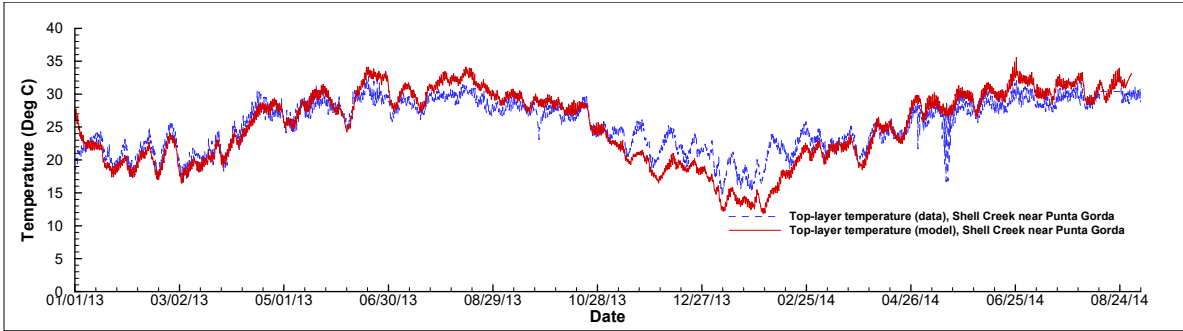


Figure 33. Comparisons of simulated (red solid lines) and measured (blue dashed lines) temperatures at the top and bottom layers at the SC_PG station during the 20-month period between January 2013 and August 2014.

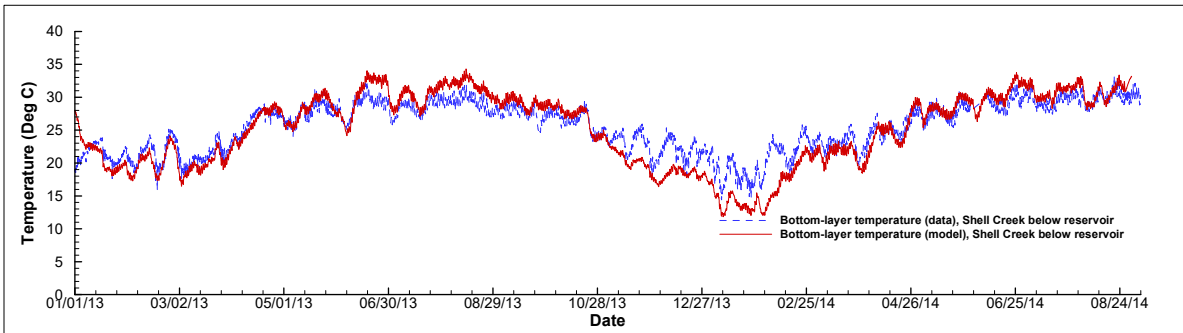
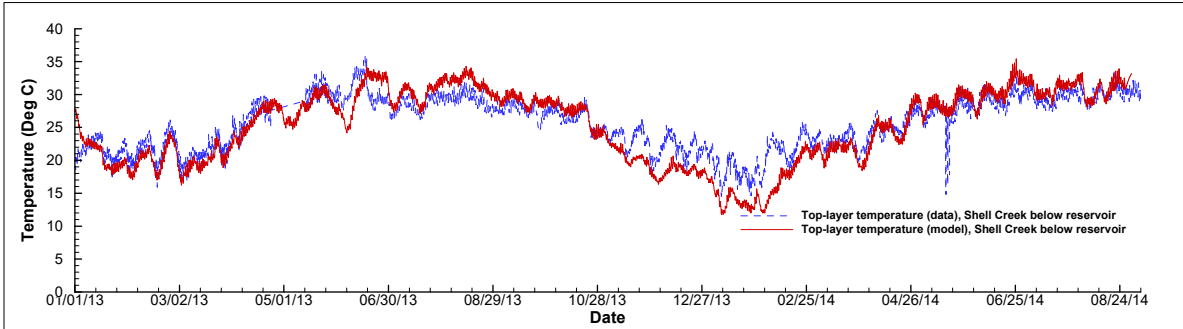


Figure 34. Comparisons of simulated (red solid lines) and measured (blue dashed lines) temperatures at the top and bottom layers at the SC_BR station during the 20-month period between January 2013 and August 2014.

3.3 Model Skill Assessment

Similar to the previous hydrodynamic modeling studies performed for MFL evaluations of the estuarine systems in the SWFWMD, a skill assessment parameter introduced by Willmott (1981) was used to judge the agreement between model results and measured data. This skill assessment parameter was used by Warner et al. (2005) to assess the performance of an estuary hydrodynamic model for the Hudson River estuary. The Willmott skill assessment parameter takes the following form

$$Skill = 1 - \frac{\sum(y^M - y^D)^2}{\sum(|y^M - \bar{y}^D| + |\bar{y}^M - y^D|)^2} \quad (17)$$

where y^M and y^D are simulated and measured variables (surface elevation or salinity) and \bar{y}^D and \bar{y}^M are means of y_i^D and y_i^M , respectively. Skill in Equation (17) varies between 0 and 1: a perfect agreement between simulated results and measured data yields a skill of one and a complete disagreement yields a skill of zero.

Skill parameters using Equation (17) for simulated water levels, salinities, and temperatures at the five stations were calculated. Additional statistical parameters such as the coefficient of determination (R^2 value), the mean error (ME), and the mean absolute error (MAE) were also calculated to analyze the error of the model.

Table 2 lists mean errors, mean absolute errors, R^2 values and skills for simulated water levels at the five stations during the calibration and verification periods, respectively from August 1, 2013 to August 31, 2014 and from January 1, 2013 to August 1, 2013. The mean error for the simulated water level ranged from -1.37 cm to 0.60 cm, with an overall mean error of -0.34 cm during the calibration period and from -0.33 cm to 1.08 cm, with an overall ME of 0.52 cm during the verification period. The ranges for the mean absolute error for the water level simulation were 5.65 – 9.15 cm and 5.60 – 8.15 cm, respectively for the calibration and verification periods, with their respective overall MAEs being 7.90 cm and 7.36 cm. The R^2 value ranged between 0.75 and 0.85, with an overall R^2 of 0.78 during the calibration period. The model verification had a R^2 ranging between 0.79 and 0.83, with an overall R^2 of 0.80. The skill of the simulated water level during the calibration period varied between 0.92 and 0.96 for the five stations, among which the overall R^2 was 0.94. During the verification period, the skill of simulated water level was 0.94 - 0.95 with an overall skill of 0.94.

Table 2. Values of ME (in cm), MAE (in cm), R^2 , and skill of simulated water levels at the five measurement stations during the calibration and verification periods.

Station	Calibration Period				Verification Period			
	ME	MAE	R^2	Skill	ME	MAE	R^2	Skill
Mote	-0.61	5.65	0.85	0.96	1.08	5.60	0.83	0.95
PR PG	0.19	8.17	0.78	0.94	0.36	7.42	0.79	0.94
PR HT	0.60	7.65	0.81	0.95	1.18	7.77	0.80	0.94
SC PG	-1.37	8.88	0.76	0.93	-0.33	7.84	0.79	0.94
SC BR	-0.54	9.15	0.75	0.92	0.33	8.15	0.81	0.94
<i>Overall</i>	-0.34	7.90	0.78	0.94	0.52	7.36	0.80	0.94

Table 3 shows MEs, MAEs, R^2 -values, and skills for the salinity simulation of the estuarine system during model calibration and verification. The mean error for simulated salinity ranged

from -1.01 psu to 0.20 psu, with an overall mean error of -0.35 psu during the calibration period. MEs for the verification period were between -1.61 psu and 0.25 psu, with an overall ME of -0.33 psu during the verification period. Ranges for the mean absolute error for modeled salinity were 0.11 – 2.41 psu and 0.27 – 2.70 psu, respectively for the calibration and verification periods, during which overall MAEs were both approximately 0.99 psu. The coefficient of determination for simulated salinity during the calibration period ranged between 0.66 and 0.89 for model calibration and between 0.67 and 0.92 for model verification. The overall R^2 values for all the stations (sensors) were very high: 0.99 during the calibration period and 0.98 during the verification period. The skill of the simulated salinity varied between 0.80 and 0.97 for the five stations during the calibration period and between 0.90 and 0.98 during the verification period. The overall skills during the calibration and verification periods were both 0.99.

Overall coefficient of determination and skill parameters approaching 1 for simulated salinity suggested that the UnLESS model has great capability for simulating horizontal salinity distribution across the simulation domain, with saltier ocean water in Charlotte Harbor and brackish or fresh water in the upstream areas of the LPR and LSC.

Table 3. Values of ME (in psu), MAE (in psu), R^2 , and skill of simulated salinities at the five measurement stations during the calibration and verification periods.

Station (sensor)	Calibration Period				Verification Period			
	ME	MAE	R^2	Skill	ME	MAE	R^2	Skill
Mote (top)	-0.61	1.16	0.89	0.97	-0.51	1.18	0.90	0.97
Mote (middle)	-0.69	1.05	0.88	0.96	-0.62	1.04	0.91	0.97
Mote (bottom)	-1.01	1.19	0.82	0.93	-0.91	1.12	0.89	0.96
PR PG (top)	0.05	2.41	0.74	0.91	-0.51	2.70	0.78	0.92
PR PG (bottom)	-1.01	2.20	0.74	0.90	-1.61	2.47	0.80	0.91
PR HT (top)	-0.10	0.11	0.67	0.81	0.04	0.27	0.67	0.90
PR HT (bottom)	-0.10	0.11	0.66	0.80	0.05	0.28	0.67	0.90
SC PG (top)	0.20	0.58	0.80	0.94	0.14	0.82	0.92	0.98
SC PG (bottom)	0.12	0.51	0.84	0.96	0.11	0.73	0.93	0.98
SC BR (top)	0.16	0.31	0.73	0.91	0.25	0.61	0.89	0.97
SC BR (bottom)	0.11	0.31	0.74	0.92	0.16	0.57	0.92	0.98
<i>Overall</i>	-0.35	0.83	0.99	0.99	-0.33	0.99	0.98	0.99

MEs, MAEs, R^2 values, and skills for the temperature simulation for the calibration and verification periods are listed in Table 4. The ME for simulated temperature ranged from -1.18 °C to 0.97 °C, with an overall ME of -0.15 °C during model calibration and from -1.09 °C to 1.14 °C, with an overall ME of 0.02 °C during model verification. The range for the MAE for the simulated temperature was 1.31 – 2.45 °C, with an overall MAE of 1.84 °C for model calibration. For model verification, the MAE was 1.38 – 2.40 °C, with an overall MAE of 1.74 °C. The R^2 values were in the range of 0.90 - 0.94 for model calibration and of 0.88 - 0.93 for model verification. The overall R^2 values during the calibration and verification period were 0.89 and 0.87, respectively. The skill of temperature simulation during both the calibration and verification periods varied between 0.91 and 0.97 for the five stations. The overall skill among all the stations (sensors) were 0.94 and 0.95, respectively for model calibration and model verification.

The overall coefficient of determination for simulated temperature behaves differently from the overall coefficient of determination for simulated salinity. While the latter is higher than that for any of the sensors, the former is lower than those for all individual sensors. This difference of the overall R^2 in relation to individual R^2 should not be a surprise if the temporal variabilities and spatial distributions of salinity and temperature are considered.

Table 4. Values of ME (in °C), MAE (in °C), R^2 , and skill of simulated temperatures at the five measurement stations during the calibration and verification periods.

Station (sensor)	Calibration Period				Verification Period			
	ME	MAE	R^2	Skill	ME	MAE	R^2	Skill
Mote (top)	0.58	1.31	0.92	0.97	0.82	1.38	0.90	0.97
Mote (middle)	0.79	1.37	0.93	0.97	1.00	1.42	0.92	0.97
Mote (bottom)	0.97	1.47	0.94	0.97	1.14	1.50	0.93	0.97
PR PG (top)	0.32	1.43	0.92	0.97	0.49	1.38	0.91	0.97
PR PG (bottom)	0.64	1.51	0.94	0.97	0.73	1.39	0.93	0.97
PR HT (top)	-1.04	2.44	0.91	0.91	-0.95	2.39	0.90	0.91
PR HT (bottom)	-1.18	2.45	0.92	0.91	-1.09	2.40	0.91	0.91
SC PG (top)	-0.41	2.06	0.90	0.93	-0.23	1.77	0.90	0.94
SC PG (bottom)	-0.68	1.87	0.93	0.94	-0.36	1.63	0.92	0.95
SC BR (top)	-0.77	2.14	0.90	0.92	-0.75	2.04	0.88	0.93
SC BR (bottom)	-0.82	2.13	0.92	0.92	-0.58	1.86	0.92	0.93
<i>Overall</i>	-0.15	1.84	0.89	0.94	0.02	1.74	0.87	0.95

Because Charlotte Harbor runs in the south-north direction, currents in the y -direction are much stronger than those in the x -direction at the Mote station. The relatively weak cross-sectional currents in the x -direction are affected by wind, barotropic and baroclinic pressure gradients, bathymetry, etc. and have low readings that are often in the comparable magnitude of the uncertainty (noise) of the field measurement. As such, it is not meaningful to assess the model performance for currents in the x -velocity. As a result, model performance assessment for current simulation is only done for those in the y -direction. Table 5 lists MEs, MAEs, R^2 values, and skills for the current simulation at the bottom 5 depths at the Mote station during the calibration and verification periods. Simulated y -velocity at the 6th (top) depth is not included in the table because data contains too many problematic or missing data points.

From Table 5, it can be seen that the ME for simulated current in the y -direction at the Mote station was in the range of -0.79 cm/s to 0.03 cm/s, with an overall ME of -0.38 cm/s during the calibration period. The ME range of simulated v -velocity during the verification period was -0.72 cm/s to 0.06 cm/s, with an overall ME of -0.31 cm/s. The mean absolute errors of simulated v -velocity during model calibration and verification were 4.63 – 7.29 cm/s and 4.61 – 7.12 cm/s, respectively. The overall MAEs are 5.64 cm/s and 5.49 cm/s, respectively for model calibration and verification. The R^2 value of the v -velocity simulation ranged between 0.77 and 0.83 during model calibration and between 0.76 and 0.84 during model verification. The overall R^2 values were all 0.81 for both simulation periods. The skill of the simulated v -velocity varied between 0.93 and 0.95 for model calibration and between 0.93 and 0.96 for model verification. The overall skills were 0.95 during both the calibration and verification periods.

Table 5. Values of ME (in °C), MAE (in °C), R², and skill of simulated currents during the calibration and verification periods at Mote’s five measurement elevations in ascending order, with v1 being close to the bottom.

Station	Calibration Period				Verification Period			
	ME	MAE	R ²	Skill	ME	MAE	R ²	Skill
Mote v1	0.03	4.63	0.80	0.95	0.06	4.61	0.80	0.95
Mote v2	-0.15	4.97	0.82	0.95	-0.07	4.87	0.82	0.95
Mote v3	-0.54	5.36	0.83	0.95	-0.42	5.18	0.84	0.96
Mote v4	-0.79	5.97	0.83	0.95	-0.72	5.68	0.84	0.96
Mote v5	-0.47	7.29	0.77	0.93	-0.40	7.12	0.76	0.93
<i>Overall</i>	-0.38	5.64	0.81	0.95	-0.31	5.49	0.81	0.95

In summary, the dynamically coupled 3D – 2DV model, UnLESS developed for the MFL re-evaluations of the LPR and LSC, is capable of simulating hydrodynamics, salinity transport processes, and thermodynamics in the Charlotte Harbor estuary, including its major tributaries. The model has been calibrated and verified against real-time data of water elevation, salinity, and temperature at five stations in the simulation domain. It was also calibrated and verified against real-time velocity data at a station in upper Charlotte Harbor.

4. Simulations for the Determination of MFLs

4.1 Flow Reduction Scenarios

With the hydrodynamic model UnLESS calibrated and verified, a series of scenario runs were conducted to evaluate effects of different flow reductions on salinity habitats. The simulation period for the scenario runs was from January 2007 through August 2014, a total of 92 months. Input data used to drive the model were obtained in the same way as those for model calibration and verification. Flow reduction scenarios simulated included baseline, 5%, 10%, 15%, 20%, 25%, 30%, 35%, and 40% for LPR and/or LSC (Table 6).

Table 6. Flow reduction scenarios simulated for the MFL re-evaluations of the LPR and LSC.

Scenario #	Scenario Name	LPR Flow Reduction (%)	LSC Flow Reduction (%)
0	Baseline	0	0
1	P5% S5%	5	5
2	P10% S10%	10	10
3	P15% S15%	15	15
4	P20% S20%	20	20
5	P25% S25%	25	25
6	P30% S30%	30	30
7	P35% S35%	35	35
8	P40% S40%	40	40
9	P5% S0%	5	0
10	P10% S0%	10	0
11	P15% S0%	15	0
12	P20% S0%	20	0
13	P25% S0%	25	0
14	P30% S0%	30	0
15	P35% S0%	35	0
16	P40% S0%	40	0
17	P0% S5%	0	5
18	P0% S10%	0	10
19	P0% S15%	0	15
20	P0% S20%	0	20
21	P0% S25%	0	25
22	P0% S30%	0	30
23	P0% S35%	0	35
24	P0% S40%	0	40

Table 6 lists 25 scenarios that have been simulated using the UnLESS model for the estuarine system. However, only Scenarios 0 - 8 were analyzed for the MFL re-evaluations for the

LPR and LSC. Although Scenarios 9 – 24 were important in studying effects of flow reduction on salinity habitats in the LPR and LSC individually and could be very helpful in investigating interactions between the LPR and LSC, they are not practical in the water withdrawal permitting process. As such, the following discussion focuses on model results for Scenarios 0 – 8 only.

4.2 Simulated Salinity Habitats

In the scenario simulations, model results of water level, velocity, salinity, and temperature at each grid cell were saved and analyzed to evaluate how a flow reduction would affect critical habitats in the LPR and LSC. As thermal habitats are of less importance for the estuarine systems, only salinity habitats, including volumes, bottom areas and shoreline lengths for various salinity ranges (e.g., $\leq 1, 2, 3, 5, 10, 15, 20$ psu), were calculated and analyzed, at an hourly interval for the 92-month period. Here, volumes and bottom areas of various salinity ranges were calculated based on simulated salinity distributions, simulated water levels, bathymetry data input to the model, as well as dimensions of the model grids. Shoreline lengths for various salinity ranges were the lengths of the edge of the LPR and LSC for salinities $\leq 1, 2, 3, 5, 10, 15,$ and 20 psu and were calculated based on surface salinity distributions, bathymetry data input to the model, and dimensions of the model grids.

It should be noted that because the upstream boundary of the simulation domain for the LPR is at the confluence of Horse Creek with the Peace River, the salinity habitat calculation for the LPR was only done for the segment from this confluence down to the river mouth. Any low salinity habitats upstream of the confluence of Horse Creek with the Peace River were not included in calculation and thereby not included in the MFL re-evaluation for the LPR. The exclusion of the low salinity habitats upstream of the model boundary will result in a more conservative MFL for the LPR.

Previous MFL evaluations for the LPR and LSC (SWFWMD, 2007 & 2010) identified that the ≤ 2 psu habitats as most critical for the health of the estuarine system. Figure 35 shows time series of water volume for salinity ≤ 2 psu in the LPR (top panel) and in LSC (bottom panel) for the period from January 2007 to August 2014 for the baseline scenario. For comparison, water volumes for salinity $\leq 1, 3, 5, 10,$ and 15 psu are also included in the figure. Major ticks on the x -axis are placed with a time interval of 182 days, or approximately every 1/2 year. It can be seen from the figure that during January 2007 - August 2014, low salinity volumes (≤ 1 psu, ≤ 2 psu, ≤ 3 psu, and ≤ 5 psu) in the LPR were generally low in 2007 but were relatively high in 2013. This temporal variation of low salinity volume matches those of gauged and ungauged flows shown in Figure 8. During the dry seasons of 2007, 2009, and 2012, freshwater inflows to the LPR were very low and water volumes for salinity ≤ 1 psu and ≤ 2 psu dropped to a few thousands of cubic meters or less. On the other hand, the summer of 2013 was quite wet and low salinity volumes in these wet days reached to 40 – 50 million m^3 in the LPR, representing more than 50% of the entire volume of the LPR.

Because LSC is a very small waterbody (about one magnitude smaller than the LPR in terms of water volume), effects of the freshwater inflow on low salinity habitats are significant. As a result, salinity volumes in LSC varied dramatically, in a way that is very different from those in the LPR. From Figure 35, it can be seen that there were many times when salinity volumes for ≤ 1 psu, ≤ 2 psu, ≤ 3 psu, ≤ 5 psu, and ≤ 10 psu dropped to zero during dry seasons. There were days when ≤ 15 psu water volume did not exist in LSC. This occurred during April 11, 2009 – May 19, 2009 and was caused by a continuous zero flow event during April 7, 2009 – May 13,

2009. During the wet summer, however, the salt wedge could often be pushed out of LSC when freshwater inflow from the Shell Creek dam was large enough, resulting in many days when salinity in the entire LSC was ≤ 1 psu.

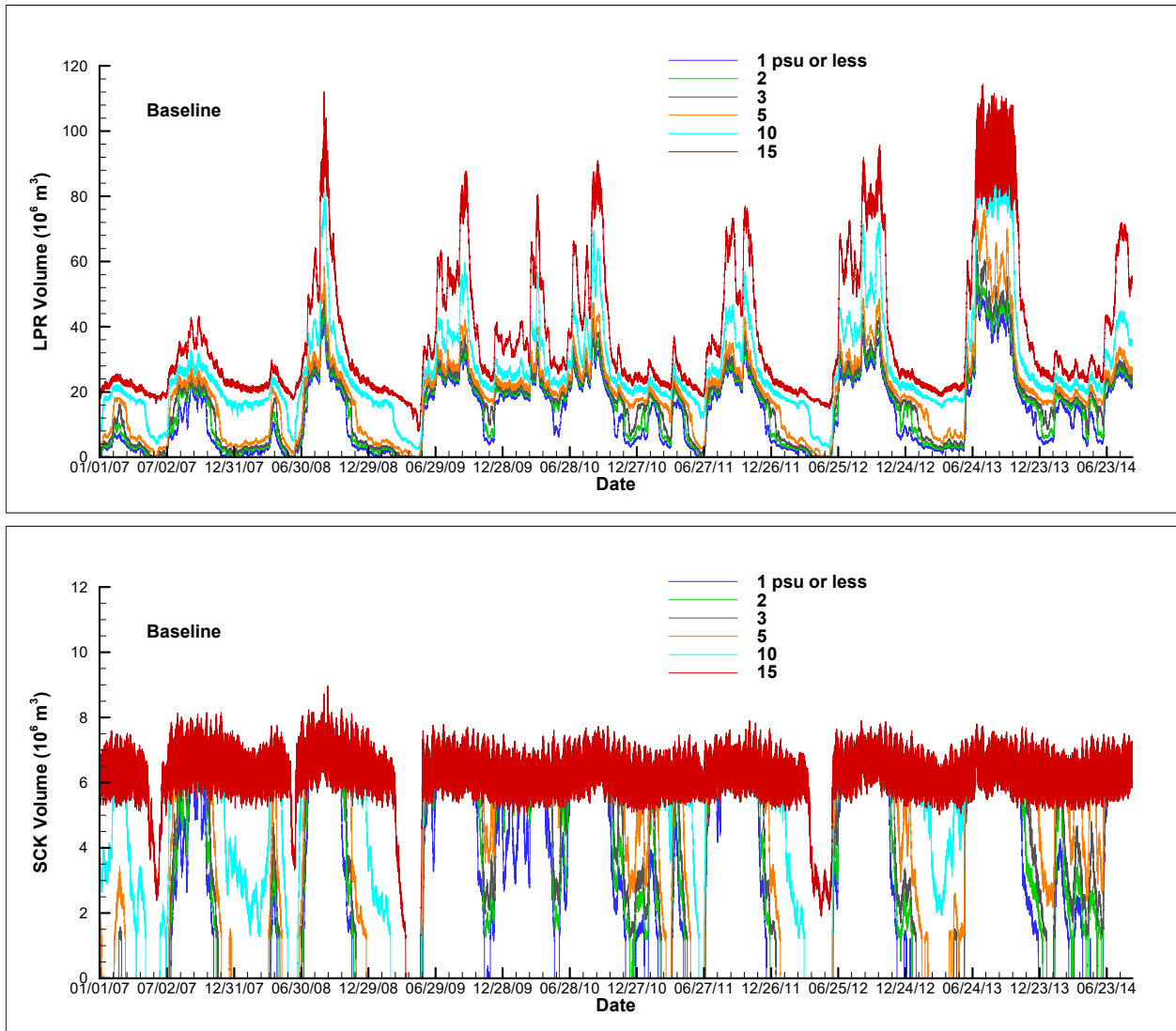


Figure 35. Water volumes for salinity $\leq 1, 2, 3, 5, 10,$ and 15 psu in the LPR (top panel) and in the LSC (bottom panel) during the simulation period of January 2007 - August 2014 for the baseline scenario.

Figure 36 shows time series of bottom area for salinity $\leq 1, 2, 3, 5, 10,$ and 15 psu in LPR (top panel) and in LSC (bottom panel) from January 2017 through August 2014 for the baseline scenario. Similar to salinity volumes shown in Figure 35, temporal variations of low salinity bottom areas in the LPR generally follows that of the freshwater inflow to the LPR. It can be seen from the figure that except for salinity $\leq 1, 2,$ and 3 psu, bottom areas for other salinity ranges contained substantial tidal signals, which were more significant than those contained in the corresponding salinity volumes. This phenomenon can be explained by the general estuarine flow pattern, with saltier water migrating at the bottom layer and directly affecting the bottom area.

Similar to salinity volumes, bottom areas for different salinity ranges exhibited dramatic variabilities in LSC because of its small water volume. If no freshwater entered LSC for certain days continuously in the dry season, no low salinity bottom area existed in the creek; however, when freshwater flow from the dam was large enough, the entire creek would be ≤ 1 psu.

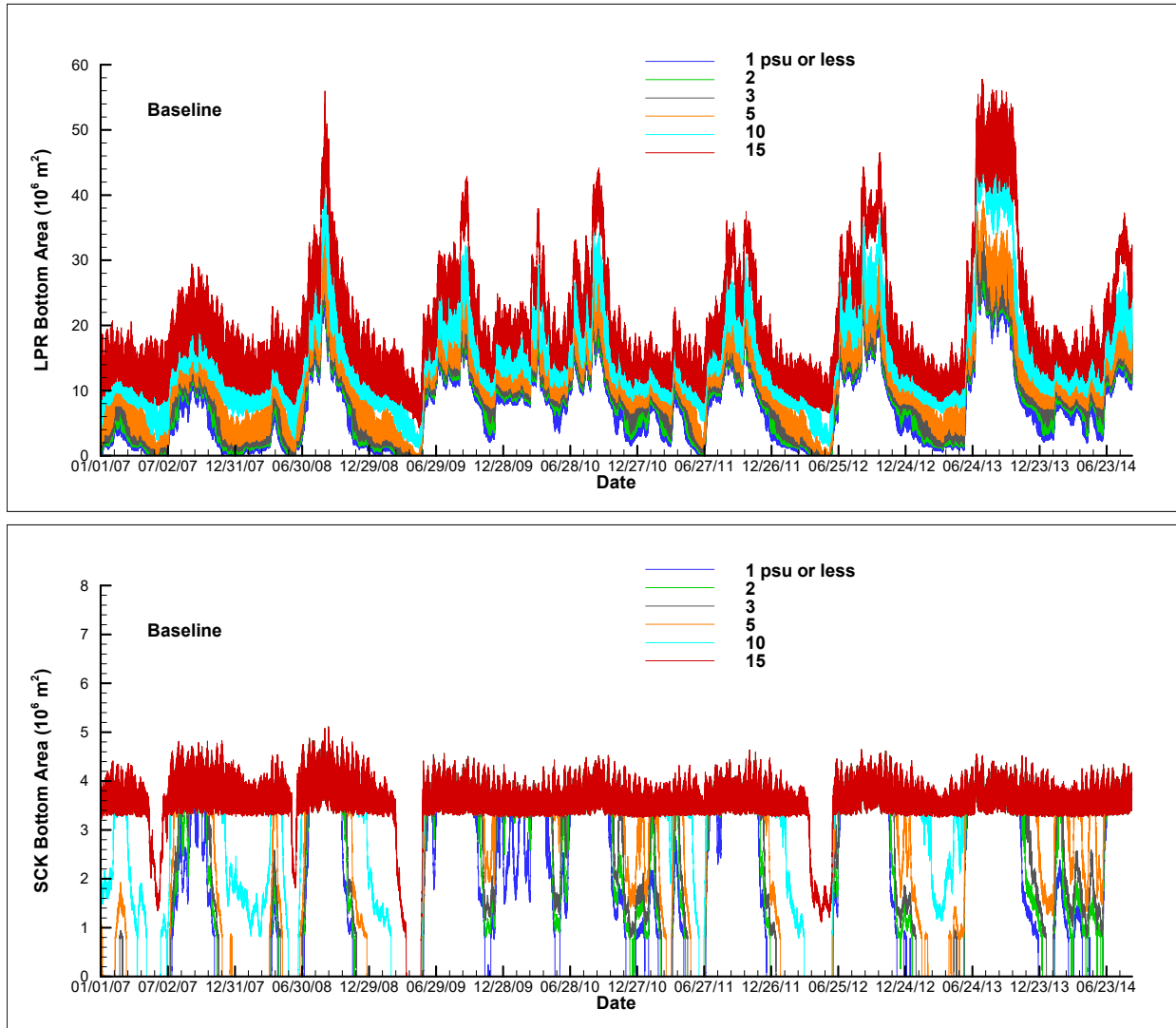


Figure 36. Bottom areas for salinity $\leq 1, 2, 3, 5, 10,$ and 15 psu in the LPR (top panel) and in the LSC (bottom panel) during the simulation period of January 2007 - August 2014 for the baseline scenario.

Figure 37 shows time series of shoreline lengths for salinity $\leq 1, 2, 3, 5, 10,$ and 15 psu in the LPR (top panel) and in the LSC (bottom panel) during January 2007 - August 2014 for the baseline scenario. It can be seen from the figure that low salinity shoreline lengths in both the LPR and LSC had large long-term variabilities during the 92-month simulation period. The short-term tidal variations were also significant for shoreline lengths of salinity $\leq 5, 10,$ and 15 psu in the LPR. The dramatic effect of freshwater flow on shoreline lengths is similar to that on salinity volumes or bottom areas in LSC.

Time series of water volumes, bottom areas, and shoreline lengths of different salinity ranges in the LPR and LSC for Scenarios 1 – 8 are similar to those shown in Figures 35 – 37 and are presented in Appendix A.

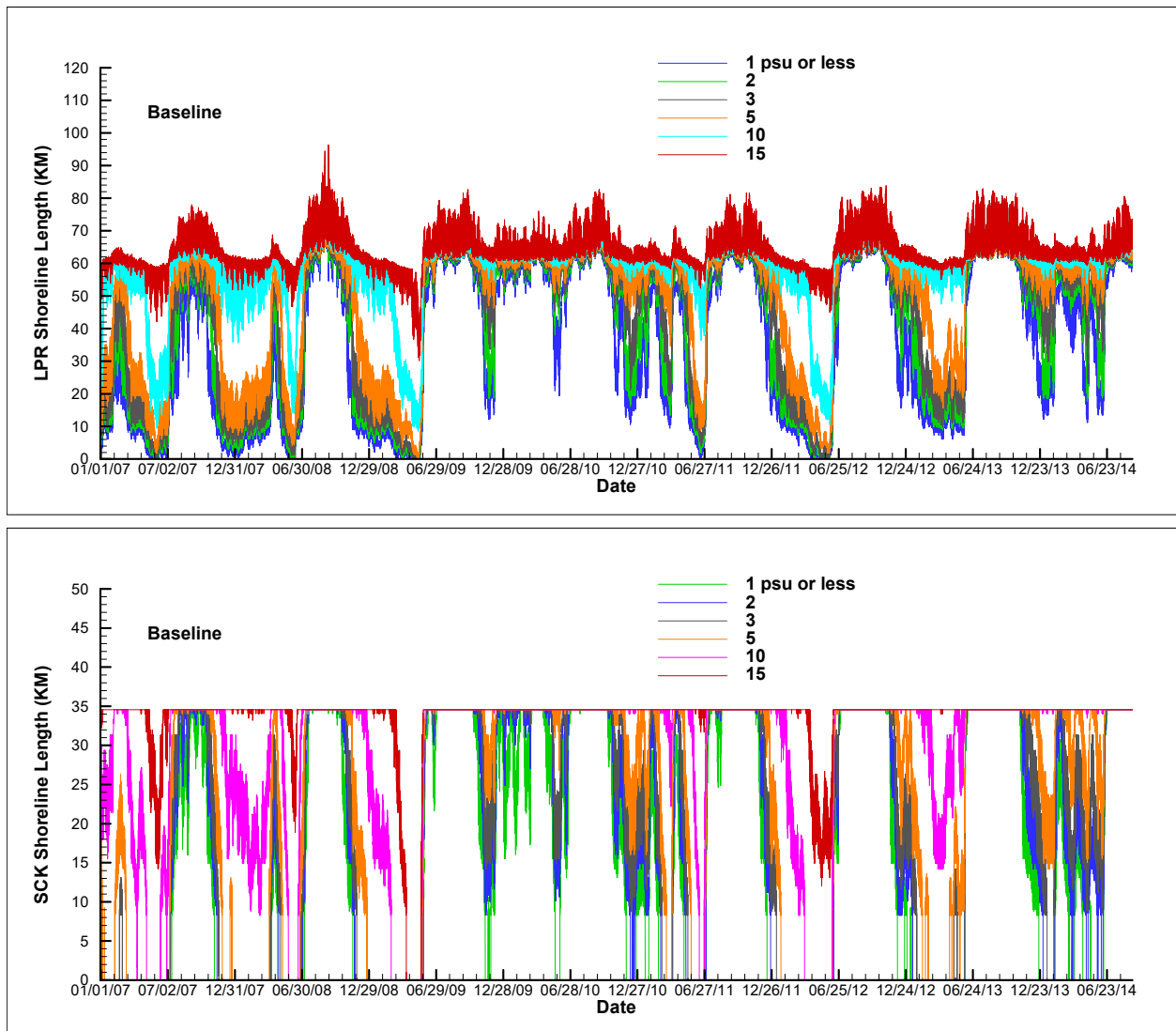


Figure 37. Shoreline lengths for salinity $\leq 1, 2, 3, 5, 10,$ and 15 psu in the LPR (top panel) and in the LSC (bottom panel) during the simulation period of January 2007 - August 2014 for the baseline scenario.

The top panel in Figure 38 compares water volumes for salinity ≤ 2 psu in the LPR during the period between January 2007 and August 2014 among the baseline scenario and the 10%, 20%, 30%, and 40% flow reduction scenarios. The middle and bottom panels in Figure 38 compare bottom areas and shoreline lengths, respectively, for salinity ≤ 2 psu in the LPR from January 2007 through August 2014 among these scenarios. For legibility, results for 5%, 15%, 25%, and 35% flow reductions are not included in the figure.

Similar comparisons of volumes, bottom areas, and shoreline lengths for salinity ≤ 1 psu during the period from January 2007 to August 2014 are shown in Figure B-1 in Appendix B,

while the volume, bottom area, and shoreline length comparisons for salinity ≤ 3 , ≤ 5 , ≤ 10 , and ≤ 15 psu in the LPR are shown in Figures B-2 – B-5, respectively.

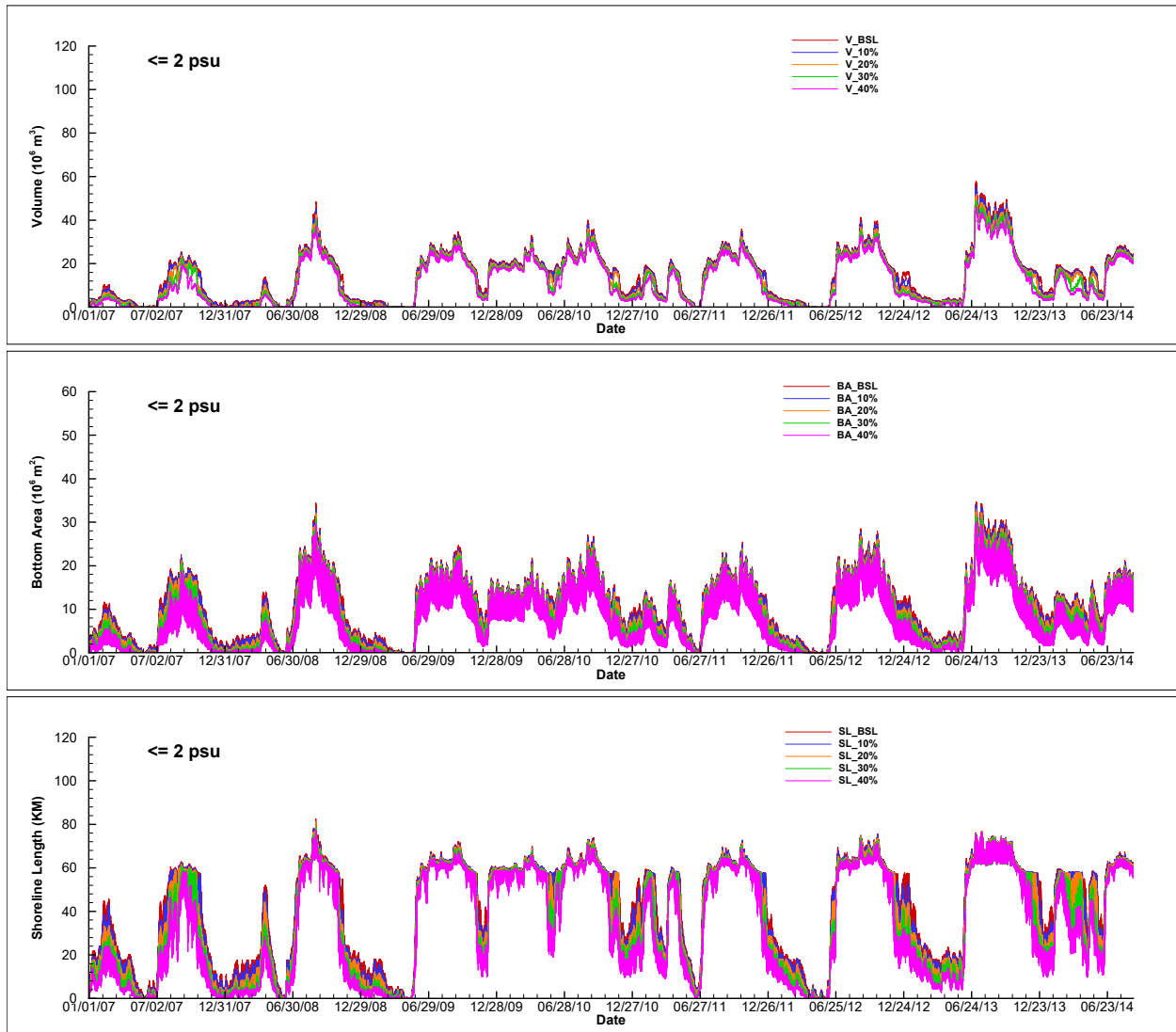


Figure 38. Comparisons of time series of water volume (top panel), bottom area (middle panel), and shoreline length (bottom panel) for salinity ≤ 2 psu in the LPR during the simulation period of January 2007 - August 2014 for different flow reduction scenarios.

Figure 39 shows comparisons of water volumes (top panel), bottom areas (middle panel), and shoreline lengths (bottom panel) for salinity ≤ 2 psu in LSC from January 2007 through August 2014 among baseline and the 10%, 20%, 30%, and 40% flow reduction scenarios. For the same reason, model results for 5%, 15%, 25%, and 35% flow reductions are not included in the figure.

As shown in Figure 39, because of its small water volume, LSC had dramatic variations of salinity habitats. During the wet seasons, the entire waterbody could be ≤ 2 psu even when the freshwater inflow was reduced by 40%. On the other hand, during the dry seasons, there was no salinity habitats ≤ 2 psu even under the baseline flow condition.

Similar comparisons of volumes, bottom areas, and shoreline lengths for salinity ≤ 12 psu in LSC from January 2007 to August 2014 are shown in Figure B-6 in Appendix B, while volume,

bottom area, and shoreline length comparisons for ≤ 3 , ≤ 5 , ≤ 10 , and ≤ 15 psu in LSC are shown in Figures B-7 – B-10, respectively.

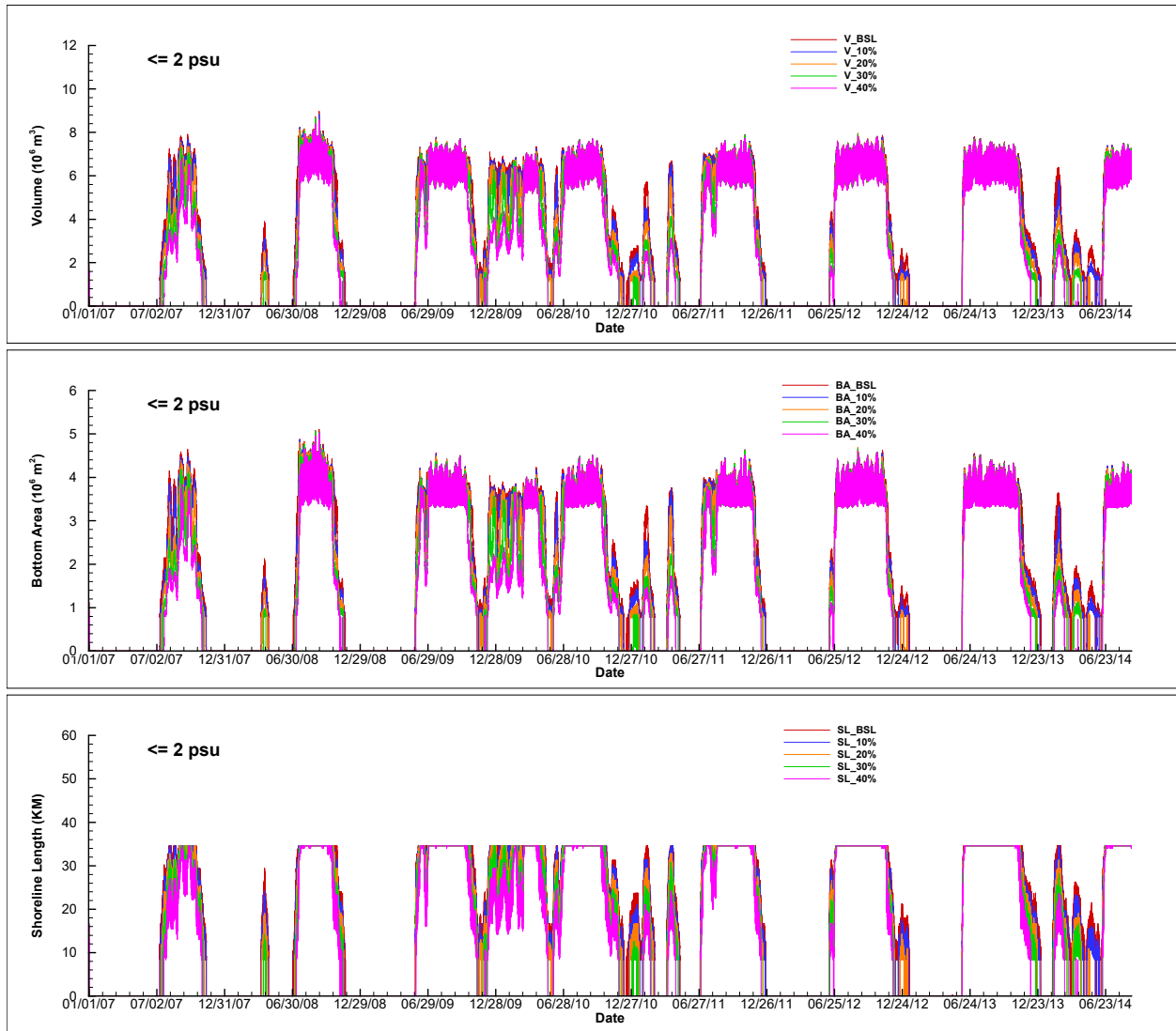


Figure 39. Comparisons of time series of water volume (top panel), bottom area (middle panel), and shoreline length (bottom panel) for salinity ≤ 1 psu in LSC during the simulation period of January 2007 - August 2014 for different flow reduction scenarios.

Figure 40 shows plots of cumulative distribution functions (CDFs) for salinity ≤ 2 psu water volumes, bottom areas, and shoreline lengths in the LPR (left three panels) and in LSC (right three panels) from January 2007 to August 2014. CDFs of water volumes, bottom areas, and shoreline lengths for salinity $\leq 1, 3, 5, 10,$ and 15 psu are plotted in Figures C-1 – C-5 in Appendix C. In these CDF graphs, areas bounded by the curves and the vertical axis (Percent) represent the 92-month averages of the corresponding salinity habitats.

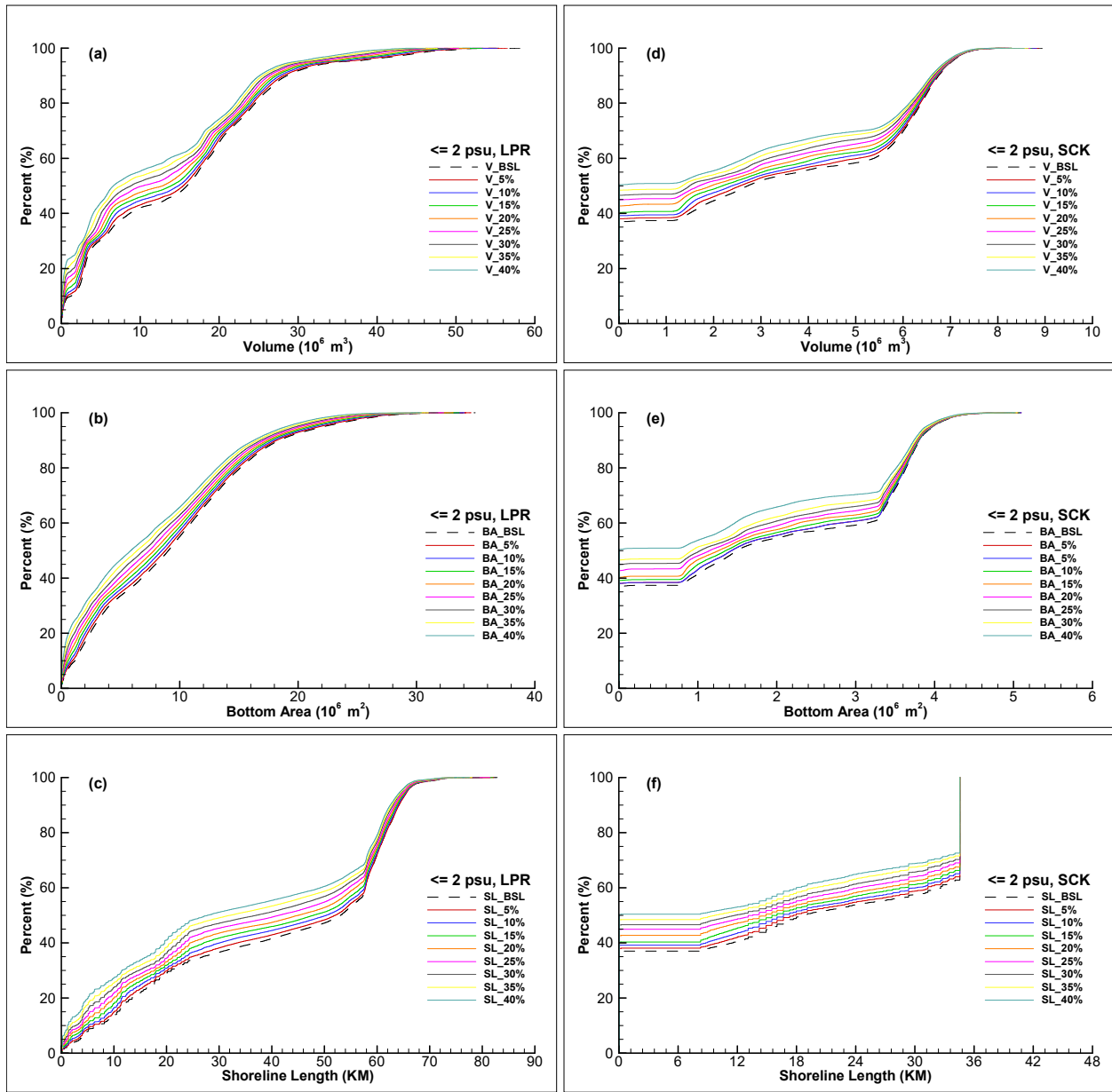


Figure 40. CDFs of ≤ 2 psu water volume (a & d), bottom area (b & e), and shoreline length (c & f) in the LPR and LSC during the simulation period of January 2007 - August 2014 for different flow reduction scenarios.

Like many other prior MFL evaluations conducted in the SWFWMD, the re-evaluations for the LPR and LSC MFLs are principally based on averages of simulated salinity habitats during certain time periods, with the considerations of the wet, dry, and extremely dry seasons. The need for the consideration of seasonality in the MFL evaluation is due to the fact that the response of salinity habitats is different for different flow regimes. Low salinity habitats are generally more sensitive to the flow reduction under the low flow condition than under the high flow condition.

Although wet and dry seasons are climatology terms strictly for the tropical climates according to the Köppen climate classification and are determined from monthly average precipitation, they have been loosely used in previous SWFWMD MFL evaluations to describe different flow regimes. In the original MFL evaluation for the LPR and LSC, three seasonal blocks were determined based upon the available historical flow data, with Block 1 being the extremely dry season, Block 2 the dry season, and Block 3 the wet season. Using the 25th and the 50th percentiles as criteria, Block 1 was found to be during April 20 - June 25 and Block 3 was during June 26 – October 26. The rest of the year, or October 27 - April 19, was Block 2 (Table 7.) With more flow data collected during recent years, the three seasonal blocks were re-calculated and updated. Blocks 1 and 3 are April 19 – June 23 and June 24 – October 21, respectively (Table 7.)

A direct way of classifying different flow regimes is to simply define daily flow below the 25th percentile as extremely low flow, above the 50th percentile as high flow, and between the 25th and 50th percentiles as low flow. Although one may call days with extremely low flows Block 1, with low flows Block 2, and with high flows Block 3, these blocks are not necessarily composed of sequential calendar days which would form a “season” or a “block.” Based on the available period-of-record flow data, 25th and 50th percentiles of the LPR flow are 297 cfs and 622 cfs, respectively. For LSC, 25th and 50th percentiles of the flow are 56 cfs and 137 cfs, respectively. Correspondingly, the flow-based blocks for extremely dry (Block 1), dry (Block 2), and wet (Block 3) conditions for both the LPR and LSC can be defined (Table 7.) Although More details on the flow-based blocks for the LPR and LSC can be found in the MFL report.

Table 7. Various definitions of blocks for the LPR and LSC.

	LPR	LSC
Block 1 (original)	April 20 - June 25	
Block 2 (original)	October 27 - April 19	
Block 3 (original)	June 26 – October 26	
Block 1 (updated)	April 19 – June 23	
Block 2 (updated)	October 22 - April 18	
Block 3 (updated)	June 24 – October 21	
Block 1 (flow-based)	$Q \leq 297$ cfs	$Q \leq 56$ cfs
Block 2 (flow-based)	$297 < Q \leq 622$ cfs	$56 < Q \leq 137$ cfs
Block 3 (flow-based)	$Q > 622$ cfs	$Q > 137$ cfs

Simulated salinity habitats were analyzed for both updated seasonal blocks and flow-based blocks; however, because the flow-based blocks are more reasonable and conservative in MFL re-evaluations for the LPR and LSC, results for flow-based blocks are discussed here.

Same as previous MFL evaluations, we defined the significant harm to the waterbody using a 15% reduction of salinity habitats as a criterium in the MFL re-evaluations for the LPR and LSC. The most sensitive salinity habitat, which is critically important for the LPR and LSC, were found to be ≤ 2 psu volume for the extremely dry and dry flow regimes (flow-based Blocks 1 and 2).

Figures 41 presents CDF plots for salinity ≤ 2 psu water volumes, bottom areas, and shoreline lengths in the LPR (left three panels) and in LSC (right three panels) during extremely dry (Block 1) days of January 2007 through August 2014. CDF plots for salinity ≤ 2 psu water volumes, bottom areas, and shoreline lengths in the LPR and in LSC during dry (Block 2) and wet (Block 3) days of the 92-month period are shown in Figures 42 and 43, respectively.

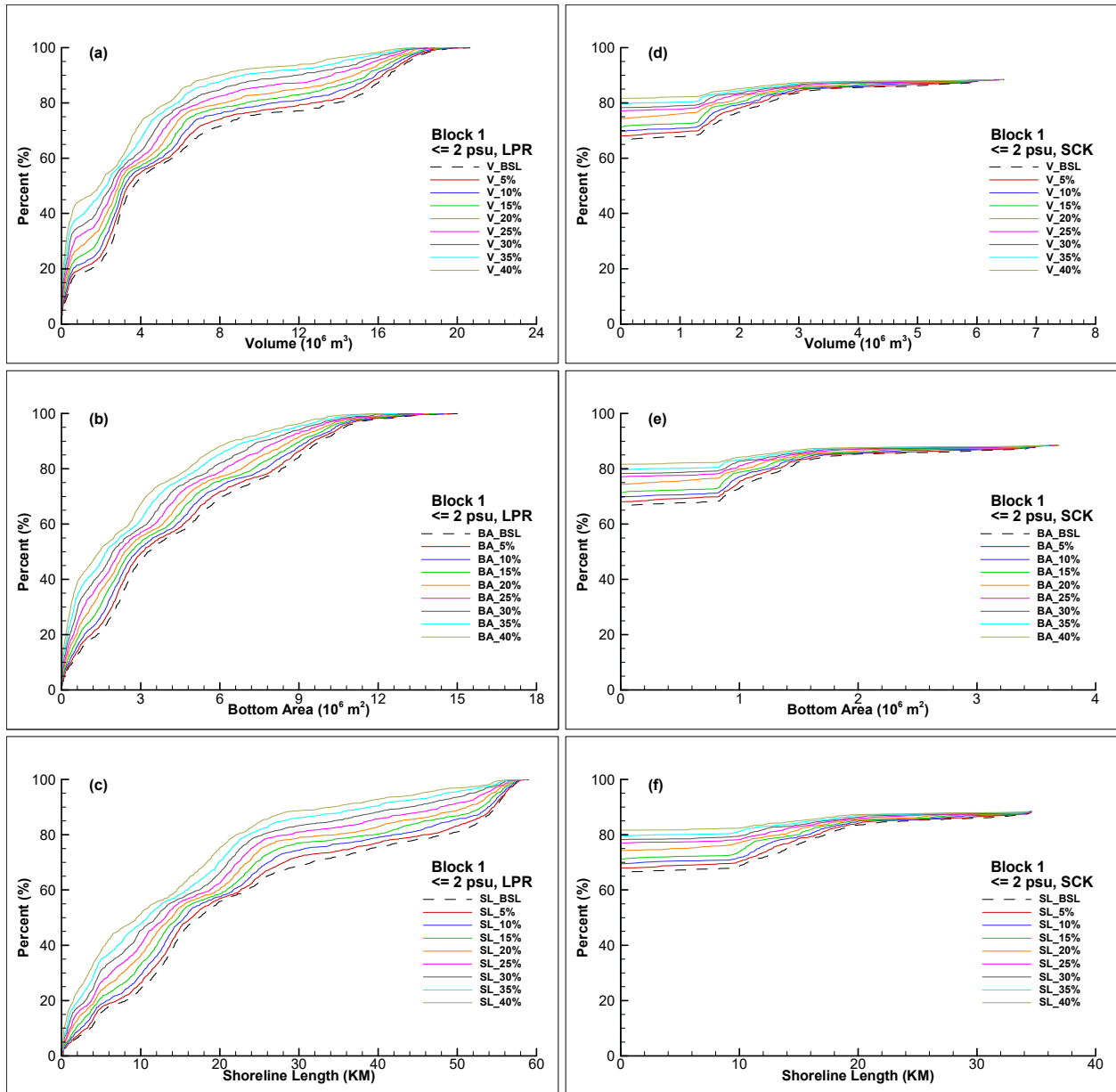


Figure 41. CDFs of ≤ 2 psu water volume (a & d), bottom area (b & e), and shoreline length (c & f) in the LPR and LSC during extremely dry (Block 1) days of January 2007 through August 2014 for different flow reduction scenarios

An examination of the CDF plots shown in Figures 41 – 43 indicates that salinity ≤ 2 psu water volumes, bottom areas, and shoreline lengths in the LPR and LSC are much more sensitive during Blocks 1 and 2 than during Block 3, as the relative reductions of the areas bounded by the curves and the vertical axes are much larger, LPR during Blocks 1 and 2 than during Block 3. As the response of low salinity habitats to flow reduction in the LPR is not necessarily the same as that in LSC, average ≤ 2 psu water volumes, bottom areas, and shoreline lengths in the two water bodies were combined before they were evaluated, because it is desirable that the same MFLs are established for the LPR and LSC. This way of evaluation is not based on any scientific reasons but

purely for the purpose of effective and reasonable regulation of freshwater resources of the LPR and LSC, from which two separate utilities withdraw water.

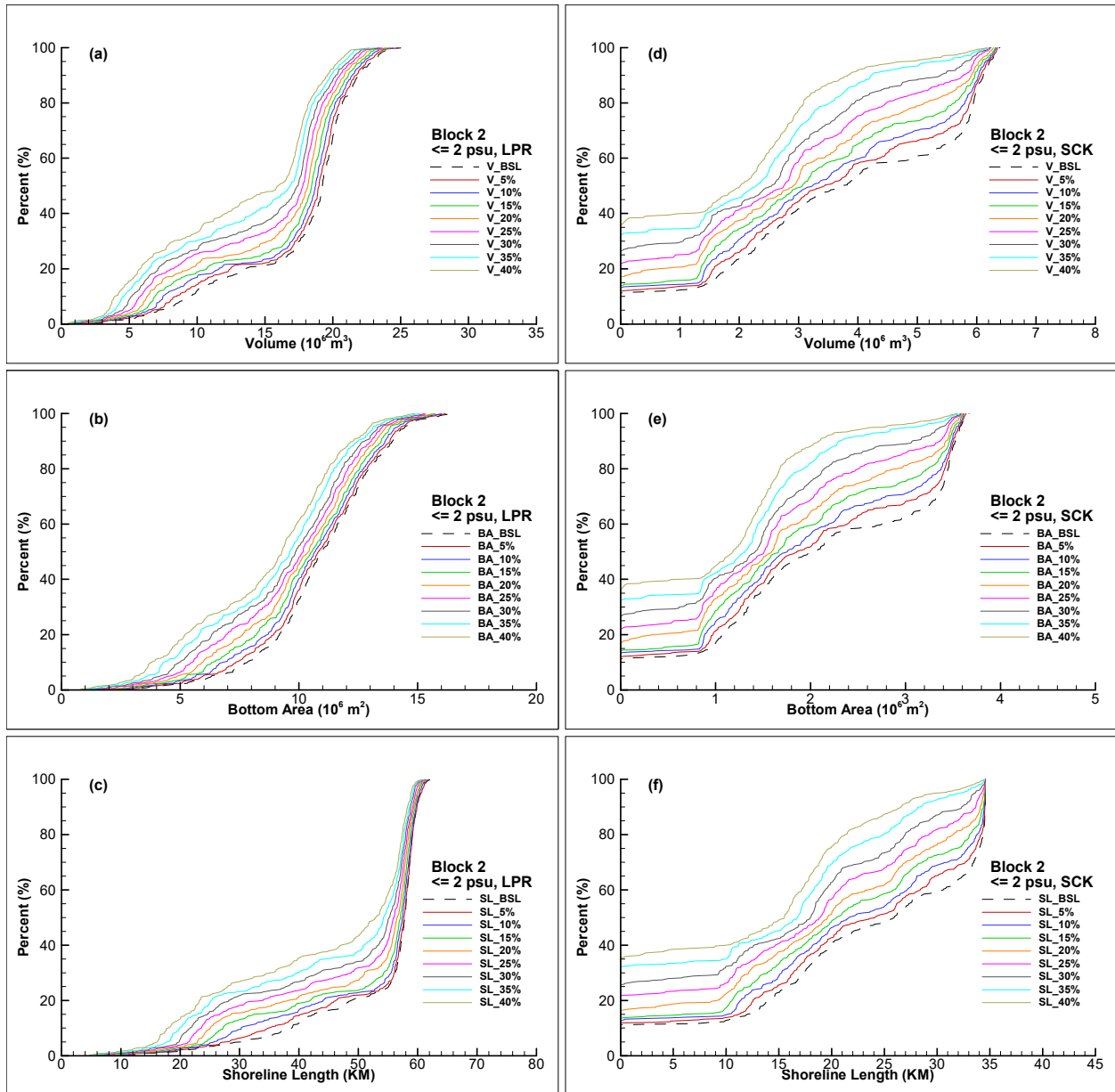


Figure 42. CDFs of ≤ 2 psu water volume (a & d), bottom area (b & e), and shoreline length (c & f) in the LPR and LSC during dry (Block 2) days of January 2007 through August 2014 for different flow reduction scenarios.

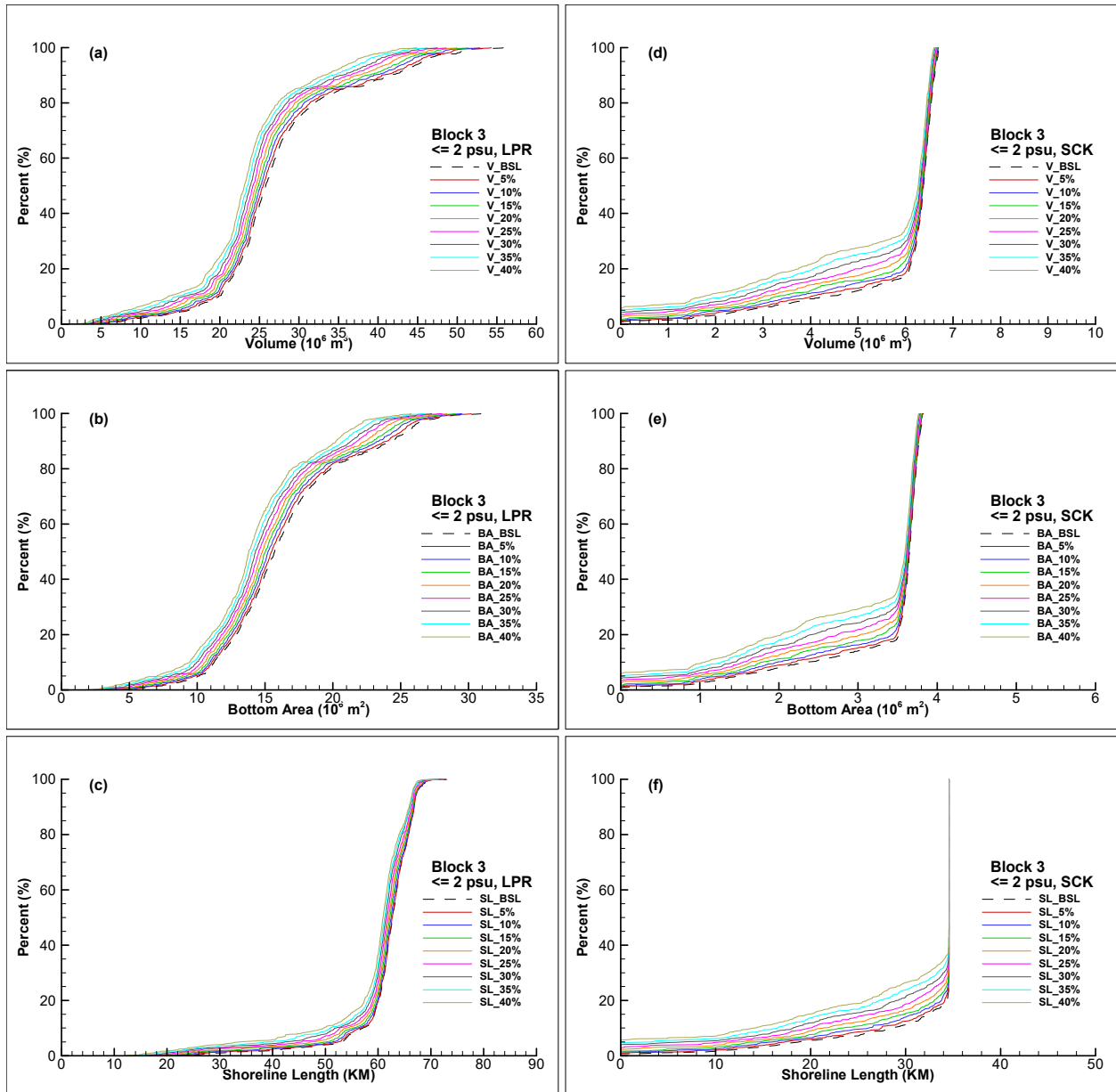


Figure 43. CDFs of ≤ 2 psu water volume (a & d), bottom area (b & e), and shoreline length (c & f) in the LPR and LSC during wet (Block 3) days of January 2007 through August 2014 for different flow reduction scenarios.

Tables 8 through 10 list combined average water volumes, bottom area, and shoreline lengths for salinity ≤ 2 psu in the LPR and LSC during extremely dry (Block 1), dry (Block 2), and wet (Block 3) days, respectively. The ≤ 2 psu salinity habitats are more sensitive to a flow reduction during Block 1 than they do during Blocks 2 and 3. Same as what was observed in the previous MFL evaluation for the LPR, ≤ 2 psu salinity volume is more sensitive to flow reductions than ≤ 2 psu bottom area, which is more sensitive than ≤ 2 psu shoreline length.

Table 8. Average water volumes, bottom areas, and shoreline lengths for salinity ≤ 2 psu under various flow reduction conditions and their ratios (in %) to the corresponding values under the baseline (BSL) flow condition during extremely dry (Block 1) days in the LPR and LSC.

Reduction Scenarios	Volume (10^6 m ³)		Bottom Area (10^6 m ²)		Shoreline (KM)	
	Value	% of BSL	Value	% of BSL	Value	% of BSL
Baseline (BSL)	6.9229		4.8457		28.3129	
5%	6.5205	94.2%	4.5962	94.9%	26.8884	95.0%
10%	6.0923	88.0%	4.3352	89.5%	25.2877	89.3%
15%	5.6556	81.7%	4.0590	83.8%	23.6636	83.6%
20%	5.1828	74.9%	3.7621	77.6%	21.8367	77.1%
25%	4.6882	67.7%	3.4690	71.6%	20.0550	70.8%
30%	4.2084	60.8%	3.1757	65.5%	18.2888	64.6%
35%	3.7193	53.7%	2.8691	59.2%	16.5347	58.4%
40%	3.2706	47.2%	2.5697	53.0%	14.7646	52.1%

Table 9. Average water volumes, bottom areas, and shoreline lengths for salinity ≤ 2 psu under various flow reduction conditions and their ratios (in %) to the corresponding values under the BSL flow condition during dry (Block 2) days in the LPR and LSC.

Reduction Scenarios	Volume (10^6 m ³)		Bottom Area (10^6 m ²)		Shoreline (KM)	
	Value	% of BSL	Value	% of BSL	Value	% of BSL
Baseline	21.3231		13.0499		76.8193	
5%	20.7449	97.3%	12.7416	97.6%	75.3034	98.0%
10%	20.1751	94.6%	12.4287	95.2%	73.5346	95.7%
15%	19.5124	91.5%	12.0738	92.5%	71.5295	93.1%
20%	18.6793	87.6%	11.6483	89.3%	69.0059	89.8%
25%	17.7890	83.4%	11.1957	85.8%	66.1598	86.1%
30%	16.9007	79.3%	10.7136	82.1%	63.1974	82.3%
35%	15.9183	74.7%	10.1719	77.9%	59.9249	78.0%
40%	14.9364	70.0%	9.6501	73.9%	56.7208	73.8%

Table 10. Average water volumes, bottom areas, and shoreline lengths for salinity ≤ 2 psu under various flow reduction conditions and their ratios (in %) to the corresponding values under the BSL flow condition during wet (Block 3) days in the LPR and LSC.

Reduction Scenarios	Volume (10^6 m ³)		Bottom Area (10^6 m ²)		Shoreline (KM)	
	Value	% of BSL	Value	% of BSL	Value	% of BSL
Baseline	33.5729		19.9592		94.7239	
5%	33.0597	98.5%	19.6818	98.6%	94.4041	99.7%
10%	32.4803	96.7%	19.3713	97.1%	93.8431	99.1%
15%	31.9167	95.1%	19.0568	95.5%	93.2207	98.4%
20%	31.3060	93.2%	18.7246	93.8%	92.4946	97.6%
25%	30.6381	91.3%	18.3533	92.0%	91.6847	96.8%
30%	30.0189	89.4%	18.0032	90.2%	90.7151	95.8%

35%	29.3111	87.3%	17.6091	88.2%	89.8268	94.8%
40%	28.5793	85.1%	17.2036	86.2%	88.7122	93.7%

From Tables 8 – 10, it could be determined that in order to protect the LPR and LSC from significant harms, flow reduction should not be larger than 13% during the extremely low flow days and 23% during low flow days. During high flow days, flow reduction is allowed up to 40% without causing sensitive salinity habitats to decrease 15% or more. More details on how model results of salinity habitats were analyzed and how MFLs for the LPR and LSC were determined can be found in the MFL report.

With these proposed MFLs for the LPR and LSC, it is meaningful to examine how the MFLs would affect ≤ 2 psu salinity habitats if withdrawals would be carried out with the rates of the MFLs. Figure 44 shown in the next page compares time series of ≤ 2 psu water volumes, bottom area, and shoreline length in the LPR during January 2007 - August 2014 for the baseline scenario to those for the MFL scenario, in which freshwater flows to the LPR and LSC were reduced by 13% during the extremely low flow days, by 23% during low flow days, and by 40% during high flow days.

Comparisons of time series of ≤ 2 psu water volume, bottom area, and shoreline length in LSC during January 2007 - August 2014 for the baseline scenario to those for the MFL scenario are plotted in Figure 45. As observed in Figures 44 and 45, losses of ≤ 2 psu volume, bottom area, and shoreline for MFL scenario, in comparison with the salinity habitats for the baseline scenario, varied with time; however, the variabilities of the salinity habitat losses were generally smaller than the short-term variabilities and much smaller than the long-term variabilities of the salinity habitats themselves.

Because the MFL was determined based on the criterium of $\leq 15\%$ reduction of average salinity habitats over all high flow, low flow, and extremely low flow days, it should not be a surprise that the 15% criterium is violated many times if Figures 44 and 45 are examined in an hourly or daily time scale. It is assumed that a temporary short-term violation of the 15% criterium is acceptable as far as the low salinity habitats do not experience 15% or more reduction over a long period of time.

Figure 46 are plots of CDFs of ≤ 2 psu water volume, bottom area, and shore length in the LPR and LSC for the baseline and MFL scenarios. Same as those shown in Figure 40, CDFs for the baseline scenario are plotted with black dashed lines. It should be noted that in the CDF plots, data points for the same percentage may not occur at the same time points.

Because the area bounded by the CDF curve and the vertical axis represents the average value of the corresponding salinity habitat, reductions of ≤ 2 psu salinity habitats in the LPR and LSC due to the allowable withdrawals in different flow regimes are clearly demonstrated in Figure 46. In LSC, it can be seen from the right three panels of Figure 46 that the occurrence of non-existence of ≤ 2 psu habitats is roughly increased by 5% with the withdrawal rates of proposed MFLs for the LPR and LSC.

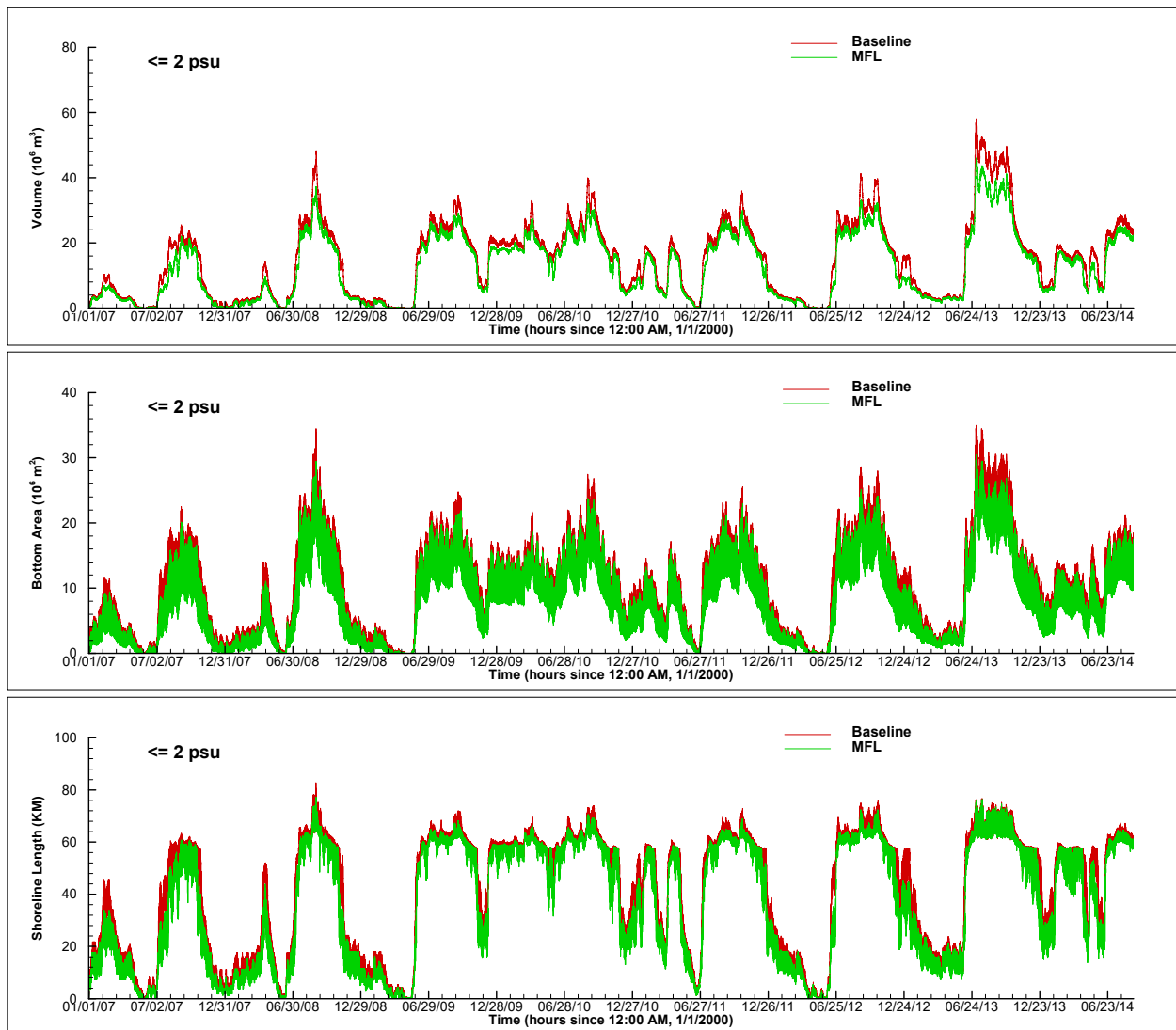


Figure 44. Comparisons of time series of water volume (top panel), bottom area (middle panel), and shoreline length (bottom panel) for salinity ≤ 2 psu in the LPR during the simulation period of January 2007 - August 2014 for the baseline and MFL scenarios.

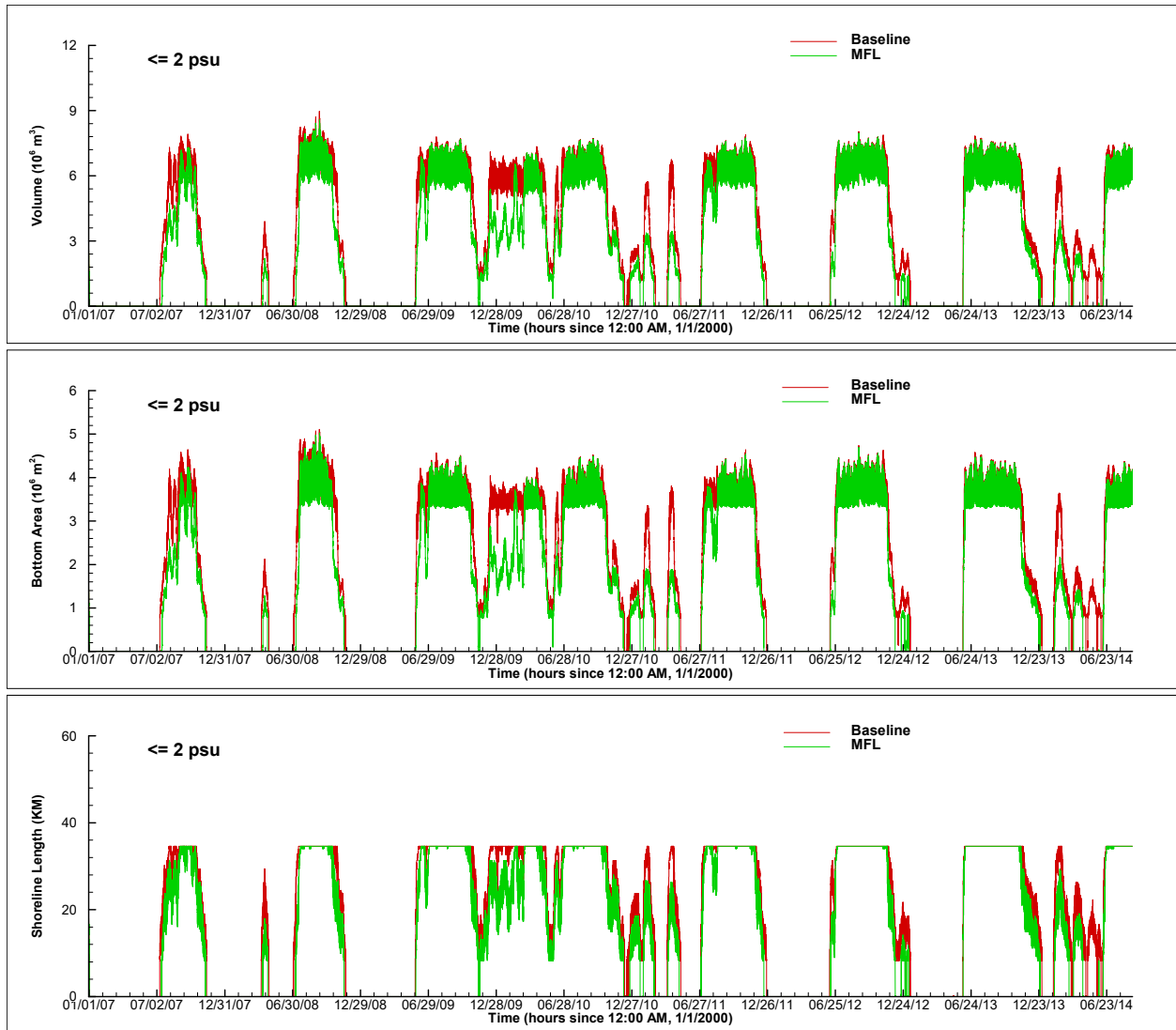


Figure 45. Comparisons of time series of water volume (top panel), bottom area (middle panel), and shoreline length (bottom panel) for salinity ≤ 2 psu in LSC during the simulation period of January 2007 - August 2014 for the baseline and MFL scenarios.

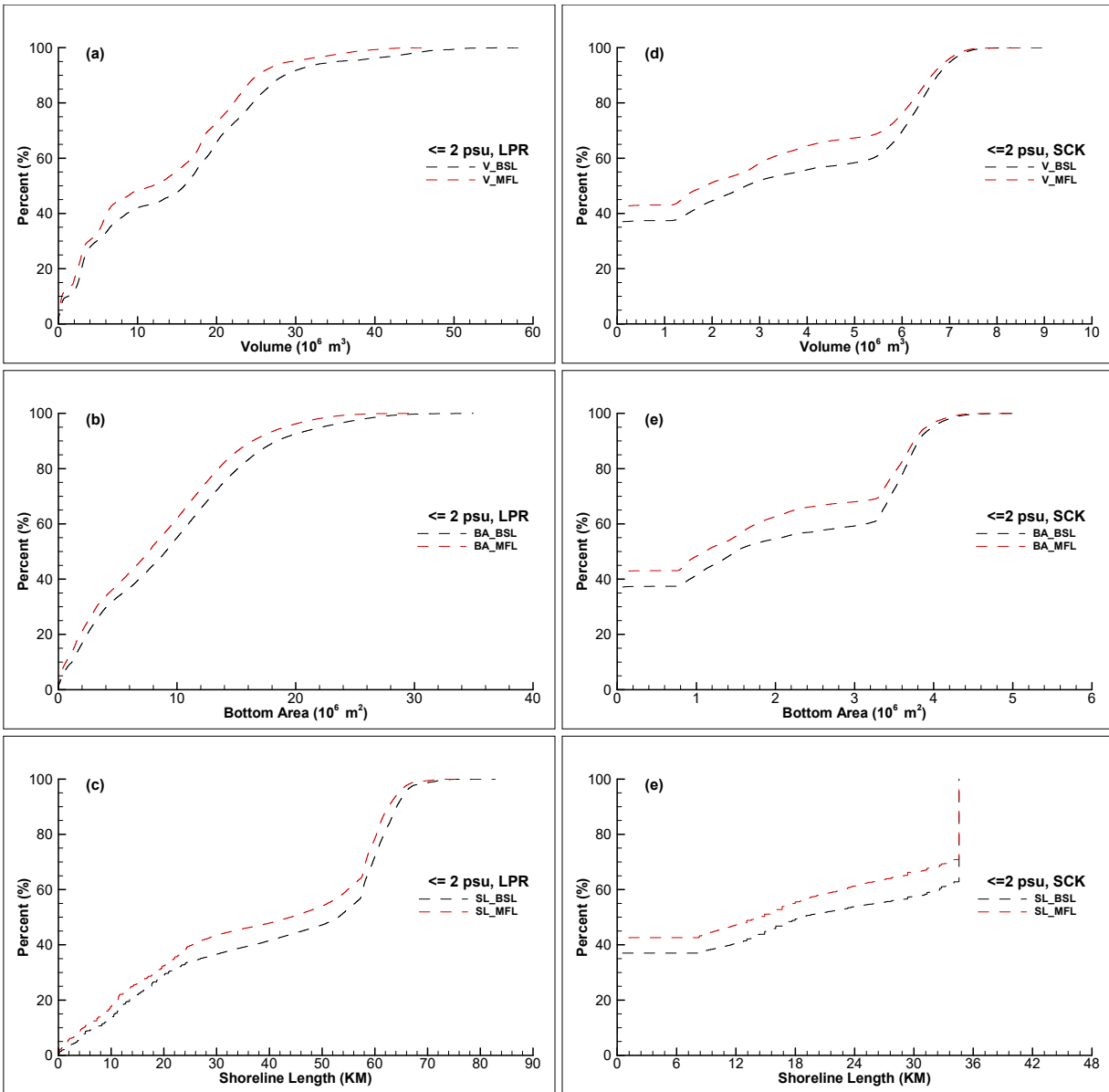


Figure 46. CDFs of ≤ 2 psu water volume (a & d), bottom area (b & e), and shoreline length (c & f) in the LPR and LSC during the simulation period of January 2007 - August 2014 for the baseline (black dashed lines) and MFL (red dashed lines) scenarios.

4.3 Consideration of Sea Level Rise

Sea level rise (SLR) scenarios were considered in the MFL re-evaluations for the LPR and LSC. Similar to previous MFL evaluations for Crystal River/Kings Bay and for Manatee/Bradens Rivers, sea level conditions in 2035 were evaluated, because the SWFWMD's regional water supply planning horizon ends in 2035. Estimates for the SLR at a NOAA station at the mouth of Caloosahatchee River near Ft. Myers, which is very close to the open boundaries of the simulation domain, can be obtained from Sea-Level Change Curve Calculator provided by the United States Army Corps of Engineers (USACE) http://corpsmapu.usace.army.mil/rccinfo/slc/slcc_calc.html

At the website, one has an option to choose from several scenario sources. In the first draft of the report, USACE 2013 was chosen for the SLR scenario source and the low, intermediate, and high SLR estimates during 2010 and 2035 were estimated at 0.20', 0.33', and 0.76' (or 6.096 cm, 10.058 cm, and 23.165 cm), respectively at the NOAA Ft. Myers station. Following a suggestion by a review panelist, NOAA's results of US Global Change Research Program 2017 (Sweet et al., 2017, also referred as NOAA et al. 2017 at the USACE website) was used to estimate low, intermediate, and high SLRs, because NOAA et al 2017 is newer than USACE 2013. It was found that the NOAA et al. 2017 SLRs are generally higher than the USACE 2013 SLRs by 50% - 106% and the low, intermediate, and high SLRs between 2010 and 2035 based on NOAA et al. 2017 are 0.38', 0.68', and 1.14' (11.58 cm, 20.57 cm, and 34.75 cm), respectively at the NOAA Ft. Myers station.

In the SLR model runs, 11.58 cm, 20.57 cm, and 34.75 cm were added to the water level boundary conditions at the open boundaries for the entire 92-month simulation period for the low, intermediate and high SLR estimates, respectively. The added layer of water is assumed to have the same salinity and temperature values as the top-layer salinity and temperature during the 92-month simulation period. The modified boundary conditions at these open boundaries were then used to drive the model to simulate effects of low, intermediate, and high SLR estimates on salinity habitats in the LPR and LSC.

Adding the SLR estimate to the water level at the open boundary is a simple but very rough way of considering effects of SLR on salinity habitats in the estuary. This approach only takes into account the direct effects of increased sea level on the estuary, which will be deeper than before and thereby has less bottom friction, allowing the salt wedge to migrate further upstream. Nevertheless, there are many other factors that are associated with SLR but not included in the consideration of its effects on salinity habitats. These other factors may include altered rain pattern in the region and different salinity and temperature characteristics in the GOM.

The SLR runs were conducted for the baseline flow scenario (baseline with SLRs) and the MFL flow scenario (MFL with SLRs.) Similar to the flow reduction scenario runs, simulated results of salinity habitats are presented with plots of time series and CDFs. Figures 47 – 49 are time series of water volume, bottom area, and shoreline length, respectively, for salinity $\leq 1, 2, 3, 5, 10,$ and 15 psu in the LPR and LSC for the baseline flow scenario with the intermediate SLR estimate. Although the simulation period was during 2007 – 2014, it is expected that tides used to drive the model at the open boundaries represent those during 2031 – 2039 if the intermediate SLR occurs.

By comparing Figure 47 to Figure 35, one can see that effects of SLR on salinity volumes are complicated. Water volumes for different salinity ranges have different responses to the SLR, and the SLR effects on salinity volumes also depend on the flow regime and the physical characteristics of the estuary. In the LPR, low salinity volumes generally decrease with an intermediate SLR during low or extremely low flow days. Nonetheless, low salinity volumes in the LPR can either increase or decrease during high flow days, depending on how high the flow reaches on the day and the flow conditions of preceding days. In LSC, while low salinity volumes decrease more dramatically during low or extremely low flow days due to the SLR, they can also increase during most of high flow days.

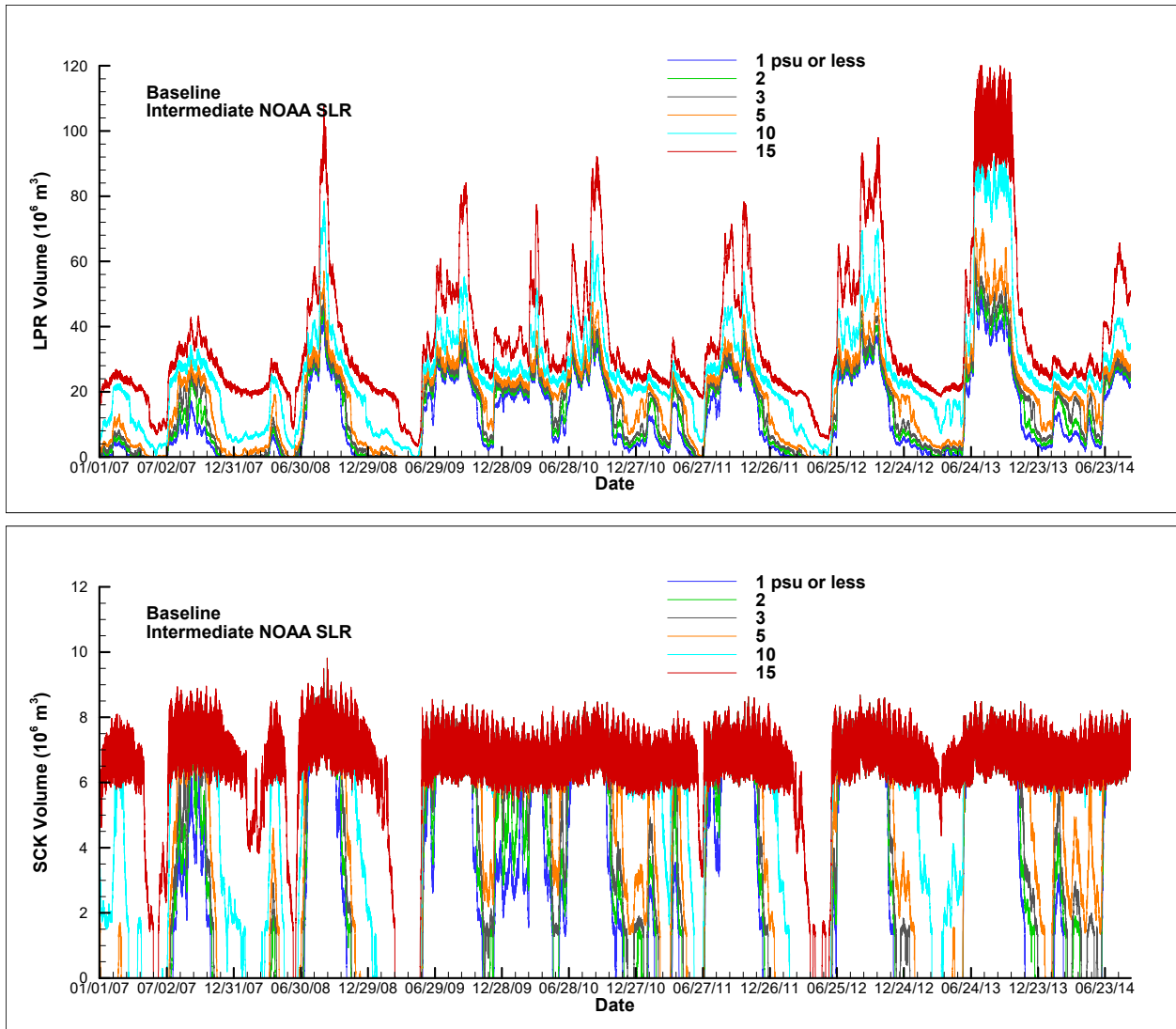


Figure 47. Water volumes for salinity $\leq 1, 2, 3, 5, 10,$ and 15 psu in the LPR (top panel) and in the LSC (bottom panel) during the simulation period of January 2007 - August 2014 for the baseline scenario with the intermediate SLR estimate.

Similar SLR effects on bottom areas as those on water volumes for different salinity ranges in the LPR and LSC can be seen by comparing Figure 48 to Figure 36. A comparison of the top panels of Figure 37 and 49 shows that for shoreline lengths in the LPR, a SLR will cause decreases of low salinity habitats almost all the time except for occasional small increases during high flow days. In LSC, a SLR will cause shorelines to decrease for all six salinity ranges, as shown in the figures.

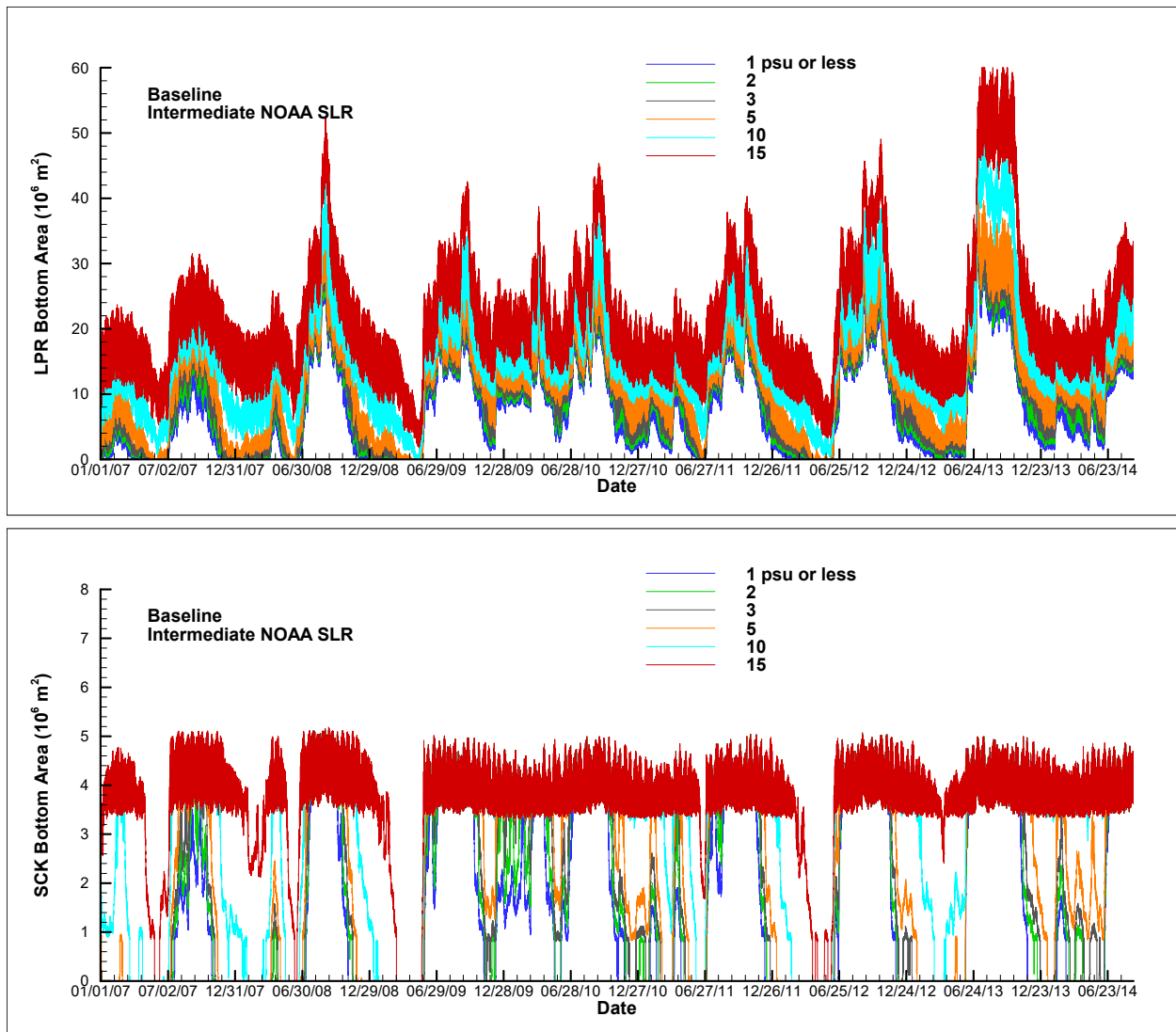


Figure 48 Bottom areas for salinity $\leq 1, 2, 3, 5, 10,$ and 15 psu in the LPR (top panel) and in LSC (bottom panel) during the simulation period of January 2007 - August 2014 for the baseline scenario with the intermediate SLR estimate.

Time series of water volume, bottom area, and shoreline length for the baseline scenarios with the high and low SLR estimates are included in Appendix D. Time series of water volume, bottom area, and shoreline length for the MFL scenarios with the high, intermediate, and low SLR estimates are also included in Appendix D. More discussions on the SLR effects on salinity habitats for both the baseline and MFL scenarios can be found in the MFL report.

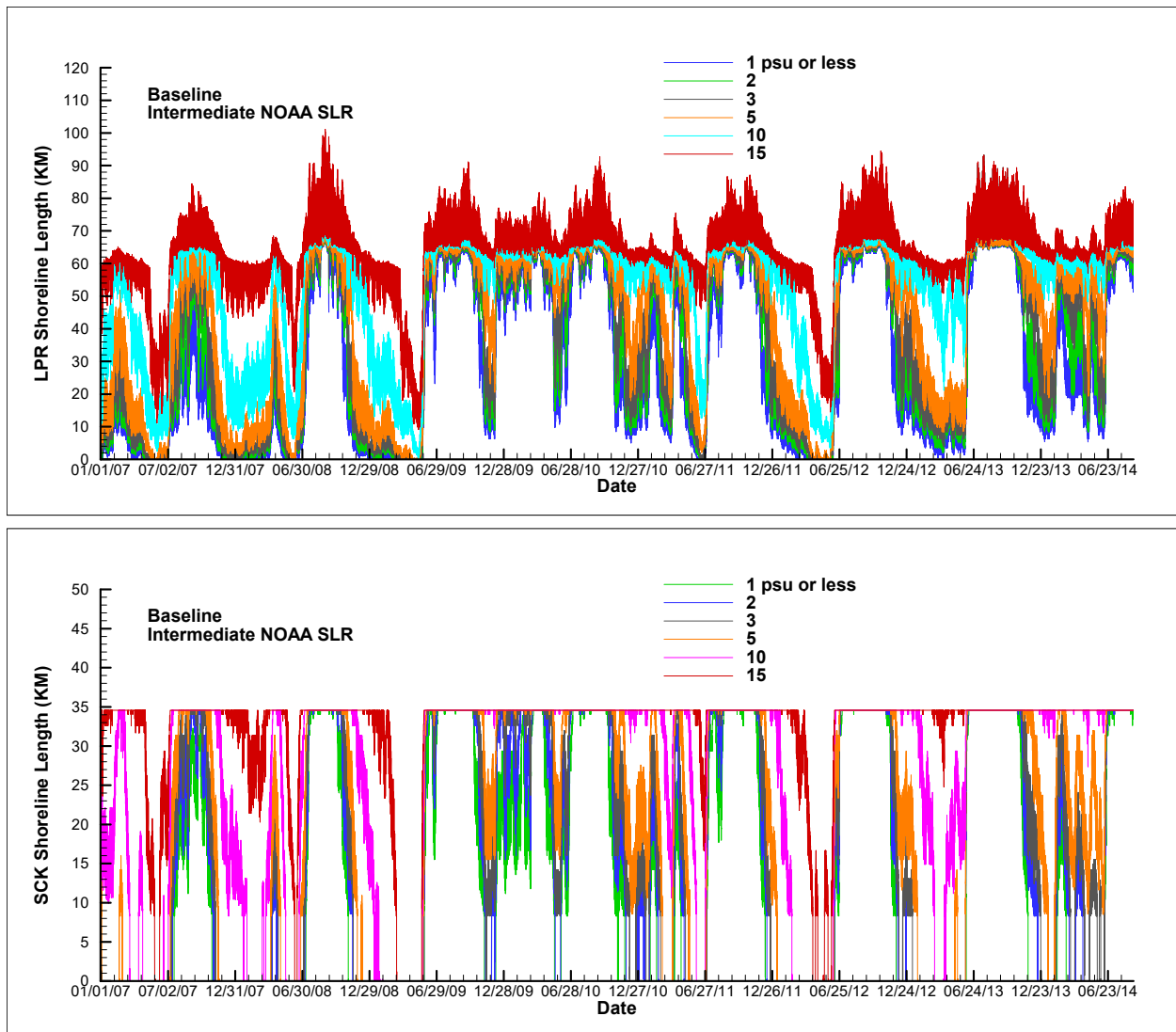


Figure 49. Shoreline lengths for salinity $\leq 1, 2, 3, 5, 10,$ and 15 psu in the LPR (top panel) and in LSC (bottom panel) during the simulation period of January 2007 - August 2014 for the baseline scenario with an intermediate SLR estimate.

The overall effects of MFL and SLR on salinity habitats can be clearly illustrated with CDF graphs. Figures 50 are CDF plots of ≤ 2 psu water volume, bottom area, and shoreline length in the LPR (left panels) and LSC (right panels) for the baseline and MFL scenarios with and without the high, intermediate, and low SLRs during the extremely dry (Block 1) days of the 92-month simulation period. Similar CDF plots during dry (Block 2) and wet (Block 3) days are shown in Figures 51 and 52, respectively.

By comparing CDF curves for ≤ 2 psu salinity habitats for the baseline and MFL scenarios with any SLRs in Figures 50 - 52, it can be observed that because MFLs were evaluated and determined for each flow-based blocks, relative reductions of ≤ 2 psu salinity habitats for the three flow blocks are similar. The CDF plots in these figures further confirm the above analysis with regard to the effects of SLRs on low salinity habitats, even though only ≤ 2 psu CDFs are shown. From Figures 50 - 52, one can see that relative reductions of salinity habitats during Block 3 are smaller than those during Blocks 1 and 2. As mentioned before, during Block 3, a 40% reduction

of flow generally does not cause significantly large decreases of ≤ 2 psu salinity habitats. Block 3 is the season when the proposed MFL is likely valid even under the high SLR condition. From Figure 52, it can be seen that a SLR actually causes ≤ 2 psu salinity habitats to be redistributed and even to increase.

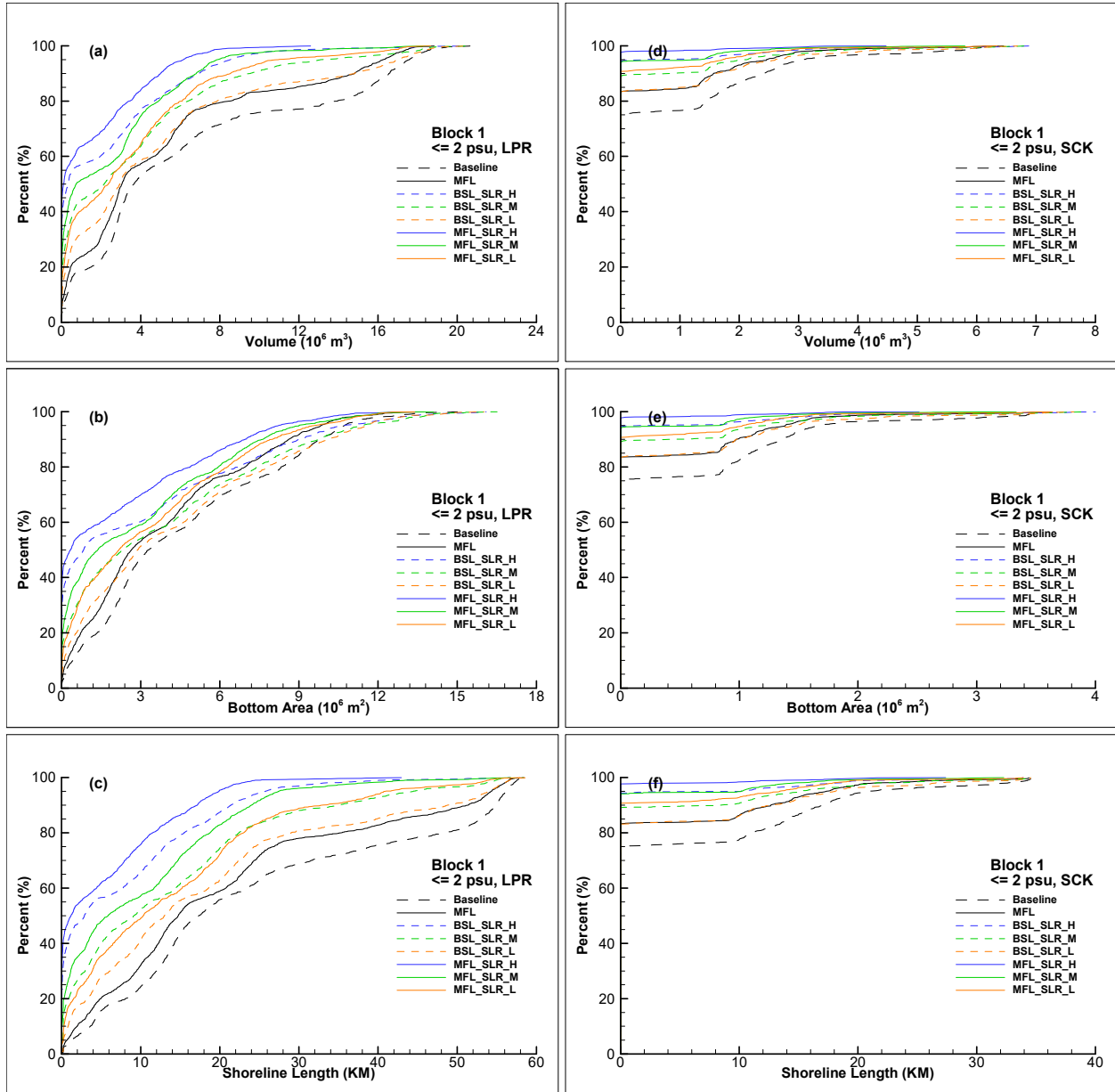


Figure 50. CDFs of ≤ 2 psu water volume (a & d), bottom area (b & e), and shoreline length (c & f) in the LPR and LSC during extremely dry (Block 1) days of January 2007 - August 2014 for the baseline flows, proposed MFLs, baseline flows with high, intermediate, and low SLRs, and MFLs with high, intermediate, and low SLRs.

Proposed MFLs under the three SLR conditions would cause similar reductions of ≤ 2 psu salinity habitats in the LPR and LSC as those caused by MFLs under the zero SLR (baseline) condition during Block 1; however, proposed MFLs under the three SLR conditions have different

effects on ≤ 2 psu salinity habitats from those during Blocks 2 and 3. During Block 2, SLRs have the highest influence on the reduction of ≤ 2 psu salinity habitats when the MFLs occur. Most significantly, medians of ≤ 2 psu volume, bottom area, and shoreline length will be reduced greatly by a 23% reduction of freshwater flow under the intermediate and high SLR conditions during Block 2.

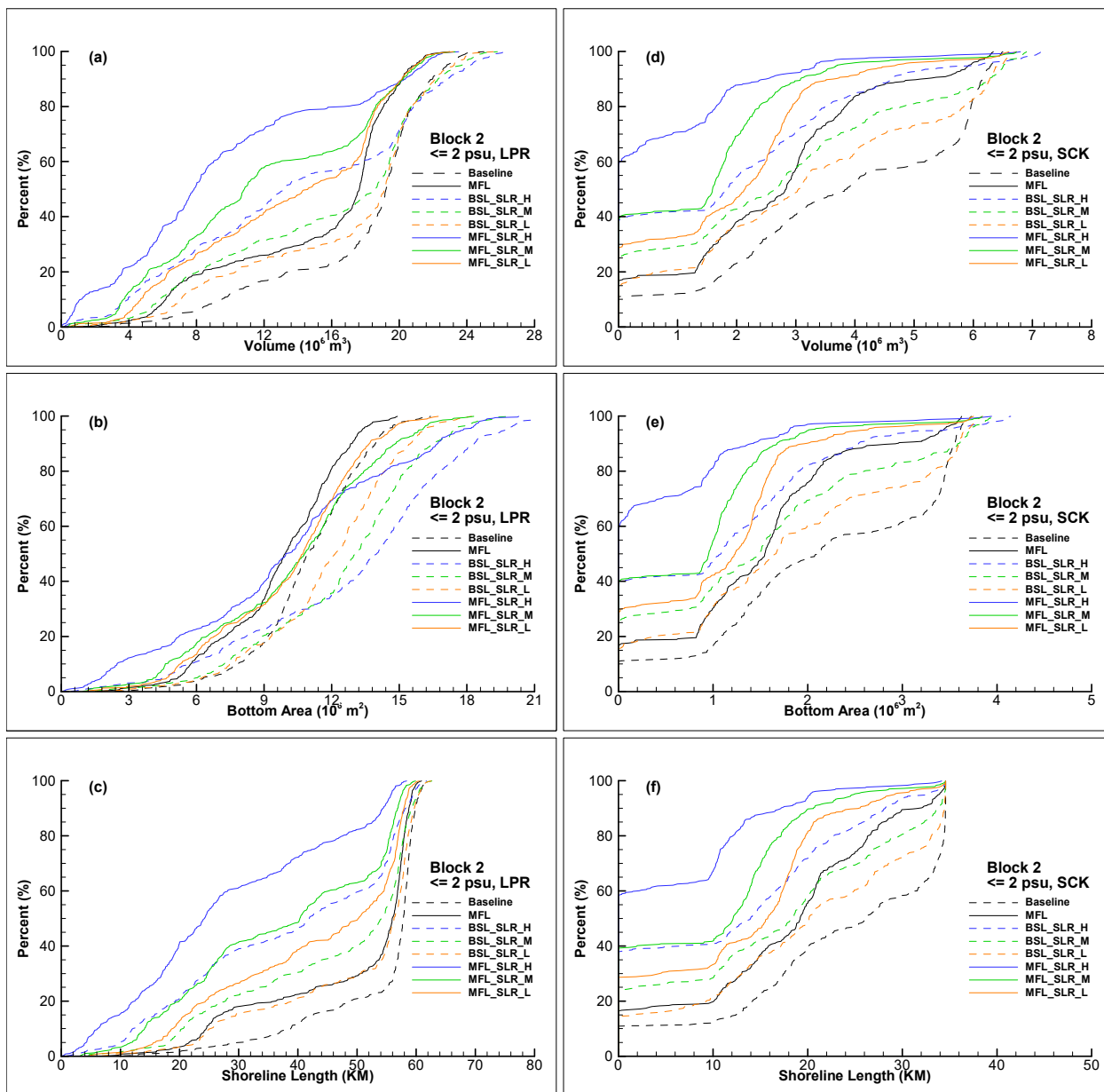


Figure 51. CDFs of ≤ 2 psu water volume (a & d), bottom area (b & e), and shoreline length (c & f) in the LPR and LSC during dry (Block 2) days during January 2007 - August 2014 for the baseline flows, proposed MFLs, baseline flows with high, intermediate, and low SLRs, and MFLs with high, intermediate, and low SLRs.

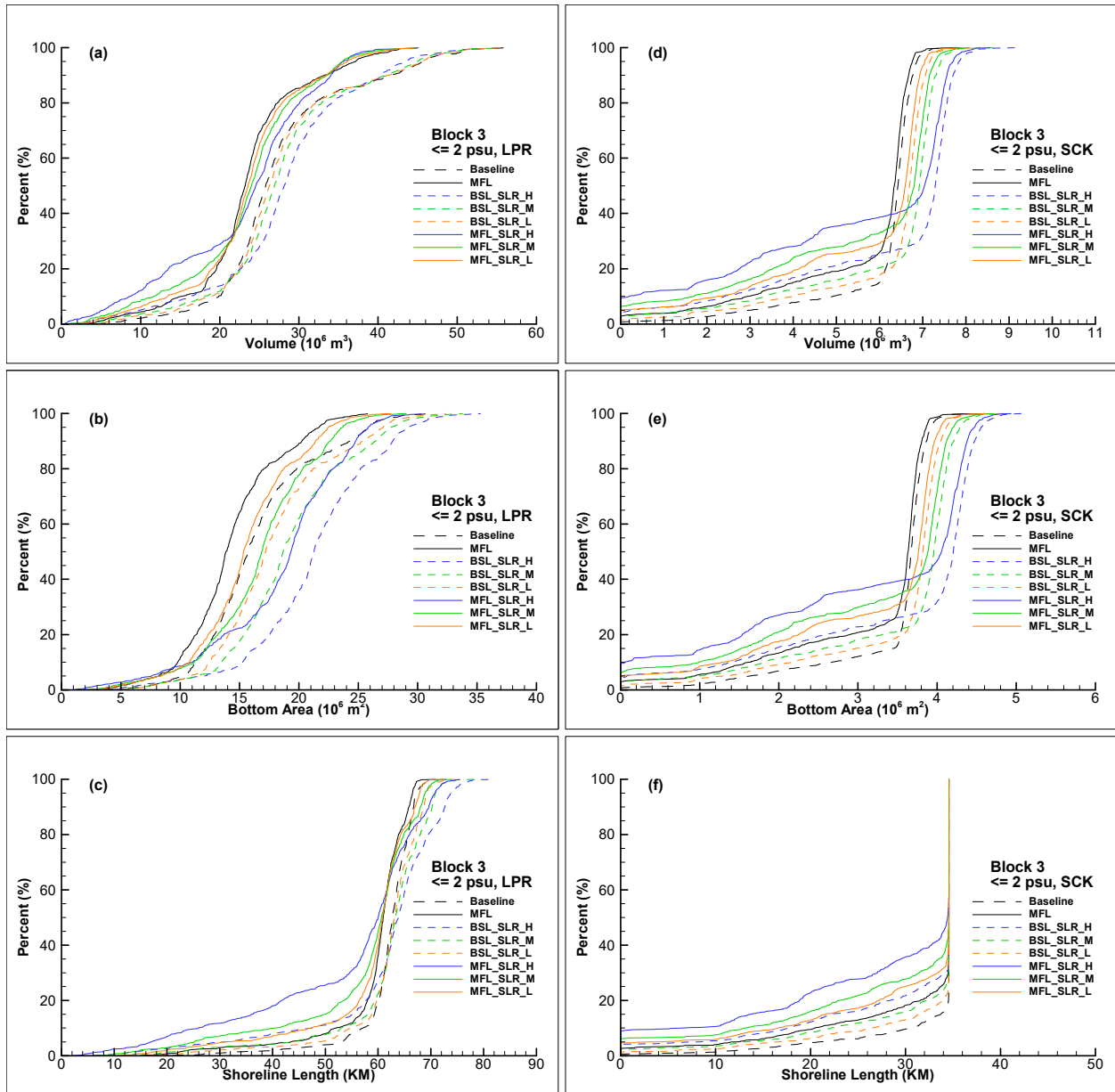


Figure 52. CDFs of ≤ 2 psu water volume (a & d), bottom area (b & e), and shoreline length (c & f) in the LPR and LSC during wet (Block 3) days during January 2007 - August 2014 for the baseline flows, proposed MFLs, baseline flows with high, intermediate, and low SLRs, and MFLs with high, intermediate, and low SLRs.

CDF plots for other salinity ranges of water volume, bottom areas, and shoreline lengths in the LPR and LSC for the baseline and MFL flows, both with and without the low, intermediate, and high SLR estimates, are included in Appendix E. More details about effects of SLR on the MFL evaluation are included in the MFL report.

Quantification of the relative reductions of ≤ 2 psu salinity habitats caused by MFLs under the three SLR conditions are listed in Tables 11 -13. In Table 11, during the extremely dry season, the proposed 13% flow reduction would cause ≤ 2 psu volume, bottom area, and shoreline length

to be reduced more than 15% from their respective values with baseline flows under the high, intermediate, and low SLR conditions. During the dry season (Table 12), MFLs would also cause more than 15% reduction of ≤ 2 psu salinity habitats compared with those with baseline flows under the high, intermediate, and low SLR conditions, though the percentage reductions by the MFLs are not as severe as these during Block 1.

Table 11. Average water volumes, bottom areas, and shoreline lengths for salinity ≤ 2 psu during extremely dry (Block 1) days in the LPR and LSC under the BSL and MFL conditions with the three SCL estimates.

Reduction Scenarios	Volume (10^6 m ³)		Bottom Area (10^6 m ²)		Shoreline (KM)	
	Value	% of BSL	Value	% of BSL	Value	% of BSL
BSL SLR H	2.4185		3.1056		8.6325	
MFL SLR H	1.5549	64%	2.1776	70%	5.7598	67%
BSL SLR M	3.8297		3.9128		15.1639	
MFL SLR M	2.6124	68%	2.9240	75%	10.6610	70%
BSL SLR L	5.1440		4.3817		20.6444	
MFL SLR L	3.5667	69%	3.3633	77%	15.1231	73%

Table 12. Average water volumes, bottom areas, and shoreline lengths for salinity ≤ 2 psu during dry (Block 2) days in the LPR and LSC under the BSL and MFL conditions with the three SCL estimates.

Reduction Scenarios	Volume (10^6 m ³)		Bottom Area (10^6 m ²)		Shoreline (KM)	
	Value	% of BSL	Value	% of BSL	Value	% of BSL
BSL SLR H	15.6773		13.9690		50.6943	
MFL SLR H	10.0637	64%	10.3067	74%	33.4854	66%
BSL SLR M	18.2717		13.8958		62.4904	
MFL SLR M	13.2657	73%	11.0376	79%	47.1902	76%
BSL SLR L	19.7749		13.5786		69.4400	
MFL SLR L	15.1945	77%	11.1212	82%	55.7507	80%

Table 13 shows that during the wet season, the proposed MFLs would not cause either ≤ 2 psu bottom area or ≤ 2 psu shoreline length to decline by more than 15% under the high, intermediate, or low SLR conditions. Under the low and intermediate SLR conditions during Block 3, the ≤ 2 psu volume would not be reduced by the proposed MFLs more than 15% either. However, under the high SLR, the MFLs would cause the salinity habitat to decline 18%, or 3% more the 15% criterion.

From Table 11 – 13, one can conclude that SLR would have significant effects on the establishment of MFLs for the LPR and LSC. Although during the high flow day, the proposed MFL (40% flow reduction) would not cause most salinity habitats to decline by more than 15% under the high, intermediate, and low SLR conditions, it would become invalid during Blocks 1 and 2 if the three SLRs were to occur. As such, it is recommended that MFLs for the LPR and LSC to be re-evaluated in the future.

Table 13. Average water volumes, bottom areas, and shoreline lengths for salinity ≤ 2 psu during wet (Block 3) days in the LPR and LSC under the BSL and MFL conditions with the three SCL estimates.

Reduction Scenarios	Volume (10^6 m ³)		Bottom Area (10^6 m ²)		Shoreline (KM)	
	Value	% of BSL	Value	% of BSL	Value	% of BSL
BSL SLR H	34.2994		24.7921		91.5801	
MFL SLR H	28.2630	82%	21.4845	87%	81.5044	89%
BSL SLR M	33.9613		22.6947		93.3297	
MFL SLR M	28.7912	85%	19.8494	88%	86.1668	92%
BSL SLR L	33.6895		21.3527		94.0543	
MFL SLR L	28.9759	86%	18.7336	88%	88.3353	94%

5. Conclusions

In the previous MFL evaluation for the LPR and LMR, a dynamically coupled 3D-2DV model named LESS was developed, which couples a 3D model (LESS3D) with a 2DV model (LAMFE). The LESS model was very efficient in dealing with the complex geometry of the LPR, LMR, and LSC, because it solves laterally averaged 2D equations in the narrow upstream tributaries and 3D equations in the large downstream waterbody. The dynamically coupling of the two models is facilitated with a FSC method that is unconditionally stable with respect to gravity waves, wind and bottom shear stresses, and vertical eddy viscosity terms.

To support the re-evaluations of minimum freshwater flows to the LPR and LSC to prevent the two riverine estuaries from significant harm, the previously used hydrodynamic model LESS was upgraded to UnLESS, in which an unstructured Cartesian grid model UnLESS3D and the LAMFE model were dynamically coupled in the same way as that in the LESS model. Unlike the 2007 simulation, which restricted the simulation domain to the SWFWMD portion of the Charlotte Harbor, the new modeling effort had a new simulation domain which included the entire Charlotte Harbor and an offshore area about 20 – 30 KM into the GOM. The simulation domain was discretized with 4790 unstructured Cartesian grids in the horizontal plane and 17 layers in the vertical direction for the 3D subdomain, which included the entire Charlotte Harbor, the downstream 1.74 KM of LSC, the downstream 16.13 KM of the LPR, and the downstream 12.64 KM of the LMR, and 311 grids and 17 layers for the 2DV subdomain, which included the LPR from river - KM 16.13 to the confluence with Horse Creek, the LMR from River-KM 12.64 to River-KM 37.27, LSC from River-KM 1.74 to the dam, and the downstream 3.67 KM of Myakkahatchee Creek.

Input data used to drive the UnLESS model included freshwater inflows at the upstream open boundaries, wind, rainfall, air temperature, air humidity, and solar radiation for the free surface boundary, as well as tides, salinities, and temperatures at the downstream open boundaries. Freshwater inflows included gauged flows, ungauged flows, and flow losses. Tides, salinities, and temperatures at the open boundary were provided by Zheng and Weisberg (2014).

The UnLESS model was calibrated and verified with 20 months of real-time data of water level, salinity, and temperature at five stations, two in the 3D subdomain and three in the 2DV subdomain. The model calibration period was from August 2013 to August 2014, while the model verification period was from January 2013 to July 2013. Although there are many uncertainties in the input data used to drive the UnLESS model, including measured data, ungauged flows, and boundary conditions provided by the USF, the UnLESS model was successfully calibrated and verified against measured real-time data of water levels, currents, salinities, and temperatures at the five stations from January 2013 to August 2014.

The calibrated UnLESS model was run for a 92-month period between January 2007 and August 2014 for various flow reduction scenarios from the baseline flows of the LPR and/or LSC. Flow reductions simulated ranged from 5% to 40%, with a 5% interval. Based on these scenario simulations, it was found that a 13% flow reduction during extremely dry days and a 23% flow reduction during dry days for both the LPR and LSC would cause the most sensitive low salinity habitat to lose 15% from its baseline levels in the two water bodies. During high flow days, there are enough low salinity habitats in both the LPR and LSC and a 40% flow reduction does not trigger a 15% reduction of any of the low salinity habitats.

The scenario runs also included the consideration of the SLR. From the USACE website http://corpsmapu.usace.army.mil/rccinfo/slc/slcc_calc.html, three SLR estimates by NOAA et al. 2017 were obtained for the period 2010 through 2035 at the NOAA Ft. Myers station, which is

very close to the open boundaries of the simulation domain. SLRs during the 25-year period are 11.58 cm, 20.57 cm, and 34.75 cm, respectively, for the low, intermediate, and high estimates. The SLR simulations were done for the baseline flow scenario and for the MFL flow scenario, in which flows for both LPR and LSC were reduced by 13%, 23%, and 40% during extremely dry, dry, and high flow days, respectively. From simulation results of salinity habitats, the proposed MFLs would become invalid during Blocks 1 and 2 under any of the estimated SLR conditions. During Block 3, the ≤ 2 psu salinity habitats would not be reduced by more than 15% by the proposed MFLs under any or the SLR conditions, except for the ≤ 2 psu volume under the high SLR condition. Under the low SLR condition, ≤ 2 psu salinity habitats will have a decline of $< 15\%$ with the proposed MFLs, except for the ≤ 2 psu water volume, which will be reduced about 18%. It is recommended that MFLs for the LPR and LSC to be re-evaluated in the future.

6. References

- Bicknell, B.R., Imhoff, J.C., Kittle, J.L. Jr., Donigian, A.S. Jr. and Johanson R.C., 1997. Hydrological Simulation Program-FORTRAN, User's Manual for Version 11. EPA/600/SR-97/080. U.S. Environmental Protection Agency, National Exposure Research Laboratory, Research Triangle Park, NC 27711.
- Chen, X. and M.S. Flannery. 1997. Use of a Hydrodynamic Model for Establishing a Minimum Freshwater Flow to the Lower Hillsborough River. In (M. L. Spaulding and A. F. Blumberg, eds.) Estuarine and Coastal Modeling (V), Proceedings of the 5th International Conference, ASCE, pp. 663-678.
- Chen, X. 1999. Three-Dimensional, Hydrostatic and Non-Hydrostatic Modeling of Seiching in a Rectangular Basin. In (M. L. Spaulding and H. L. Butler, eds.) Estuarine and Coastal Modeling (VI), Proceedings of the 6th International Conference, ASCE, pp. 148-161.
- Chen, X., M.S. Flannery, and D.L. Moore. 2000. Salinity Response to the Change of the Upstream Freshwater Flow in the Lower Hillsborough River, Florida. *Estuaries*, 23: 735-742.
- Chen, X. 2003a. An efficient finite difference scheme for simulating hydrodynamics in narrow rivers and estuaries. *International Journal for Numerical Methods in Fluids*. 42: 233-247.
- Chen, X. 2003b. A Free-Surface Correction Method for Simulating Shallow Water Flows. *Journal of Computational Physics*, 189:557-578.
- Chen, X. 2003c, Coupling a 3D model with a 2DV model using a free-surface correction method, In (M. L. Spaulding, ed.) Estuarine and Coastal Modeling (IIX), Proceedings of the 8th International Conference, ASCE, pp. 769 - 783.
- Chen, X. 2004a. Using a piecewise linear bottom to fit the bed variation in a laterally averaged, z-co-ordinate hydrodynamic model. *International Journal for Numerical Methods in Fluids*. 44: 1185-1205.
- Chen, X. 2004b. A Cartesian method for fitting the bathymetry and tracking the dynamic position of the shoreline in a three-dimensional, hydrodynamic model. *Journal of Computational Physics*, 200: 749 - 768.
- Chen, X. 2005. Using a Dynamically Coupled 3D-2DV Model to Simulate Hydrodynamics in the Lower Peace River – Upper Charlotte harbor System in Southwest Florida, In (M.L. Spaulding, ed.) Estuarine and Coastal Modeling (V), Proceedings of the 9th International Conference, ASCE, pp. 72 - 87.
- Chen, X. 2007a. Dynamic coupling of a three-dimensional hydrodynamic model with a laterally averaged, two-dimensional hydrodynamic model. In production, *Journal of Geophysical Research*.
- Chen, X. 2007b. Simulations of Minimum Flow Scenarios for the Lower Myakka River Estuary Using a Dynamically Coupled 3D-2DV Model. Technical Report. Southwest Florida Water Management District, Tampa, Fla.
- Chen, X., 2011. A three-dimensional hydrodynamic model for shallow waters using unstructured Cartesian grids. *International Journal for Numerical Methods in Fluids* 66, 885–905. doi:10.1002/fld.2290.
- Chen, X., 2012. Simulating hydrodynamics in a spring-fed estuary using a three-dimensional unstructured Cartesian grid model. *Estuarine, Coastal, and Shelf Science*, 115: 246 – 259. doi:10.1016/j.ecss.2012.09.007.
- Chen, X., 2020. Coupling an Unstructured Grid three-dimensional Model with a Laterally Averaged two-dimensional Model for Shallow Water Hydrodynamics and Transport Processes, submitted for publication.

- Ghile, Y.B. and D.A., Leeper. 2015. Initial Reevaluation of the Minimum Flows and Levels for the Lower Peace River, Internal Review Draft June 30, 2015. Southwest Florida Water Management District. Brooksville, Florida.
- Sucsy P.V., F.W. Morris, M.J. Bergman, and L.J. Donnangelo. 1997. A 3-D Model of Florida's Sebastian River Estuary, In (M. L. Spaulding and A. F. Blumberg, eds.) Estuarine and Coastal Modeling (V), Proceedings of the 5th International Conference, ASCE, pp. 59 - 74.
- Johnson, B.H. K.W. Kim, R. Heath, B. Hsieh, and L. Butler. 1991. Validation of a Three-Dimensional Hydrodynamic Model of Chesapeake Bay, *Journal of Hydraulic Engineering*, 117 (1): 2 – 20.
- Mendelsohn, D.L., S. Peene, E. Yassuda, and S. Davie, 1999. A Hydrodynamic Model Calibration Study of the Savannah River Estuary with an Examination of Factors Affecting Salinity Intrusion, In (M. L. Spaulding and L. Butler, eds.) Estuarine and Coastal Modeling (VI), Proceedings of the 6th International Conference, ASCE, pp. 663-685.
- Ross, M.A., A. Said, K. Trout, and J. Zhang, 2005. Hydrologic Modeling of Streamflow from Ungaged Areas in the Upper Charlotte Harbor Basin – Phase 2, Prepared for the Southwest Florida Water Management District. Department of Civil and Environmental Engineering, University of South Florida, Tampa, Florida.
- SFWMF, 2005. Caloosahatchee River/Estuary Nutrient Issues, White Paper, South Florida Water Management District, West Palm Beach, Florida 33406, 128p.
- SFWMD, FDEP, FDACS, 2009. Caloosahatchee River Watershed Protection Plan, West Palm Beach, Florida 33406, 276p.
- SFWMD, 2001. Peace River Comprehensive Management Plan, Volume I (Draft), Southwest Florida Water Management District Brooksville, Fla.
- SFWMD, 2007. Proposed Minimum Flows and Levels for the Lower Peace River and Shell Creek. Southwest Florida Water Management District, Brooksville, Fla., August 24, 2007 PEER REVIEW DRAFT.
- SFWMD, 2010. Proposed Minimum Flows and Levels for the Lower Peace River and Shell Creek. Southwest Florida Water Management District, Brooksville, Fla., April 2010 – Final Report and Appendix 1.
- Sweet, W.V., R.E. Kopp, C.P. Weaver, J. Obeysekera, R.M. Horton, E.R. Thieler, and C. Zervas, 2017. Global and Regional Sea Level Rise Scenarios for the United States, NOAA Technical Report NOS CO-OPS 083, Silver Spring, Maryland, January 2017, 189p.
- UNESCO, 1983. Algorithms for computation of fundamental properties of seawater, UNESCO Technical Papers in Marine Science, Number 44, 53 pp., Paris.
- Van der Vorst, H.A.. 1992. Bi-CGSTAB: A fast and smoothly converging variant of Bi-CG for solution of non-symmetric linear systems, *SIAM J. Sci. Statist. Comput.* 13: 631-644.
- Warner, J.C., Geyer, W.R., Lerczak, J.A., 2005. Numerical modeling of an estuary: A comprehensive skill assessment. *Journal of Geophysical Research* 110, C05001, doi:10.1029/2004JC002691.
- Willmott, C.J., 1981. On the validation of models. *Physical Geography* 2, 184-194.
- Zheng, L. and R.H. Weisberg, 2014. Water Level, Salinity and Temperature Simulations near Charlotte Harbor from the West Florida Coastal Ocean Model. Submitted to Southwest Florida Water Management District. University of South Florida, St. Petersburg, Fla.

7. Appendix A

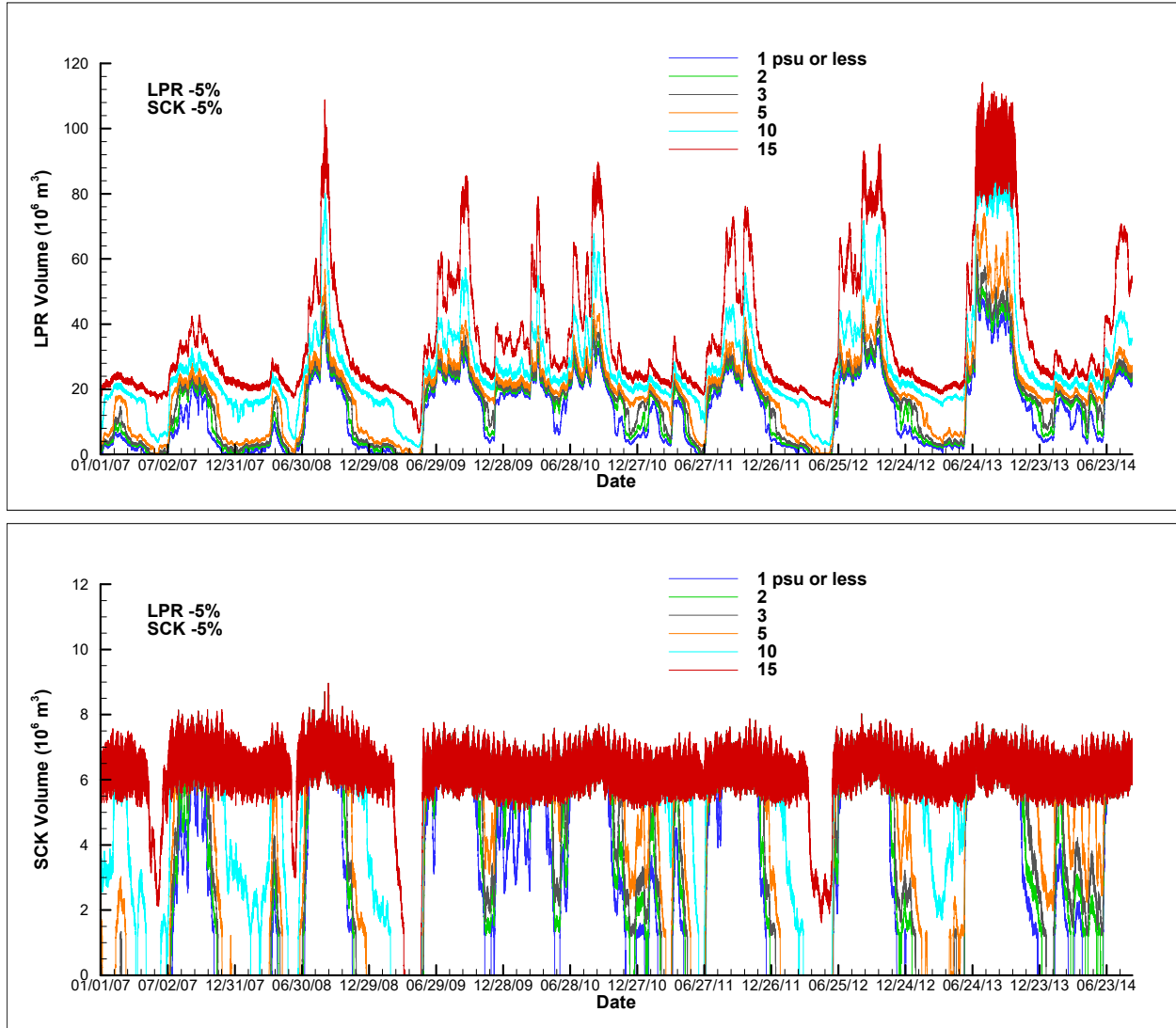


Figure A - 1. Water volumes for salinity $\leq 1, 2, 3, 5, 10,$ and 15 psu in the LPR (top panel) and in LSC (bottom panel) during the simulation period of January 2007 - August 2014 for the 5% flow reduction scenario.

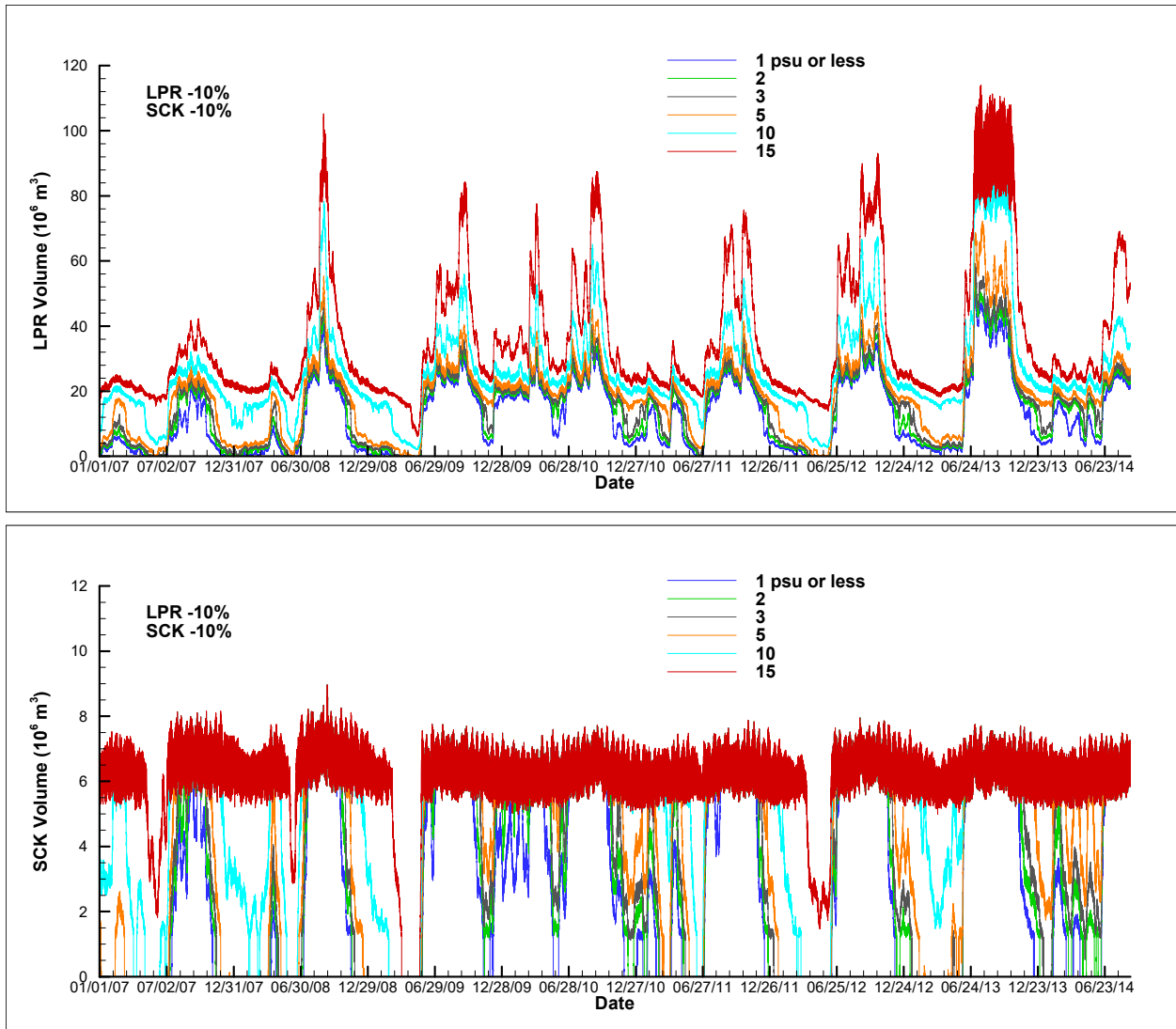


Figure A - 2. Water volumes for salinity $\leq 1, 2, 3, 5, 10,$ and 15 psu in the LPR (top panel) and in LSC (bottom panel) during the simulation period of January 2007 - August 2014 for the 10% flow reduction scenario.

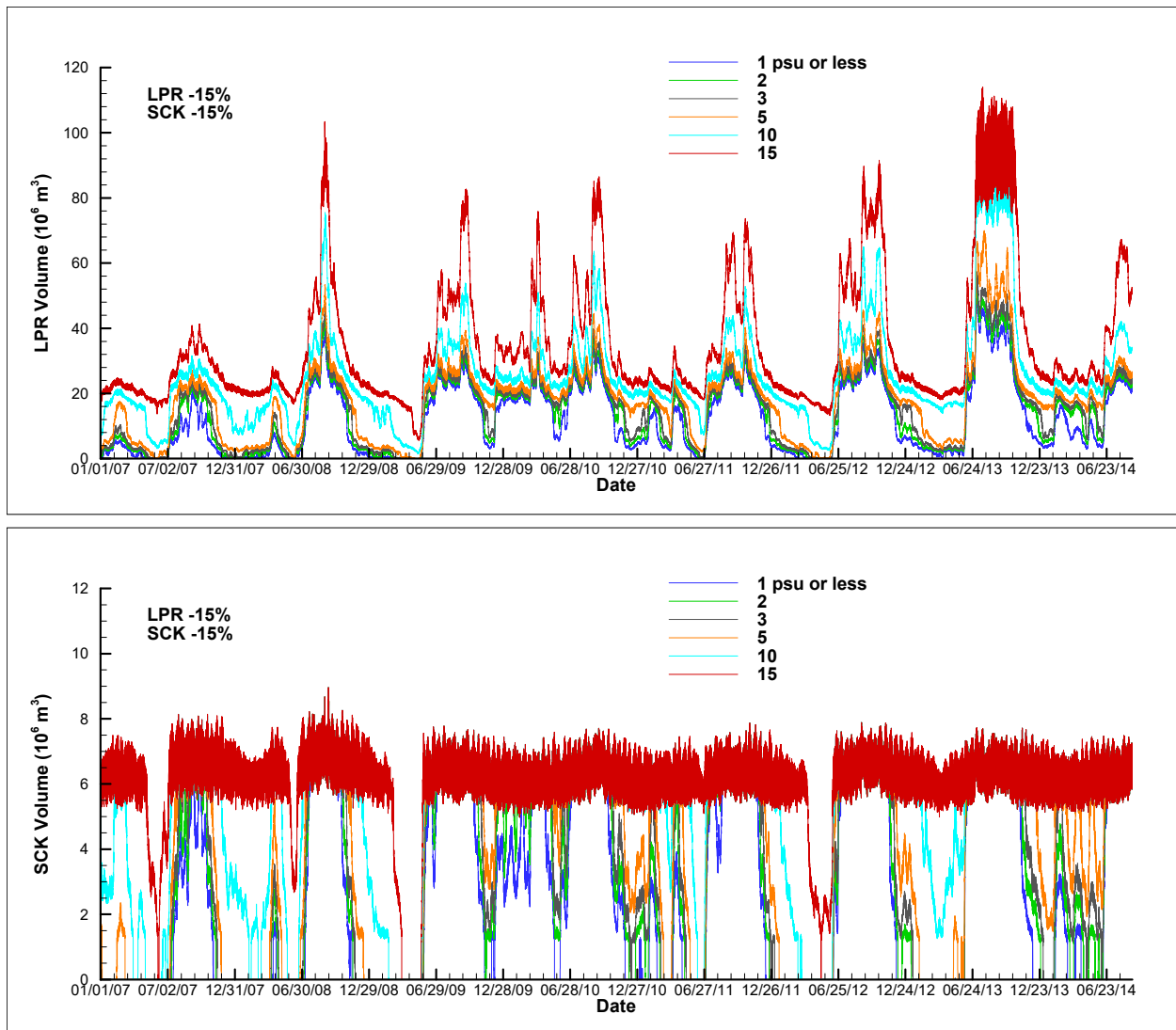


Figure A - 3. Water volumes for salinity $\leq 1, 2, 3, 5, 10,$ and 15 psu in the LPR (top panel) and in LSC (bottom panel) during the simulation period of January 2007 - August 2014 for the 15% flow reduction scenario.

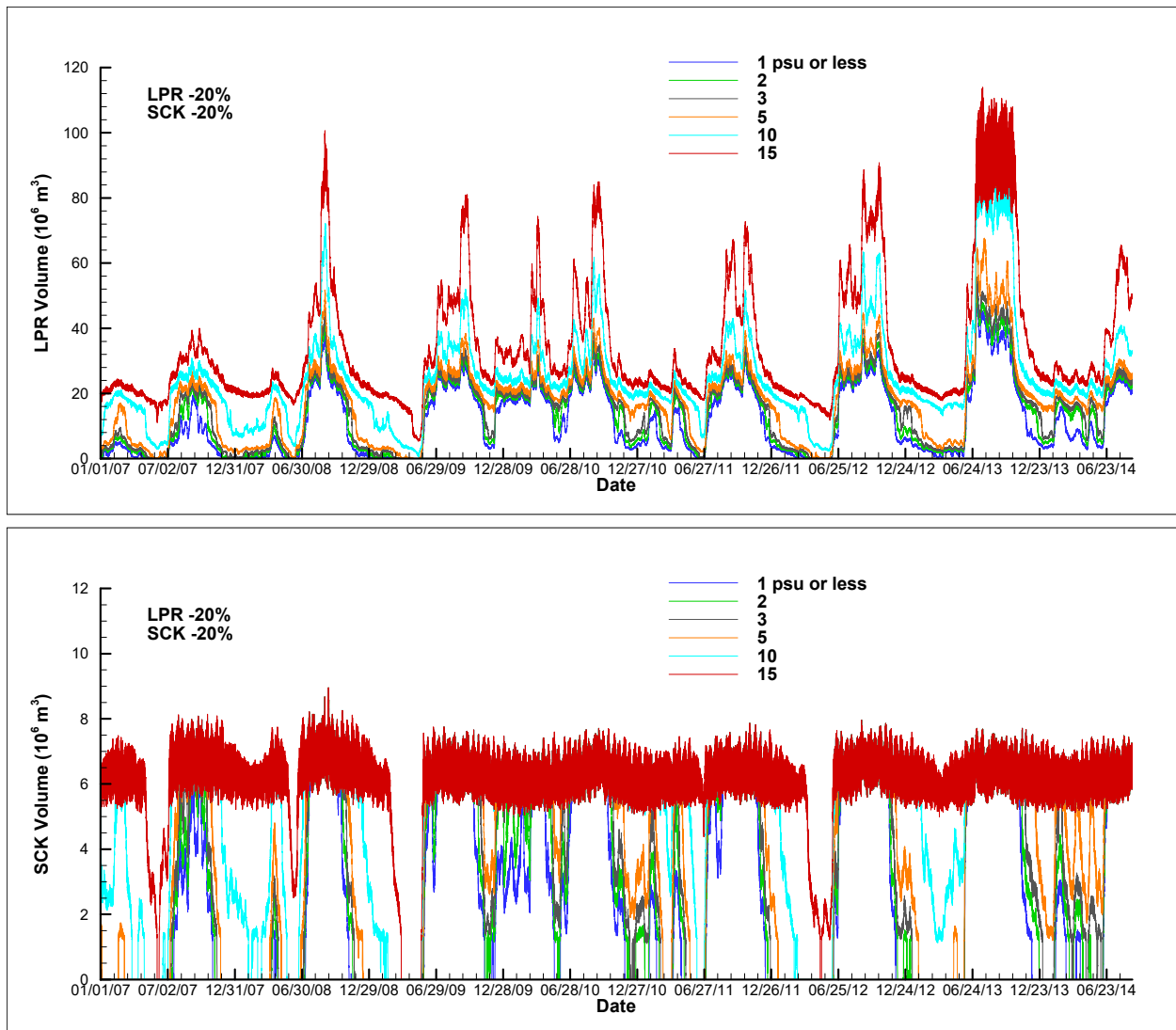


Figure A - 4. Water volumes for salinity $\leq 1, 2, 3, 5, 10,$ and 15 psu in the LPR (top panel) and in LSC (bottom panel) during the simulation period of January 2007 - August 2014 for the 20% flow reduction scenario.

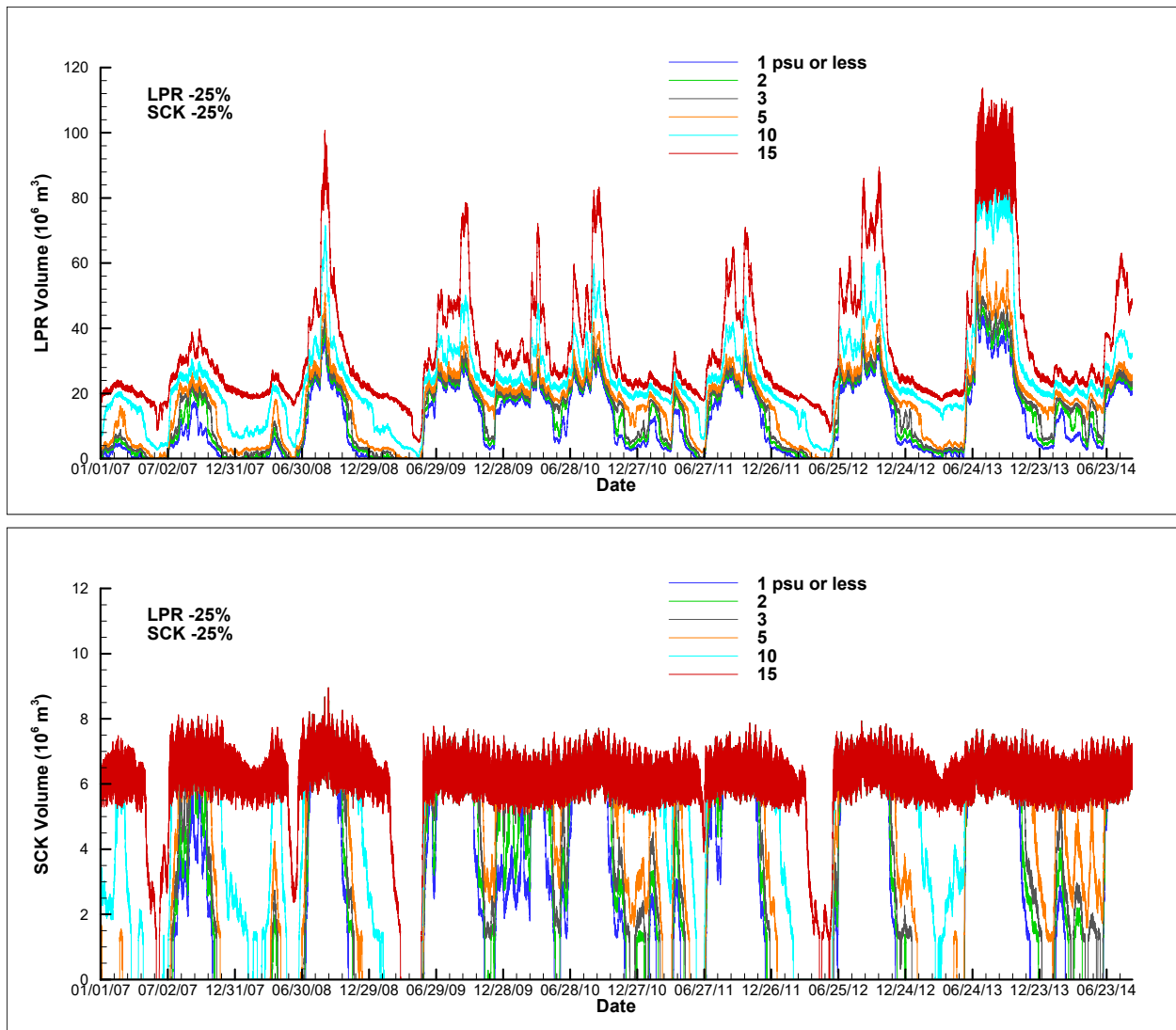


Figure A - 5. Water volumes for salinity $\leq 1, 2, 3, 5, 10,$ and 15 psu in the LPR (top panel) and in LSC (bottom panel) during the simulation period of January 2007 - August 2014 for the 25% flow reduction scenario.

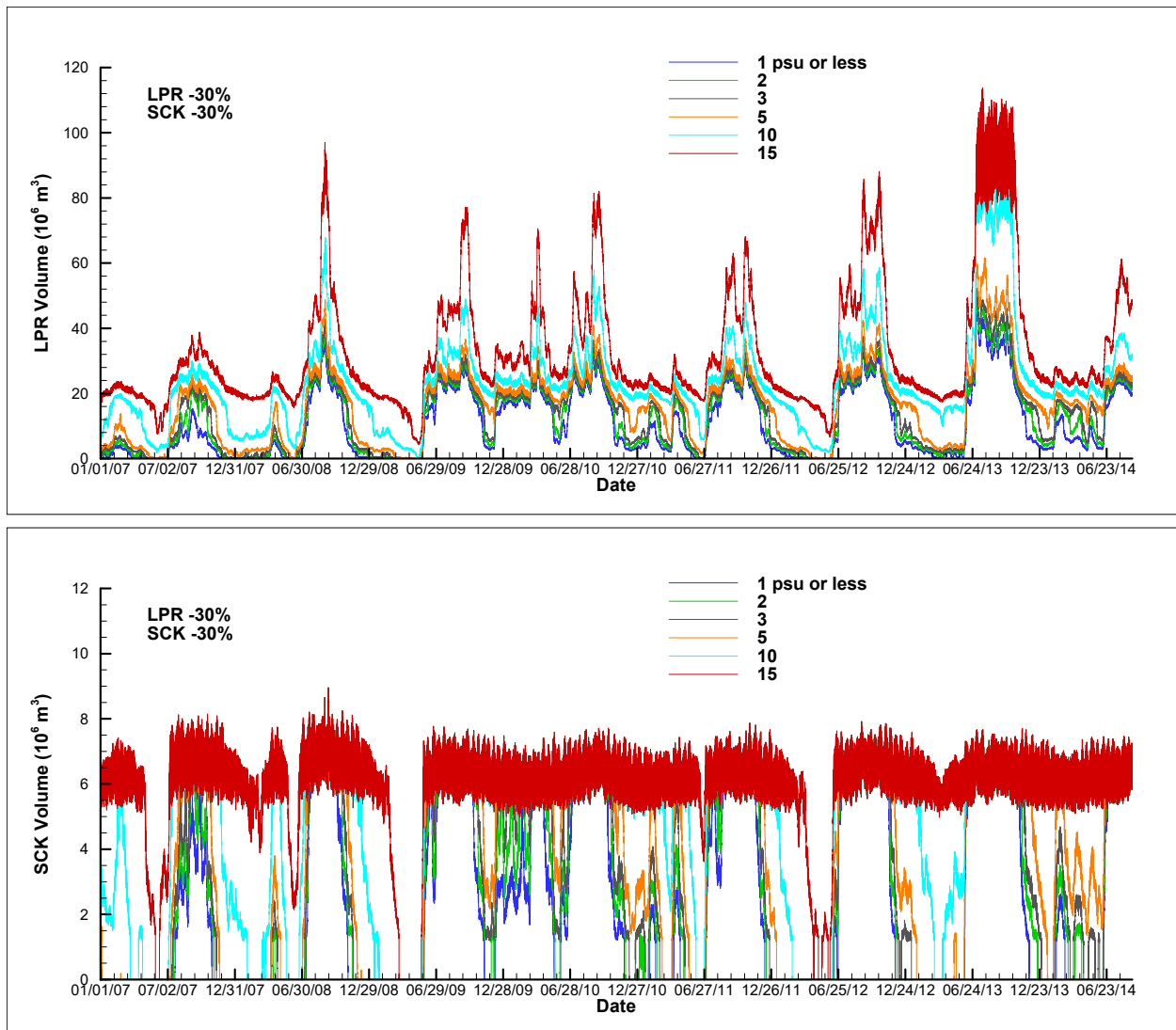


Figure A - 6. Water volumes for salinity $\leq 1, 2, 3, 5, 10,$ and 15 psu in the LPR (top panel) and in LSC (bottom panel) during the simulation period of January 2007 - August 2014 for the 30% flow reduction scenario.

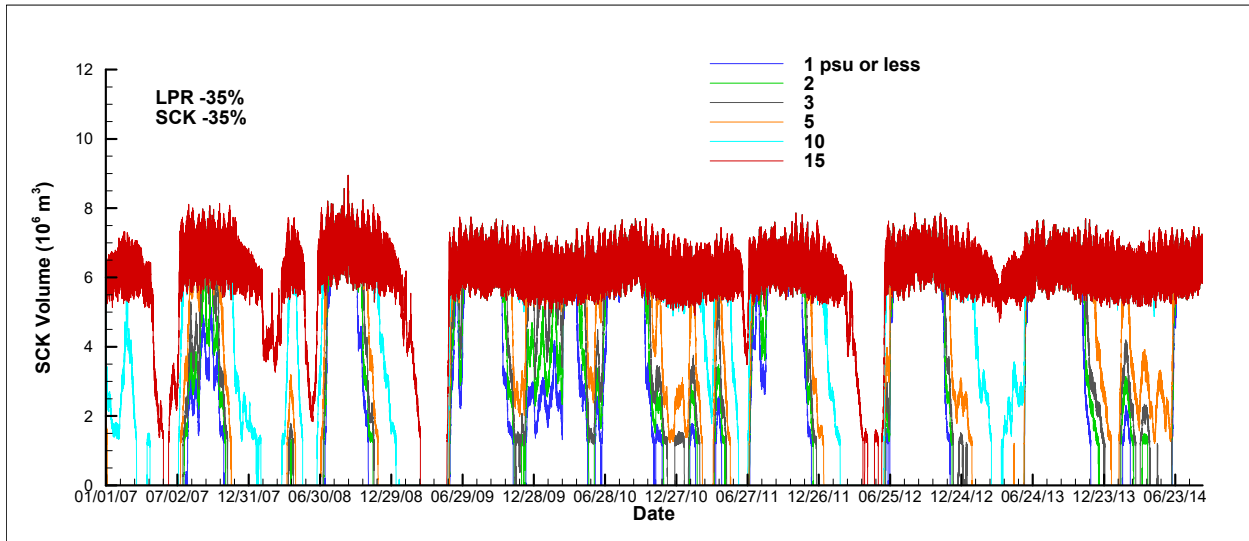
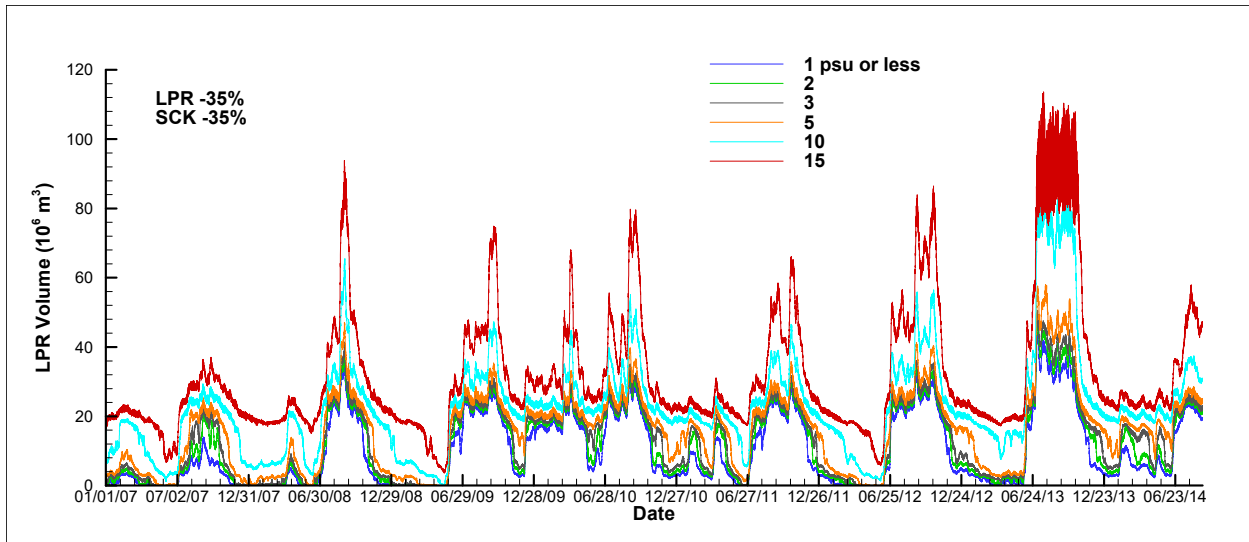


Figure A - 7. Water volumes for salinity $\leq 1, 2, 3, 5, 10,$ and 15 psu in the LPR (top panel) and in LSC (bottom panel) during the simulation period of January 2007 - August 2014 for the 35% flow reduction scenario.

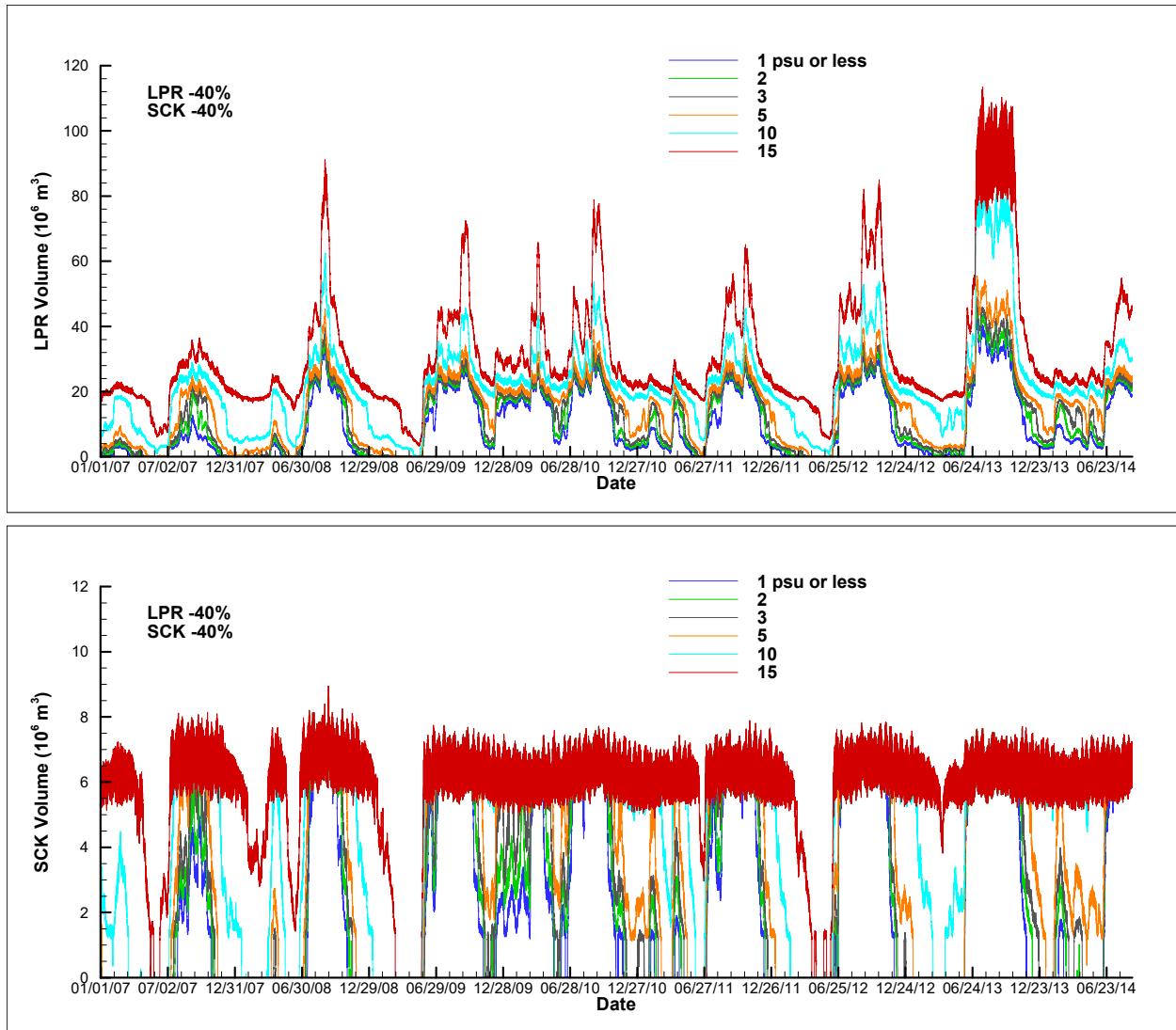


Figure A - 8. Water volumes for salinity $\leq 1, 2, 3, 5, 10,$ and 15 psu in the LPR (top panel) and in LSC (bottom panel) during the simulation period of January 2007 - August 2014 for the 40% flow reduction scenario.

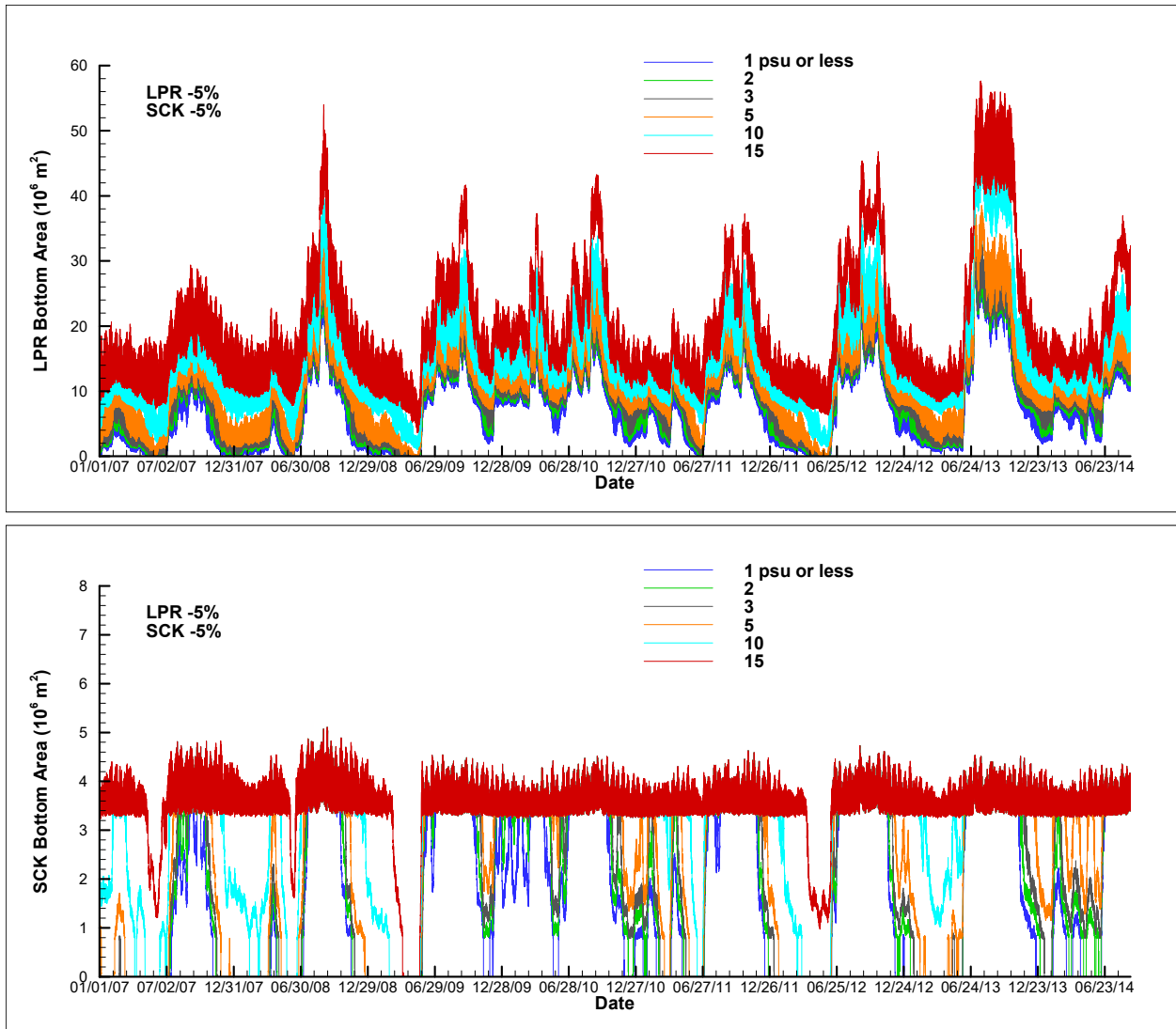


Figure A - 9. Bottom areas for salinity $\leq 1, 2, 3, 5, 10,$ and 15 psu in the LPR (top panel) and in LSC (bottom panel) during the simulation period of January 2007 - August 2014 for the 5% flow reduction scenario.

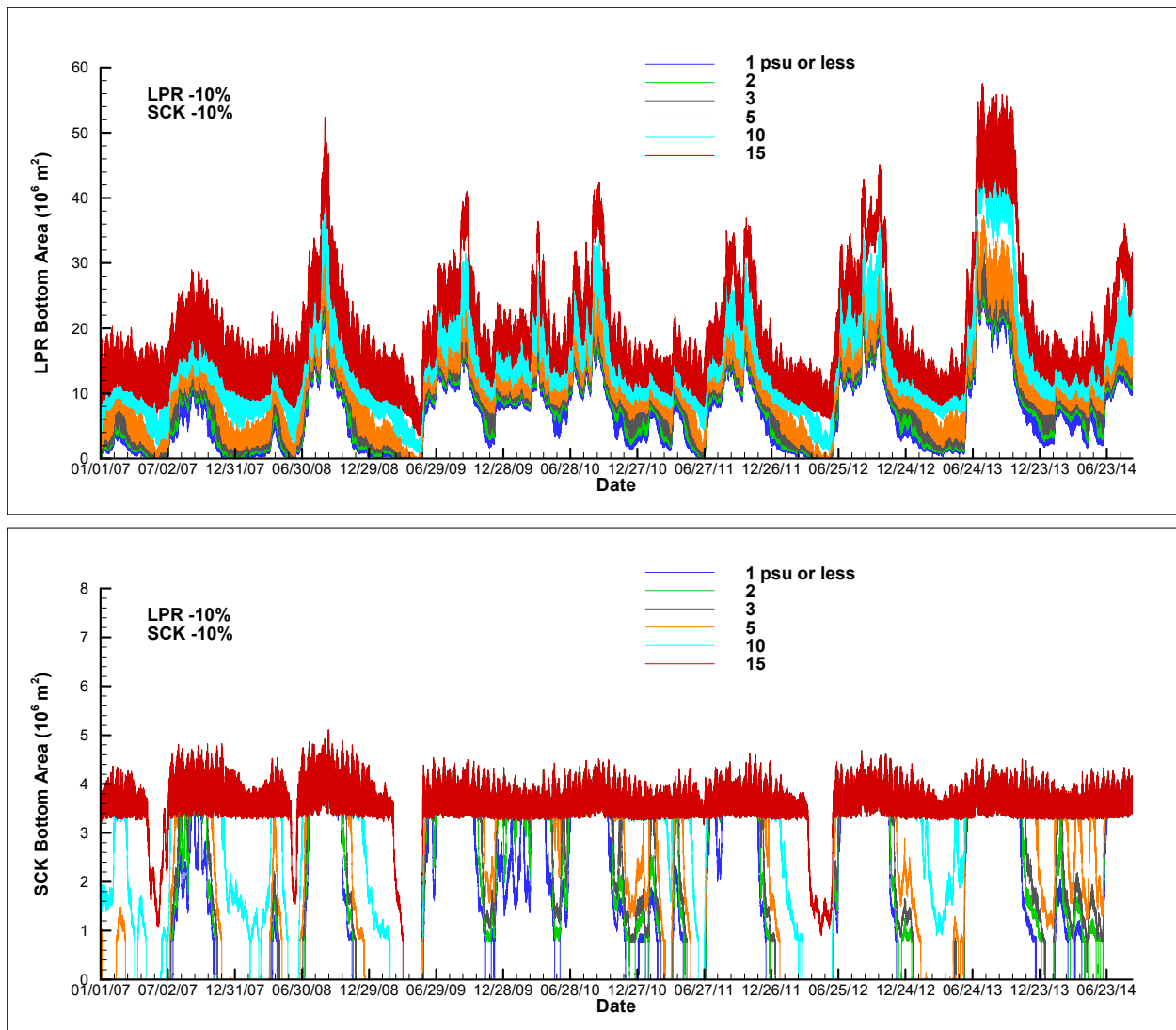


Figure A - 10. Bottom areas for salinity $\leq 1, 2, 3, 5, 10,$ and 15 psu in the LPR (top panel) and in LSC (bottom panel) during the simulation period of January 2007 - August 2014 for the 10% flow reduction scenario.

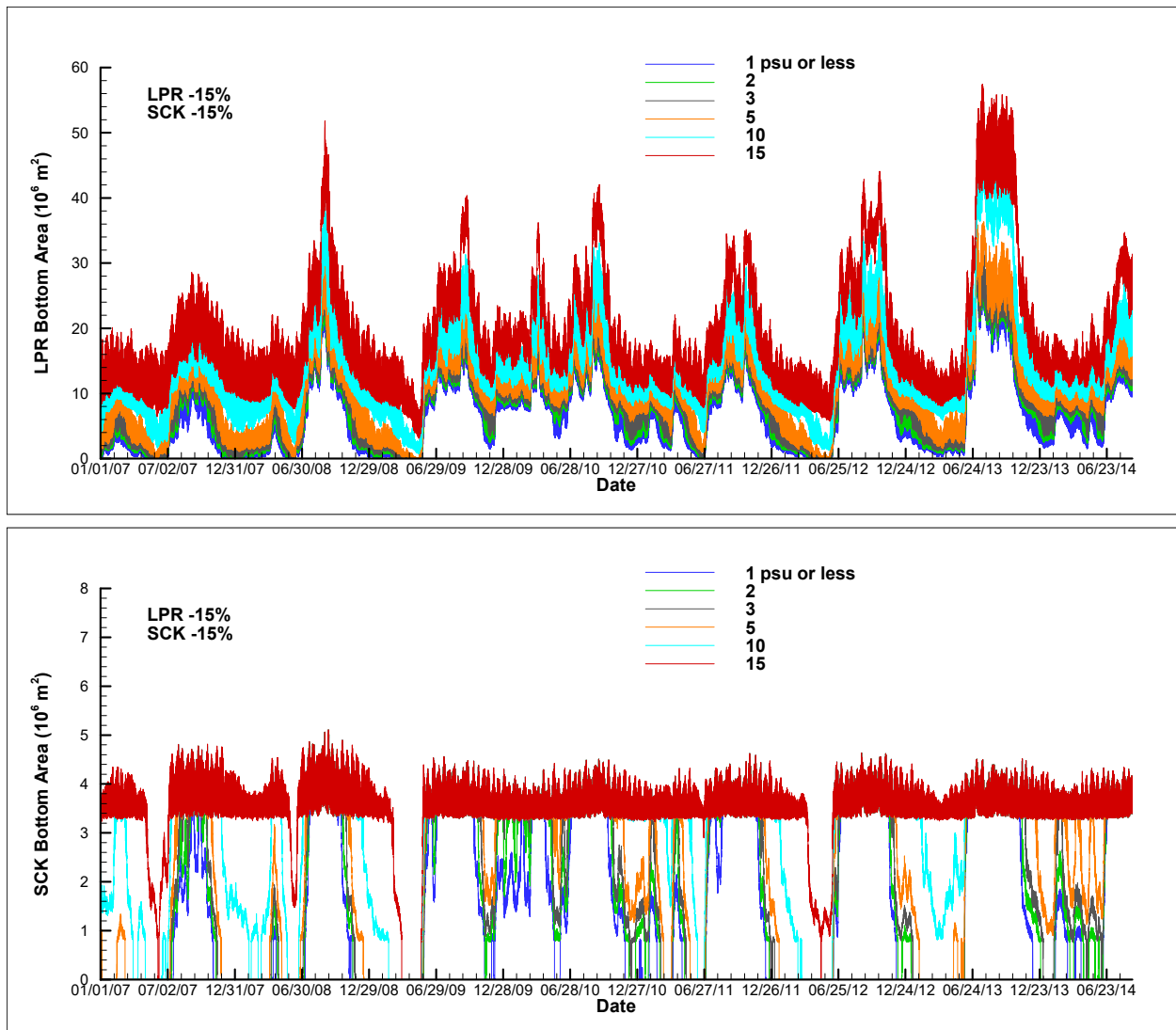


Figure A - 11. Bottom areas for salinity $\leq 1, 2, 3, 5, 10,$ and 15 psu in the LPR (top panel) and in LSC (bottom panel) during the simulation period of January 2007 - August 2014 for the 15% flow reduction scenario.

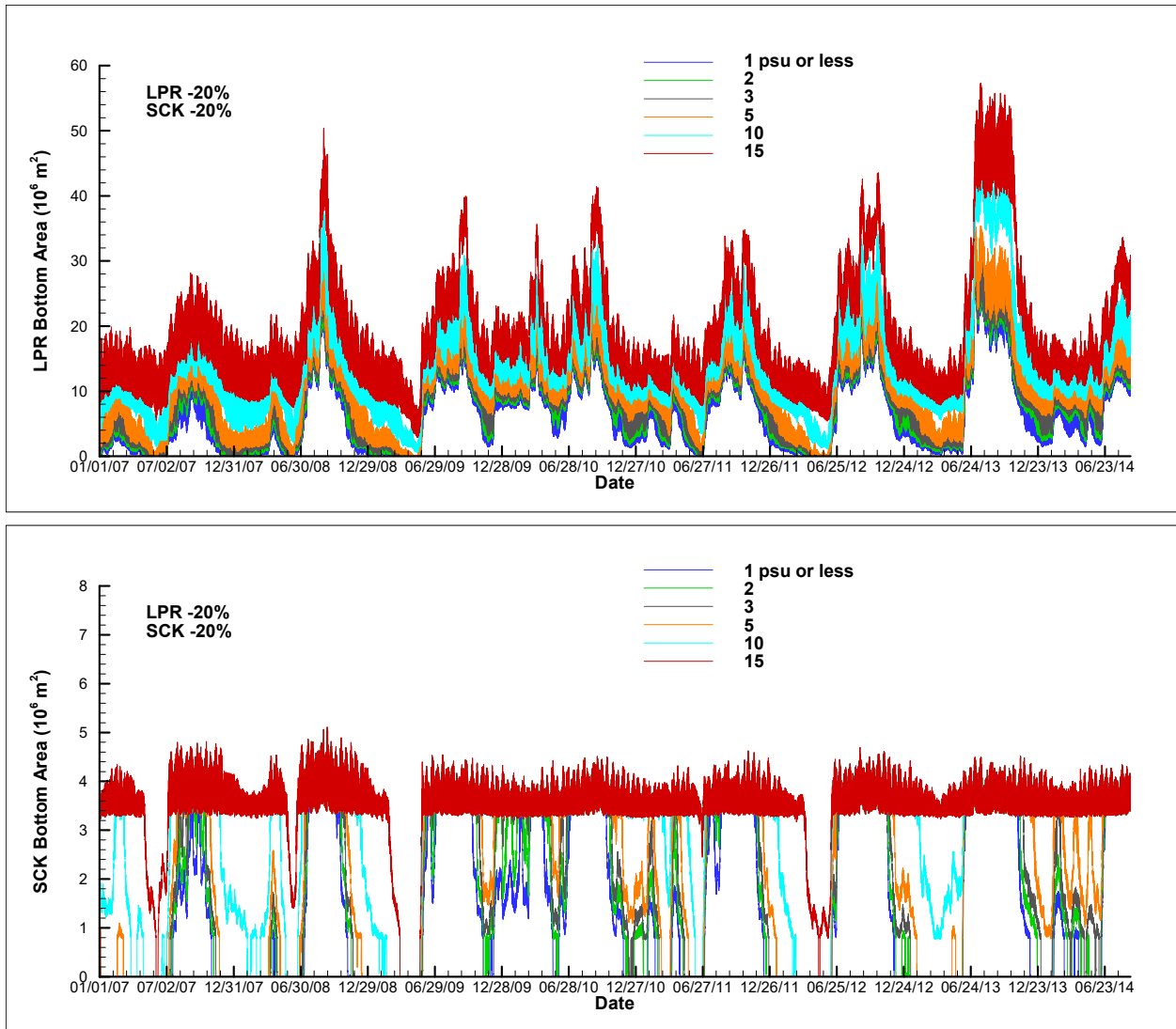


Figure A - 12. Bottom areas for salinity $\leq 1, 2, 3, 5, 10,$ and 15 psu in the LPR (top panel) and in LSC (bottom panel) during the simulation period of January 2007 - August 2014 for the 20% flow reduction scenario.

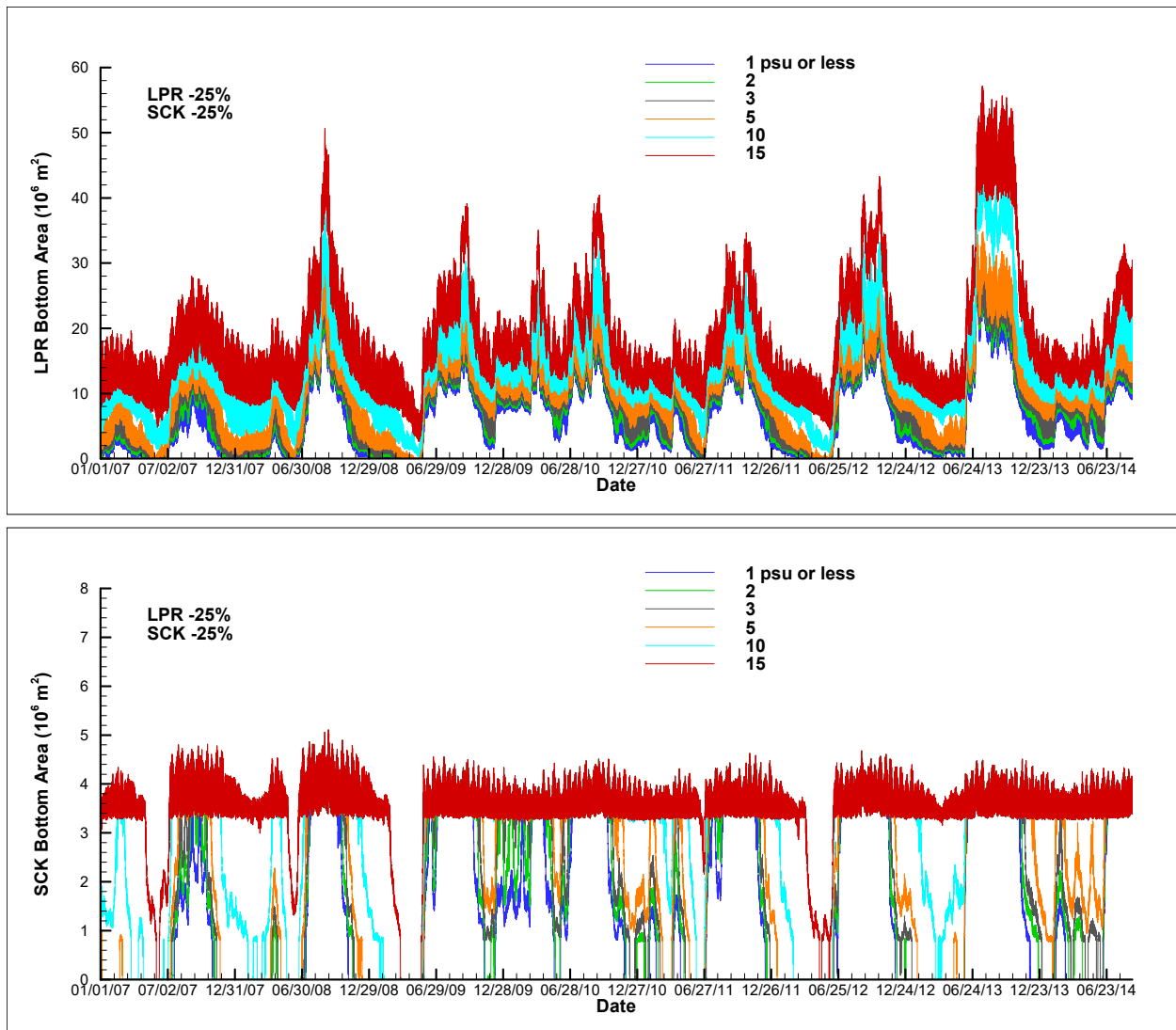


Figure A - 13. Bottom areas for salinity $\leq 1, 2, 3, 5, 10,$ and 15 psu in the LPR (top panel) and in LSC (bottom panel) during the simulation period of January 2007 - August 2014 for the 25% flow reduction scenario.

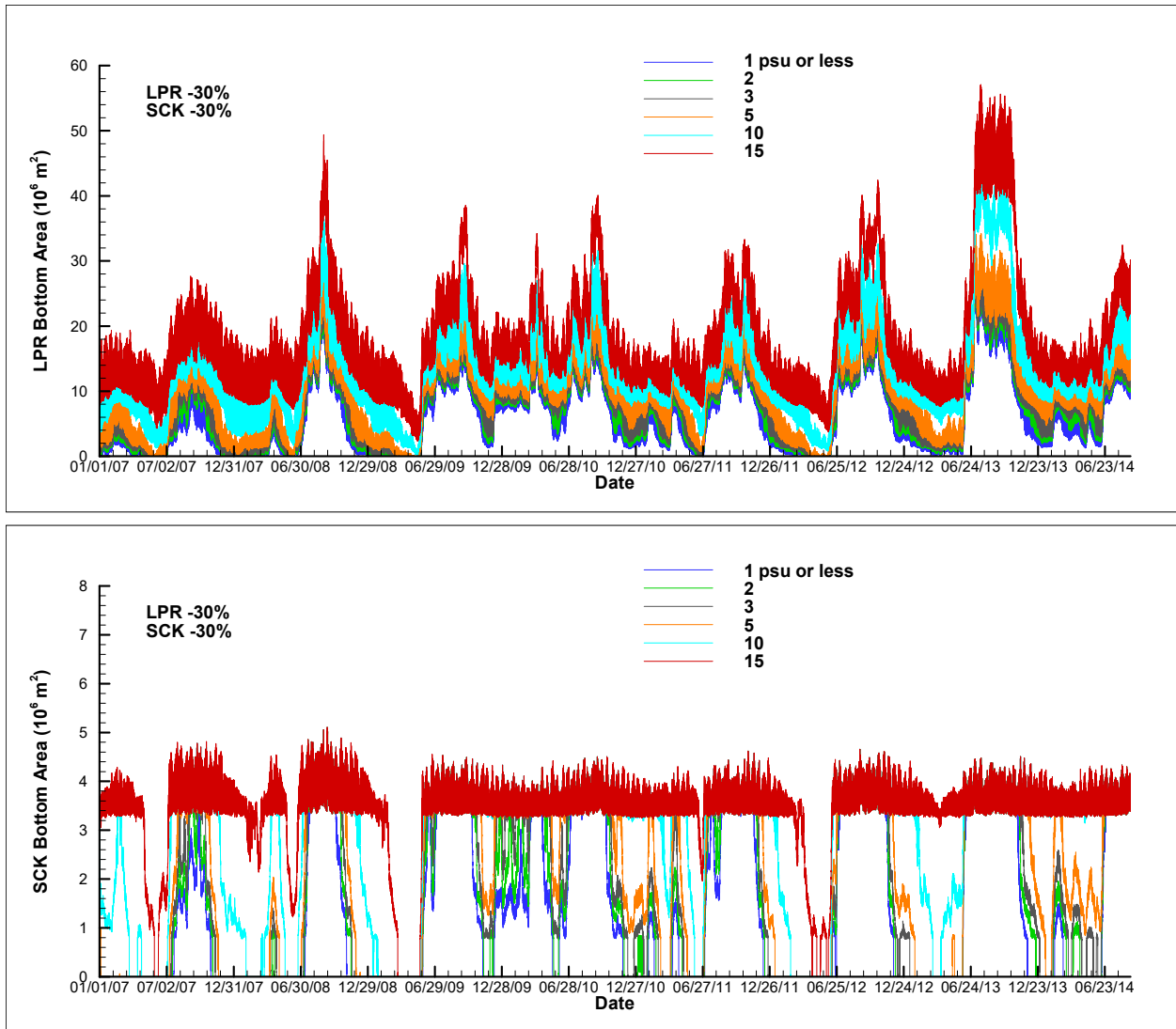


Figure A - 14. Bottom areas for salinity $\leq 1, 2, 3, 5, 10,$ and 15 psu in the LPR (top panel) and in LSC (bottom panel) during the simulation period of January 2007 - August 2014 for the 30% flow reduction scenario.

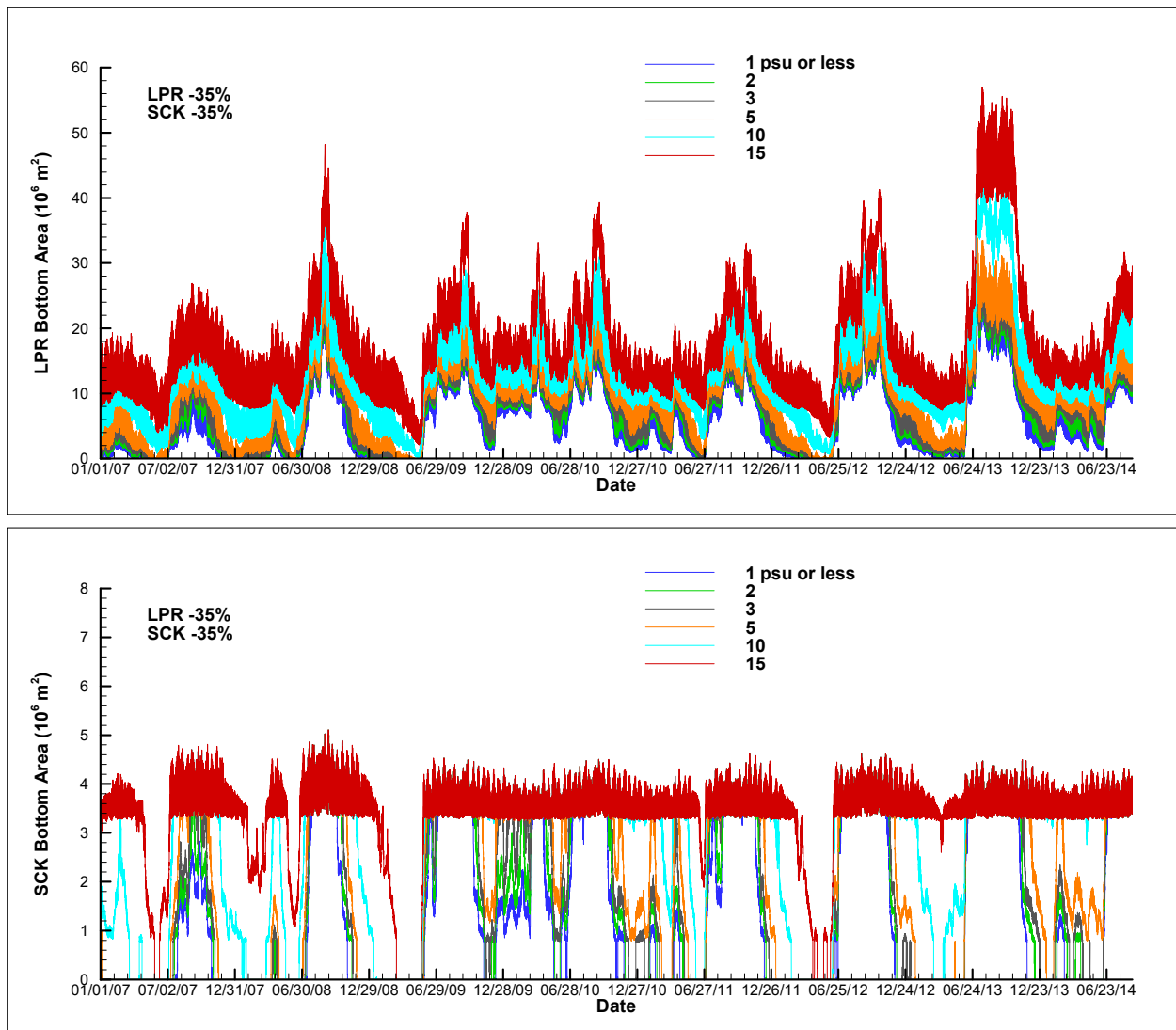


Figure A - 15. Bottom areas for salinity $\leq 1, 2, 3, 5, 10,$ and 15 psu in the LPR (top panel) and in LSC (bottom panel) during the simulation period of January 2007 - August 2014 for the 35% flow reduction scenario.

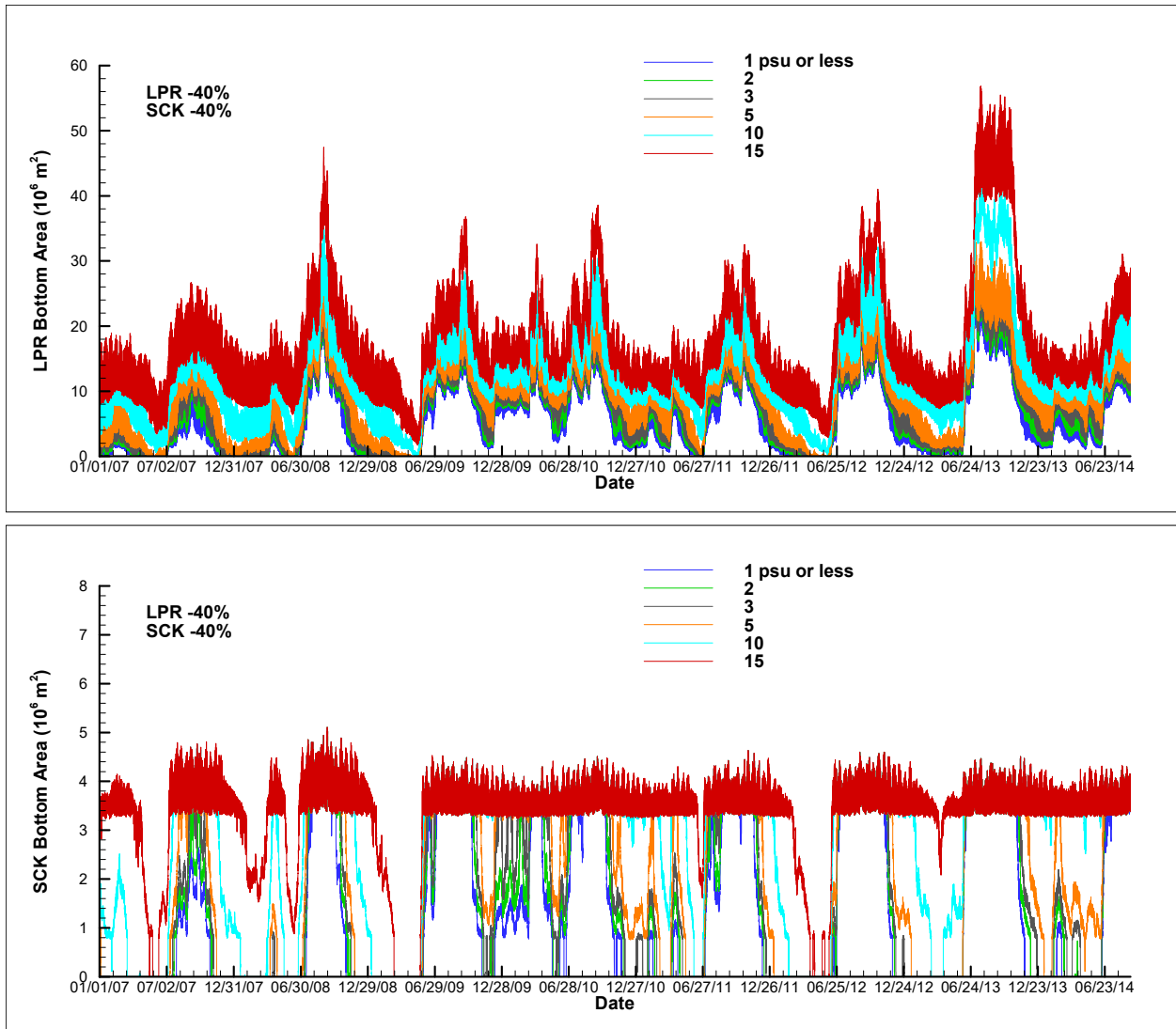


Figure A - 16. Bottom areas for salinity $\leq 1, 2, 3, 5, 10,$ and 15 psu in the LPR (top panel) and in LSC (bottom panel) during the simulation period of January 2007 - August 2014 for the 40% flow reduction scenario.

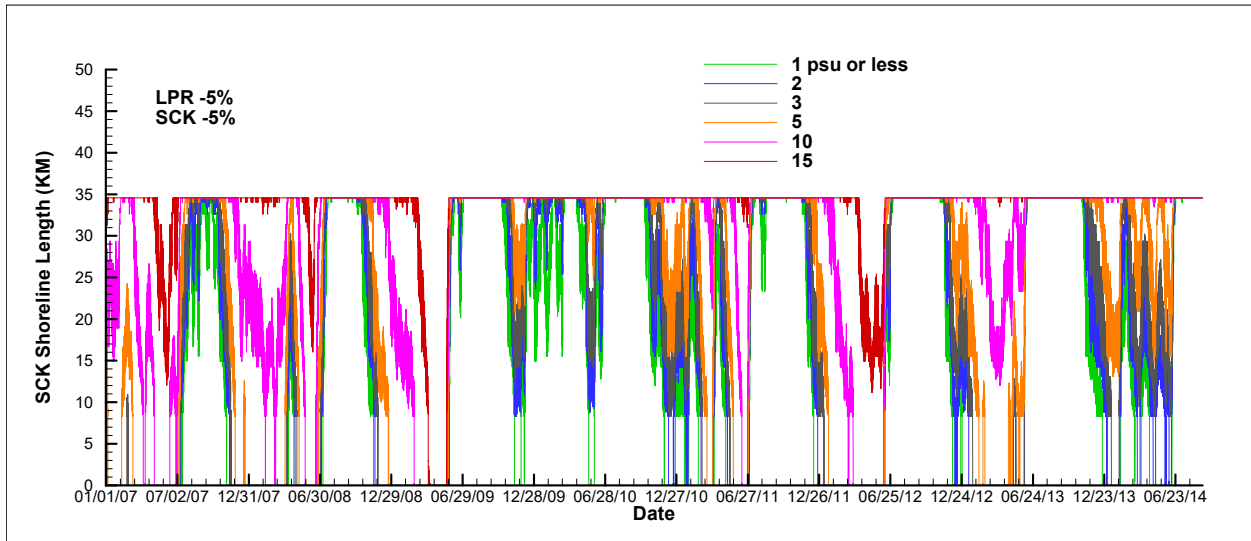
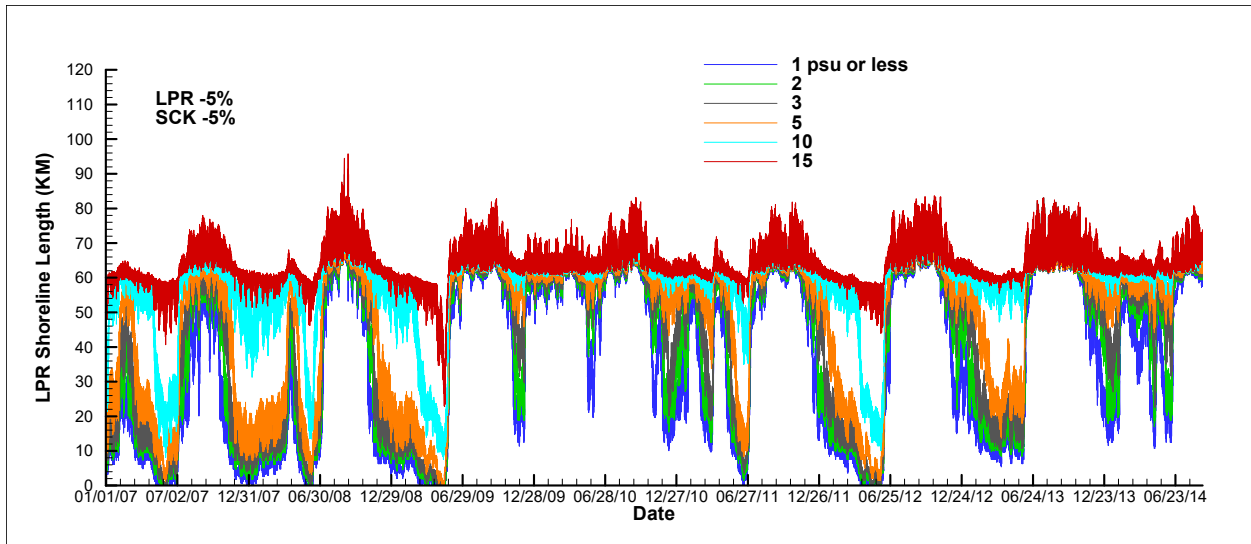


Figure A - 17. Shoreline lengths for salinity $\leq 1, 2, 3, 5, 10,$ and 15 psu in the LPR (top panel) and in LSC (bottom panel) during the simulation period of January 2007 - August 2014 for the 5% flow reduction scenario.

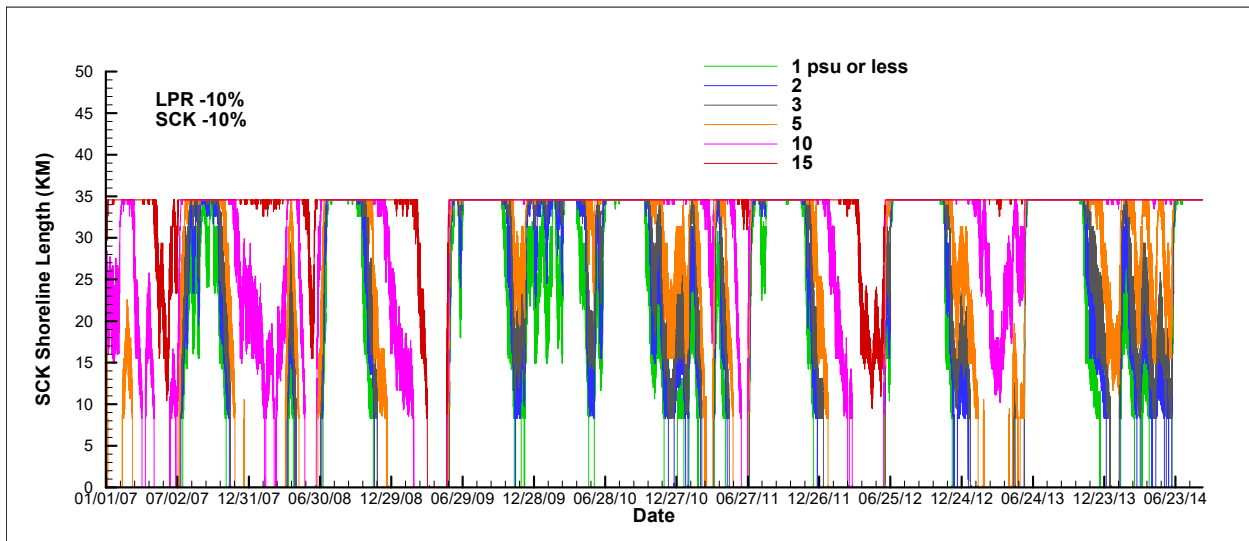
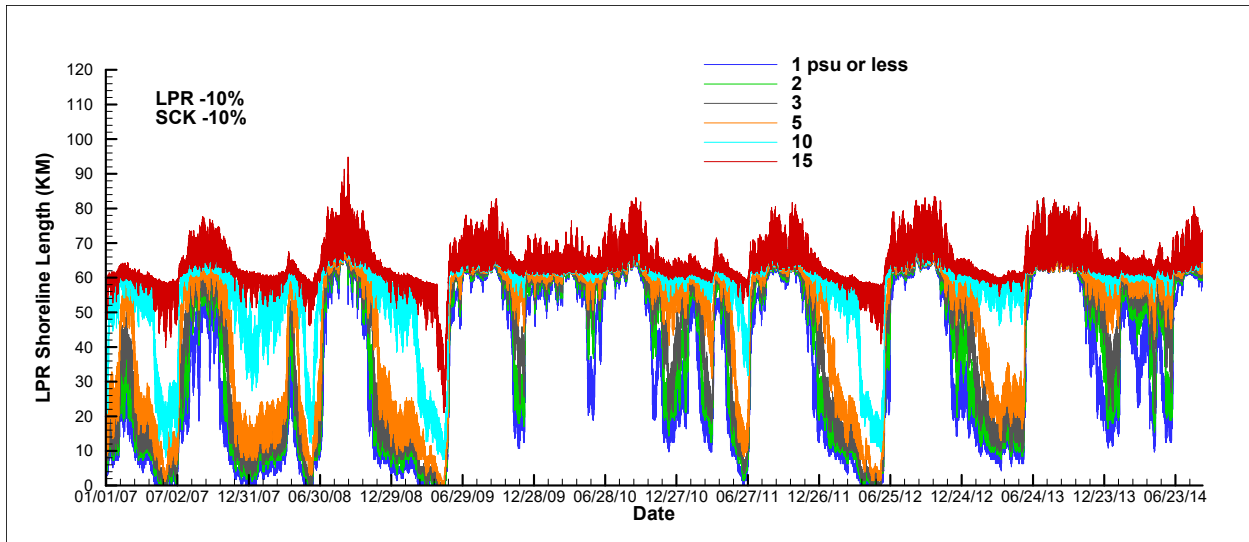


Figure A - 18. Shoreline lengths for salinity $\leq 1, 2, 3, 5, 10,$ and 15 psu in the LPR (top panel) and in LSC (bottom panel) during the simulation period of January 2007 - August 2014 for the 10% flow reduction scenario.

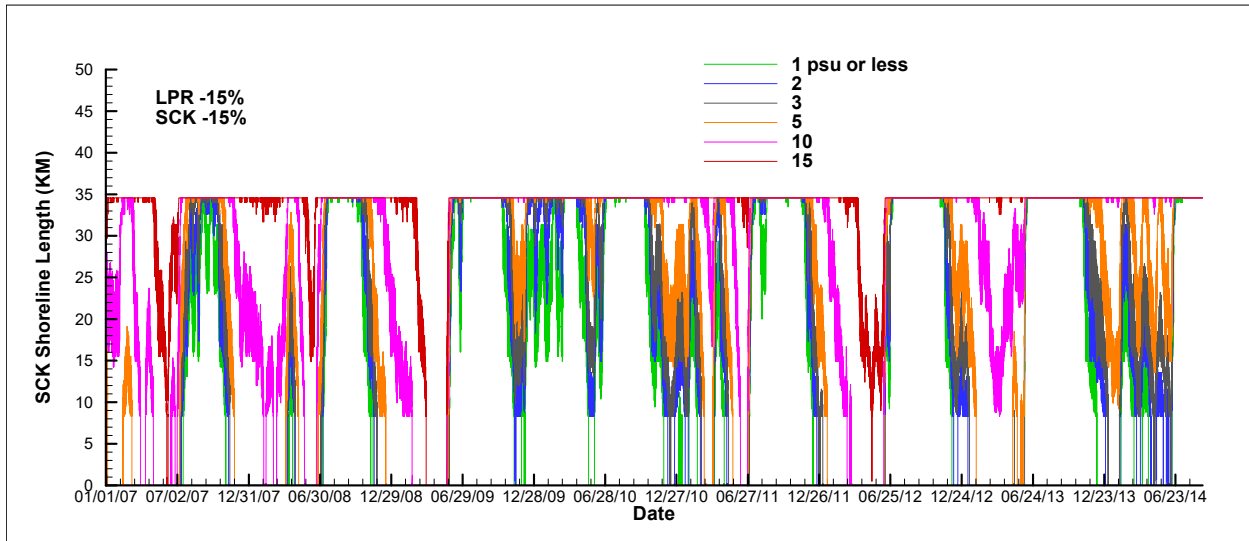
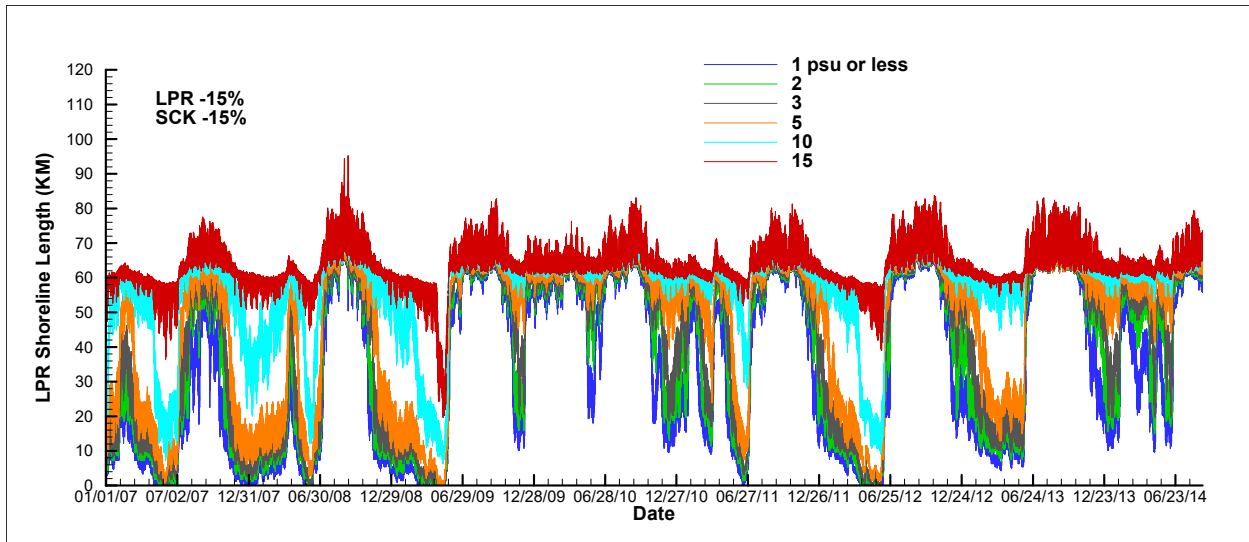


Figure A - 19. Shoreline lengths for salinity $\leq 1, 2, 3, 5, 10,$ and 15 psu in the LPR (top panel) and in LSC (bottom panel) during the simulation period of January 2007 - August 2014 for the 15% flow reduction scenario.

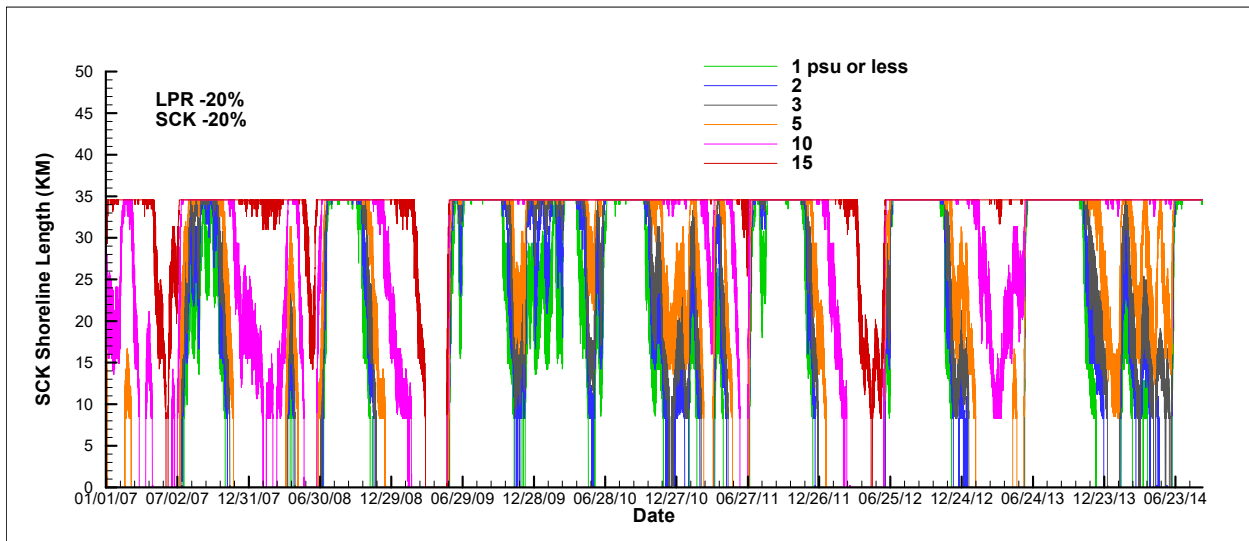
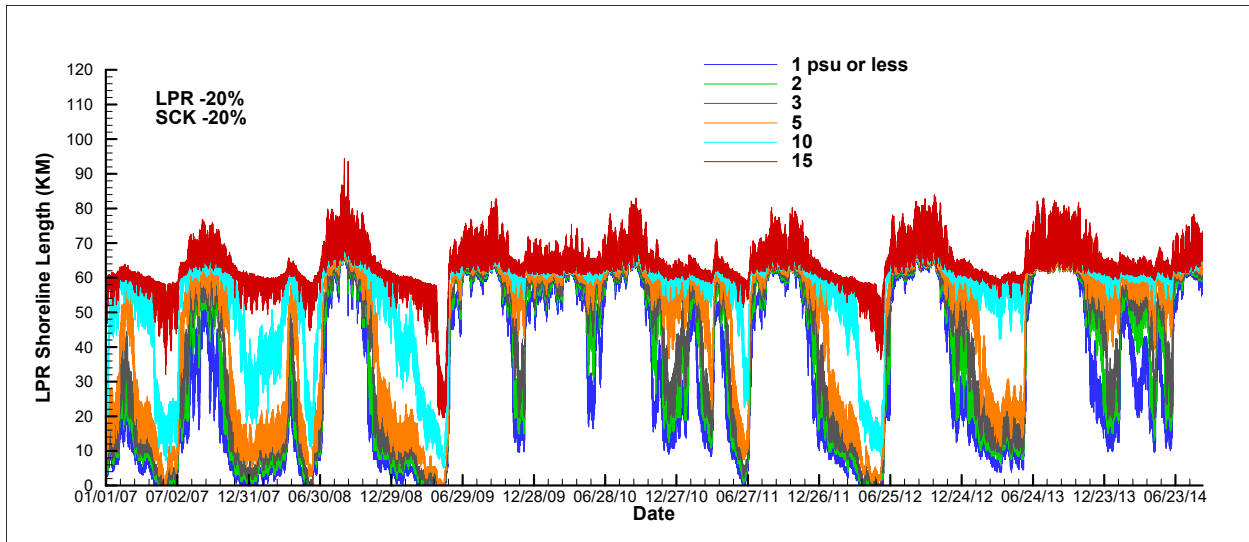


Figure A - 20. Shoreline lengths for salinity $\leq 1, 2, 3, 5, 10,$ and 15 psu in the LPR (top panel) and in LSC (bottom panel) during the simulation period of January 2007 - August 2014 for the 20% flow reduction scenario.

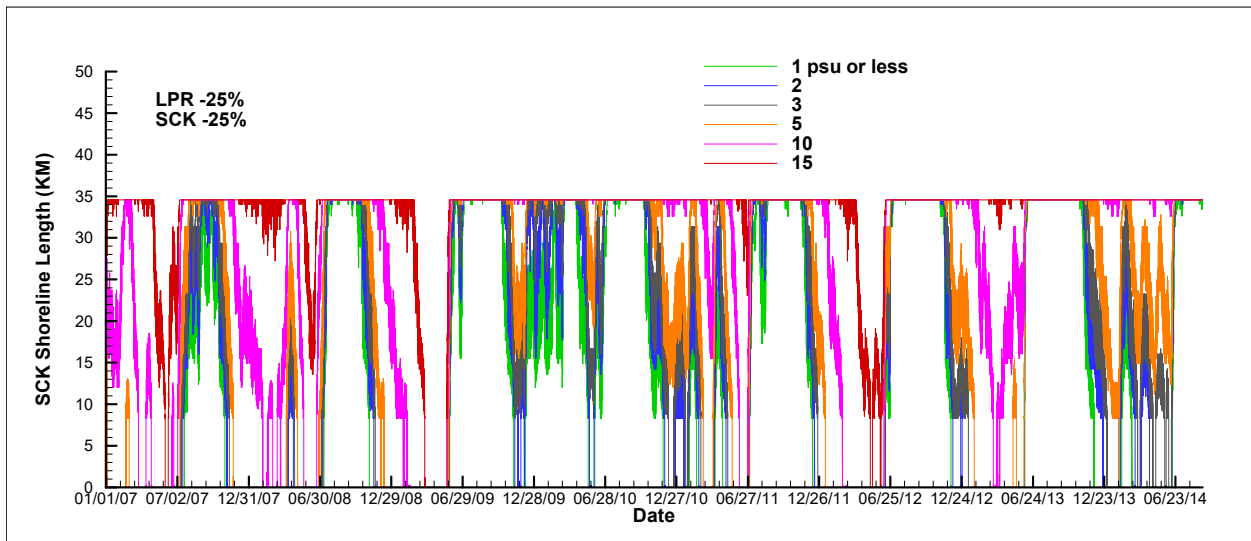
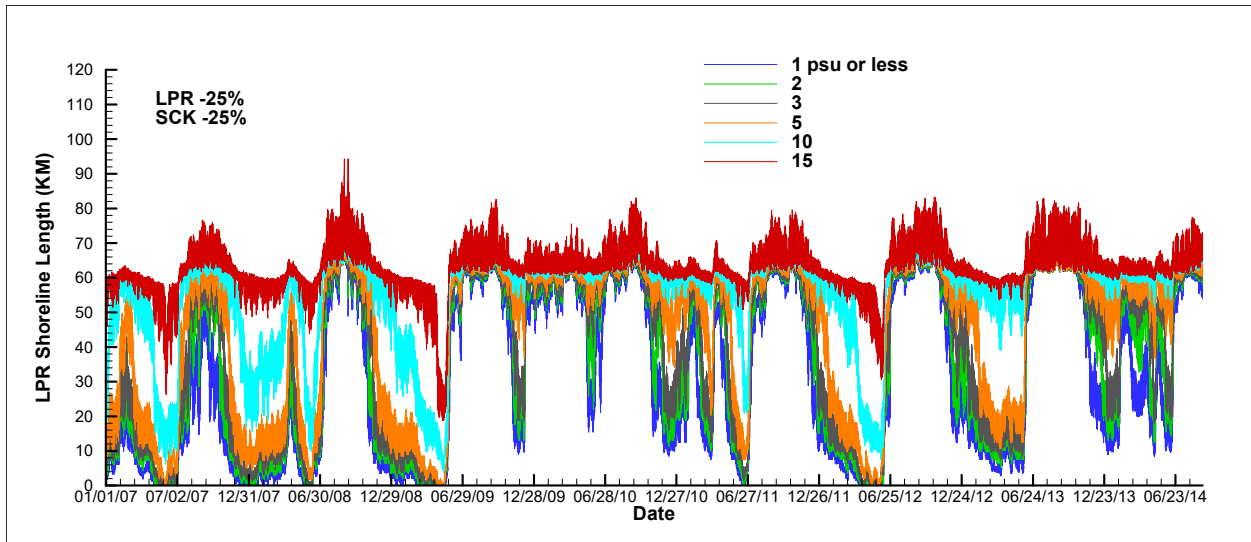


Figure A - 21. Shoreline lengths for salinity $\leq 1, 2, 3, 5, 10,$ and 15 psu in the LPR (top panel) and in LSC (bottom panel) during the simulation period of January 2007 - August 2014 for the 25% flow reduction scenario.

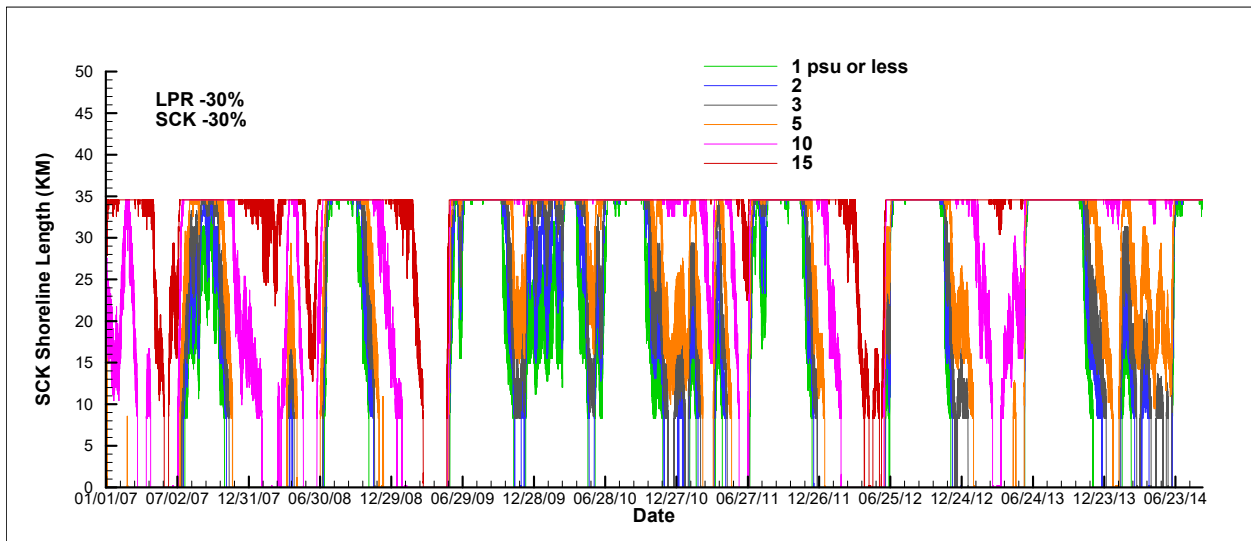
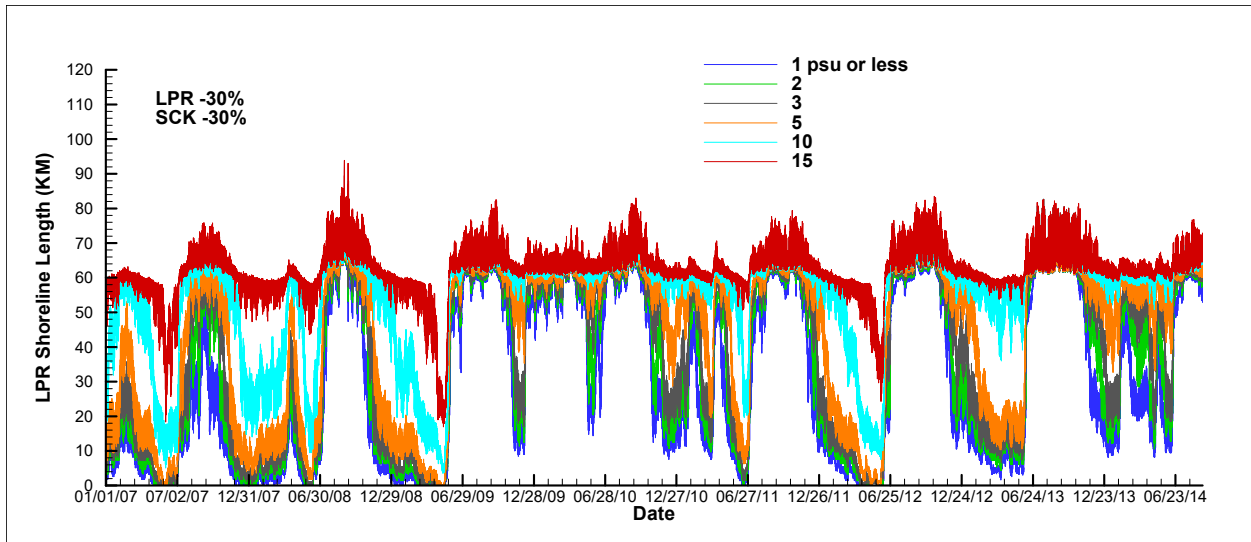


Figure A - 22. Shoreline lengths for salinity $\leq 1, 2, 3, 5, 10,$ and 15 psu in the LPR (top panel) and in LSC (bottom panel) during the simulation period of January 2007 - August 2014 for the 30% flow reduction scenario.

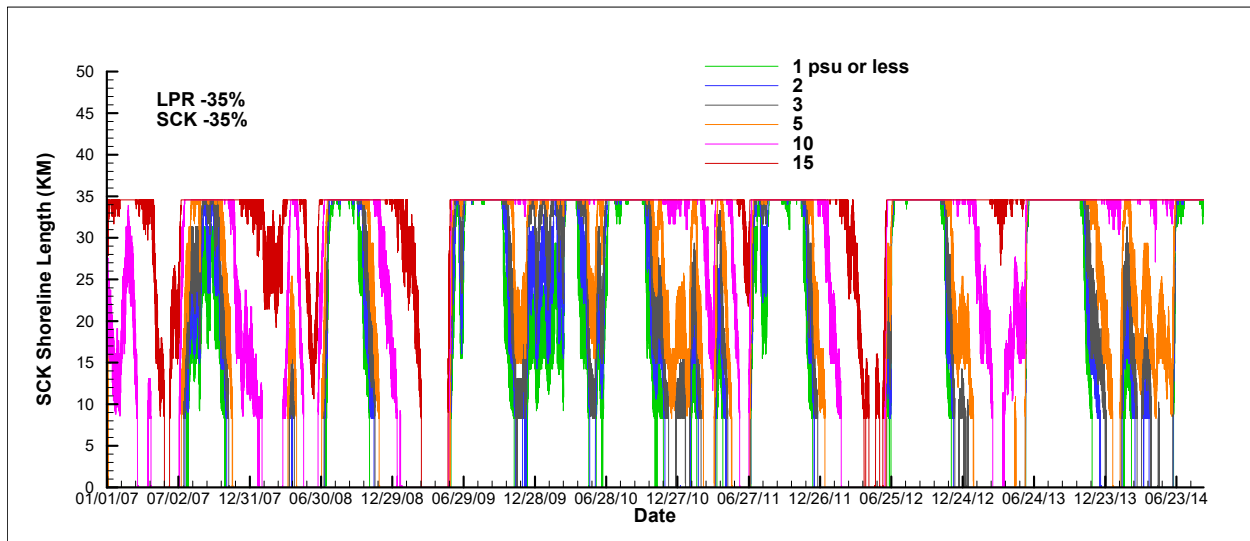
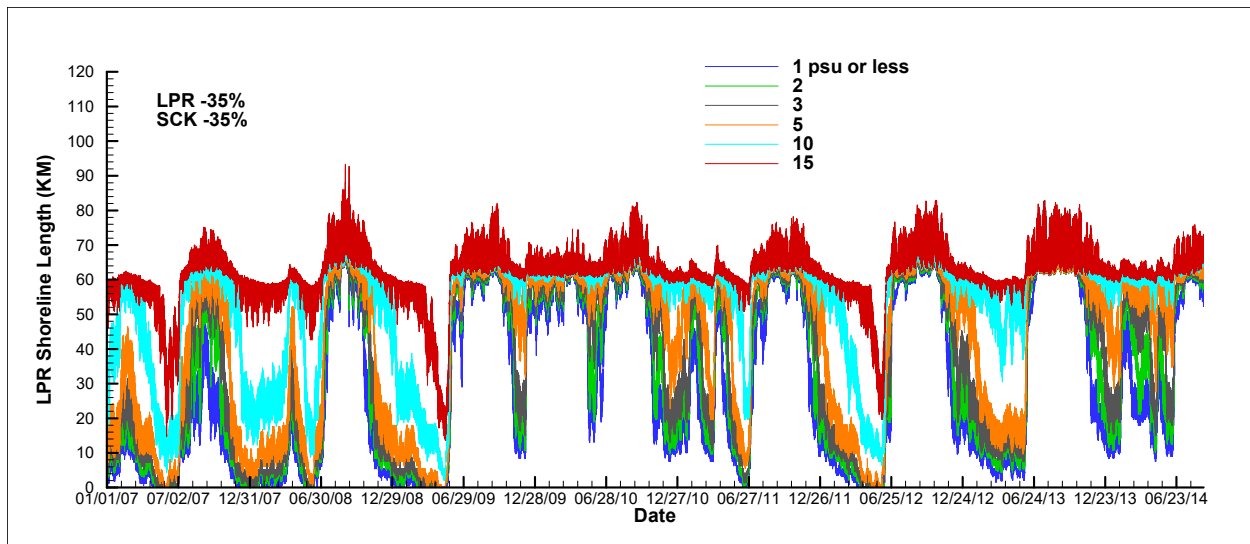


Figure A - 23. Shoreline lengths for salinity $\leq 1, 2, 3, 5, 10,$ and 15 psu in the LPR (top panel) and in LSC (bottom panel) during the simulation period of January 2007 - August 2014 for the 35% flow reduction scenario.

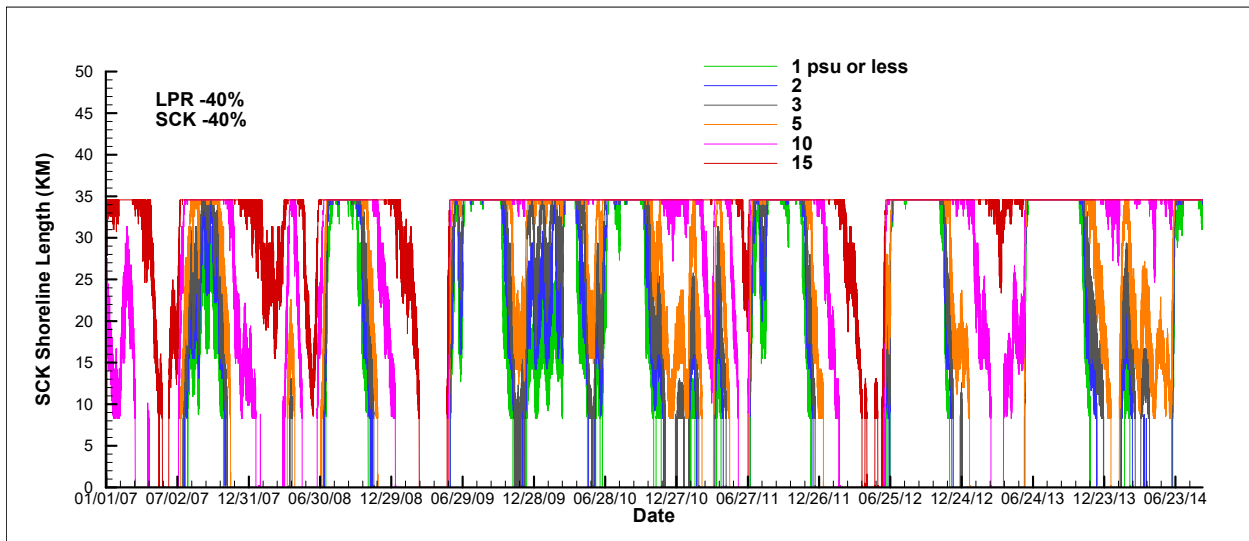
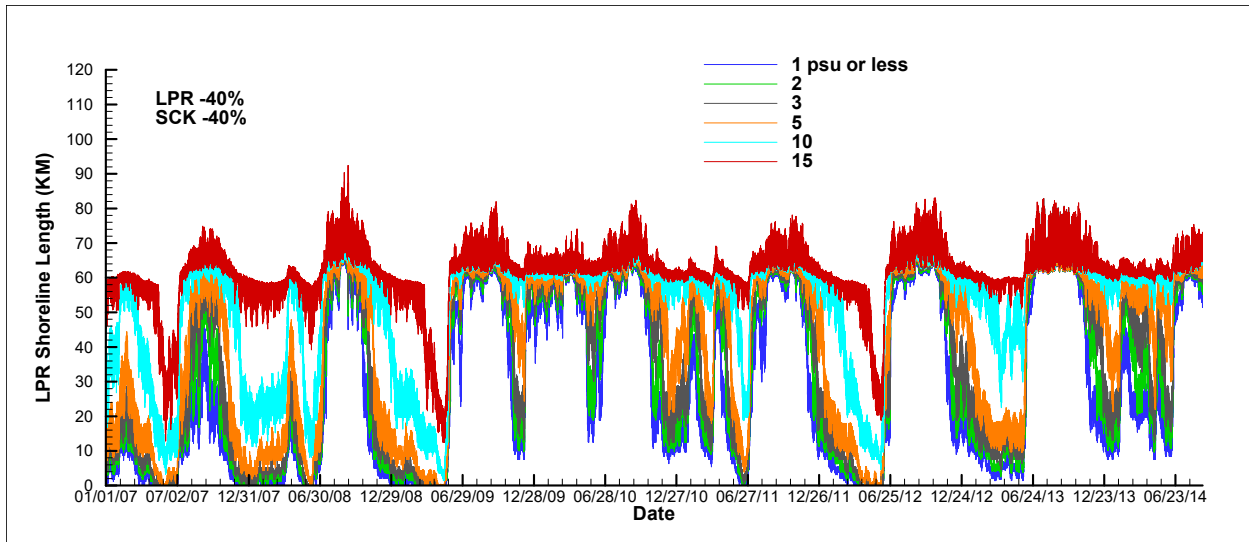


Figure A - 24. Shoreline lengths for salinity $\leq 1, 2, 3, 5, 10,$ and 15 psu in the LPR (top panel) and in LSC (bottom panel) during the simulation period of January 2007 - August 2014 for the 40% flow reduction scenario.

8. Appendix B

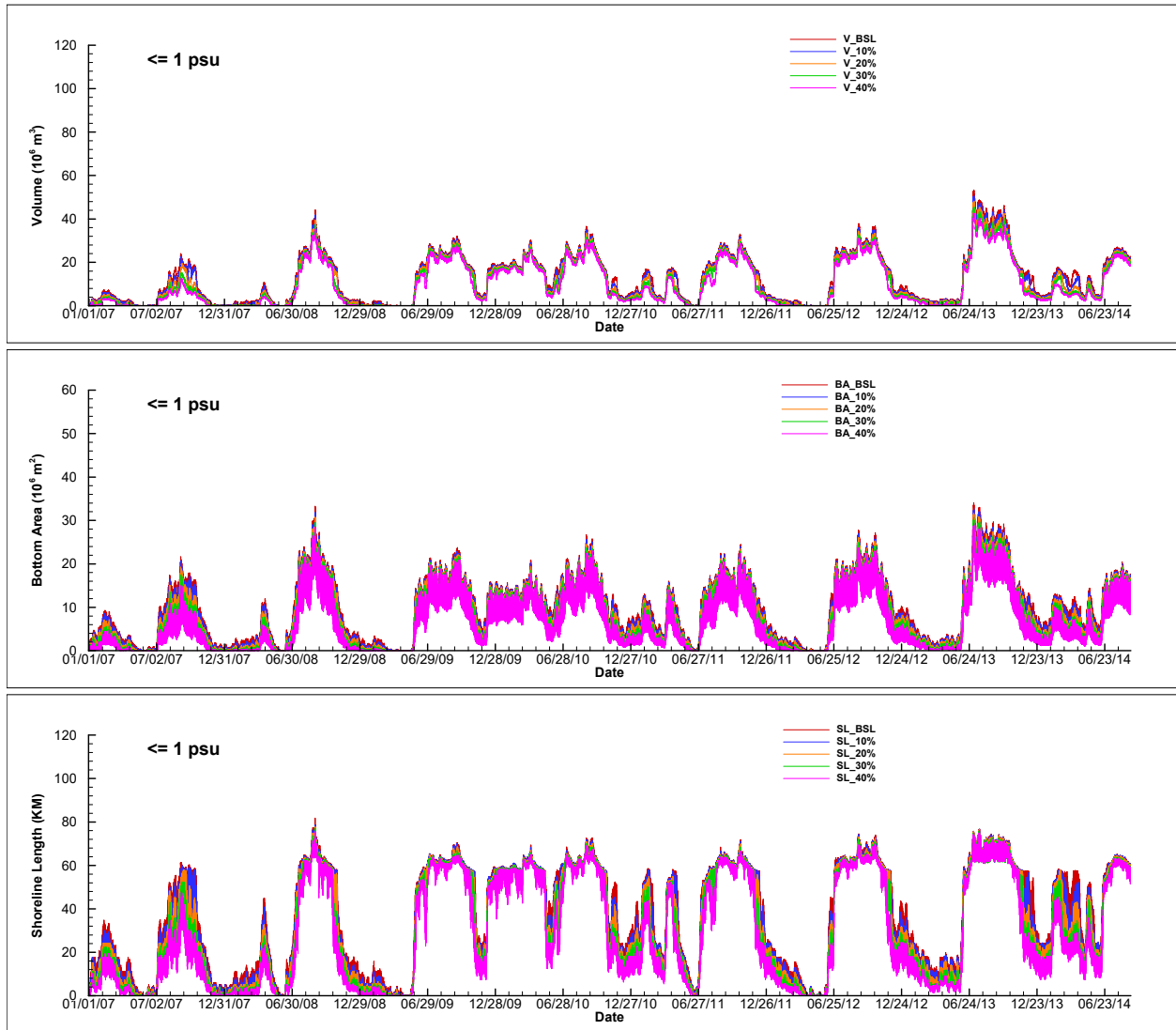


Figure B- 1. Comparisons of time series of water volume (top panel), bottom area (middle panel), and shoreline length (bottom panel) for salinity ≤ 1 psu in the LPR during the simulation period of January 2007 - August 2014 for different flow reduction scenarios.

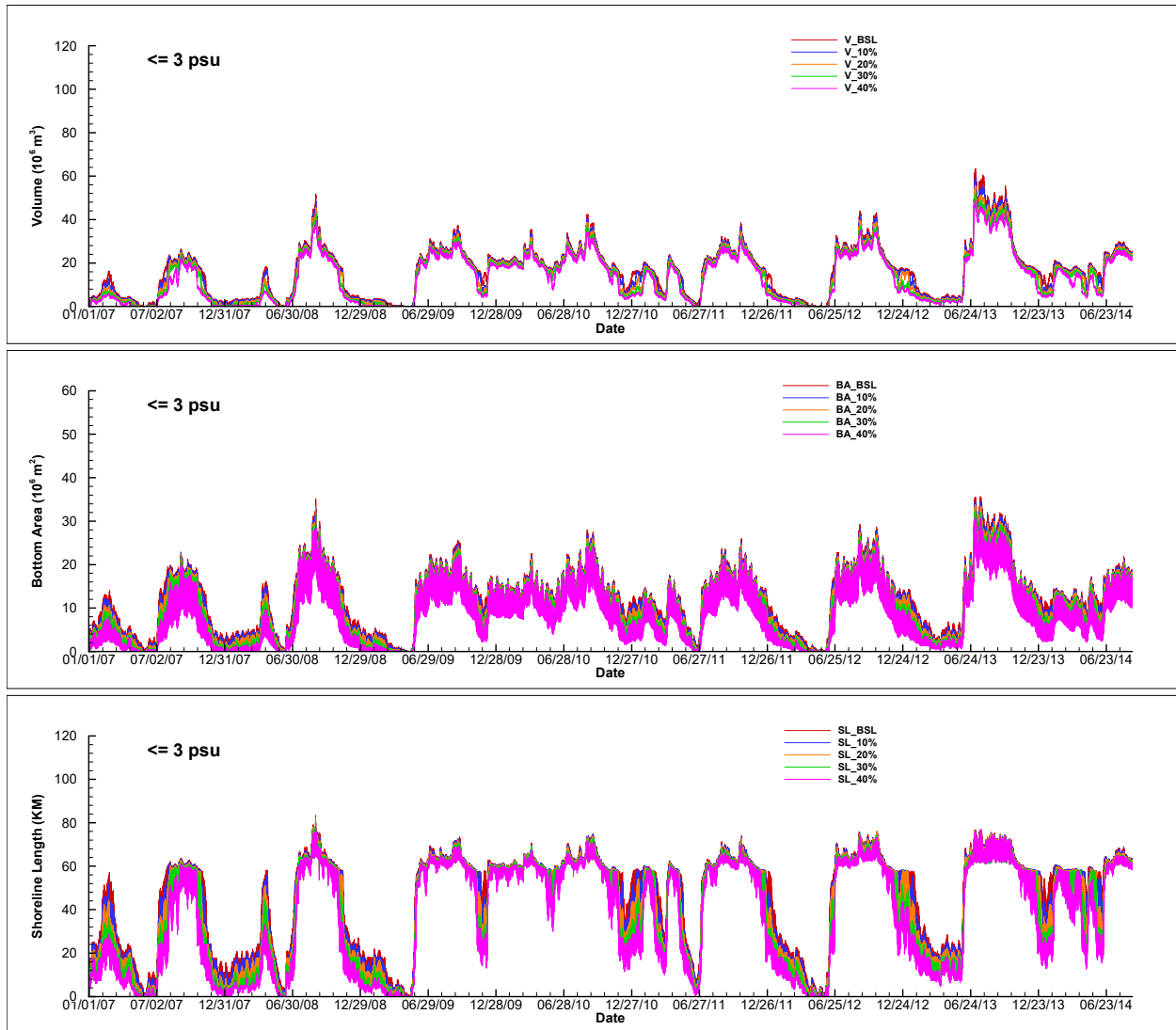


Figure B- 2. Comparisons of time series of water volume (top panel), bottom area (middle panel), and shoreline length (bottom panel) for salinity ≤ 3 psu in the LPR during the simulation period of January 2007 - August 2014 for different flow reduction scenarios.

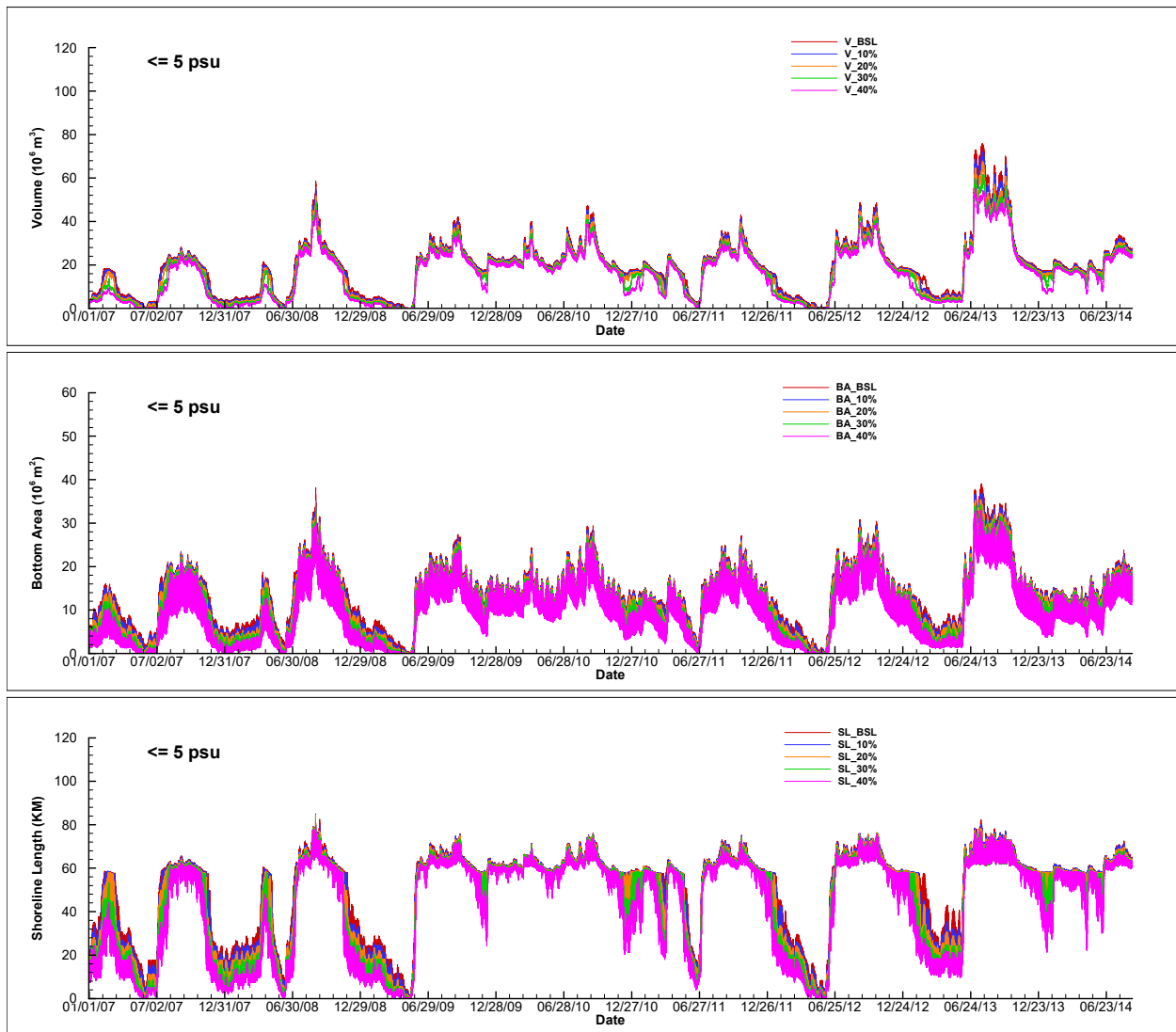


Figure B- 3. Comparisons of time series of water volume (top panel), bottom area (middle panel), and shoreline length (bottom panel) for salinity ≤ 5 psu in the LPR during the simulation period of January 2007 - August 2014 for different flow reduction scenarios.

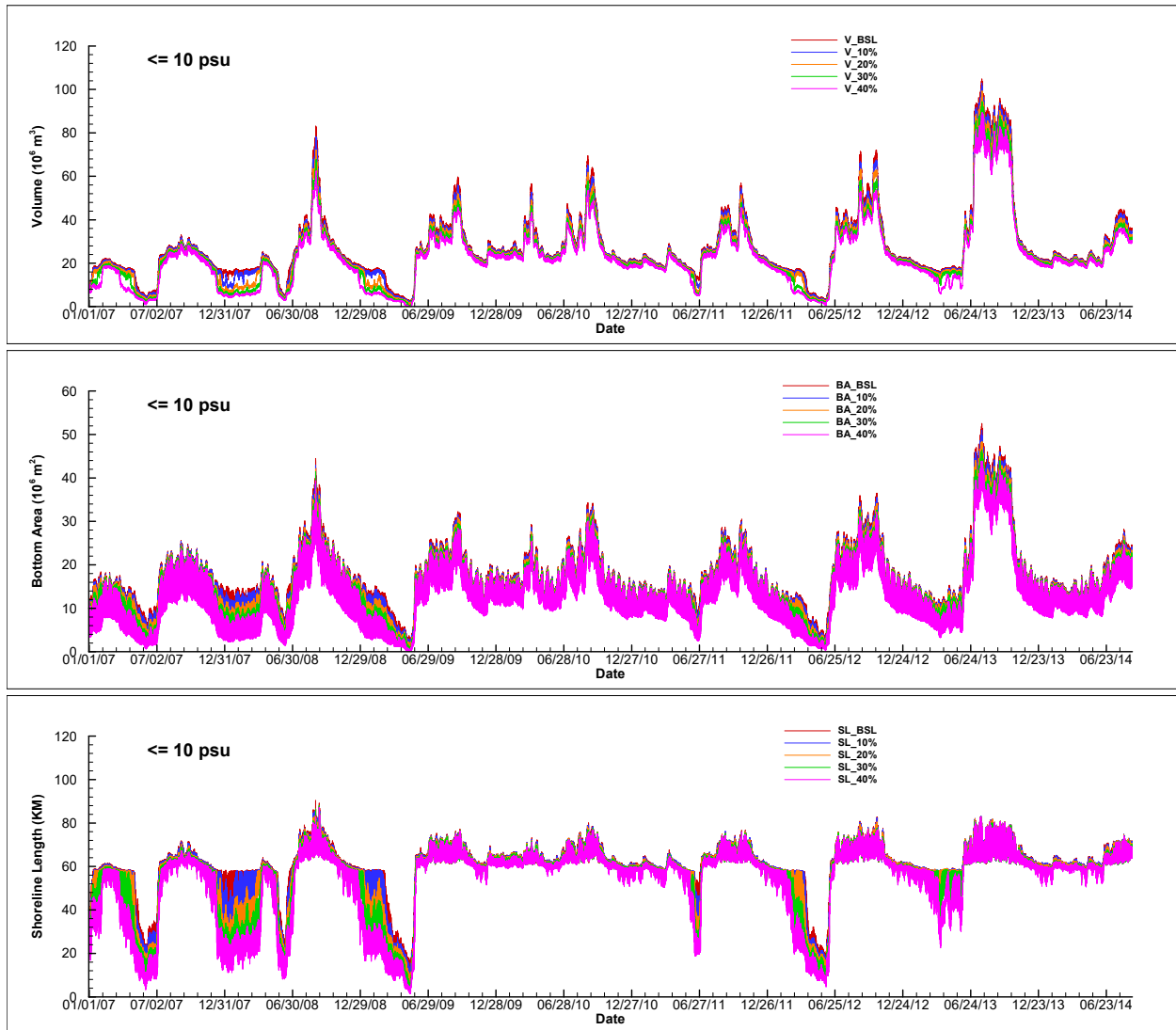


Figure B- 4. Comparisons of time series of water volume (top panel), bottom area (middle panel), and shoreline length (bottom panel) for salinity ≤ 10 psu in the LPR during the simulation period of January 2007 - August 2014 for different flow reduction scenarios.

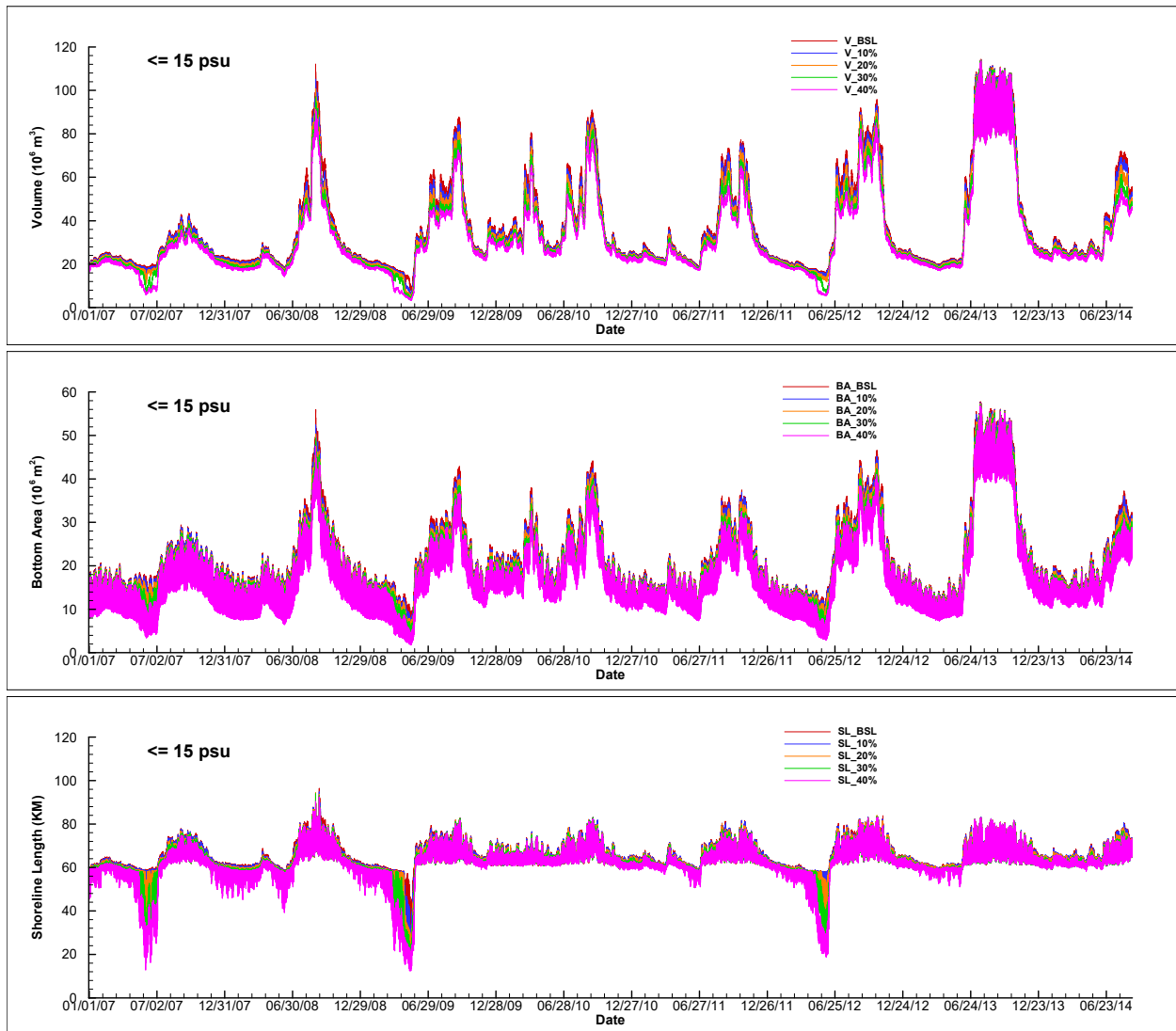


Figure B- 5. Comparisons of time series of water volume (top panel), bottom area (middle panel), and shoreline length (bottom panel) for salinity ≤ 15 psu in the LPR during the simulation period of January 2007 - August 2014 for different flow reduction scenarios.

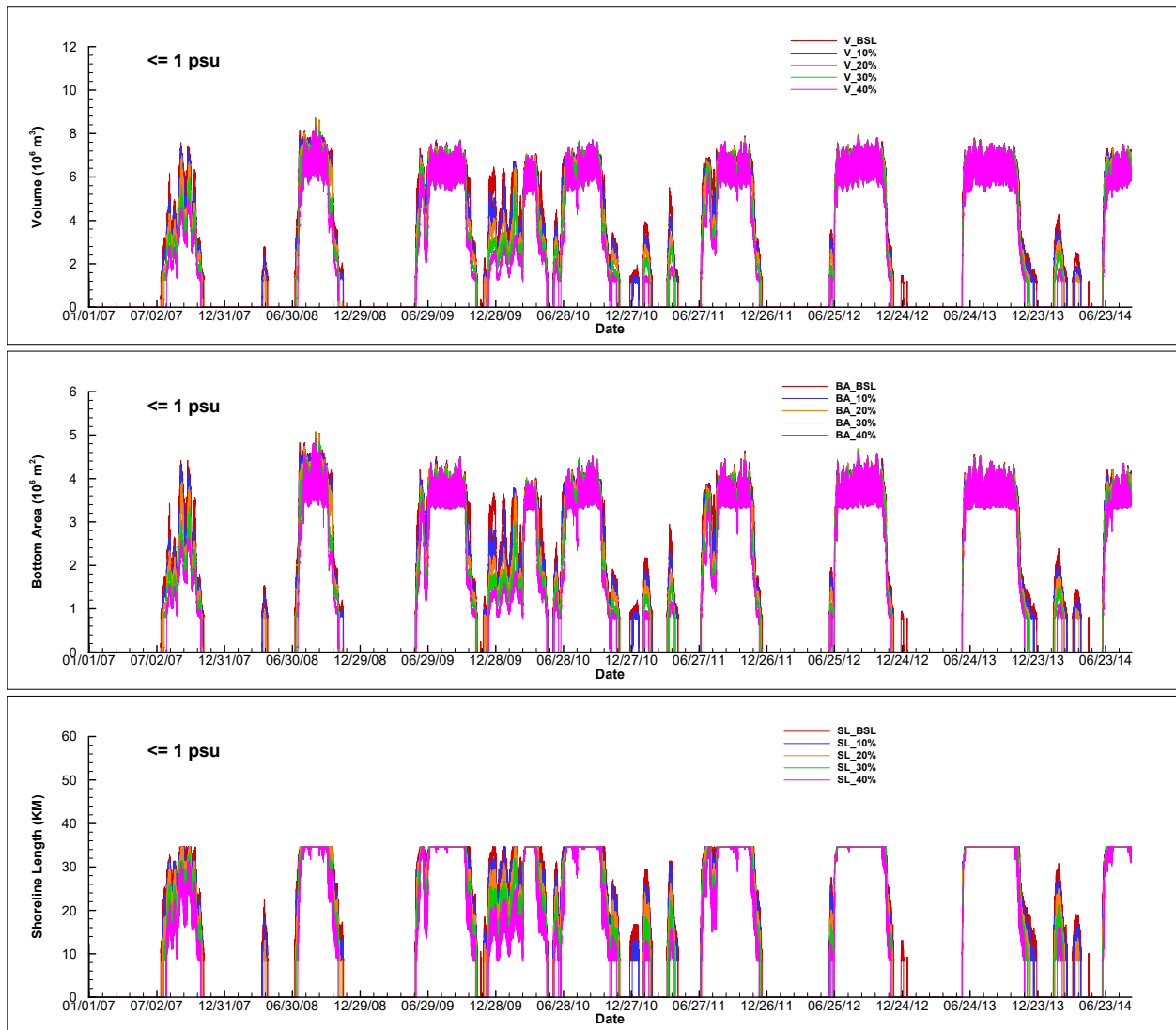


Figure B- 6. Comparisons of time series of water volume (top panel), bottom area (middle panel), and shoreline length (bottom panel) for salinity ≤ 2 psu in LSC during the simulation period of January 2007 - August 2014 for different flow reduction scenarios.

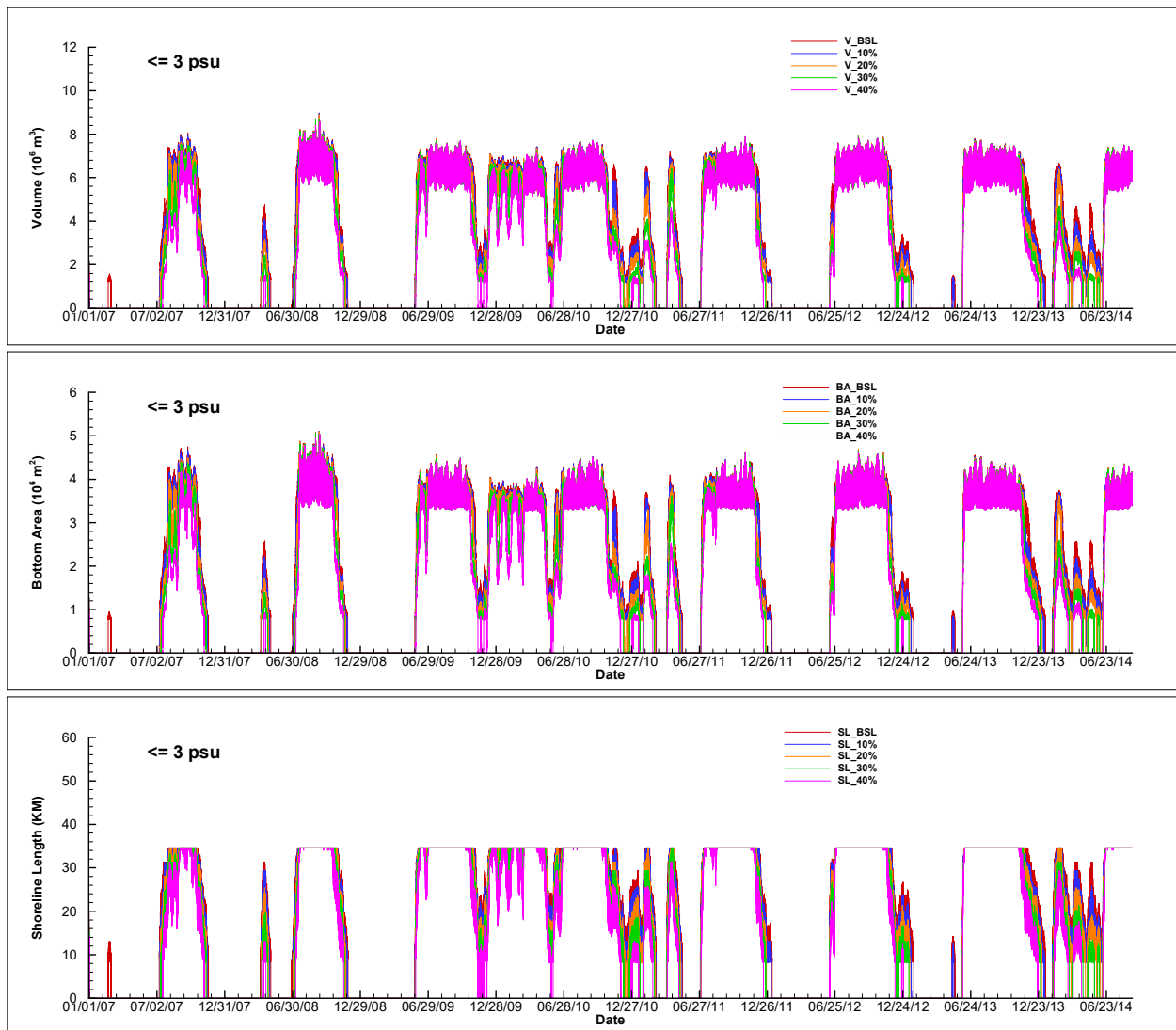


Figure B- 7. Comparisons of time series of water volume (top panel), bottom area (middle panel), and shoreline length (bottom panel) for salinity ≤ 3 psu in LSC during the simulation period of January 2007 - August 2014 for different flow reduction scenarios.

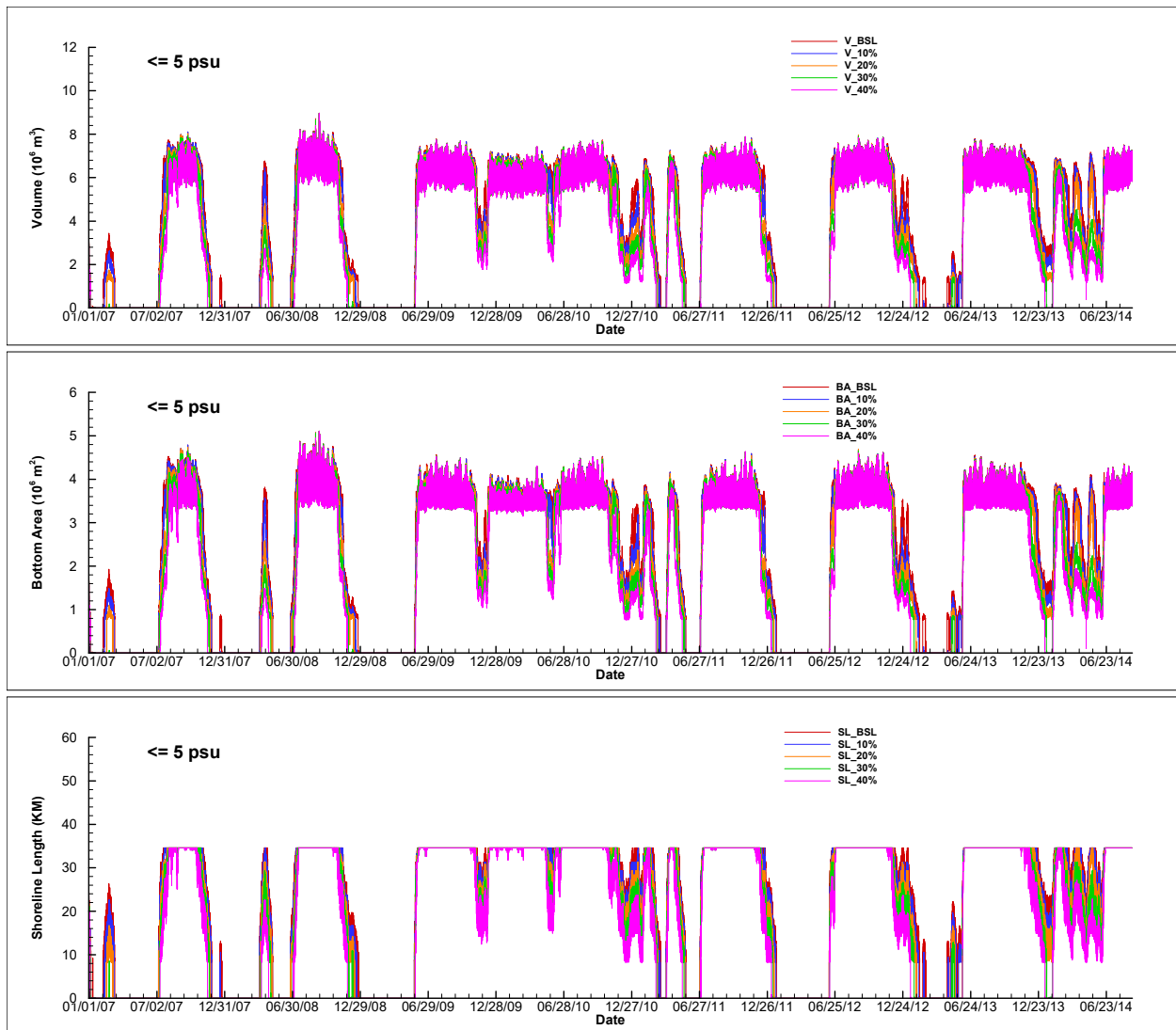


Figure B- 8. Comparisons of time series of water volume (top panel), bottom area (middle panel), and shoreline length (bottom panel) for salinity ≤ 5 psu in LSC during the simulation period of January 2007 - August 2014 for different flow reduction scenarios.

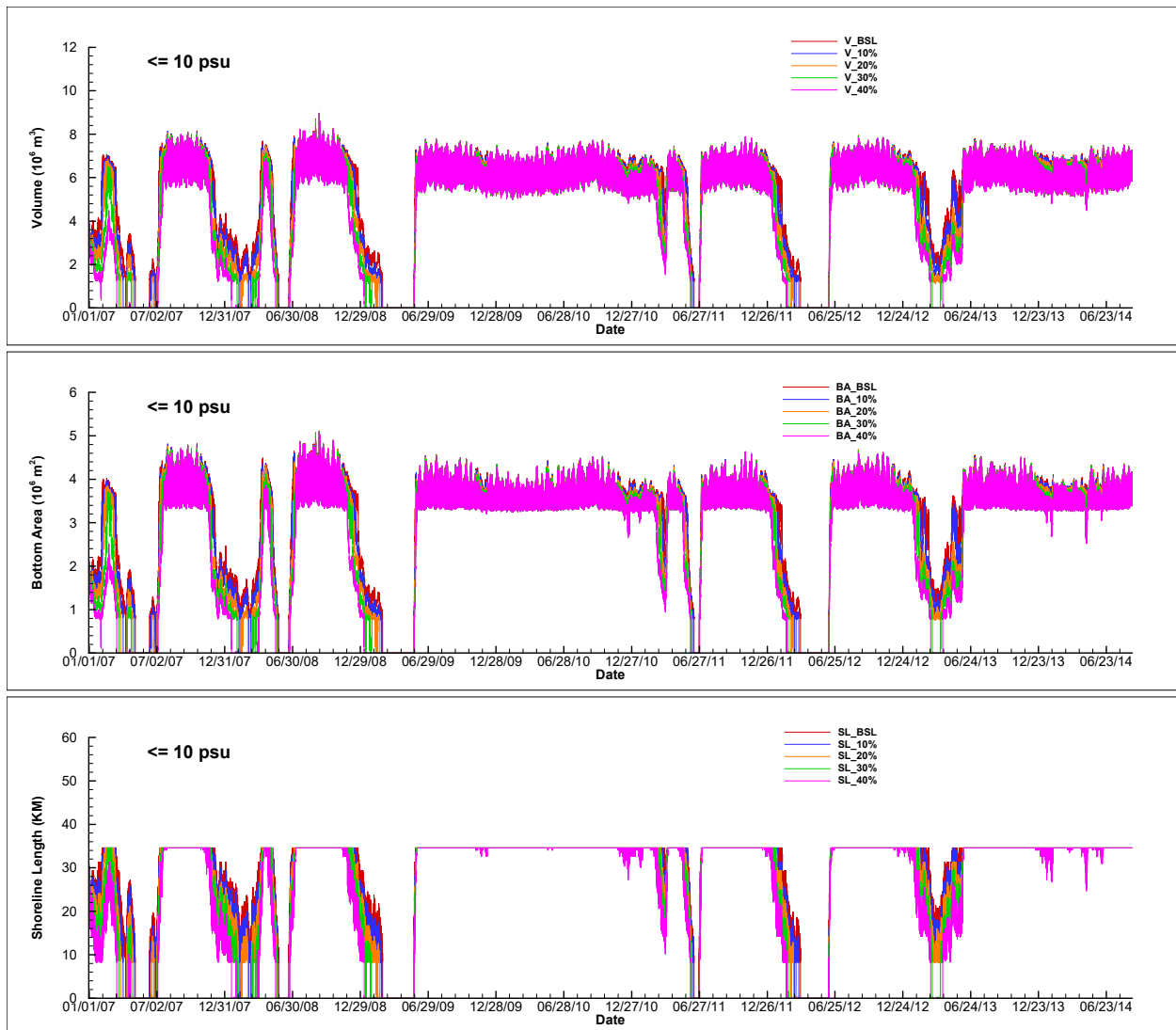


Figure B- 9. Comparisons of time series of water volume (top panel), bottom area (middle panel), and shoreline length (bottom panel) for salinity ≤ 10 psu in LSC during the simulation period of January 2007 - August 2014 for different flow reduction scenarios.

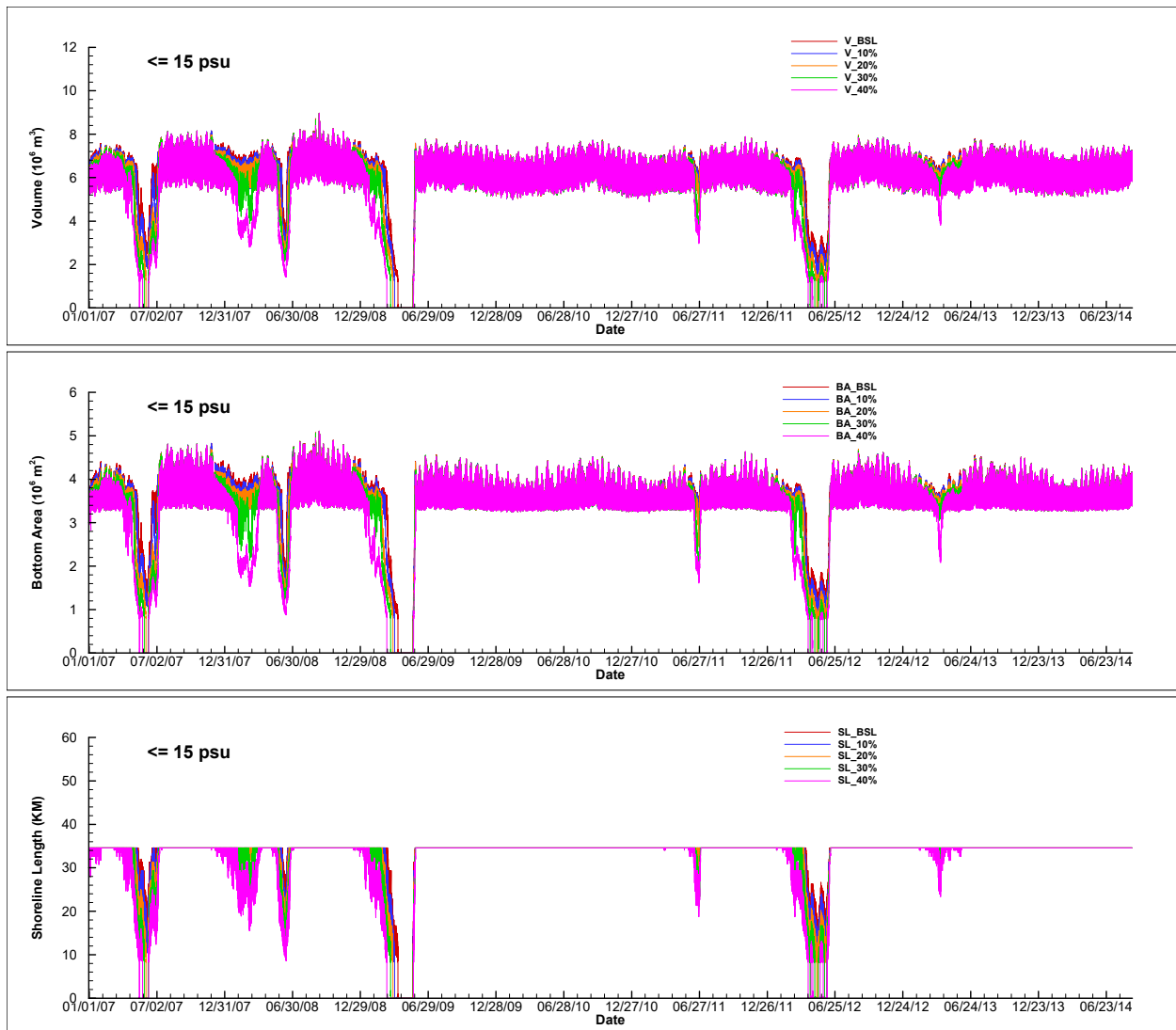


Figure B- 10. Comparisons of time series of water volume (top panel), bottom area (middle panel), and shoreline length (bottom panel) for salinity ≤ 15 psu in LSC during the simulation period of January 2007 - August 2014 for different flow reduction scenarios.

9. Appendix C

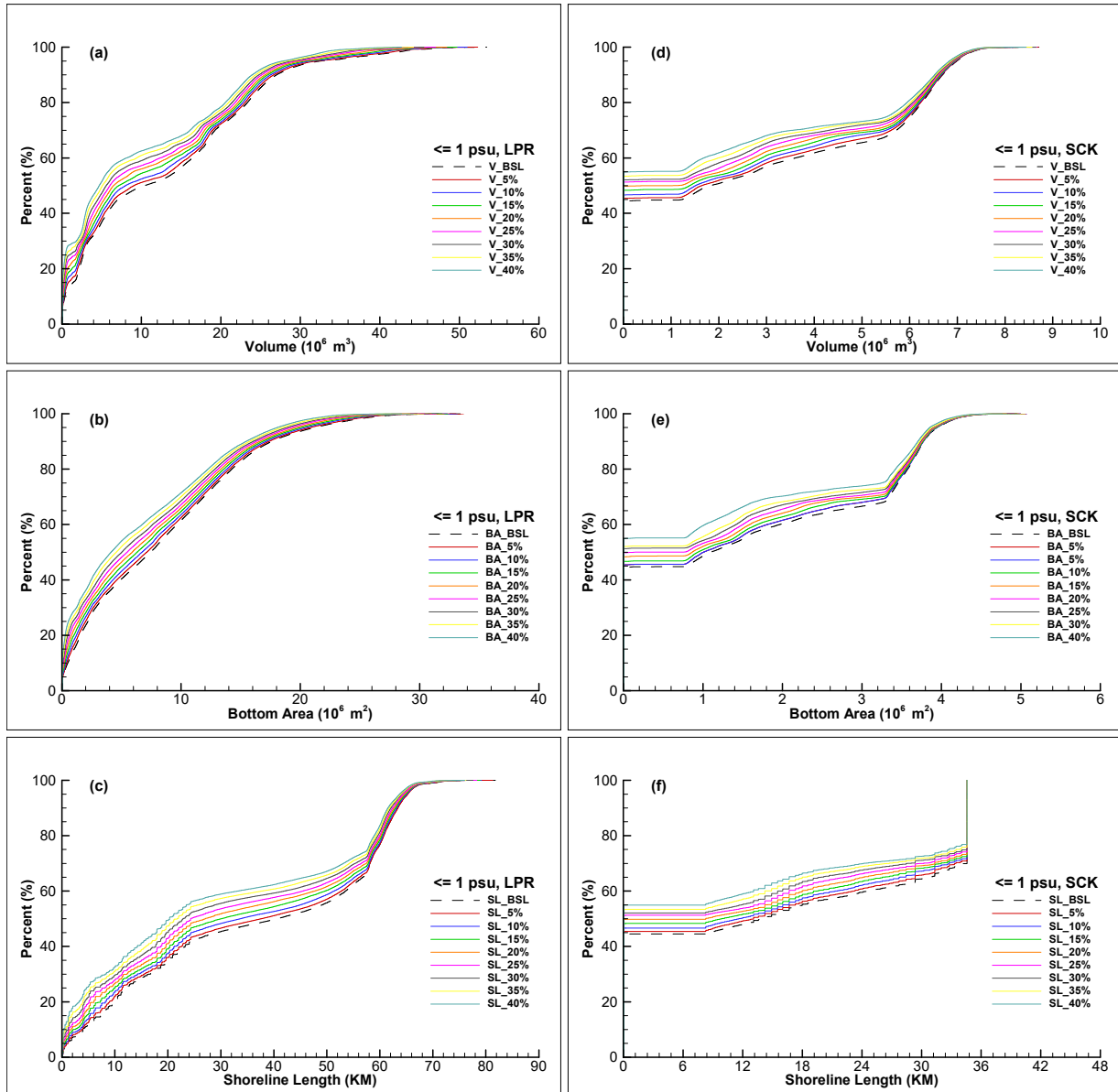


Figure C - 1. CDFs of ≤ 1 psu water volume (a & d), bottom area (b & e), and shoreline length (c & f) in the LPR and LSC during the simulation period of January 2007 - August 2014 for different flow reduction scenarios.

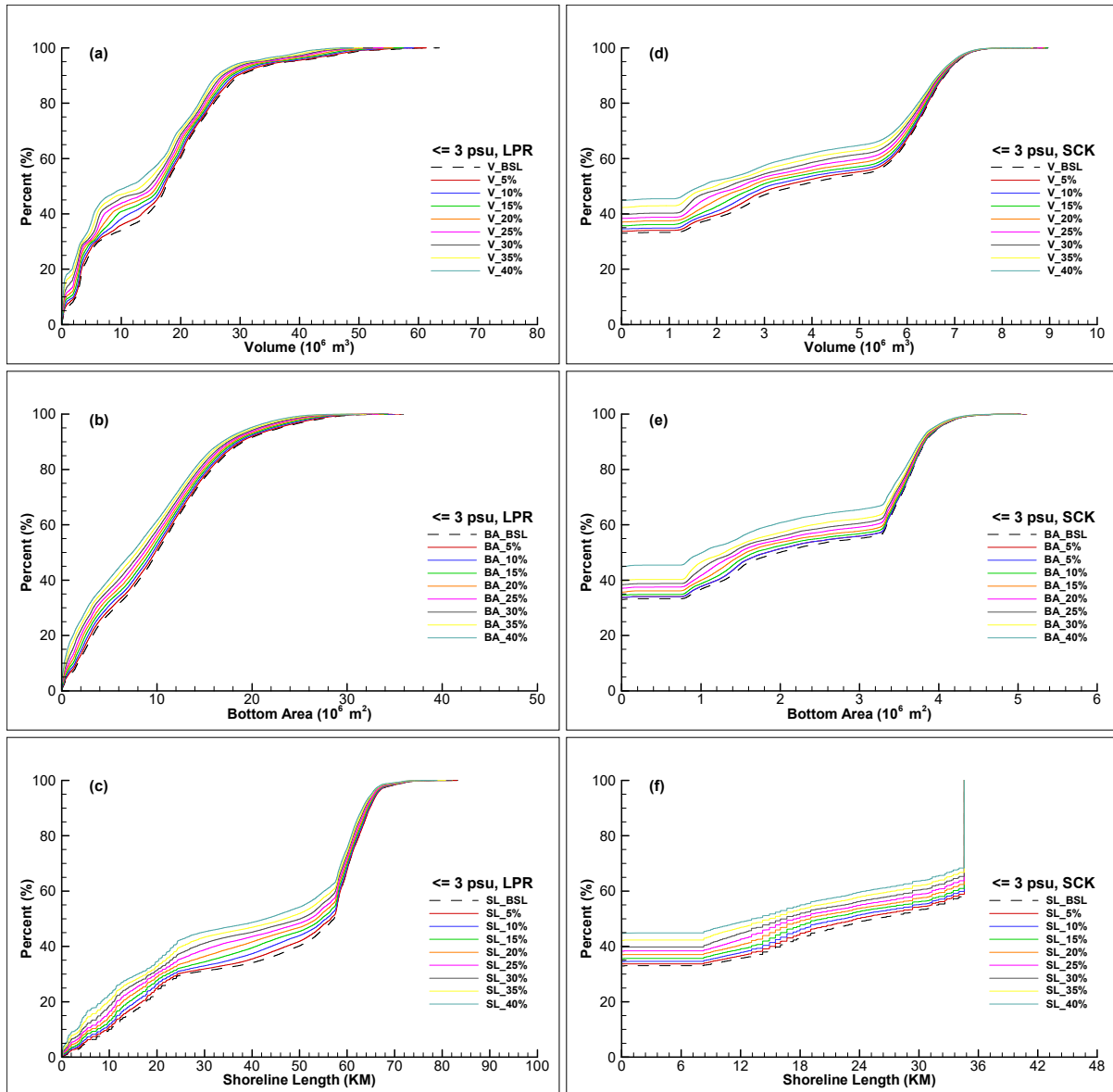


Figure C - 2. CDFs of ≤ 3 psu water volume (a & d), bottom area (b & e), and shoreline length (c & f) in the LPR and LSC during the simulation period of January 2007 - August 2014 for different flow reduction scenarios.

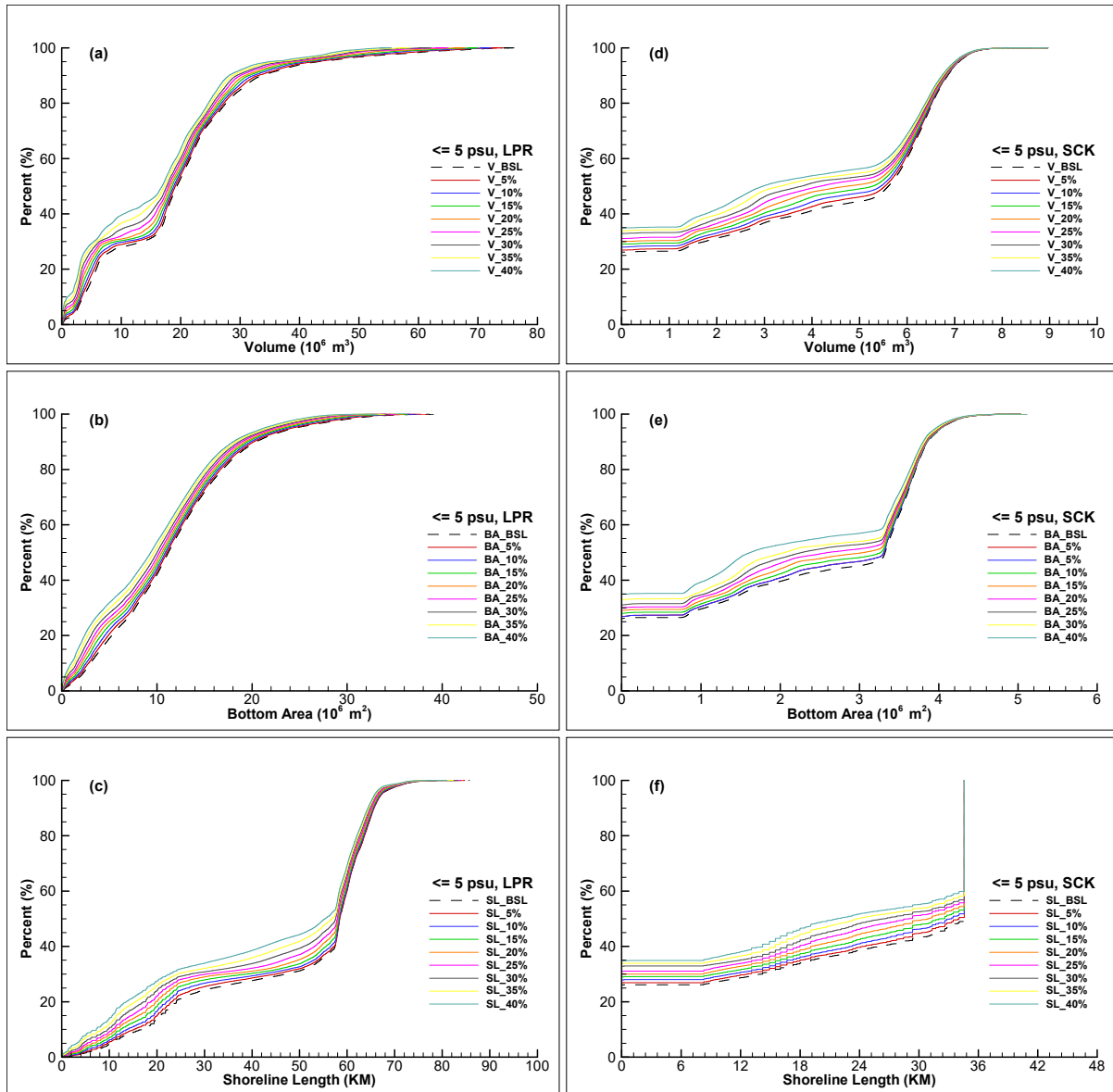


Figure C - 3. CDFs of ≤ 5 psu water volume (a & d), bottom area (b & e), and shoreline length (c & f) in the LPR and LSC during the simulation period of January 2007 - August 2014 for different flow reduction scenarios.

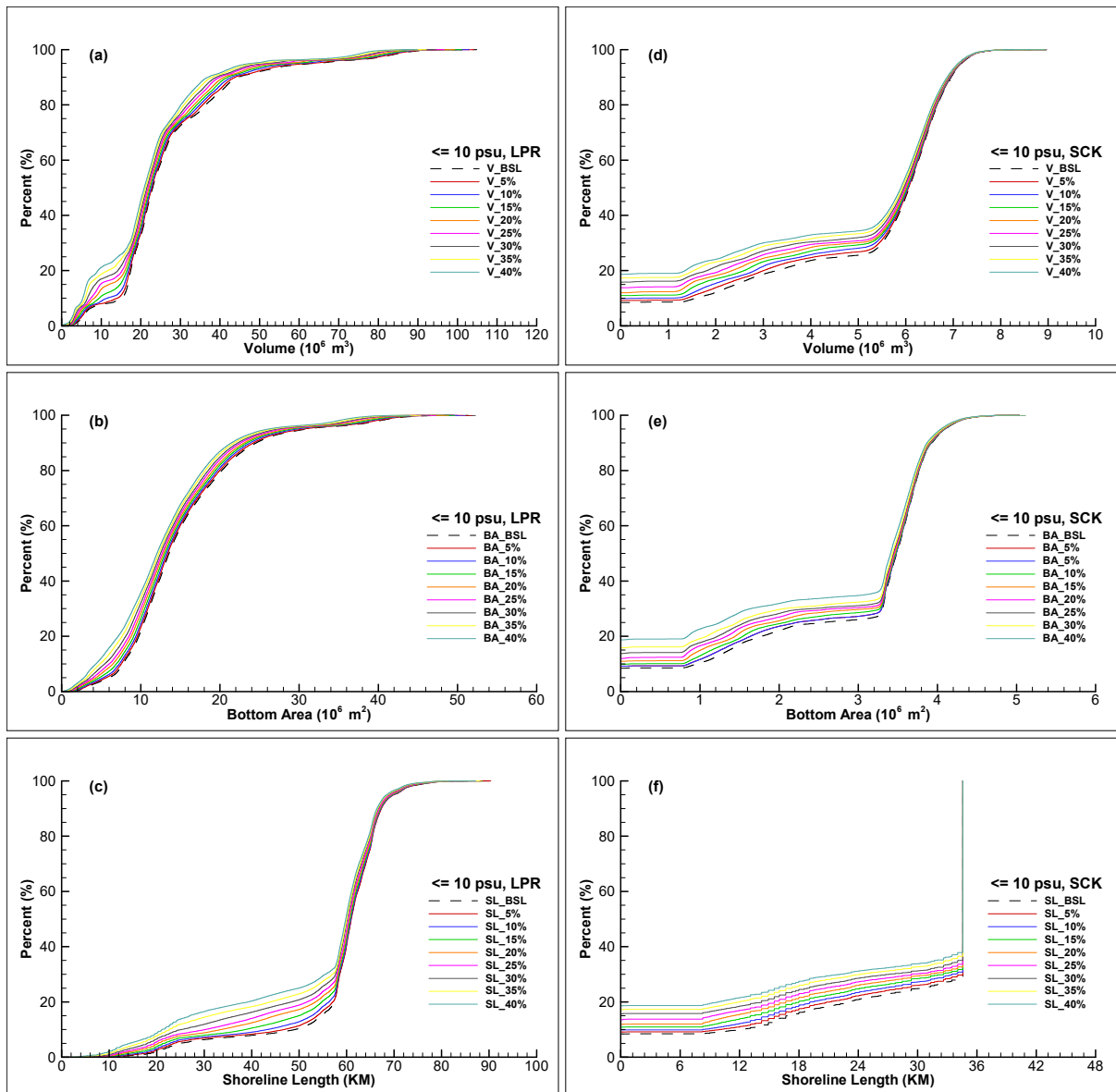


Figure C - 4. CDFs of ≤ 10 psu water volume (a & d), bottom area (b & e), and shoreline length (c & f) in the LPR and LSC during the simulation period of January 2007 - August 2014 for different flow reduction scenarios.

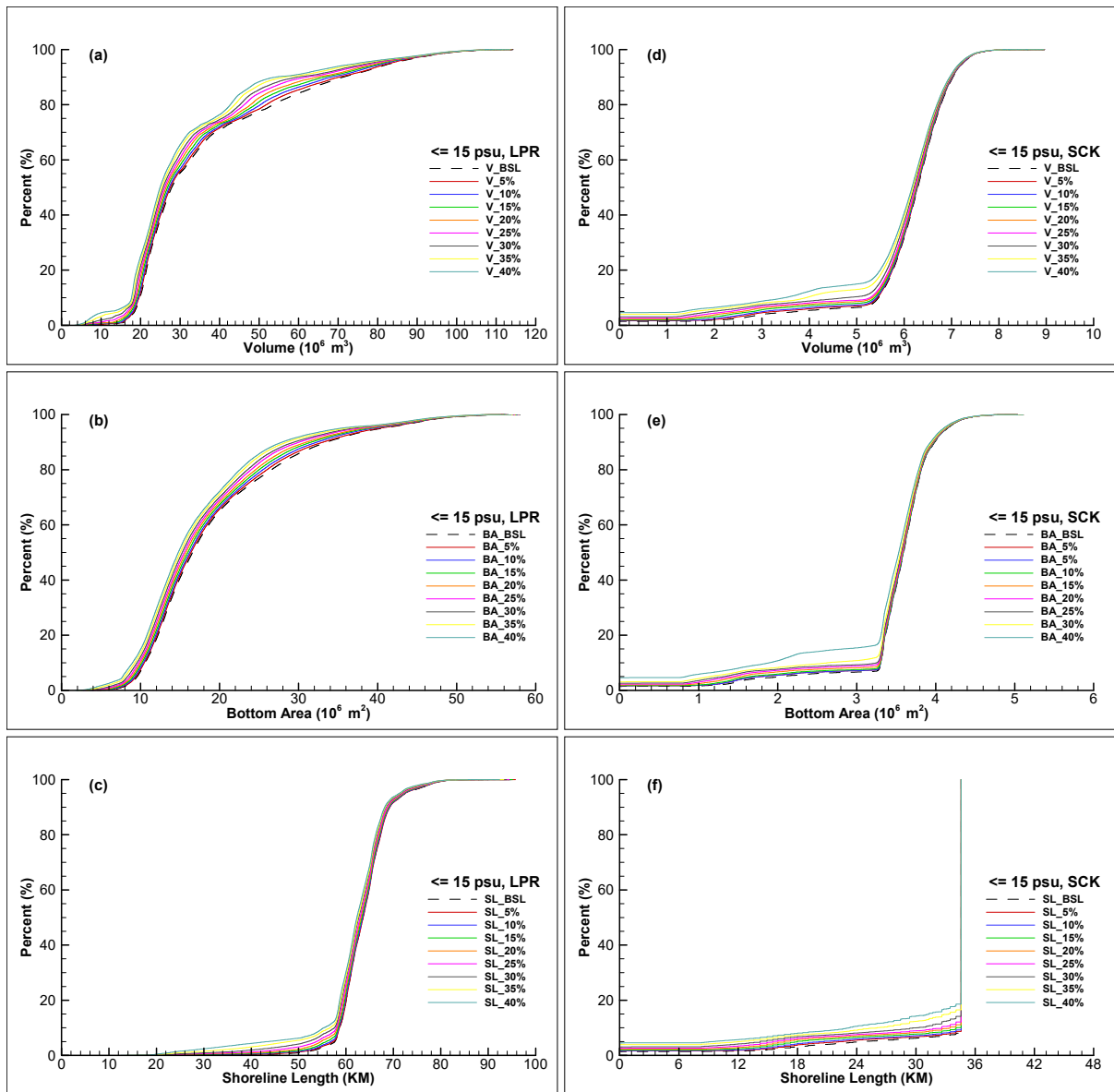


Figure C - 5. CDFs of ≤ 15 psu water volume (a & d), bottom area (b & e), and shoreline length (c & f) in the LPR and LSC during the simulation period of January 2007 - August 2014 for different flow reduction scenarios.

10. Appendix D

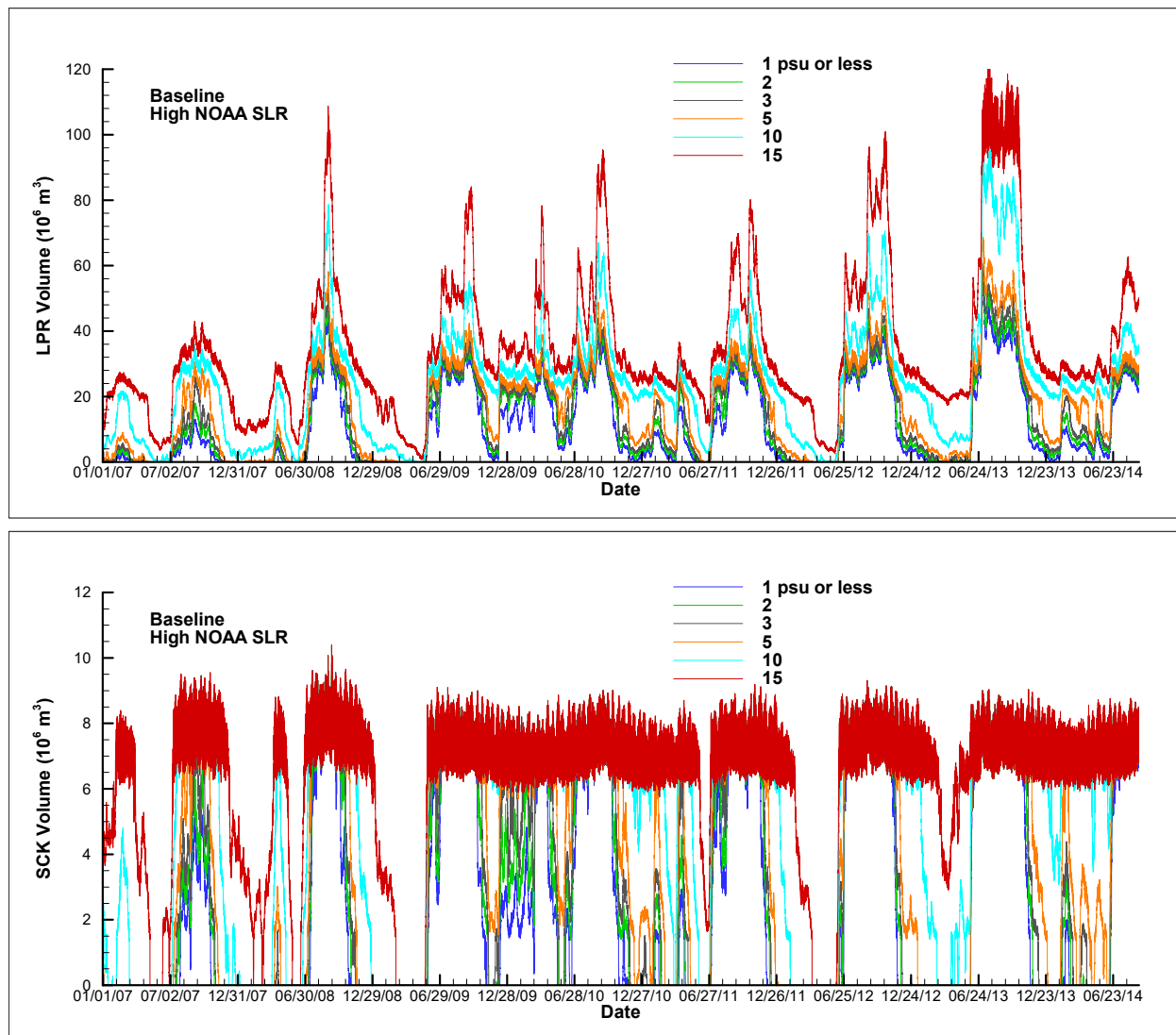


Figure D - 1. Water volumes for salinity $\leq 1, 2, 3, 5, 10,$ and 15 psu in the LPR (top panel) and in LSC (bottom panel) during the simulation period of January 2007 - August 2014 for the baseline scenario with the high SLR estimate.

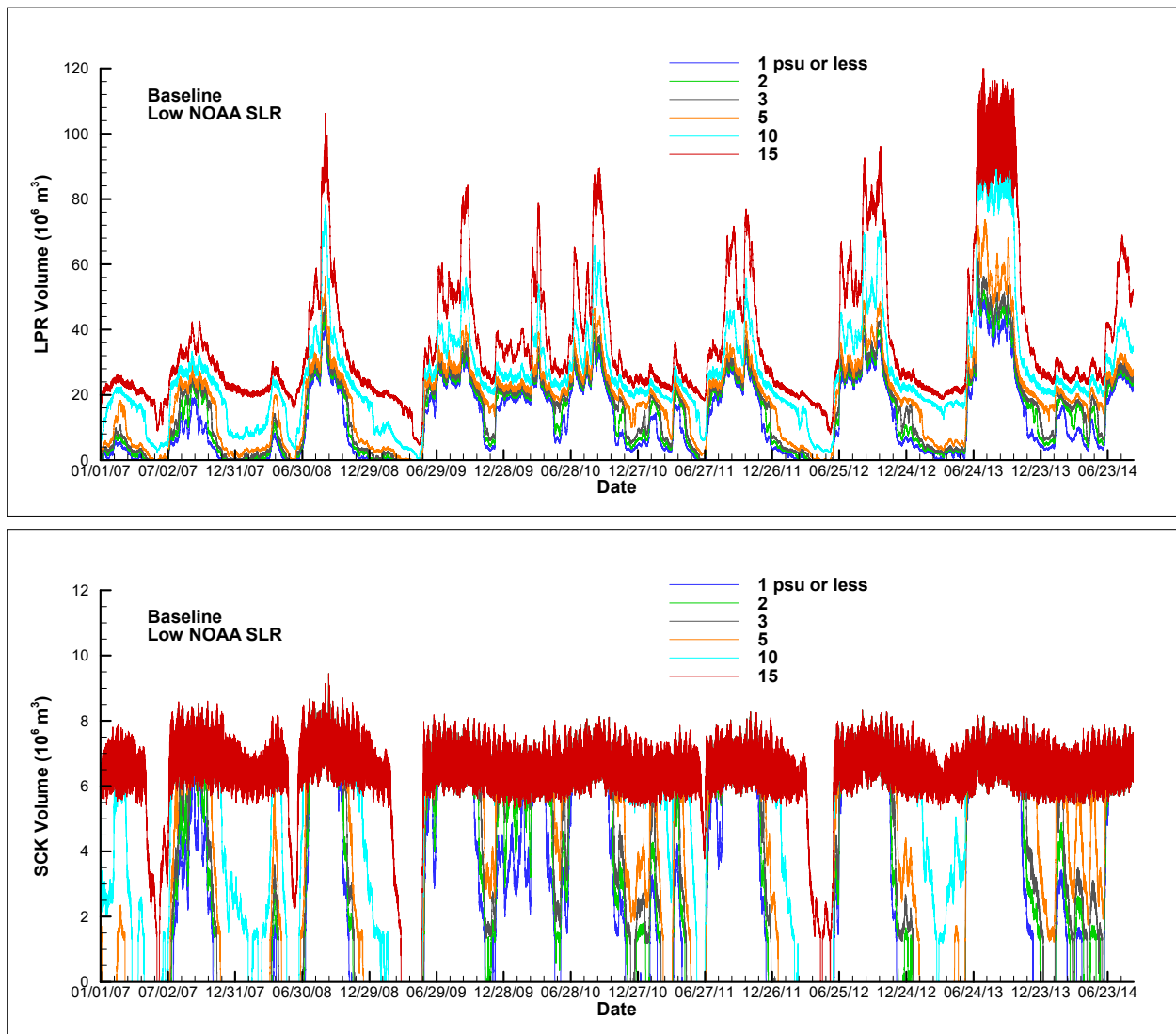


Figure D - 2. Water volumes for salinity $\leq 1, 2, 3, 5, 10,$ and 15 psu in the LPR (top panel) and in LSC (bottom panel) during the simulation period of January 2007 - August 2014 for the baseline scenario with the low SLR estimate.

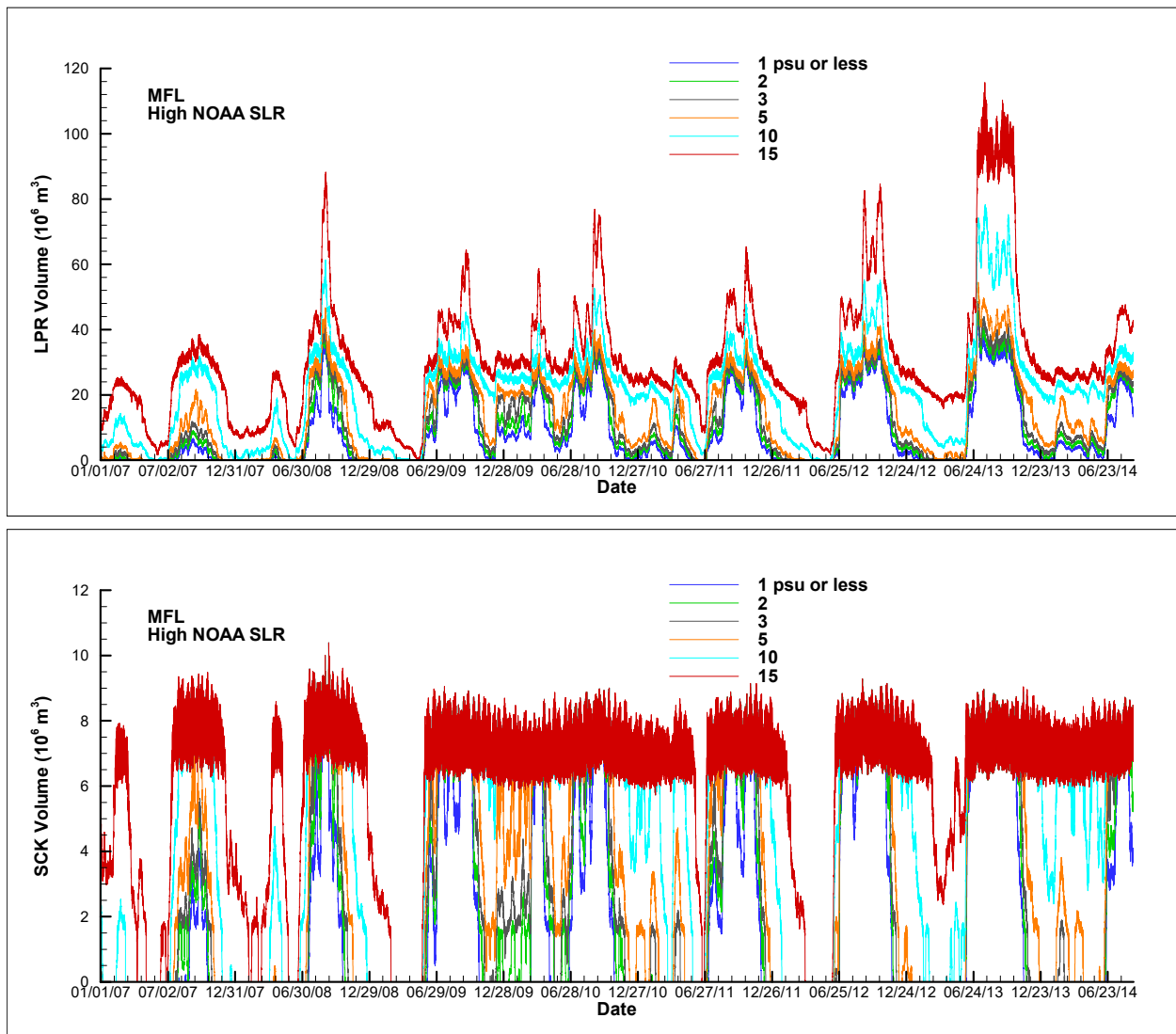


Figure D - 3. Water volumes for salinity $\leq 1, 2, 3, 5, 10,$ and 15 psu in the LPR (top panel) and in LSC (bottom panel) during the simulation period of January 2007 - August 2014 for the MFL scenario with the high SLR estimate.

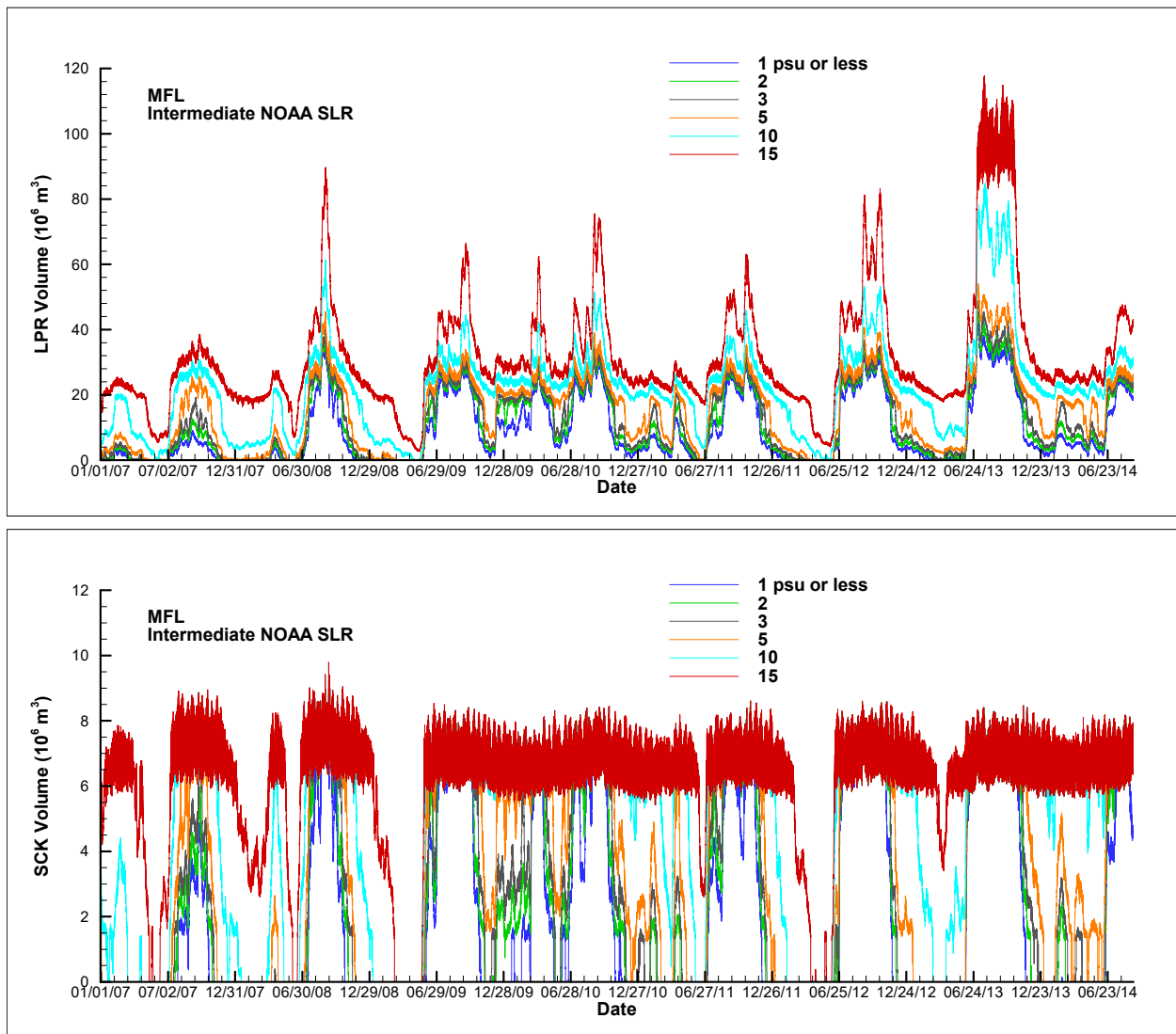


Figure D - 4. Water volumes for salinity $\leq 1, 2, 3, 5, 10,$ and 15 psu in the LPR (top panel) and in LSC (bottom panel) during the simulation period of January 2007 - August 2014 for the MFL scenario with the intermediate SLR estimate.

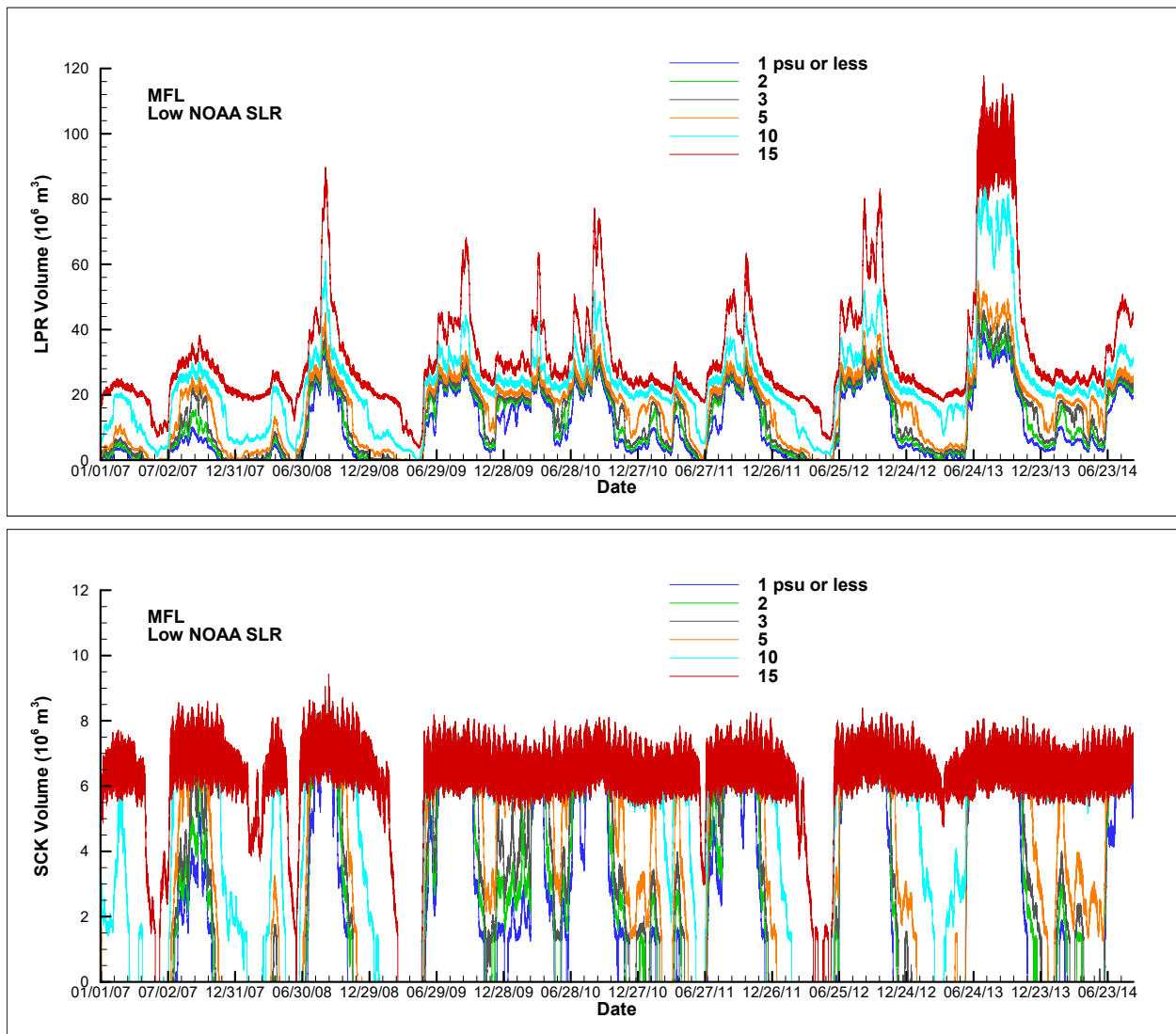


Figure D - 5. Water volumes for salinity $\leq 1, 2, 3, 5, 10,$ and 15 psu in the LPR (top panel) and in LSC (bottom panel) during the simulation period of January 2007 - August 2014 for the MFL scenario with the low SLR estimate.

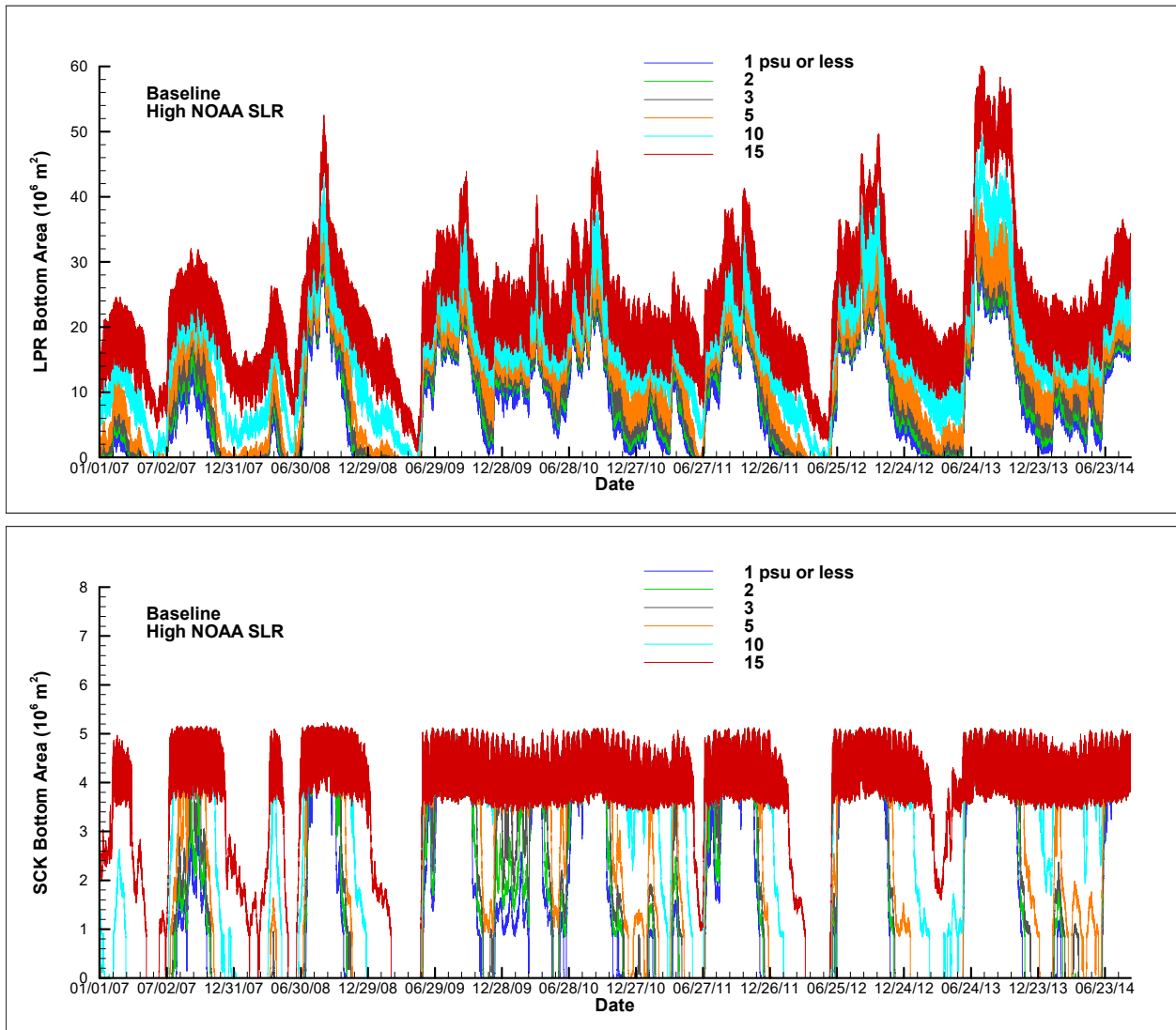


Figure D - 6. Bottom areas for salinity $\leq 1, 2, 3, 5, 10,$ and 15 psu in the LPR (top panel) and in LSC (bottom panel) during the simulation period of January 2007 - August 2014 for the baseline scenario with the high SLR estimate.

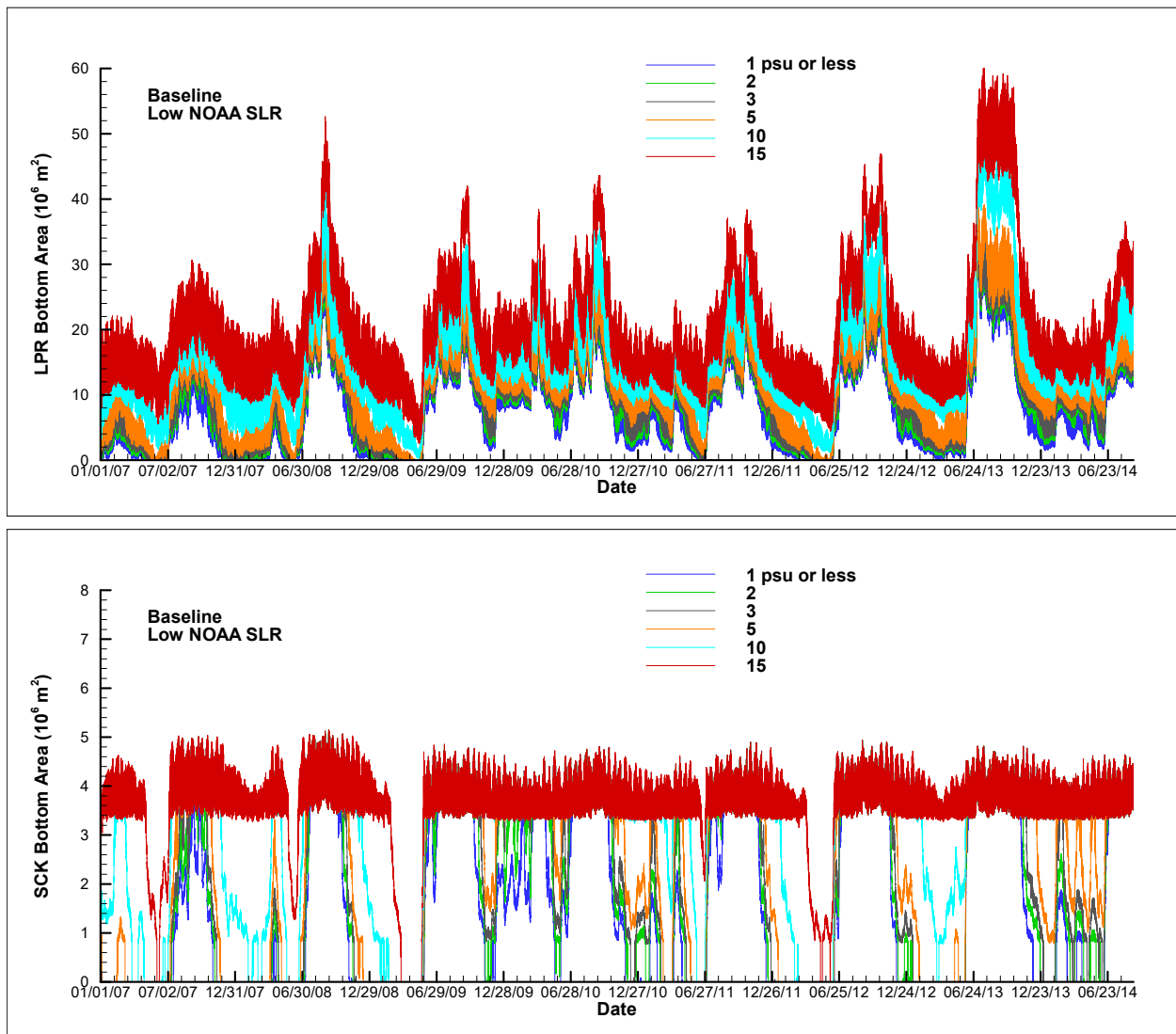


Figure D - 7. Bottom areas for salinity $\leq 1, 2, 3, 5, 10,$ and 15 psu in the LPR (top panel) and in LSC (bottom panel) during the simulation period of January 2007 - August 2014 for the baseline scenario with the low SLR estimate.

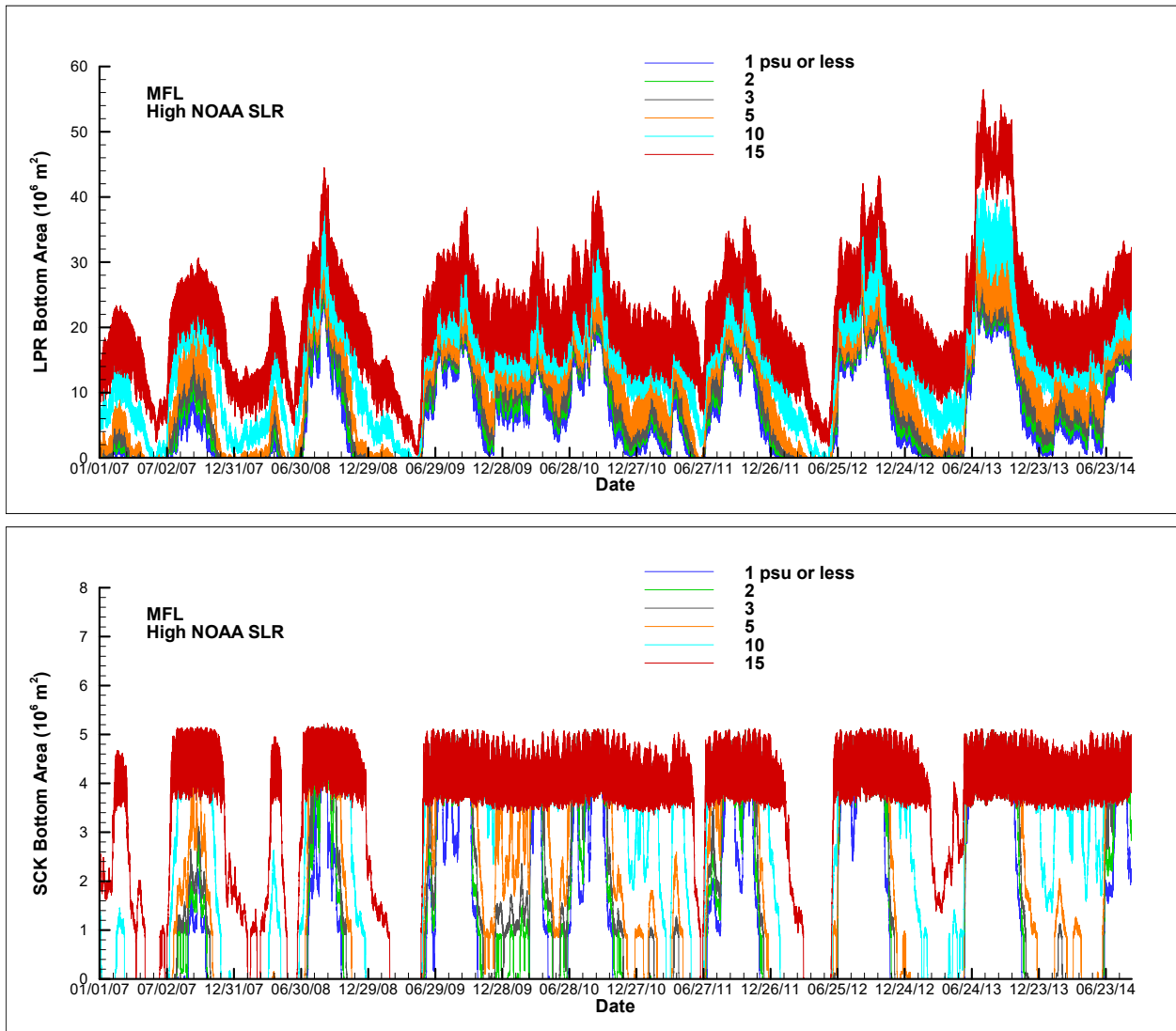


Figure D - 8. Bottom areas for salinity $\leq 1, 2, 3, 5, 10,$ and 15 psu in the LPR (top panel) and in LSC (bottom panel) during the simulation period of January 2007 - August 2014 for the MFL scenario with the high SLR estimate.

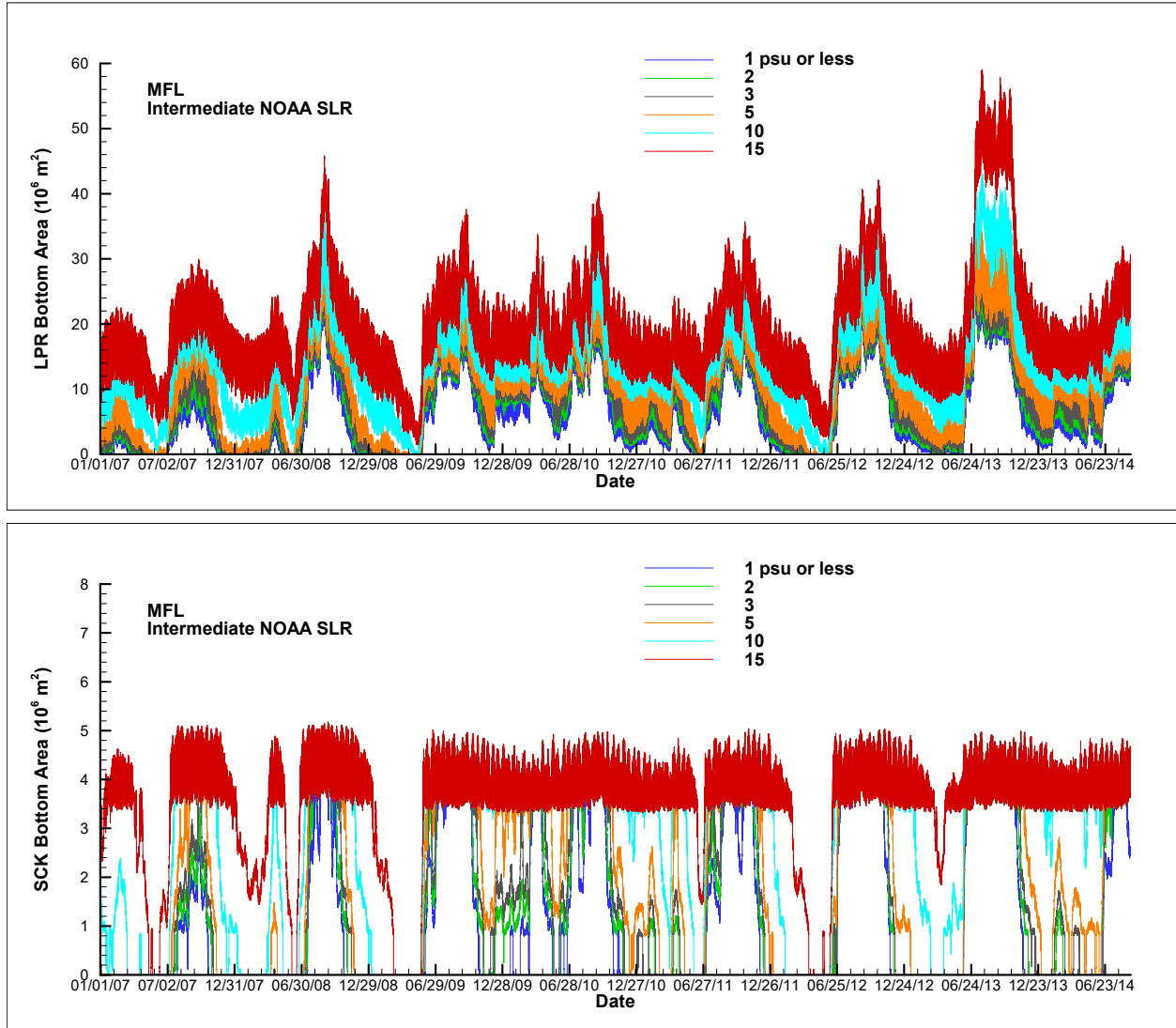


Figure D - 9. Bottom areas for salinity $\leq 1, 2, 3, 5, 10,$ and 15 psu in the LPR (top panel) and in LSC (bottom panel) during the simulation period of January 2007 - August 2014 for the MFL scenario with the intermediate SLR estimate.

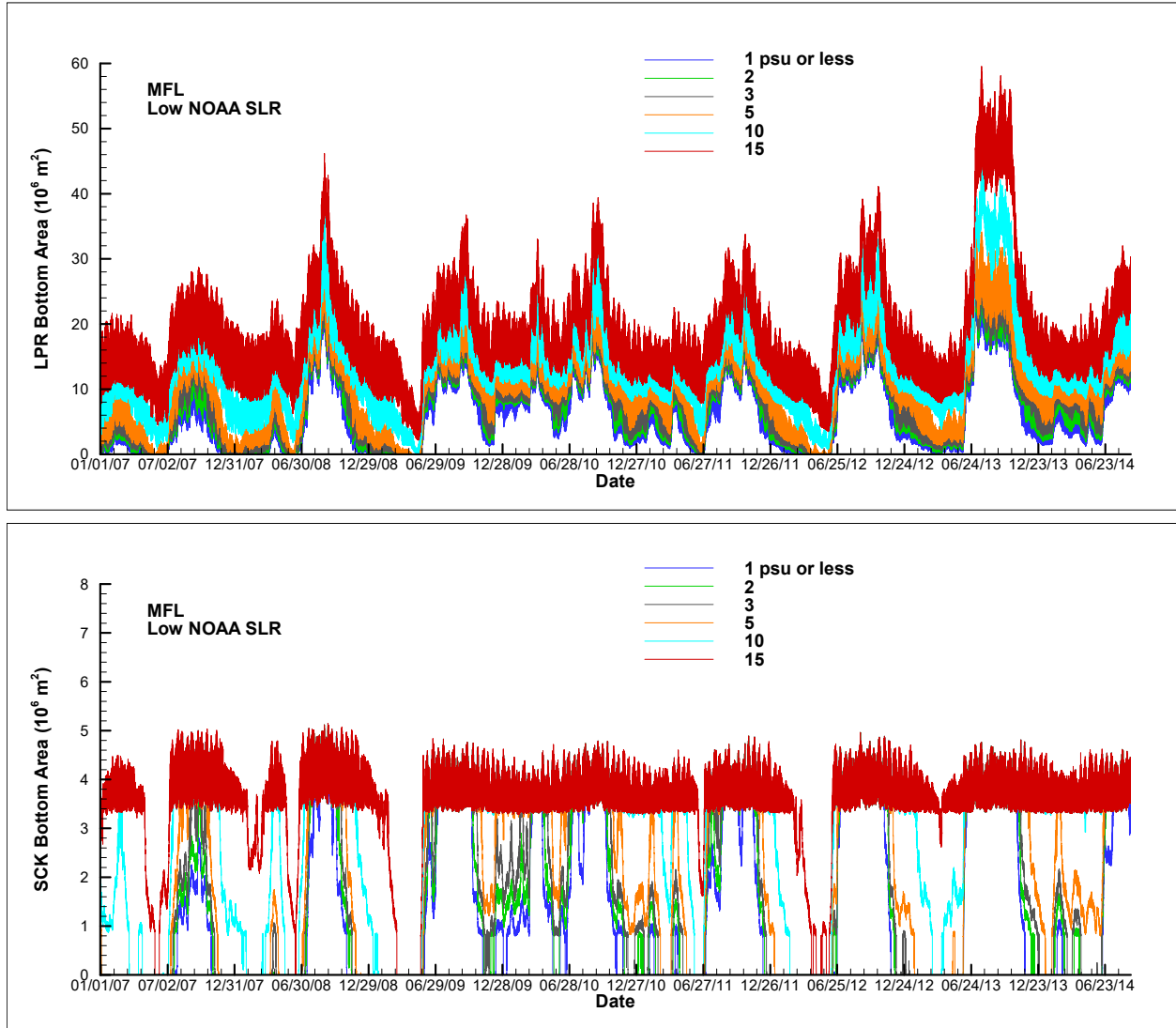


Figure D - 10. Bottom areas for salinity $\leq 1, 2, 3, 5, 10,$ and 15 psu in the LPR (top panel) and in LSC (bottom panel) during the simulation period of January 2007 - August 2014 for the MFL scenario with the low SLR estimate.

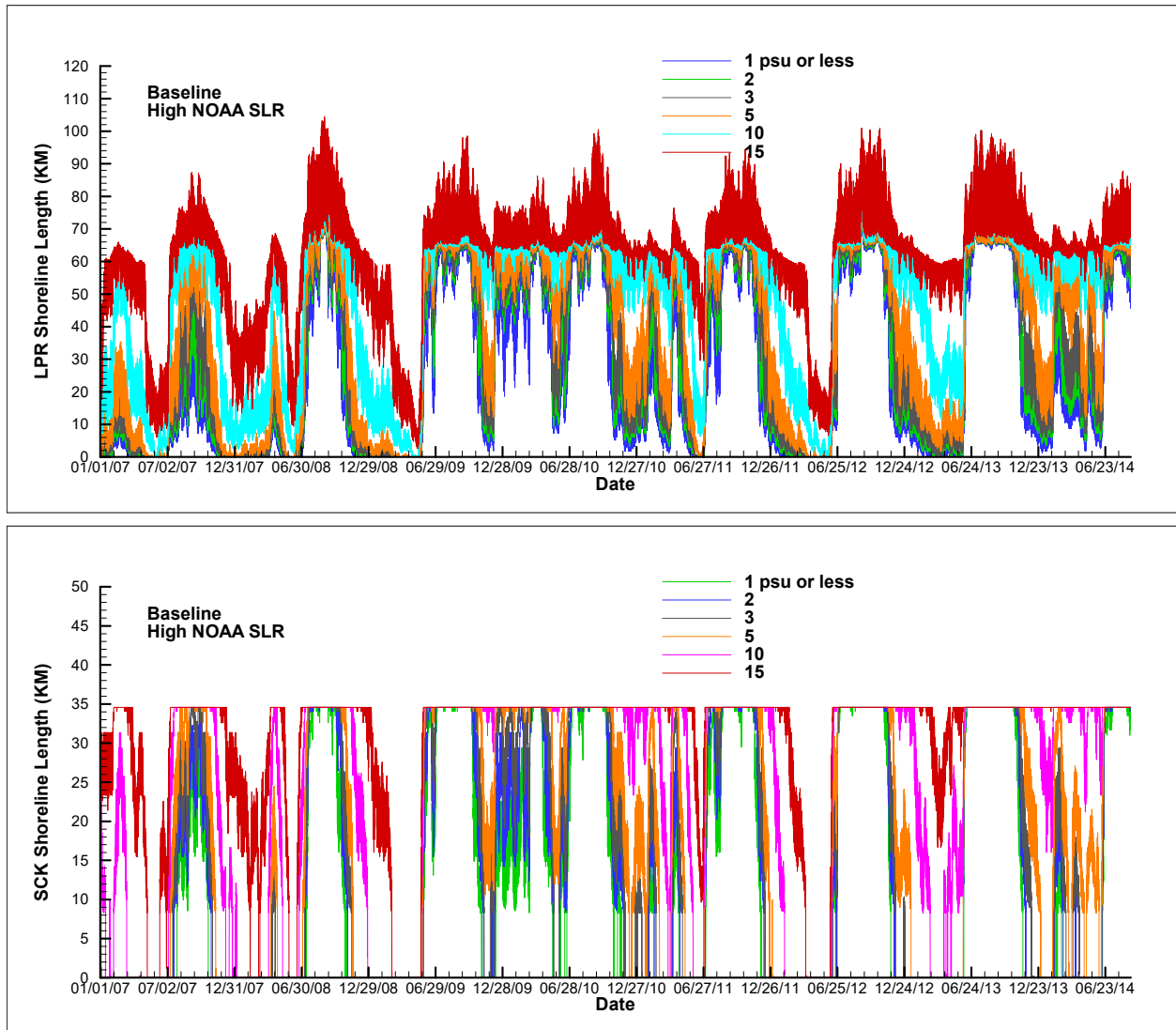


Figure D - 11. Shoreline lengths areas for salinity $\leq 1, 2, 3, 5, 10,$ and 15 psu in the LPR (top panel) and in LSC (bottom panel) during the simulation period of January 2007 - August 2014 for the baseline scenario with the high SLR estimate.

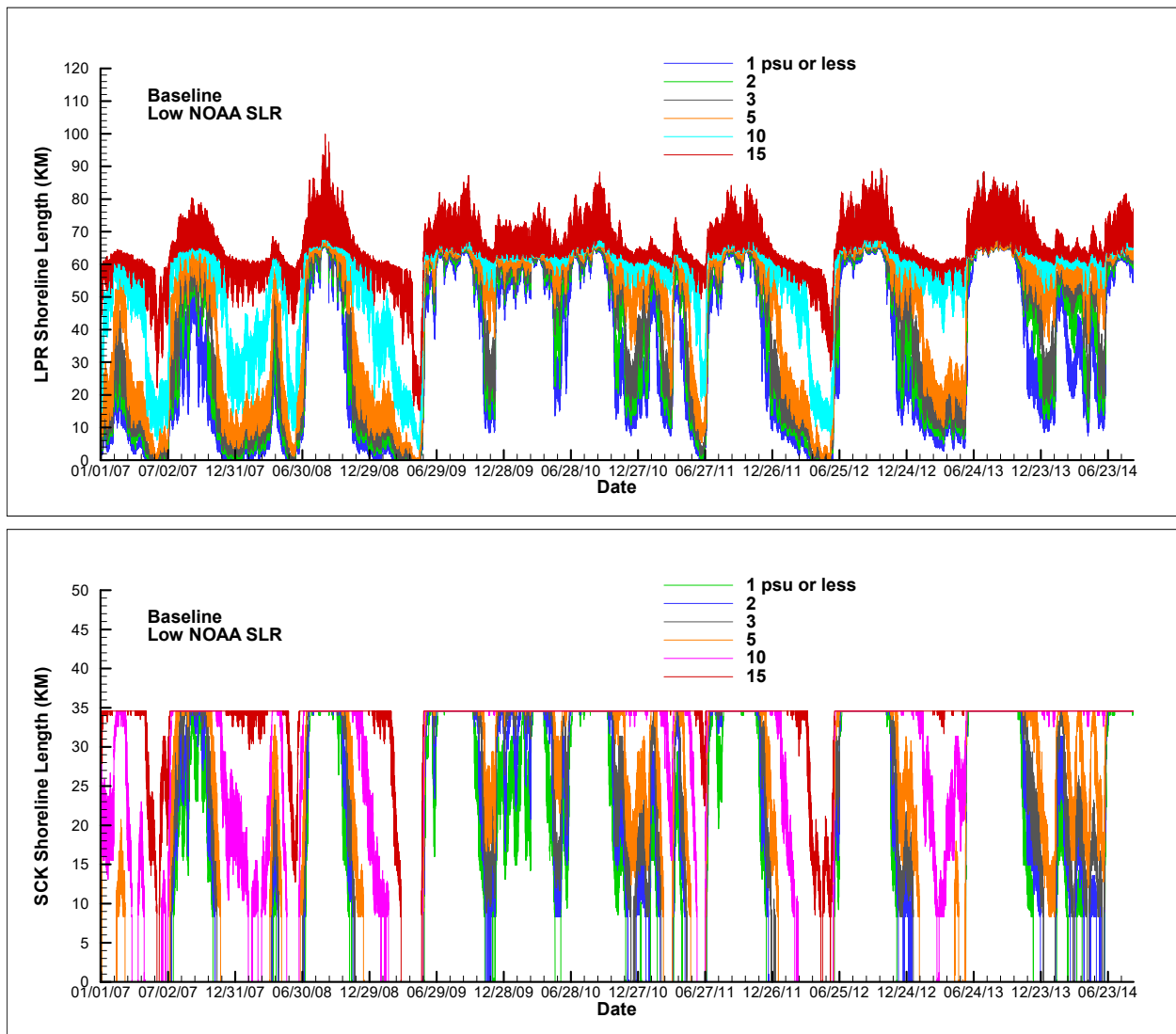


Figure D - 12. Shoreline lengths areas for salinity $\leq 1, 2, 3, 5, 10,$ and 15 psu in the LPR (top panel) and in LSC (bottom panel) during the simulation period of January 2007 - August 2014 for the baseline scenario with the low SLR estimate.

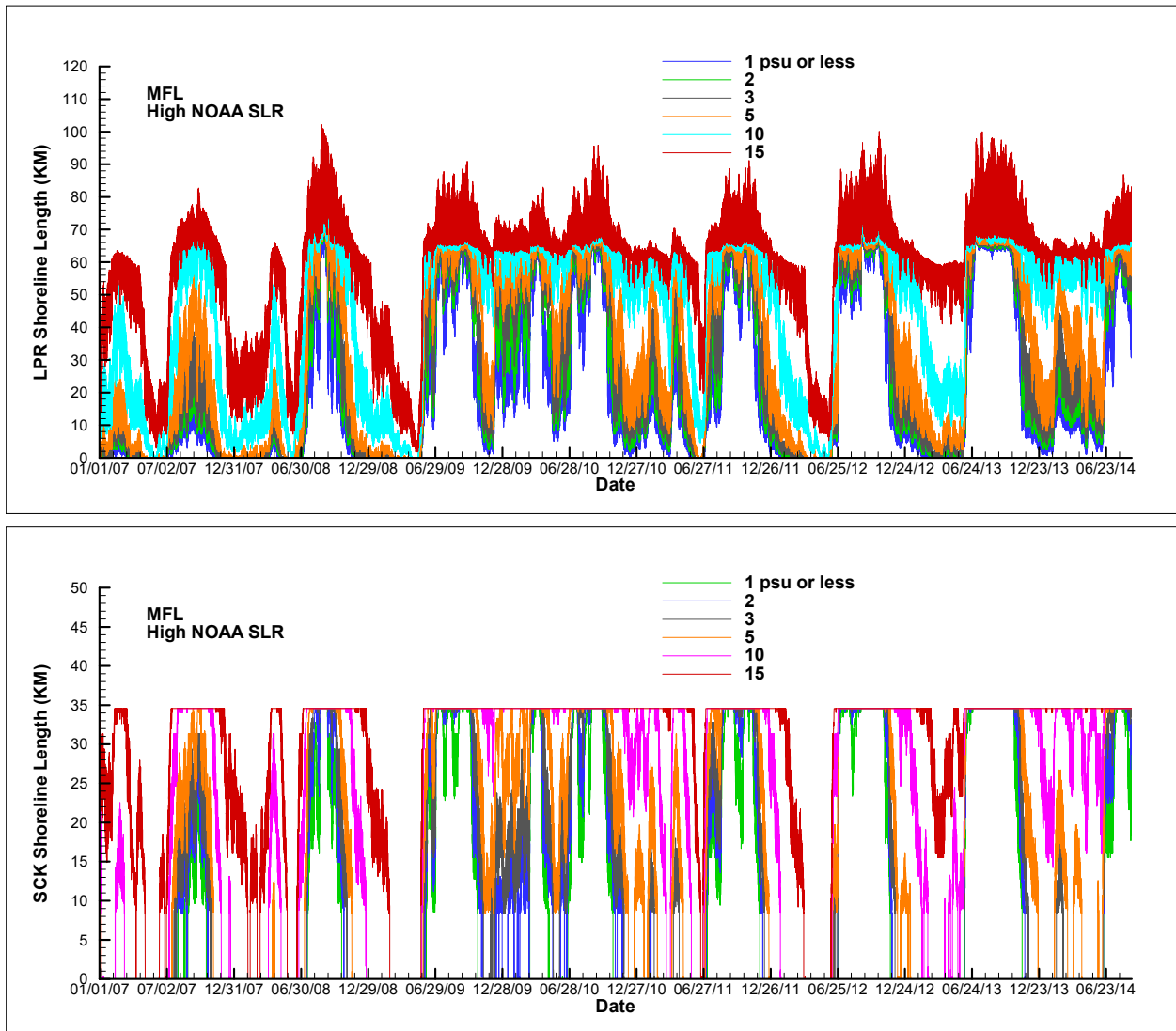


Figure D - 13. Shoreline lengths areas for salinity $\leq 1, 2, 3, 5, 10,$ and 15 psu in the LPR (top panel) and in LSC (bottom panel) during the simulation period of January 2007 - August 2014 for the MFL scenario with the high SLR estimate.

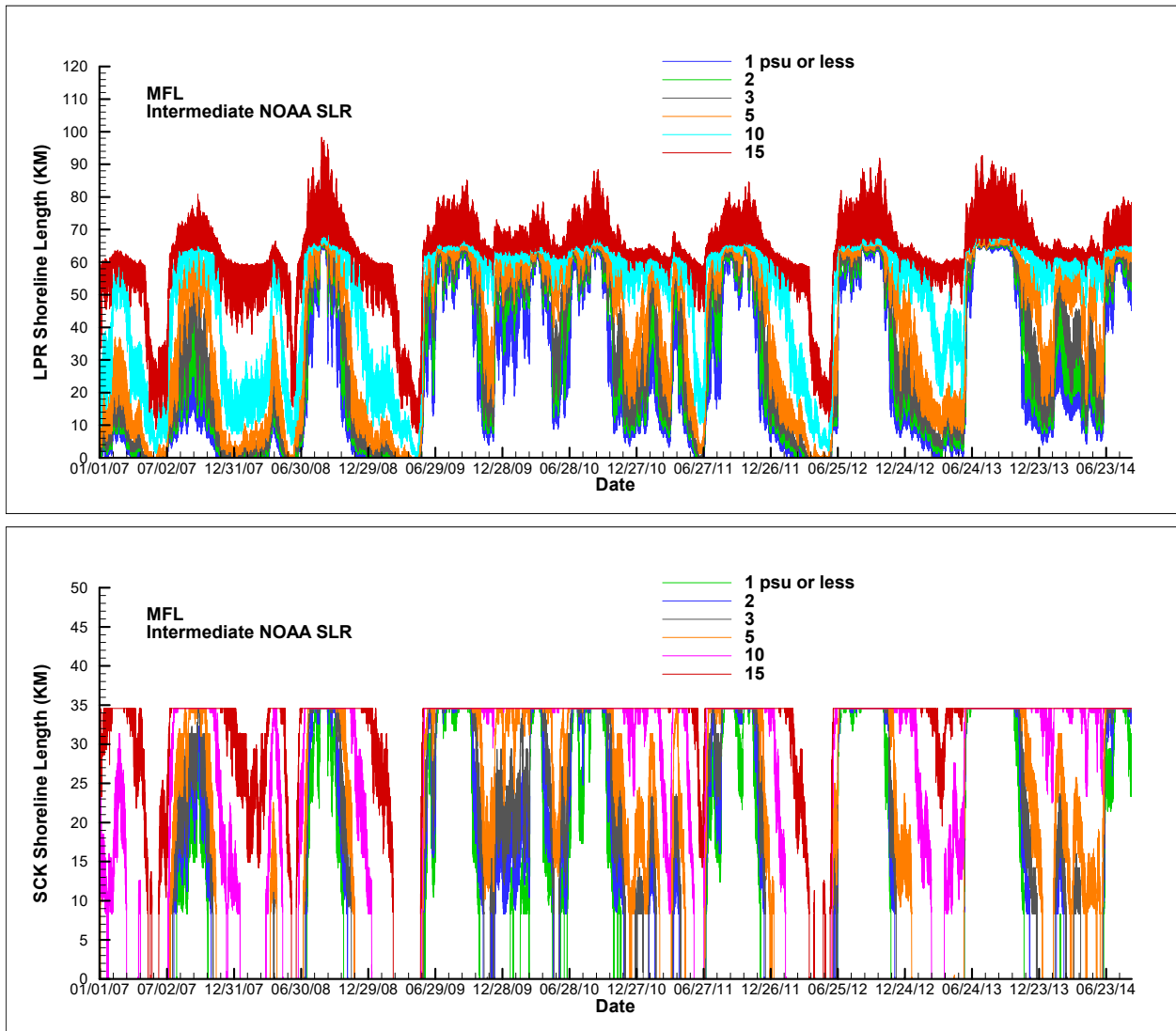


Figure D - 14. Shoreline lengths areas for salinity $\leq 1, 2, 3, 5, 10,$ and 15 psu in the LPR (top panel) and in LSC (bottom panel) during the simulation period of January 2007 - August 2014 for the MFL scenario with the intermediate SLR estimate.

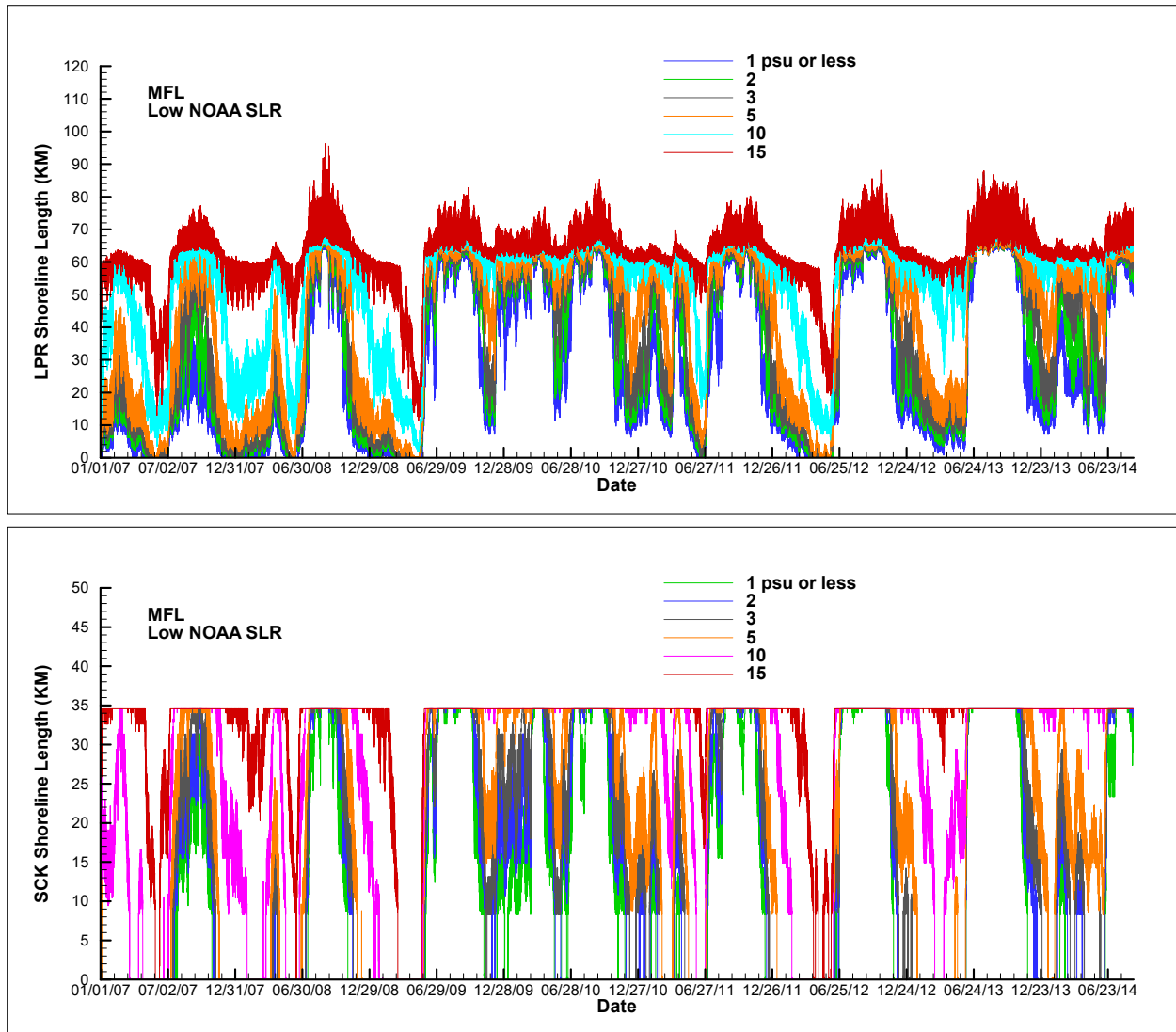


Figure D - 15. Shoreline lengths areas for salinity $\leq 1, 2, 3, 5, 10,$ and 15 psu in the LPR (top panel) and in LSC (bottom panel) during the simulation period of January 2007 - August 2014 for the MFL scenario with the low SLR estimate.

11. Appendix E

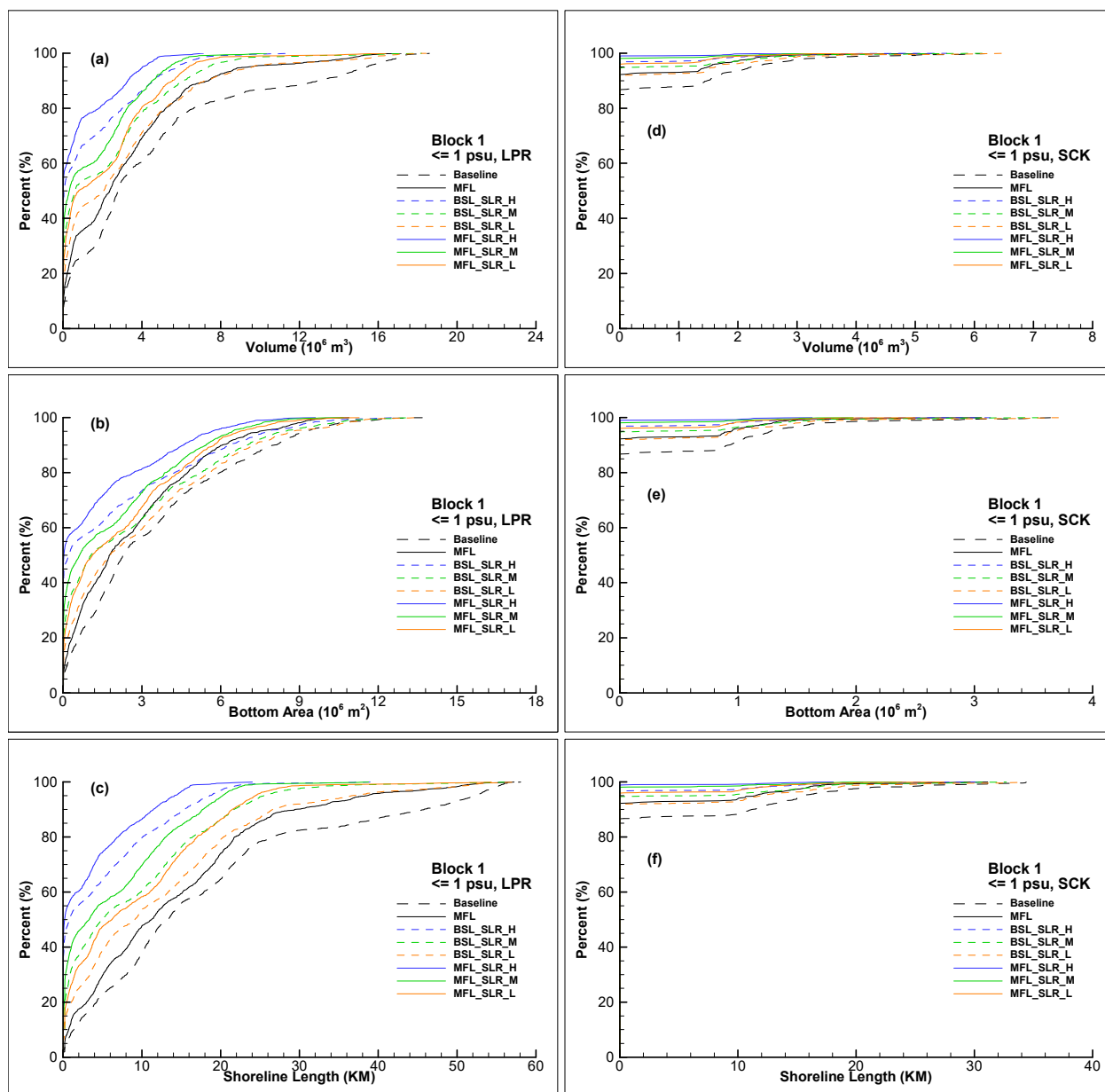


Figure E - 1. CDFs of ≤ 1 psu water volume (a & d), bottom area (b & e), and shoreline length (c & f) in the LPR and LSC during extremely dry (Block 1) days during January 2007 - August 2014 for the baseline flows, proposed MFLs, baseline flows with high, intermediate, and low SLRs, and MFLs with high, intermediate, and low SLRs.

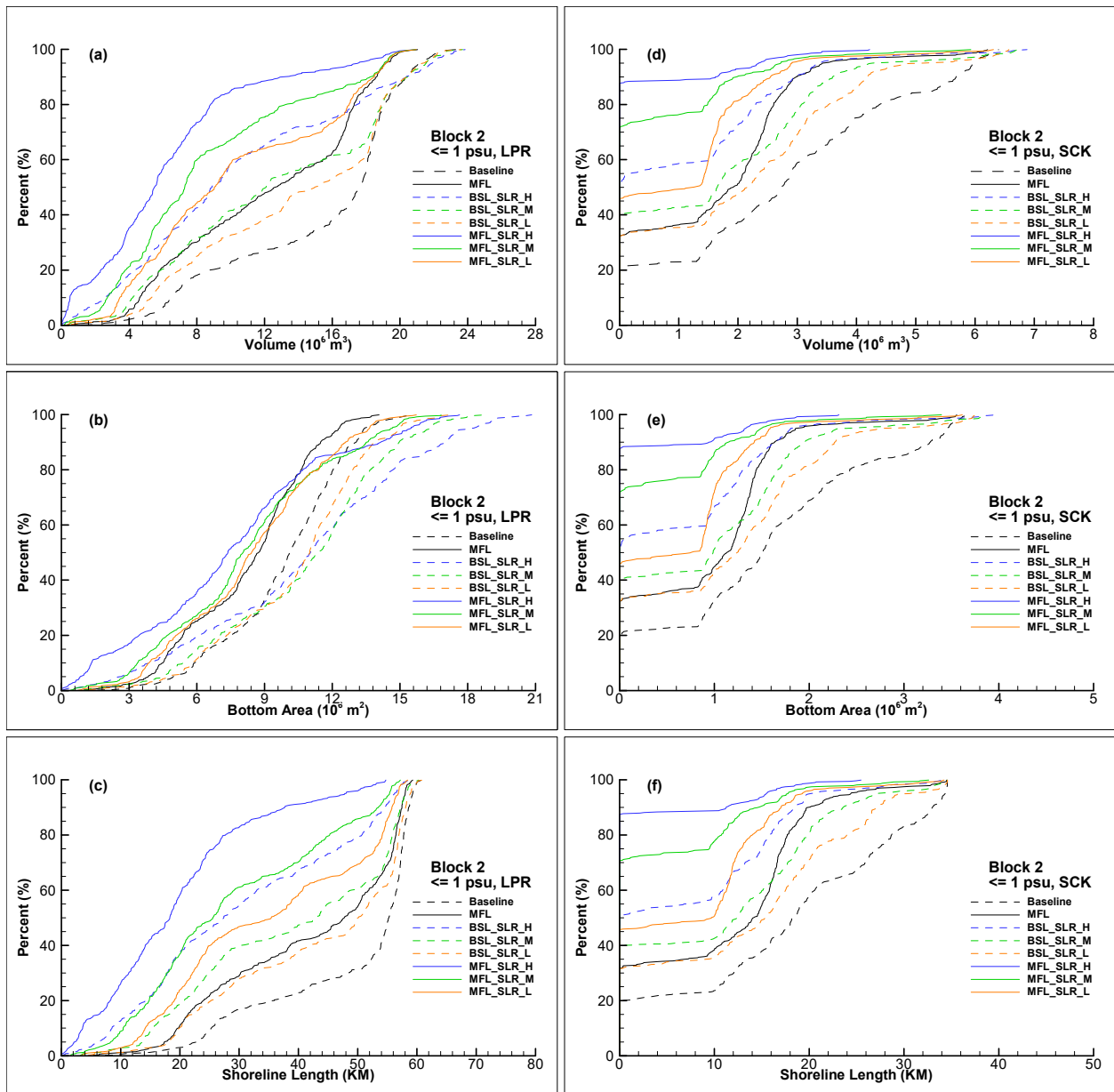


Figure E - 2. CDFs of ≤ 1 psu water volume (a & d), bottom area (b & e), and shoreline length (c & f) in the LPR and LSC during dry (Block 2) days during January 2007 - August 2014 for the baseline flows, proposed MFLs, baseline flows with high, intermediate, and low SLRs, and MFLs with high, intermediate, and low SLRs.

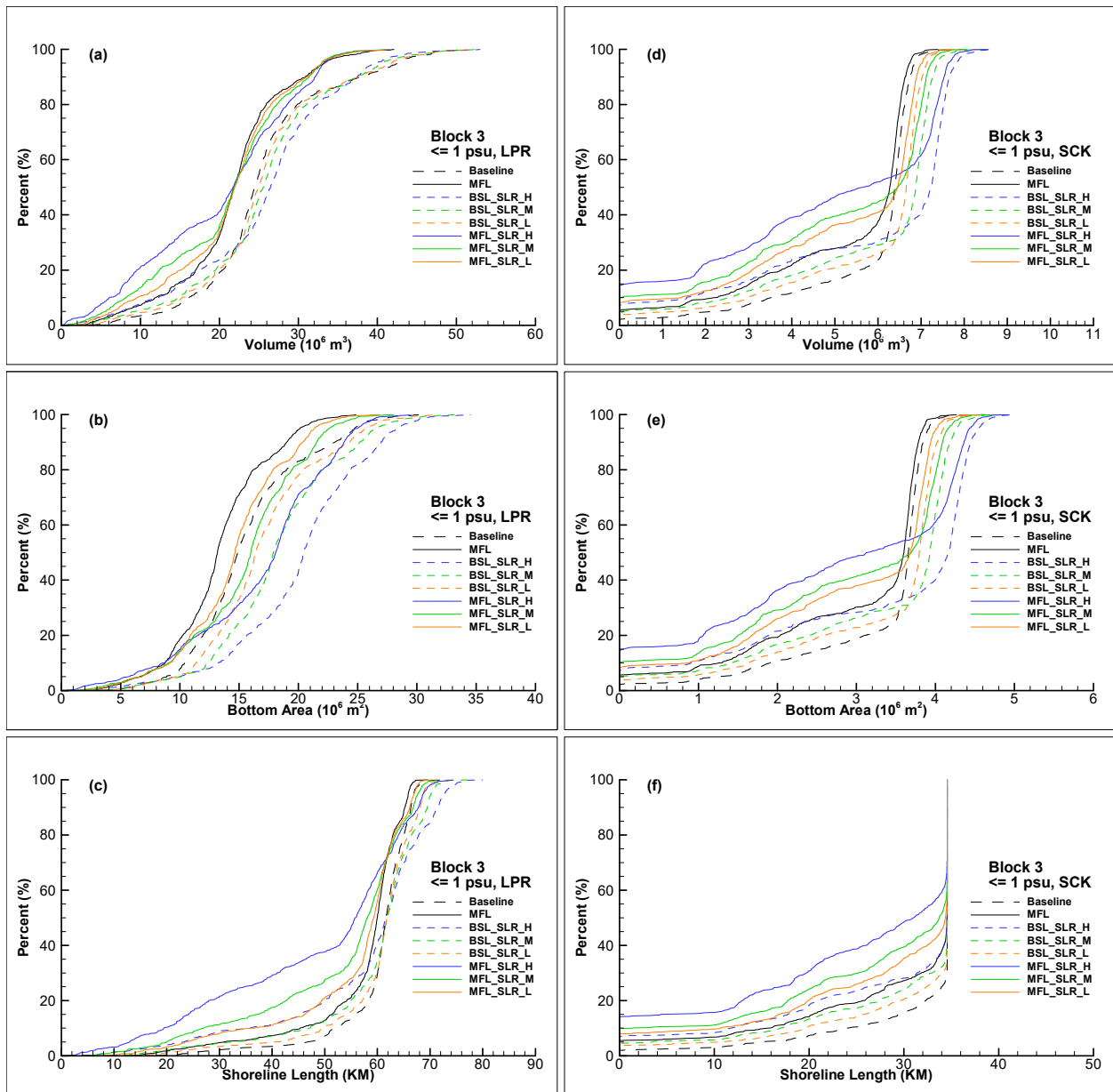


Figure E - 3. CDFs of ≤ 1 psu water volume (a & d), bottom area (b & e), and shoreline length (c & f) in the LPR and LSC during wet (Block 3) days during January 2007 - August 2014 for the baseline flows, proposed MFLs, baseline flows with high, intermediate, and low SLRs, and MFLs with high, intermediate, and low SLRs.

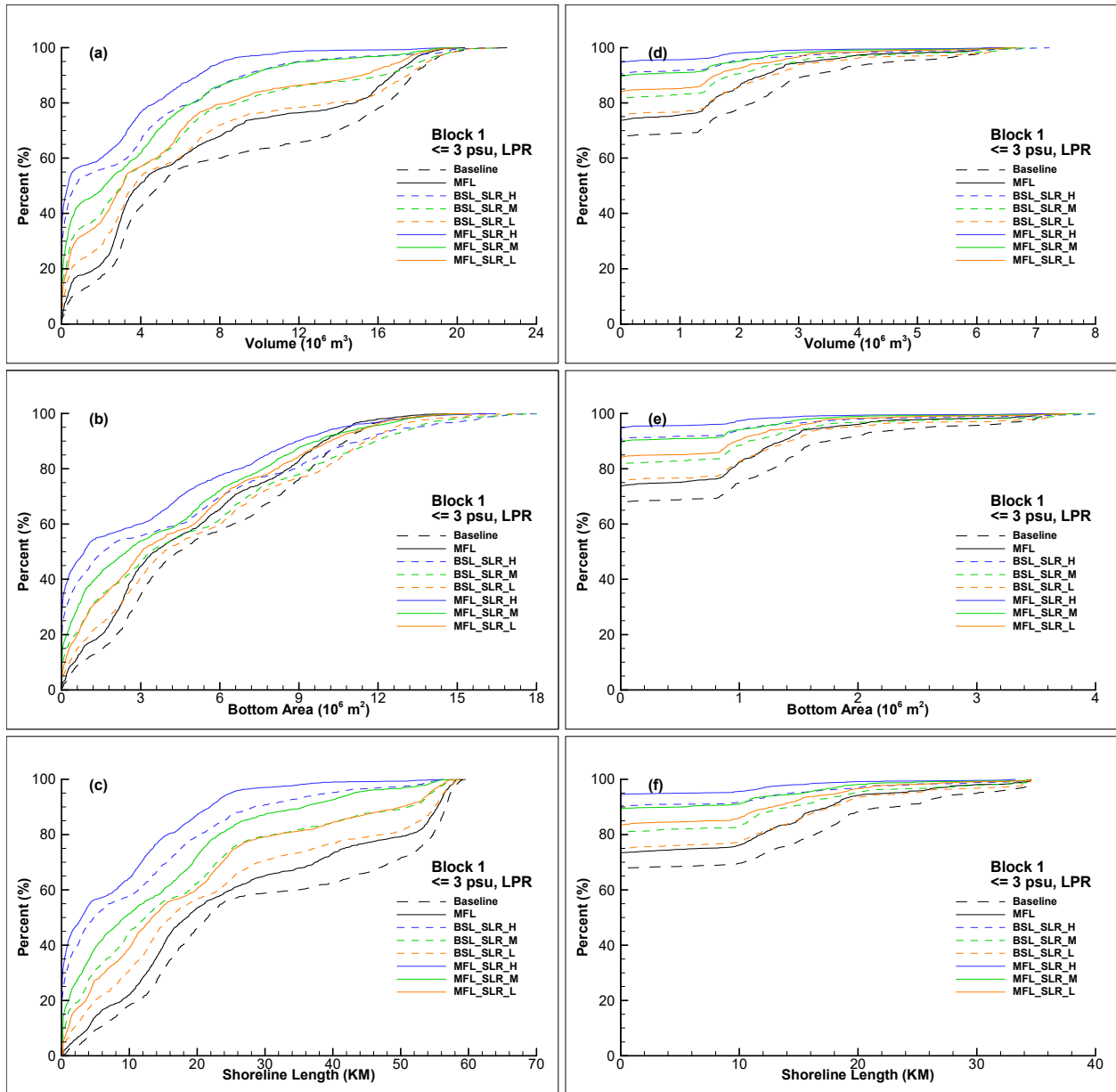


Figure E - 4. CDFs of ≤ 3 psu water volume (a & d), bottom area (b & e), and shoreline length (c & f) in the LPR and LSC during extremely dry (Block 1) days during January 2007 - August 2014 for the baseline flows, proposed MFLs, baseline flows with high, intermediate, and low SLRs, and MFLs with high, intermediate, and low SLRs.

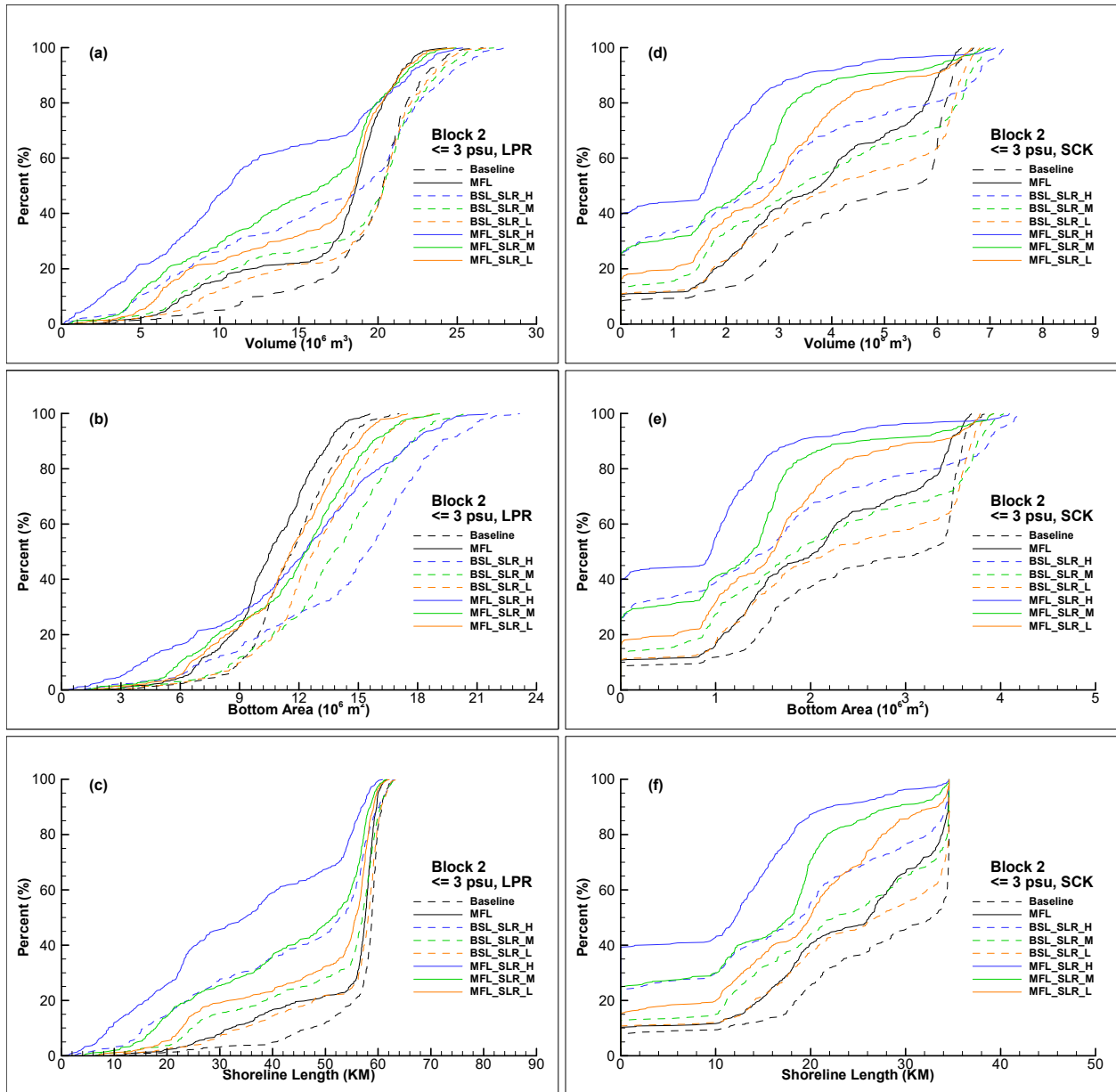


Figure E - 5. CDFs of ≤ 3 psu water volume (a & d), bottom area (b & e), and shoreline length (c & f) in the LPR and LSC during dry (Block 2) days during January 2007 - August 2014 for the baseline flows, proposed MFLs, baseline flows with high, intermediate, and low SLRs, and MFLs with high, intermediate, and low SLRs.

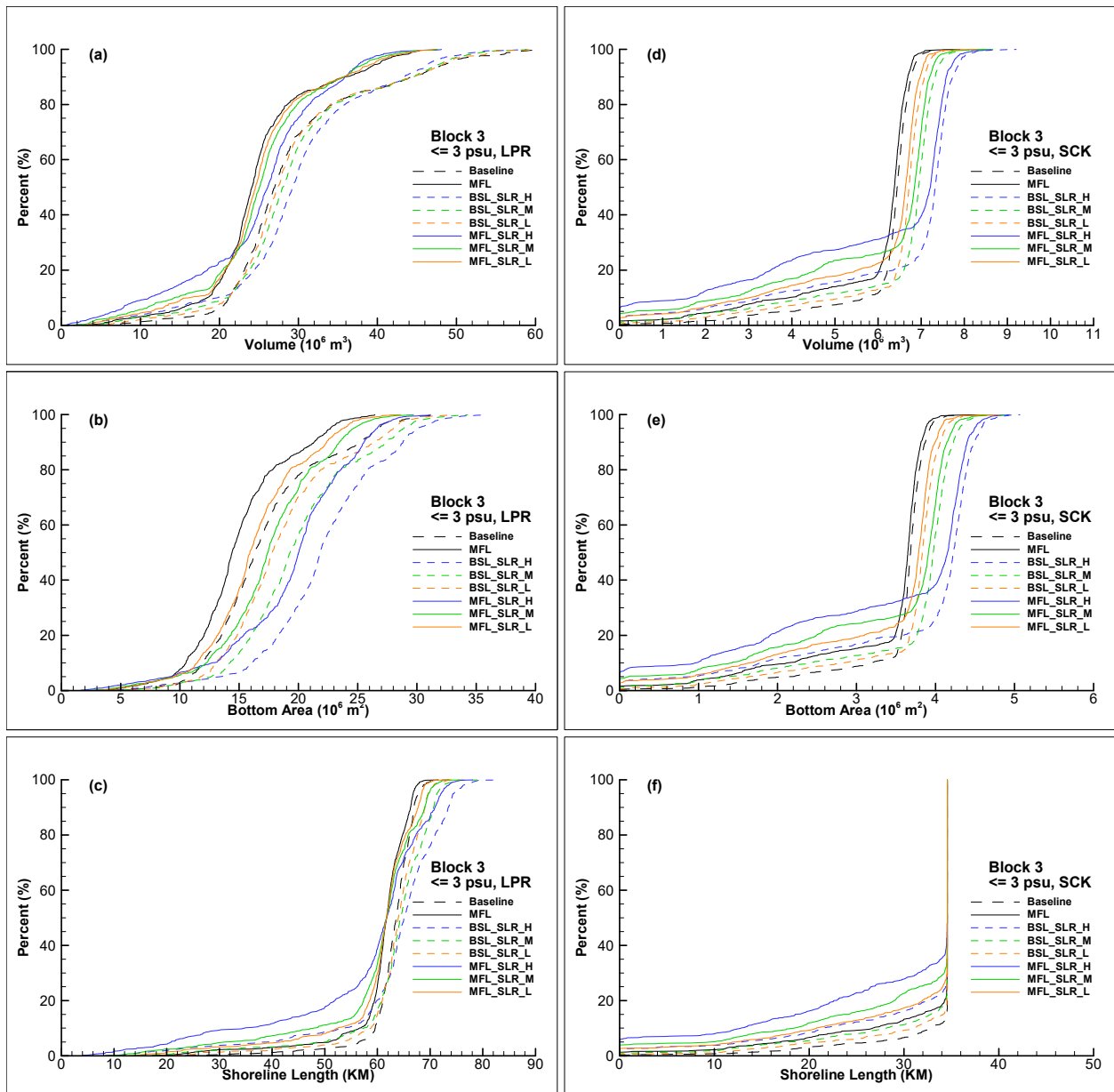


Figure E - 6. CDFs of ≤ 3 psu water volume (a & d), bottom area (b & e), and shoreline length (c & f) in the LPR and LSC during wet (Block 3) days during January 2007 - August 2014 for the baseline flows, proposed MFLs, baseline flows with high, intermediate, and low SLRs, and MFLs with high, intermediate, and low SLRs.

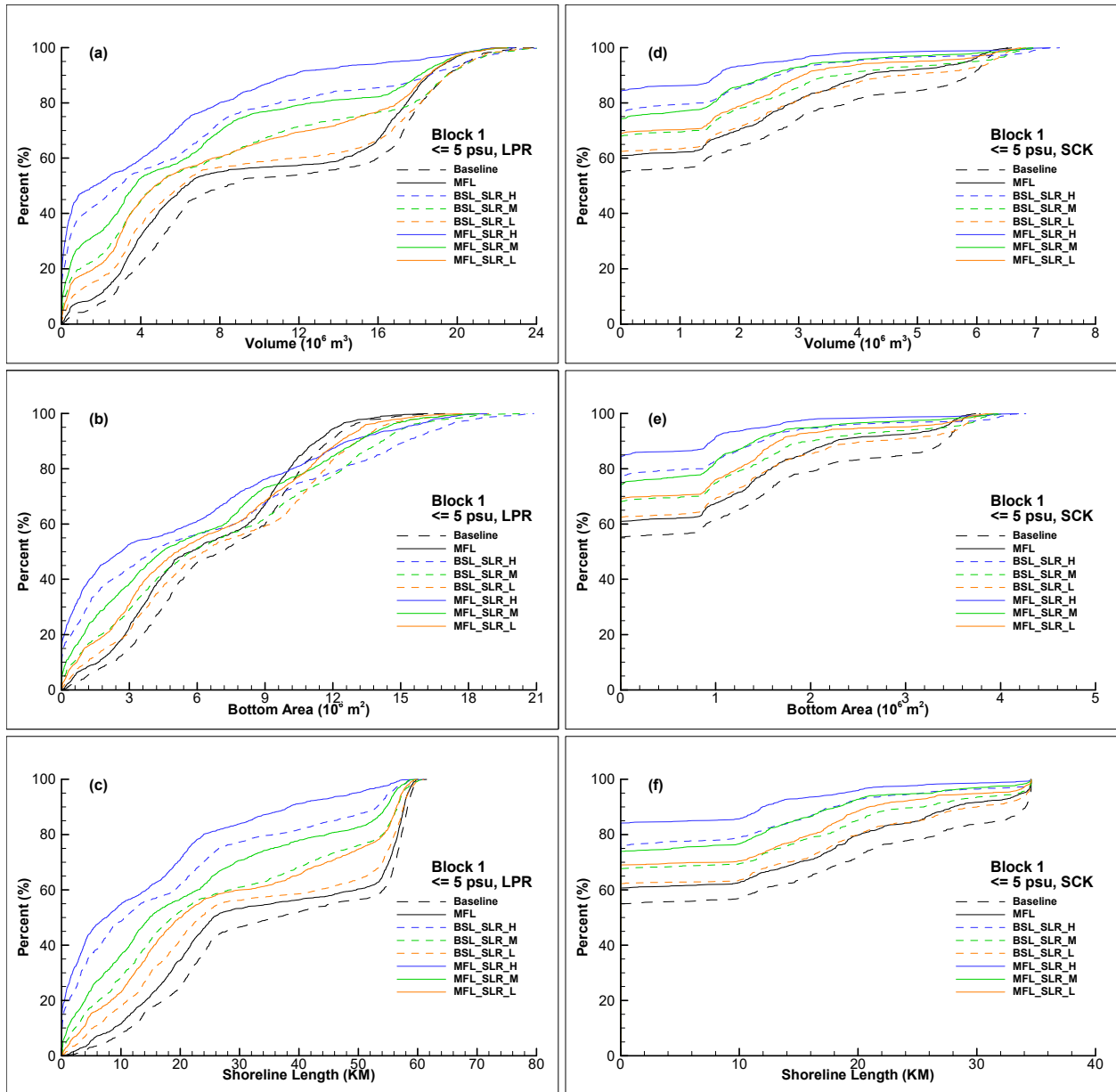


Figure E - 7. CDFs of ≤ 5 psu water volume (a & d), bottom area (b & e), and shoreline length (c & f) in the LPR and LSC during extremely dry (Block 1) days during January 2007 - August 2014 for the baseline flows, proposed MFLs, baseline flows with high, intermediate, and low SLRs, and MFLs with high, intermediate, and low SLRs.

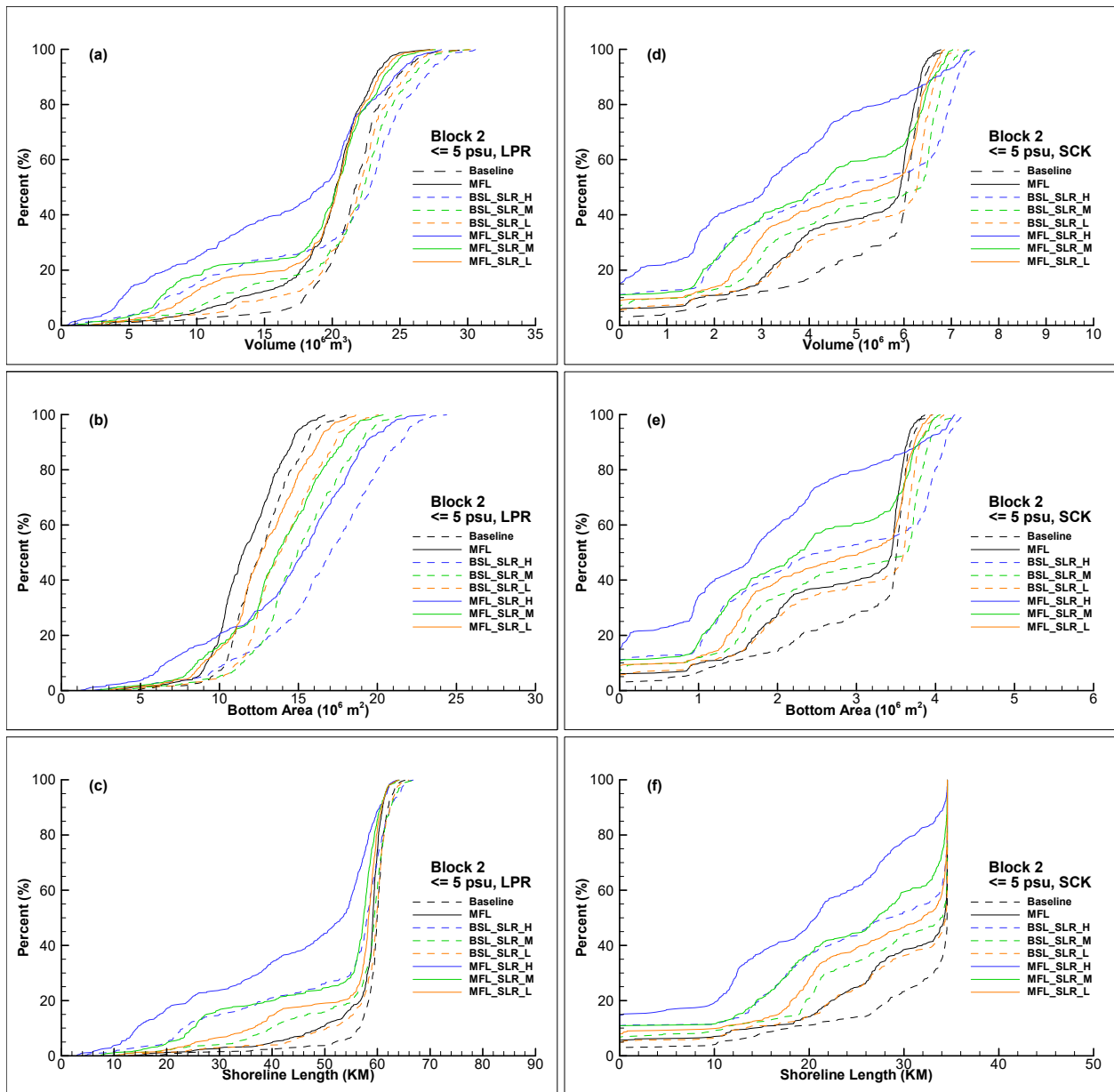


Figure E - 8. CDFs of ≤ 5 psu water volume (a & d), bottom area (b & e), and shoreline length (c & f) in the LPR and LSC during dry (Block 2) days during January 2007 - August 2014 for the baseline flows, proposed MFLs, baseline flows with high, intermediate, and low SLRs, and MFLs with high, intermediate, and low SLRs.

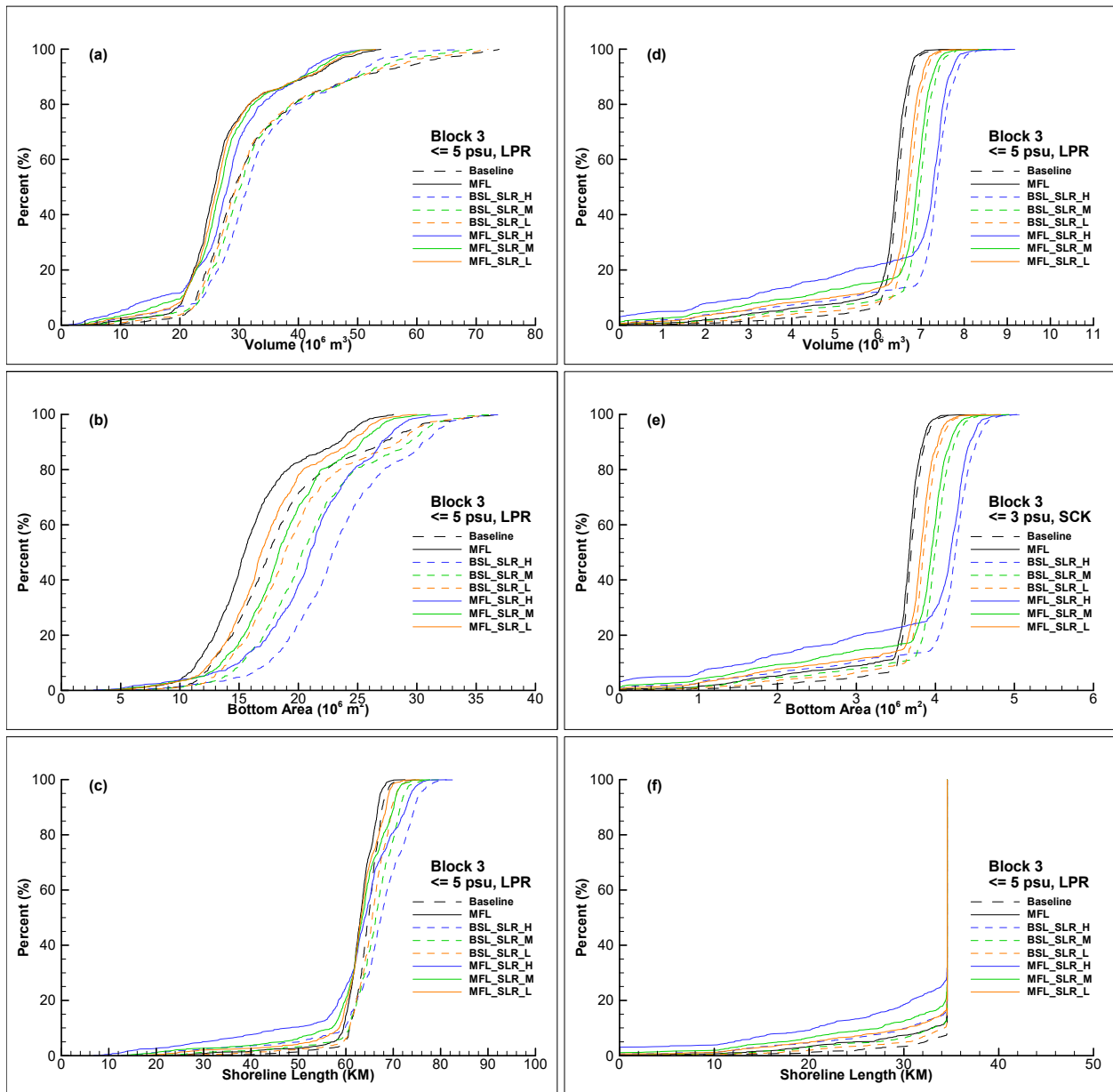


Figure E - 9. CDFs of ≤ 5 psu water volume (a & d), bottom area (b & e), and shoreline length (c & f) in the LPR and LSC during wet (Block 3) days during January 2007 - August 2014 for the baseline flows, proposed MFLs, baseline flows with high, intermediate, and low SLRs, and MFLs with high, intermediate, and low SLRs.

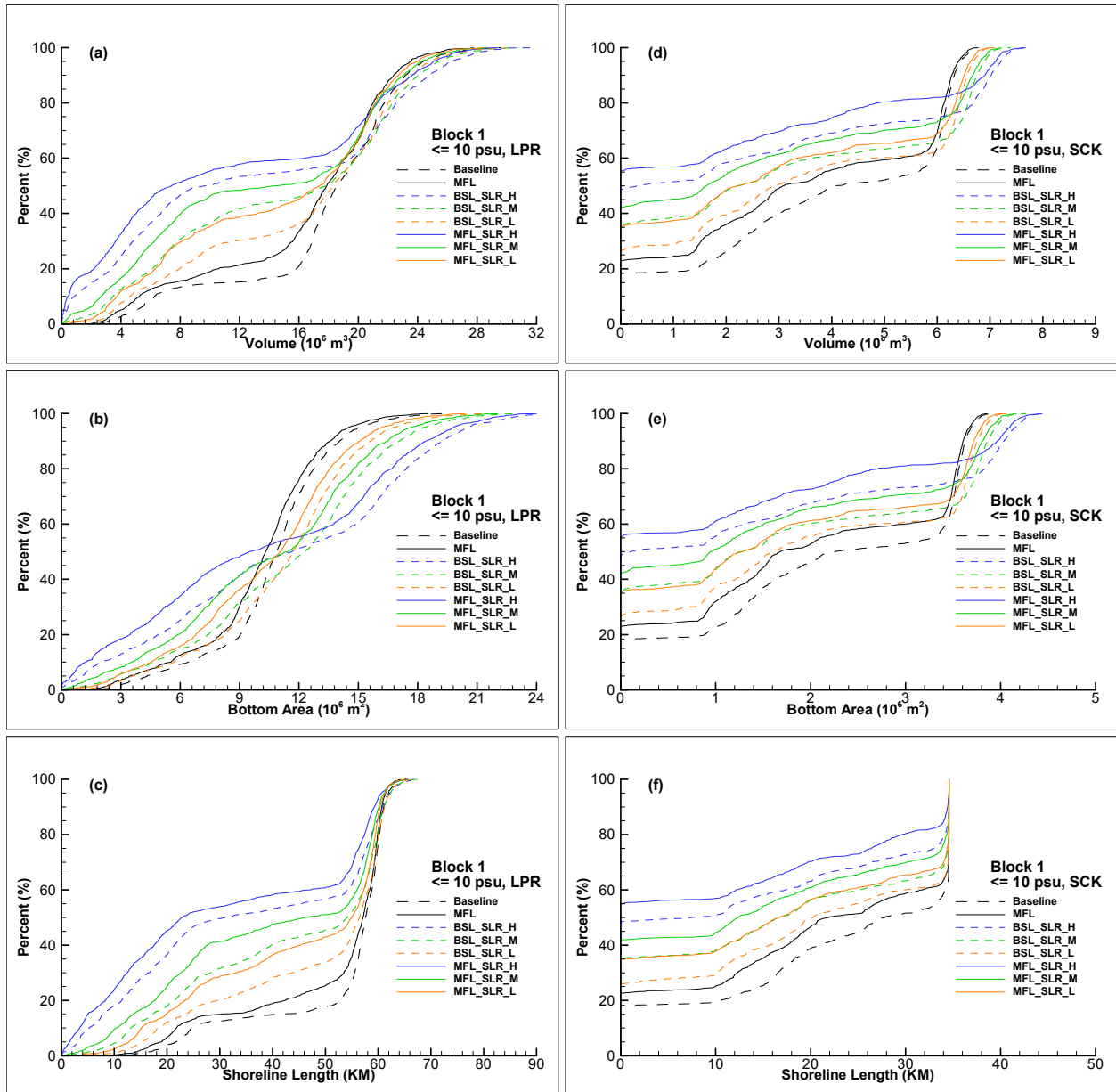


Figure E - 10. CDFs of ≤ 10 psu water volume (a & d), bottom area (b & e), and shoreline length (c & f) in the LPR and LSC during extremely dry (Block 1) days during January 2007 - August 2014 for the baseline flows, proposed MFLs, baseline flows with high, intermediate, and low SLRs, and MFLs with high, intermediate, and low SLRs.

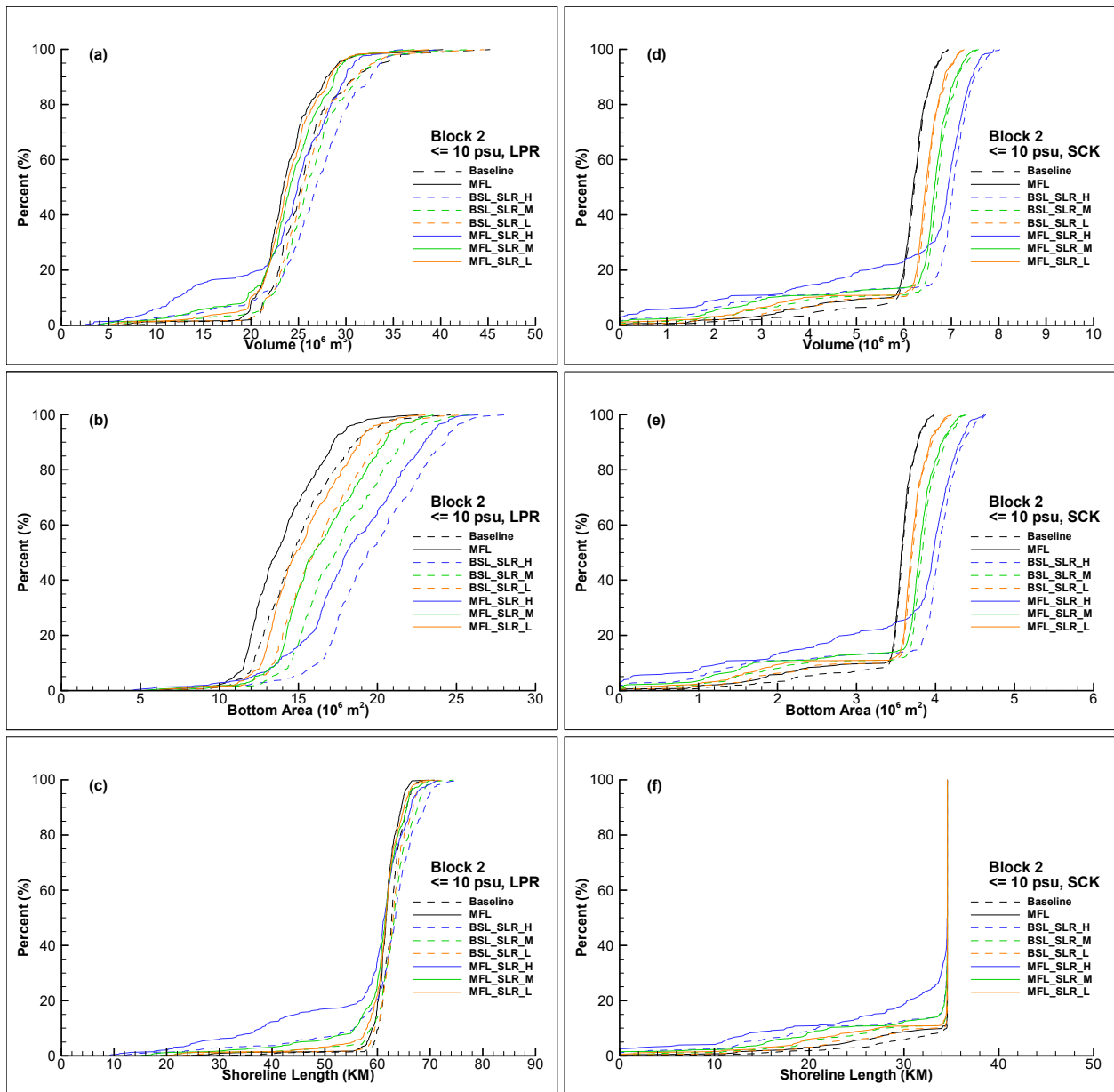


Figure E - 11. CDFs of ≤ 10 psu water volume (a & d), bottom area (b & e), and shoreline length (c & f) in the LPR and LSC during dry (Block 2) days during January 2007 - August 2014 for the baseline flows, proposed MFLs, baseline flows with high, intermediate, and low SLRs, and MFLs with high, intermediate, and low SLRs.

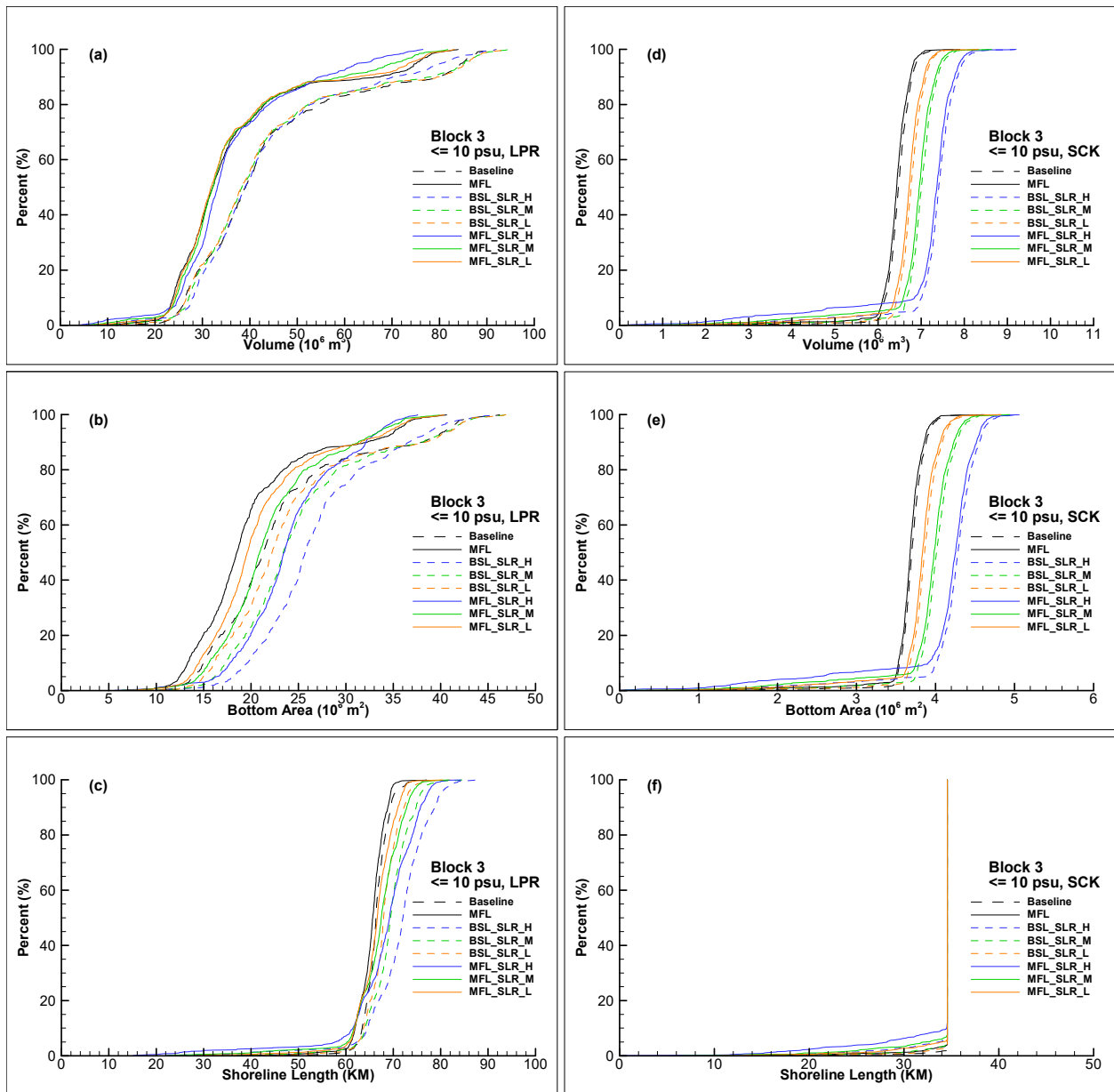


Figure E - 12. CDFs of ≤ 10 psu water volume (a & d), bottom area (b & e), and shoreline length (c & f) in the LPR and LSC during wet (Block 3) days during January 2007 - August 2014 for the baseline flows, proposed MFLs, baseline flows with high, intermediate, and low SLRs, and MFLs with high, intermediate, and low SLRs.

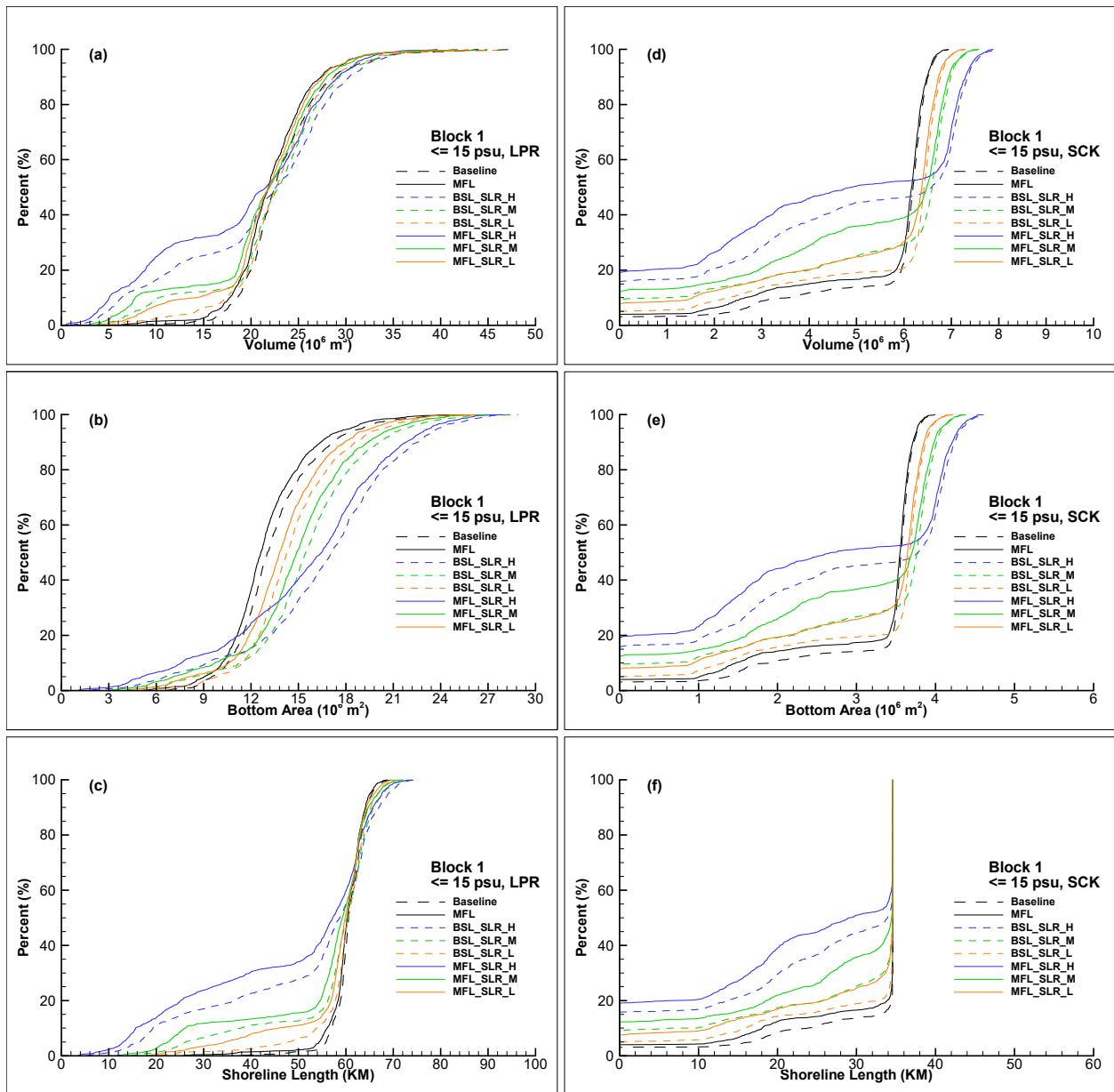


Figure E - 13. CDFs of ≤ 15 psu water volume (a & d), bottom area (b & e), and shoreline length (c & f) in the LPR and LSC during extremely dry (Block 1) days during January 2007 - August 2014 for the baseline flows, proposed MFLs, baseline flows with high, intermediate, and low SLRs, and MFLs with high, intermediate, and low SLRs.

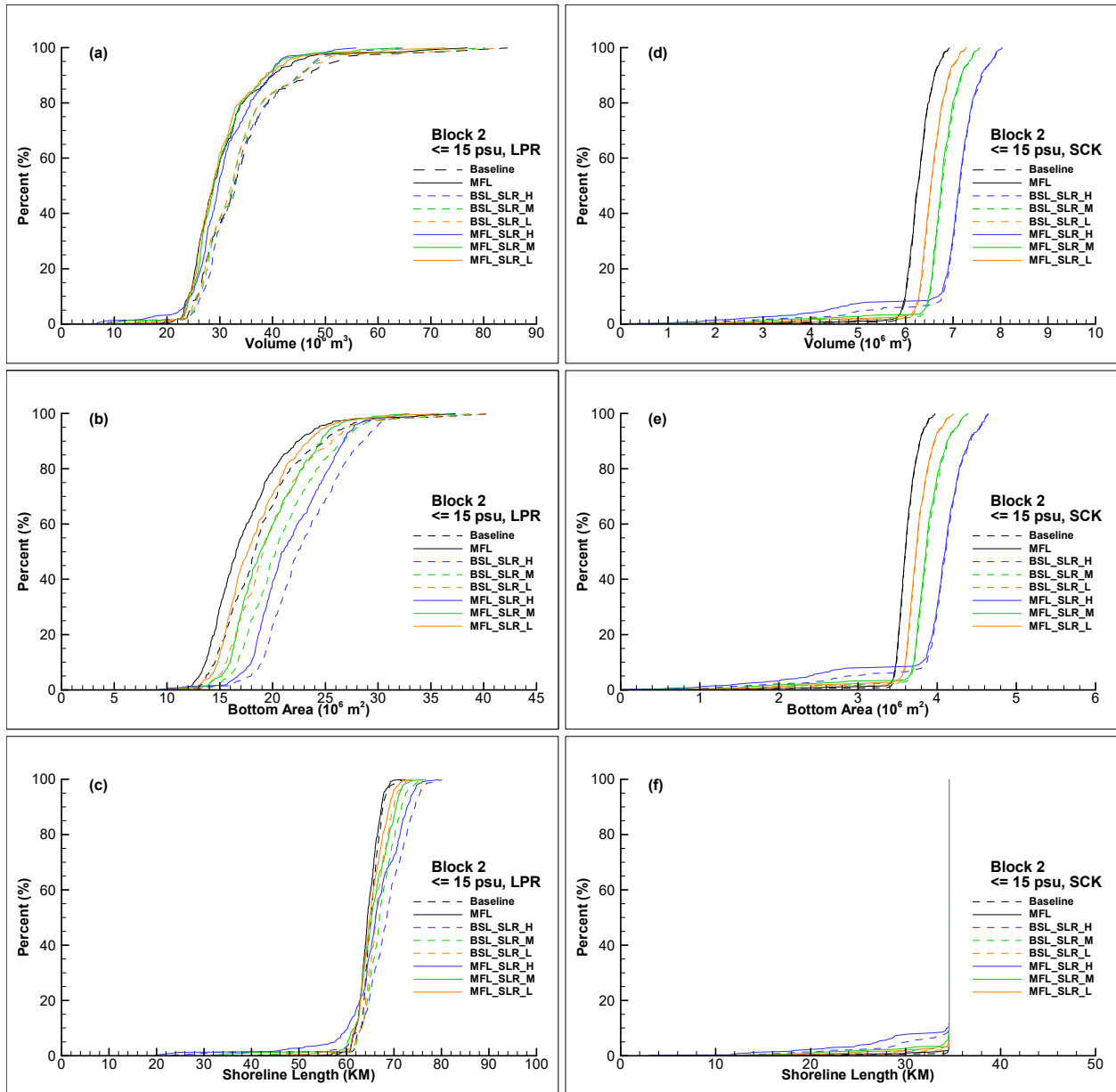


Figure E - 14. CDFs of ≤ 15 psu water volume (a & d), bottom area (b & e), and shoreline length (c & f) in the LPR and LSC during dry (Block 2) days during January 2007 - August 2014 for the baseline flows, proposed MFLs, baseline flows with high, intermediate, and low SLRs, and MFLs with high, intermediate, and low SLRs.

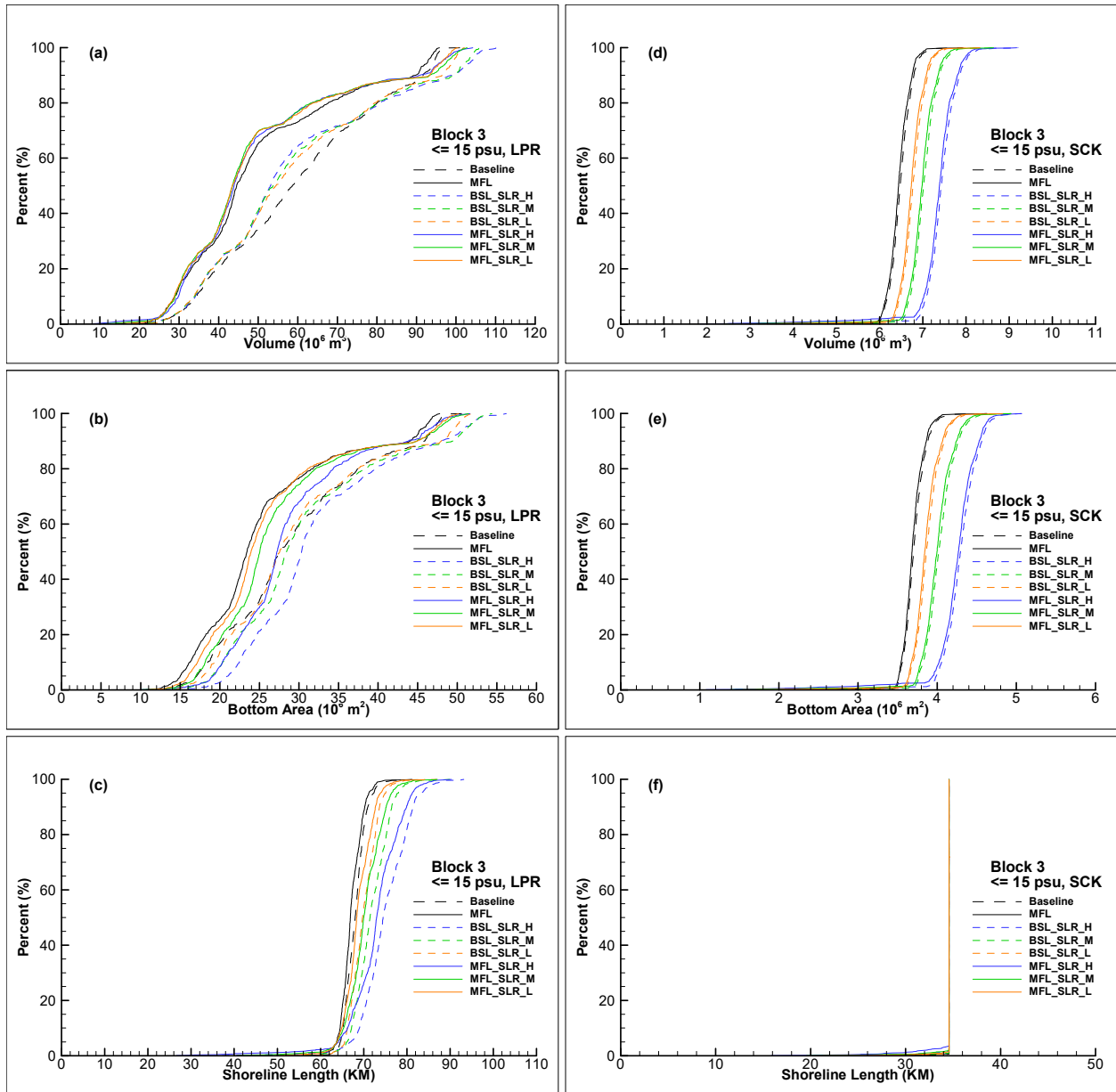


Figure E - 15. CDFs of ≤ 15 psu water volume (a & d), bottom area (b & e), and shoreline length (c & f) in the LPR and LSC during wet (Block 3) days during January 2007 - August 2014 for the baseline flows, proposed MFLs, baseline flows with high, intermediate, and low SLRs, and MFLs with high, intermediate, and low SLRs.